UNIVERSITÉ DU LUXEMBOURG

PhD-FSTC-2013-03
The Faculty of Sciences, Technology and Communication

DISSERTATION

Defense held on 28/01/2013 in Luxembourg

to obtain the degree of

DOCTEUR DE L'UNIVERSITÉ DU LUXEMBOURG

EN SCIENCES DE L'INGÉNIEUR

by

Lara ALELUIA DA SILVA REIS

Born on 06 October 1984 in Agualva-Cacém ∗ Sintra (Portugal)

Development and Application of an Asymptotic Level Transport Pollution Model for Luxembourg Energy Air Quality Project

Dissertation defense committee

Dr. Bernhard Peters, dissertation supervisor
Professor, Université du Luxembourg

Dr. Daniel Zachary
R&D Manager, CRP Henri Tudor

Dr. Geoffrey Caruso, Chairman
Professor, Université du Luxembourg

Dr. Dimitrios Melas
Professor, Aristotle University of Thessaloniki

Dr. Ulf Janicke
Executive, Janicke Consulting

Abstract

The connections between air pollution and the increase of respiratory diseases, are well known. In Europe, many efforts have been carried out towards the mitigation of the pollutants' emissions over the last decades. However the ambient levels of some air pollutants, is still worrisome and a large part of the European population is still exposed to high levels pollution.

The European Union supports the implementation of structural planning measures to control air pollution. The assessment and evaluation of these air quality policies must be carried out with the help of dedicated integrated assessment models. The use of integrated assessment models, which combine models from different fields, raises the need for developing specific modelling concepts in order to provide results to support policy decisions within a practical time frame. Integrated assessment models for air policy relate technologies, the emitting sources, with air quality levels. Existing photochemical air quality models are not directly suitable for integrated approaches as they are time intensive in terms of input preparation and simulation speed.

This work presents the methodology and the development of a dedicated air quality model for an integrated assessment model. This approach has been designed for the Luxembourg Energy and Air Quality, LEAQ, integrated assessment model. It combines an air quality model, AUSTAL2000-AYLTP, with a techno-economic model, ETEM, which computes ozone precursors emissions related to energy consumption. The models are coupled via an optimization engine, which minimizes the total energy cost for a given ozone level.

AUSTAL2000, a Lagrangian transport model, has been adapted to receive a photochemical module, the AsYmptotic Level Transport Pollution, AYLTP. This module consists of a Look-Up Table of quasi-linear reaction rates. The AUSTAL2000 model inquires the look-up table for pre-calculated initial conditions, and it reads the correspondent rate that is then used by AUSTAL2000. The look-up table has been built using a box model by simulating a large set of possible combinations of meteorological variables and precursor concentrations. A balance has been found that gives an acceptable level of accuracy, given the reduction of computational time. The development of such methodologies is important when considering integrated assessment models. Furthermore, the results of the air quality model have been compared with measurements, and with the regional model LOTOS-EUROS. The results of the validation are considered satisfactory for this type of approach. Additionally, the air quality model has been used within the in LEAQ model. Two study cases have been simulated, one including only the national emissions

from Luxembourg country, and a second one for the Luxembourg region, including the neighbouring countries emissions.

The use of quasi-linear reaction rates obtained with the help of the look-up table represents an innovative step towards the use of simplified air quality models that involve complex chemistry.

Acknowledgements

First, I would like to acknowledge that this work would have not been possible, without the guidance of my committee members and the support of my family and friends.

I would like to express my gratitude and recognition to my scientific advisor, Dr. Daniel Zachary who has proposed this research topic and has patiently guided my work throughout these four years, also for having raised my interest in integrated assessment approaches, and for being always supportive. I would, equally, like to acknowledge the help of Professor Bernhard Peters, my principal supervisor, for his guidance and advice during my Ph.D. studies, and also for the thesis management support. I am grateful to Professor Geoffrey Caruso, for the help in shaping this thesis work and for his constructive comments and encouragement. To professor Dimitrios Melas for having kindly received me as a guest student in his research group, for always providing a good and constructive advice, I express my gratitude. This thesis would not have been possible without the promptly answers of Dr. Ulf Janicke, to whom I thank for his patience to help me with the theoretical and technical details of the AUSTAL2000 model.

I acknowledge the FNR - Fonds National de la Recherche Luxembourg for the grant founding, AFR - Aide a la Formation-Recherche, under the grant identifier PHD-08-004.

My gratitude goes, also, to all the colleagues who have participated in the Luxembourg Energy Air Quality (LEAQ) project. Namely to Oliver O'Nagy and Guy Kneip for their contribution to the energy database. To Christian Braun for having introduced me to GRASS GIS and the restless help whenever some technical support was needed. To Ulrich Leopold, for being a nice company and for making me an open-source software fan, and to his wife, Elbia who always had good Brazilian food to comfort me. To Laurent Drouet, my colleague, my friend, my mentor and my life partner, for his work on the Energy-Technology-Environment Model (ETEM), without whom the LEAQ project and this thesis would have not been possible, and for his patience, ideas and suggestions my deep and sincere "Merci".

I thank all the people I have met in Resource Centre for Environmental Technologies (CRTE), especially Bianca Schmit for all the support and trust that she conceded me. A big thank you to all the people who have inhabited the "Robert's" office, for the nice coffee breaks and lunches we had together.

I am grateful to Dr. Anastasia Poupkou from the Aristotle University of Thessaloniki, for the help with the biogenic Volatile Organic Compounds (VOC) data, and the good modelling advices. To Kostas Markakis for his help

with the temporal emissions' profiles for Luxembourg, to Eleni Katragkou and Zoi Hristodoulou for having welcomed me and taken care of me in Thessaloniki, to Spiros Dimopoulos and Theodoros Giannaros my nice officemates and to all the people at the laboratory of Atmospheric Physics of the Aristotle University of Thessalonik I express my honest "ευχαριστώ πολύ".

I wish to thank professor Sergio Corrêa from the University of the State of Rio de Janeiro, for his help with OZIPR model. I acknowledge the help of Dr. Renske Timmermans for providing the LOTOS-EUROS data results, and for the constructive comments and suggestions on chapter 7 and Dr. Kumar Kannan for the help with OpenFOAM.

Obviously, friends could not be forgotten. I thank all my friends in Portugal, who always send nice e-mails from time to time asking "Have you finished yet?", and always had a little time for me whenever I was back in town. To all the nice people I have met in Luxembourg, who have made my days brighter and my weekends funnier, I dedicate a huge "villmols merci" to you all.

Finally, I express my profound gratitude, admiration and affection to my extraordinary family. To my mother Maria Teresa and my brother André Silva Reis a big thank you for your never-ending patience, support and for always finding the best words to comfort me. To my grandmother Natalia who I am sure has always sent me positive thoughts, I express my "muito obrigada". To my father, António Heitor Reis who is my idol and my hero, for all the help, patience, support and for his hints and suggestions, I express my sincere gratitude.

Contents

List of Figures

List of Tables

Chapter 1

Introduction

Contents

1.1 Motivation and Objectives

Air pollution is known to harm the environment, the materials and human health, reducing life expectancy (Almeida et al., 2011; EEA, 2010a). A significant part of Europe's population is exposed to high levels of air pollution, including the most problematic air pollutants, ozone and particulate matter (EEA, 2010a). The European Union (EU) has enforced legislation, to limit pollutants emissions and to impose thresholds on air quality ambient levels. However, European countries still show difficulties in complying with the legislative limits, specially concerning ozone, nitrogen oxides and particulate matter (EEA, 2012b).

The emission of primary air pollutants is directly linked with human activities and the use of energy devices operating with fossil fuel resources (Cohan et al., 2010). Some primary pollutants, such as nitrogen oxides (NO_x) and Volatile Organic Compounds (VOC), react in the troposphere to generate secondary pollutants, such as ozone, (Borrego et al., 2010; Kumar et al., 2008). The ambient levels of secondary pollutants are, generally, more complex to reduce, since they have to be controlled through their precursors, in the case of ozone: NO_x and VOC (Cohan et al., 2010). Therefore, the definition of mid-long term pollutant reduction strategies envisaging structural energy plans has become essential at the international, regional, national, and urban levels (EEA, 2012b).

Nevertheless, the EU adverts that air quality policies should aim at minimizing the costs to society (EEA, 2011). Accordingly, the optimization of the pollutants' emissions should include both the economic and the air quality fields of research. Integrated assessment models for air pollution are tools which combine these two areas to provide technical support to the decision makers in order to orient them towards cost-effectiveness structured policies

(Drouet, 2006). These integrated assessment models couple techno-economic models or a module which calculates emissions, and air quality models.

The LEAQ integrated assessment model aims at supplying policy makers in the Grand-Duchy of Luxembourg with technical support for the implementation of the least cost measures which respect a given air quality limit. It is composed of a techno-economic model, ETEM Luxembourg, an air quality model, AUSTAL2000-AYLTP, an emission allocator module, and an optimization engine called OBOE, which connects all the parts of the LEAQ model (Aleluia Reis et al., 2011a).

ETEM Luxembourg has been developed at CRP Henri Tudor on the context of the LEAQ project. ETEM contains the description of the energy system, and it calculates the energy supply shares such that the cost of the energy system is minimum. It includes five economic sectors, such as industry, transport, residential, commercial and agriculture. The model is evaluated for mid-long term, e.g. 20–30 years, and it is sub-divided into decision periods, e.g. 1–5 years, where the policy actions take place (Drouet and Thénié, 2008). Additionally, it considers the annual emissions of NO_x and VOC associated with the energy supply. The annual emissions, calculated by ETEM, are the link variable between the two models, ETEM Luxembourg and AUSTAL2000-AYLTP.

However, the annual emission must be "translated" to the air quality model, in the form of a time series, e.g. subsequent hourly, of spatially distributed emissions. This task is undertaken by the emission allocator module which has been developed in this thesis work. The module disaggregates the emissions spatially, by economic sector, and temporally e.g. monthly, daily and hourly.

The emissions' time series are the input of the air quality model. Additionally, the air quality model takes as input a digital elevation model, and meteorological data. In the context of the LEAQ model, the air quality model is run for a worst case pollution scenario. Since the emissions refer to the economic decision periods, thus far in the future, the use of this scenario encompasses some of the uncertainties associated with predicting for such long time horizon. The model calculates the ambient levels of ozone, which are aggregated in an ozone air quality indicator (Aleluia Reis et al., 2012).

The ozone air quality indicator is then evaluated by OBOE against a fixed limit, which is defined by the user and it might be a legislated limit, or the use of long term objectives. OBOE checks if the fixed limit is breached. When the air quality indicator is above the limit, OBOE proposes another value for the emissions of the ozone precursors in ETEM Luxembourg and the cycle is repeated. The cycle stops when the air quality indicator respects the fixed limit and the cost of the energy is minimized (Zachary et al., 2011). This approach implies that both the models must be run several times and thus the Central Processing Unit (CPU) time of each model becomes important to

achieve results in a feasible time frame. The ETEM model requires a large database, although the simulation time is very low. On the other hand, the air quality models are often CPU intensive and require great efforts in terms of data input preparation and collection (Aleluia Reis et al., 2009, 2012).

The application of air quality models which run in optimization approaches, becomes more complex for secondary pollutants, as ozone. The reason for this is that the relation between ozone precursors, NO_x and VOC, emissions and ozone concentrations is not linear. Accordingly, a reduction in NO_x emissions might not lead to a reduction of ozone, depending on the VOC/NO_x ratio (Carnevale et al., 2008). This is one of the reasons why the first prototype of the LEAQ air quality model, TAPOM-Lite was a simple model, it did not include terrain, and was based on ozone isopleths (Zachary et al., 2003).

The main goal of this work is to develop and to apply an air quality model, with the focus on the pollutant ozone, for an optimization integrated assessment model. The development of the air quality model includes the development of an emission allocation module, which disaggregates annual emissions spatially and temporally. The application aims at assessing the optimized air quality policies for the Grand-Duchy of Luxembourg.

Moussiopoulos et al. (1996) states that the coupling of air quality models with other models may require the application of reduction techniques. These are necessary due to feasibility issues which arise when coupling several models with different characteristics, such as differences in temporal and spatial scales, types of inputs, and computational resources. Often, integrated assessment models for air quality policy, especially those which work in optimization mode, require modelling reduction or emulation techniques.

Currently, optimization integrated assessment models for air quality policy use model reduction techniques, such as simplification of chemical schemes, linearisation, and emulation techniques, such as source-receptor matrices. Carnevale et al. (2008) defends the development of new approaches to better model the connections between ozone and its precursors emissions.

This work consists in building a photochemical air quality model, which is fast enough so that it can be included in the LEAQ framework. Nevertheless, the model calculates the spatially distributed ozone concentrations, accounting for the main factors that influence air pollution, including topography and meteorology (Aleluia Reis et al., 2009).

The air quality model is based on an existing transport calculator, the AUSTAL2000 model. A fast photochemical module, AYLTP, has been developed and implemented in the transport calculator.

AUSTAL2000 is a Lagrangian particle model and the official reference model of the German Regulation on Air Quality Control (TA Luft). Gen-

erally, Lagrangian models are known to be faster transport calculators than Eulerian models, however the implementation of chemical reactions is more complex (Janicke, 2000; VDI, 2000). In order to overcome this drawback, the photochemical module, AYLTP, is based on quasi-linear rates which are stored in a LUT. The LEAQ air quality model has been given the name of AUSTAL2000-AYLTP. It is assumed that under fixed given conditions, defined by temperature, relative humidity, zenith angle and the ozone precursors concentration, a linear reaction rate holds. A significant set of conditions are simulated using an existing box model, OZIPR, and the reactions rates are pre-tabulated in the LUT. AUSTAL2000-AYLTP then, at each time step and each cell of the domain, "asks" for the reaction rate which corresponds to the meteorological and precursor's concentration condition at the given cell. The rate is then applied and the Lagrangian particle's mass is upgraded with the photochemically transformed mass.

This approach represents an attempt to include a photochemical air quality model which operates in full mode in an optimization approach. Despite the fact that the approach uses a simplified method for the calculation of ozone levels, it is one of the first approaches where a full grid model is used in an optimization framework.

The outcomes of the thesis are the publication and submission of 3 journal papers, 2 peer reviewed conference papers and 3 conference papers. Namely:

Peer-Reviewed articles:

- L. Aleluia Reis, D. Melas, B. Peters, and D. S. Zachary. Developing a fast photochemical calculator for an integrated assessment model. *International Journal of Environment and Pollution*, 2012. Accepted (Follow-up of the paper presented in the HARMO14 conference).

- L. Aleluia Reis, L. Drouet, D. S. Zachary, B. Peters, and D. Melas. Implementation of a full air quality model in an integrated assessment framework – the Luxembourg energy air quality model. *Environmental Modelling & Software*, 2012. Submitted.

- D. S. Zachary, L. Drouet, U. Leopold, and L. Aleluia Reis. Trade-offs between energy cost and health impact in a regional coupled energy-air quality model: the LEAQ model. *Environ. Res. Lett.*, 6:9pp, 2011.

Conference papers:

- L. Aleluia Reis, D. S. Zachary, B. Peters, and L. Drouet. A fast air quality model using look-up tables to address integrated environmental assessment model requirements. In R. Seppelt, A.A. Voinov, S. Lange, and D. Bankamp, editors, *International Environmental Modelling and*

Software Society (iEMSs) 2012 International Congress on Environmental Modelling and Software Managing Resources of a Limited Planet, Sixth Biennial Meeting, Leipzig, Germany, 2012.(peer-reviewed)

- L. Drouet, L. Aleluia Reis, U. Leopold, and D. Zachary. Implementing the oracle-based optimisation for an integrated assessment model for air pollution: the Luxembourg energy air quality model. In R. Seppelt, A.A. Voinov, S. Lange, and D. Bankamp, editors, *International Environmental Modelling and Software Society (iEMSs) 2012 International Congress on Environmental Modelling and Software Managing Resources of a Limited Planet, Sixth Biennial Meeting*, Leipzig, Germany, 2012.(peer-reviewed)

- L. Aleluia Reis, D. Melas, B. Peters, and D. S. Zachary. Developing a fast photochemical calculator for an integrated assessment model. In J.B. Bartzis, A. Syrakos, and S. Andronopoulos, editors, *HARMO14, proceedings of the 14th international conference on harmonisation within atmospheric dispersion modelling for regulatory purposes*, pages 225—229. Environmental Technology Laboratory, Department of Mechanical Engineering, University of west Macedonia, Greece, 2011.

- L. Aleluia Reis, D. Zachary, U. Leopold, and Peters. B. Selecting a fast air quality calculator for an optimization meta-model. In C.A. Brebbia and Popov V., editors, *Air Pollution XVII*, pages 39—49. WITpress, 2009.

- D. Zachary, U. Leopold, L. Aleluia Reis, G. C., B.; Kneip, and O. O'Nagy. An energy and environmental meta-model for strategic sustainable planning. In A. Mammoli and Brebbia C.A., editors, ENERGY and Sustainability II, pages 247—255. WITpress, 2009.

1.2 Thesis Outline

The thesis is divided into 8 Chapters, including this one, the introduction, as the first chapter. In Chapter 2, the thesis background is presented giving an introduction of the concepts that will be used throughout the thesis and presenting the problematic of air quality. Additionally, a review of the existing integrated assessment models for air quality policy is carried on. Chapter 2 finishes presenting the different types of air quality models and emission reduction instruments.

The concept and structure of the LEAQ model is described in Chapter 3. Moreover a more detailed explanation about the components of the LEAQ is presented, with the focus on the ETEM Luxembourg and the emission

allocator module. Finally, the selection of the transport calculator is discussed. The details of the air quality model AUSTAL2000, which has been used as the transport calculator, are presented in Chapter 4.

The development of photochemical module, AYLTP, and the quasi-linear rates methodology is discussed in Chapter 5. Moreover an analysis of the LUT and its connections with the meteorological and precursors' concentration variables is undertaken.

The application of AUSTAL2000-AYLTP to the region of Luxembourg has been included in Chapter 6. The results of the model application are compared against air quality monitoring data and against the results of an European regional model LOTOS-EUROS.

Finally, the air quality model is integrated into the LEAQ integrated assessment model, and two study cases are analysed. The first where only national emissions are considered and a second one where transboundary emissions are taken into account, the Luxembourg region case.

The conclusion and future work have been included in Chapter 8. In this work the symbols are given by chapter for ease of notation and they are presented in the chapter List of Symbols at the end of the document.

Chapter 2

Background

Contents

2.1 Air Quality — A Major Concern

Air quality is, nowadays, a subject of major concern. The designation "air quality" refers to state of the air, likewise good air quality relates to unpolluted air. In this sense, air pollution refers to the presence of harmful substances in the atmosphere. The World Health Organisation (WHO) considers "clean air" as a requirement for human health. Moreover the European Environmental Agency (EEA) alerts for important damages on human health, climate and ecosystems due to air pollution, e.g. eutrophication, acidification, vegetation degradation and increase of human morbidity.

In Europe, legislation on air quality through emission management of damaging substances has been developed since the 70's. Consequently emissions of some pollutants, sulphur dioxide (SO_2) and lead (Pb) for instances, have been significantly reduced in the last decades. However some emission control policies have not been completely successful in the abatement of ambient levels. This happens because the relation between emissions and air quality is not linear, due to the effects of chemistry and meteorology, especially for the pollutants which are chemically very active.

Air pollution was once considered just a local problem, where high concentrations were observed near the sources. But as human industrial activities grew so did the impacts. Pollution transport in regional and intercontinental scales became significantly important. Air pollution was no longer just an urban problem but a regional and global issue.

Poor air quality has negative impacts on human well-being, ecosystems, climate change and materials. The negative relation of air pollution with human health, resulting in an increase of morbidity and mortality, is well documented and studied, (Laaidi et al., 2011; Rückerl et al., 2011; Solé et al., 2007; Ström et al., 1994; Tzivian, 2011; West et al., 2007). Known effects are: aggravation of respiratory diseases, reduction of lung function, coughing, breathing difficulties, susceptibility to respiratory infections, damage of the cardiovascular, reproductive and nervous system and cancer.

The EEA reports on five million years of lost life due to exposure to $PM_{2.5}$ in Europe (EEA, 2010a), in 2005. The ecosystems, on the other hand, are more susceptible to ozone (O_3), sulphur and nitrogen compounds. Nitrogen and sulphur are responsible for the acidification of soils and water, through deposition. Thus affecting the ecosystems and biodiversity, specially nitrogen since it is responsible for eutrophication of aquatic systems. Ozone affects crops and vegetation, high monetary damages have been reported due to high concentrations of ozone (Kuik et al., 2000; Murphy et al., 1999; Segerson, 87). As it affects the ability of plants to absorb carbon dioxide (CO_2), it indirectly affects climate. O_3 and Particulate Matter (PM) affect the earth radiative forcing hence contributing to climate change. Some pollutants are known to accelerate the degradation of buildings, mainly due to soiling of particles, acidification and oxidation.

Presently, the pollutants of major concern are SO_2, carbon monoxide (CO), VOC, NO_x, particulate matter (PM_{10} and $PM_{2.5}$) and O_3.

Sulphur dioxide SO_2 is mainly emitted from coal and oil power plants. A recent work by Peters and Smuła-Ostaszewska (2012) evaluates contribution of SO_2 by the combustion of biomass. Likewise Knudsen et al. (2004) found that 30 to 55% of the sulphur's biomass can be transformed into SO_2. This percentage varies with the temperature of the biomass combustion and on the composition of the biomass. Additionally, volcanic activity contributes as a natural source. Humans subject to high concentrations of SO_2 may feel eye, nose and throat irritation, intensification of asthma and even bronchitis. People who suffer from respiratory problems may experience an intensification of breathing difficulties.

The combination of SO_2 with rain is at the origin of acid rain, which damages vegetation, buildings, promotes soil degradation and pollutes rivers and water reservoirs.

Over the past decades, SO_2 has been substantially reduced with the reduction of domestic coal-fired heating, and the reductions of high-sulphur fuel in energy production and industry. Ambient SO_2 levels have been reduced by more than 50% in the last two decades, leading to a reduction of acid deposi-

tion. The percentage of population exposed to SO_2 levels above the EU limits is 0.1%, on the other hand 68–85% of the urban population is exposed to SO_2 levels above the WHO air quality guidelines.

Carbon monoxide CO is the result of gasoline vehicles exhaust, forest fires and waste treatment. It reduces the capacity of the blood to carry oxygen. People inhaling this pollutant exhibit headaches, fatigue, dizziness, respiratory problems, and in extremely high concentrations, in closed environments, even death.

However the legislation limits to these pollutant is rarely exceeded in Europe. Mainly because the implementation of catalytic converters in gasoline cars, which can reduce more than 95% of the CO emissions. Therefore, CO is becoming less and less a problematic pollutant (EEA, 2011; MECA, 2009; Pearson, 2001).

CO contributes to the formation of CO_2, contributing to climate change. Furthermore it is also a precursors of ozone.

Nitrogen oxides The term NO_x encompasses nitric oxide (NO) and nitrogen dioxide (NO_2). NO_x is mainly emitted by traffic, industrial possesses and power plants or any processes involving fuel burning. It can also have natural origins, such as storms, forest fires and agriculture. NO is emitted in greater quantities than NO_2, although in the atmosphere NO can oxidise to form NO_2.

Approximately 50% of the NO_x in Europe are related to road transport (Pearson, 2001). Consequently NO_x becomes more problematic in urban areas, where road traffic is intense. In the last two decades the emission reduction efforts led to a 28% decrease in NO_x emissions although NO_2 concentrations have gone down only 15%. The highest values of NO_2 are found in the cities, near the roads. The exhaust after-treatment systems that have been implemented in diesel cars may have led to an increase of NO_2 emissions despite having reduced CO, VOC and PM (EEA, 2011). This may have contributed to the increase of NO_2 share on NO_x.

Exceedances are observed all over Europe near the large roadsides. NO is not harmful to human beings however NO_2 can be responsible for inflammation of the respiratory system; asthma; increasing susceptibility to respiratory diseases; affect the liver, spleen and blood. It is the main constituent of the red brownish smog observed in some cities. NO_x is of particular concern due to its role on the production of secondary pollutants, such as ozone and secondary particles.

VOC Volatile organic compounds (VOC) represent a group of compounds that includes: hydrocarbons ,which contain hydrogen and carbon; halocarbons and oxygenates. They are the result of incomplete combustion processes, mainly in gasoline powered-vehicles, and by fuel evaporation. A great part of VOC has biogenic origins, although its share on the total contribution depends on the region. VOC can be highly toxic and carcinogenic, specially benzene and 1,3-butadiene, and they are one of the precursors of ozone.

Particulate matter Particulate matter is highly problematic due to its negative impacts on human health. Mainly, it is emitted by diesel vehicles, coal extraction, dust and spray or is the result of chemical reactions that produce secondary particles. Particles are classified according to their aerodynamic diameter, PM_{10} and $PM_{2.5}$ refers to particles with a diameter inferior to 10 and 2.5 micrometers respectively. Particulate matter is known to travel deep into the lung, causing lung diseases. Moreover the capacity to penetrate deep in the lungs tends to increase with the decreasing size of the diameter. Hence the smaller the diameter is the higher are the potentially negative impacts on health.

Ozone Tropospheric ozone is a strong oxidant, a greenhouse gas and the main constituent of photochemical smog. It is a secondary pollutant, as such it is not emitted directly by any source. Instead it is formed through a chain of complex photochemical reactions (Kumar et al., 2008). Ozone is formed by reacting with NO_x and VOC in the presence of sun light. The mechanisms which lead to the formation of ozone are very complex and high concentrations of this pollutant are generally found far from the sources of its precursors. The relationships between ozone and its precursors is non linear, and a reduction of NO_x may or may not lead to a reduction in ozone, hindering the establishment of reduction policies. According to the EEA, O_3 is one of Europe's most problematic pollutants due to its health effects (EEA, 2011). Moreover this is also the most difficult pollutant to control, and the ozone management efforts that have been undertaken in the last decades are not yet satisfying. Specifically, the reduction observed in ozone's precursors emissions has not reproduced a clear decreasing trend in ozone levels. Therefore, this issue is worthy of great attention, since it represents a great threat to human health and to vegetation. The EEA reports on 13 to 61 % of the EU urban population being exposed to ozone concentrations which exceed the EU target value of human health protection in the period 1997 to 2009 (EEA, 2011).

More effective air quality management strategies need to be implemented. The legal limits should be achieved through emission control policies. Moreover emission control must be seen as part of structural plans for cities and countries and not as episodic measures. Modelling tools, both economic and

environmental, can be used in an integrated way to help decision makers in order to achieve effective reductions.

The London smog disaster 1952, illustrated in Fig. 2.1, brought attention to the damaging effects of air pollution (Bell and Davis, 2001). Air pollution control strategies, first in individual countries and then on the international scene, started to appear.

Figure 2.1: Picture of the London great smog in December of 1952.

European legislation has been developing and becoming more strict, hence it has become more difficult for the member states to comply with EU standards. In Europe, the existent legislation on air pollution is the following:

- the Directive 2010/75/EC on sectoral emissions of industry, agriculture and waste treatment plants (EU, 2010a);
- the 2009/126/EC Directive on petrol vapour (EU, 2009b);
- the Directive 2008/50/EC on ambient air quality and cleaner air for Europe. Which sets limits on SO_2, NO_2, NO_x, PM, lead, benzene, CO, O_3 ambient levels (EU, 2008b);
- the 04/107/EC on arsenic, cadmium, mercury, nickel and polycyclic aromatic hydrocarbons (EU, 2004);
- the 2003/17/EC directive on quality of petrol and diesel fuels (EU, 2003);
- the 2001 National Emission Ceilings Directive (EU, 2001), relative to the national emission limits;

- the 1999 Gothenburg Protocol on acidification, eutrophication and ground-level ozone (UNECE, 1999);
- the 1999/32/EC directive on reduction of sulphur of certain liquid fuels (EU, 1999a);
- the Directive 1999/13/EC on emissions of VOC due to the use of organic solvents (EU, 1999b);
- the 1999/32/EC directive on reduction of sulphur of certain liquid fuels (EU, 1999a);
- the Euro 4, 5 and 6 standards for vehicles, 98/70/EC (EU, 1998), 2005/55/EC (EU, 2005), Regulation (EC) No 692/2008 (EU, 2008a), Regulation (EC) No 595/2009 (EU, 2009a);
- the 94/63/EC on the control of VOC (EU, 1994);
- the 91/676/EEC directive on nitrates from agricultural sources (EU, 1991);
- the 1979 UN LRTAP, delivering protocols on emissions limits of SO_2, NO_2, VOC and ammonia (UNECE, 1979);
- the Marine Pollution Convention, MARPOL 73/78 on air pollution from ships (IMO, 1973).

The more rigid air quality standards and regulations require structured answers from the policy makers. The compliance with current legislation in force in Europe still poses a problem for the members states, which still report every year a large number of exceedances.

In the past years, the links between air pollution and energy production and use have been the subject of interest, as decision-makers required coherent and integrated solutions. The EU states in the air quality report of 2011 (EEA, 2011) that:

> "European policies and measures increasingly seek to maximise co-benefits, managing air pollutant and greenhouse gas emissions at the least cost to society."

Achieving efficient air quality management can be done through the reduction of emissions at the source, structural planning, and behavioural changes.

Integrated assessment models have been developed to answer these needs, connecting economy with different fields of environment, to study the efficiency of environmental policies. Decision makers have become more exigent

in demanding more integrated technical support, and air pollution is pointed as one of the environmental factors to be accounted in urban planning. Consequentially, integrated assessment models that use air quality models, have emerged and became more common.

2.2 Air Quality Integrated Assessment Models

Nature is the most complex example of an integrated system. In practice much simplification is needed to model such systems. As it is impossible to model the whole environment in detail, thus the sub-systems of a bigger system are isolated. Integrated assessment models isolate the most important sub-systems in order to find integrated solutions towards a given problem, in a world with increasing complexity of questions.

An integrated assessment model combines the knowledge coming from different scientific fields to bring a better understanding of a problem which cannot be attained with a single disciplinary approach. They have two following necessary characteristics: (i) they should have added value compared to single disciplinary models; and (ii) they should provide useful information for decision makers (Rotmans and Asselt, 1996). In the case of integrated assessment models using air quality models, they combine human and natural aspects related to air pollution: pollutant emissions, either energy-related/anthropogenic or biogenic; atmospheric dispersion, chemistry, impacts on health or on the natural environment.

Historically, the first integrated assessment model has appeared in the middle of the 80's. In particular, the Regional Air Pollution INformation and Simulation (RAINS) model, developed and built in the framework of the international negotiations on acid rains (Alcamo and Hordijk, 1990). Integrated assessment models became, since then, important tools to support the policy decision in response to complex issues involving a large diversity of actors and phenomena.

They are used to explore the possible states of the human and natural systems in order to analyse the key questions related to the formulation of policies but also to address the environmental issues (IPCC, 2007). The main objective of an integrated model is to supply a consistent framework to organise the knowledge and inform the decision makers on the different possible options (Risbey et al., 1996). As a result of the needs in an interdisciplinary exercise, the integrated assessment model consists of interconnected models of different programming environments, different scales, different resolutions or even different paradigms.

The air quality integrated assessment models form a class of integrated assessment models which aims at addressing issues related to atmospheric

pollution. They relate two main different realms, emitting entities, e.g. emissions from energy production and consumption, and air pollution which are linked by a common component: emissions.

The main reasons for the focus in integrated assessment modelling is that climate change became a major concern, and that global economy models can be easily coupled with simplified carbon cycle-climate models because they share the same characteristics of size, complexity and time-horizon range. Good examples of these compact integrated assessment for climate change are DICE (Nordhaus and Boyer, 2000) and MERGE (Manne, 1995). The existing knowledge in integrated assessment for climate change, can easily be generalised and extended to integrated assessment for air pollution (Parson, 1995; Schneider, 1997; Toth and Hizsnyik, 1998).

Air pollution is highly dependent on emissions, which mainly result from processes that depend on the implementation of technologies over years such as power plants, industry facilities and cars. Therefore the implementation of air quality policies must be designed for long time-horizons.

Like all models, the integrated assessment models have intrinsic uncertainties, including uncertainty in future emissions, meteorological conditions or background emissions, as well as the uncertainties in intrinsic parameters. Integrated assessment models have natural limitations. Generally, they use simplified sub-models, and they analyse very large and complex systems. This modelling approach underlies many assumptions about the physical, chemical, demographical and social environments. Moreover assuming hypothesis about the future evolution of these disciplines is a very difficult task. Assumptions about the natural environments are based on past trends such as statistics or projections, and events like energetic, economical or social crisis and, for instance technological developments, are very difficult to predict as they evolve independently of the natural environment. Furthermore, not all the impacts of the policy measures are measurable. Different integrated assessment models make different assumptions, therefore the development of a large variety of integrated assessment models is advantageous.

Integrated assessment models aim to give technical support to the debates on the precautionary actions against the risk of air quality degradation. Also, they aim to allocate efficiently the efforts of reduction of pollutant emissions. The integrated assessment models can then describe the temporal and spatial aspects, the options of abatement or adaptation, the future technology changes, the long-term efficiency and the underlying uncertainties in order to establish the best decision, or the best sequence of decisions. The information and the models to integrate come from various disciplines such as chemistry, physics, environmental science, economy, risk analysis, amongst others.

From a general overview, the integrated assessment models for air pollution represent the fundamental interactions of the “emission management”

by the society and the physical phenomena related to air quality. Figure 2.2 shows the generic structure of such a model. It is composed of modules, e.g. M1 to M5, describing the involved processes, each module is connected to one or more modules. The system itself is split into two main components: *Society* and *Air*. The *Society* component determines the processes which emits pollution, calculates the potential abatement strategy to meet environmental targets. Additionally, it might include other modules such as land-use management. On the other side, the *Air* component of Fig. 2.2 main modules are the pollutant dispersion and atmospheric chemistry. The major interconnection are the emissions which go into the ambient air and, in the case of optimization mode, an air quality indicator, such as Accumulated Ozone Exposure (AOT) or health impact indicators.

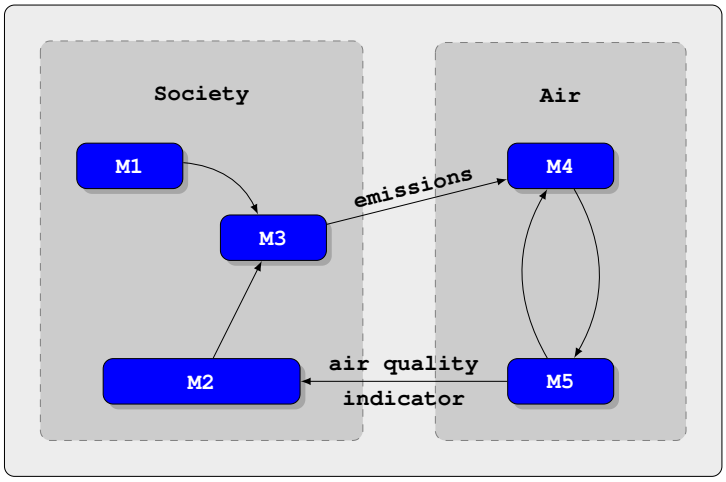

Figure 2.2: Generic structure of integrated assessment models for air pollution, composed of two systems *Society* and *Air*, composed of sub-modules M1,...,M5 which describe different phenomena including energy-related emissions or pollutant dispersion.

Two main approaches for integrated assessment models can be distinguished to analyse air quality policy: the evaluation of scenarios — *simulation* mode, or the optimisation of policies — *optimisation* mode.

In *simulation* mode, also called *cascading* mode, the model runs in series its sub-models: From a scenario defined by a socio-economic development, a land-use change or a technical progress, a module computes the pollutant emissions in time and space. Then, the air quality model calculates the dispersion and the chemistry in the atmosphere. As a result, an air quality indicator can be used to determine the impacts on the society. The analysis evaluates the outcomes of the models as a possible future of the defined policy. The simulation mode allows the use of complex high resolution models yielding a more detailed view of the future. This approach is the most used and also the easiest to implement and understand.

The *optimisation* mode determines the best policy, generally defined as an economic criterion among a set of possible policies delineated by predefined assumptions. The economic criteria can be for instance utility value or total cost. The best policy is called the "optimal" policy and the assumptions are set up as constraints in an optimisation mathematical problem. Two approaches can be distinguished. The cost-benefit approach which is based on the total cost and the cost-effectiveness one which imposes an environmental constraint. The cost-benefit approach balances the economy costs with the impact costs accounting for the adaptation costs and the indirect costs. The economic quantification of these impacts in monetary value is a difficult task, because all the cost and benefits are expressed in monetary value. This might rise controversy, specially when attributing economic values to human life and ecosystems. For these reasons, the cost-effectiveness approach is normally preferred over cost-benefit.

Figure 2.3 highlights the differences of analysis between the air quality policy and its impact on environment or health. The *simulation* mode, starting from predefined scenarios, observes the resulting impacts. On the contrary, the *optimisation* mode determines the optimal air quality policy to reach a predefined target.

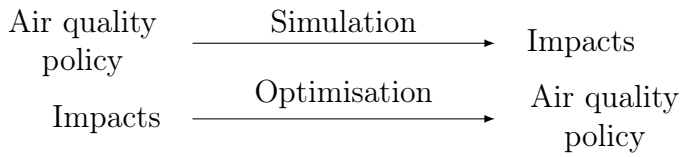

Figure 2.3: Comparison of simulation and optimisation approaches in air quality policy assessment.

The large definition of the integrated assessment models allows to have diverse levels of complexity and there is no unique framework to build them. Table 2.1 lists the characteristics of existing integrated assessment models which use air quality models. They are classified by the type of mode they are mostly used.

The MERG model (James et al., 1985) is one of the first experimentation of such an integrated approach. It uses an energy model MARKAL (Abilock et al., 1980) to produce SO_x emissions scenarios along with a compact air quality model.

RAINS model (Alcamo and Hordijk, 1990) is a major integrated assessment model, developed initially to study acid rains. The following versions, Greenhouse Gas and Air Pollution Interactions and Synergies (GAINS) extend its capacity to handle other air pollutants as defined by the Convention on LRTAP (Schoepp et al., 1998) and greenhouse gases (Klaassen et al., 2004,

Name	Emission model	Air quality model	Scale	Reference
Simulation mode				
MERG	MARKAL	SCA	regional	James et al. (1985)
RAINS	PRIMES	EMEP	regional	Alcamo and Hordijk (1990)
ASAM	EMEP/CASM	RAINS	regional	ApSimon et al. (1994)
SAMI	EMS-95/Mobile5b	URM-1ATM,...	regional	Odman et al. (2002)
USIAM	Inventory	ADMS-Urban	urban	Mediavilla and ApSimon (2003)
IMPAQT	ADMS inventory	ADMS-Urban	urban	Lim et al. (2005)
EC4MACS	GAINS	TM5,EMEP,...	regional	EC4MACS (2007)
SIMCA	CEP/SMOKE	CMAQ	regional	Borge et al. (2008)
BRUTAL	iMOVE	ADMS-Urban,...	urban	Oxley et al. (2009)
MINNI	RAINS-Italy	FARM	regional	D'Elia et al. (2009)
Mexico2050	E3MG	p-TOMCAT	regional	Barker et al. (2010)
SEA	Projection	MUAIR	urban	Nguyen and Coowanitwong (2010)
Finish IAM for PM	FRES,EMEP	SILAM	regional	Tainio et al. (2010)
Global Health Impacts	MESSAGE	TM5	global	Rao et al. (2012)
Optimisation mode				
Shih	Projections	Isopleths	urban	Shih et al. (1998)
RAINS	PRIMES	EMEP	regional	Amann et al. (2001)
UKIAM	NAEI	FRAME,PPM	regional	Oxley et al. (2003)
GENEVA	MARKAL-lite	TAPOM-lite	urban	Carlson et al. (2004)
OMEGA	EMEP	EMEP	regional	Reis et al. (2005)
MERLIN	EMEP	OFIS	regional	Reis et al. (2005)
GAMES	EMEP	TCAM	regional	Carnevale et al. (2008)
GAINS	GAINS	EMEP	regional	Amann et al. (2011)
LEAQ	ETEM	TAPOM-lite	urban	Zachary et al. (2011)

Table 2.1: Survey of integrated assessment models for air pollution

GAINS). Additionally GAINS includes an optimization approach which goes beyond a single pollutant cost curve but based on specific measures. These integrated assessment models are based on the Eulerian dispersion model EMEP (CIA, 2012) at regional level. Amann et al. (2001) presents a first attempt of using the RAINS model in optimisation mode. Later, the MERLIN model used an optimisation framework based on genetic algorithms (Reis et al., 2005).

The EC4MACS is not a model of its own but a model framework, which includes the RAINS model along with a set of multi-disciplinary models (EC4MACS, 2007). It is the integrated assessment model in simulation mode which encompasses the largest number of models. Thus describes a large spectrum of socio-economical and environmental aspects. The GAINS model, the successor of RAINS, originally dedicated to greenhouse gases, has been extended to air quality. It has been used in optimization mode, minimizing the cost of emission abatement measures and balancing it amongst countries (Amann et al., 2011). Nemet et al. (2010) presents the interest of dealing with the two issues of climate change and airquality to assess the potential of co-benefits even if it can end in a complex implementation of the policy.

Focusing on the United Kingdom, the ASAM, UKIAM and BRUTAL models have been used in a nested framework to analyse the policies at different scales (Oxley and ApSimon, 2007). Accordingly, the UKIAM model optimizes abatement strategies for human exposure to particulate PM_{10} (Oxley et al., 2003). The IMPAQT software aims at supporting transportation planning creating a more efficient air quality assessment tool for NO_2 and PM_{10} (Lim et al., 2005).

Barker et al. (2010) put forward an integrated assessment model for both climate change mitigation and air quality. The SAMI model (Odman et al., 2002) is the result of an North-America initiative. The SIMCA model (Borge et al., 2008) implements the Community Air Quality Model CMAQ based on an open-source platform. The USIAM model, based on ASAM, investigates possible strategies for reduction of PM_{10} (Mediavilla and ApSimon, 2003). The strategic environmental assessment (SEA) assesses the impact of air quality measures applied to the transport sector to reduce CO. Tainio et al. (2010) investigates the health effects of $PM_{2.5}$ emissions. MINNI (D'Elia et al., 2009) is the integrated modelling system for Italian policy support and for international negotiation on atmospheric pollution, with focus on SO_2, NO_x, PM_{10} and $PM_{2.5}$.

Shih et al. (1998) developed an optimisation model for the reduction of ozone through its precursors using linearisation techniques. OMEGA model used genetic algorithms to determinate cost-effective solutions for multi-pollutant and multi-effect problems. In the same way, GAMES has been

applied to the northern Italian region, to solve a two-objective problem, reduction of emission policy costs and air pollution.

The Geneva model (Carlson et al., 2004) is the coupling of MARKAL-lite with the reduced version of TAPOM, TAPOM-lite. The framework follows a meta-modelling approach: an interior point algorithm solves a decomposition problem, calling either the energy model or the air quality in a cost-effectiveness analysis.

The LEAQ model (Aleluia Reis et al., 2011b) is an extension of this approach for the Grand-Duchy of Luxembourg. It proposes a new approach of air pollution integrated assessment models, using a dedicated air quality model, discussed in more detail in Chapter 4.

Generally, air quality integrated assessment models which run in optimization mode, use model reduction techniques such as emulation, receptor-source matrix.

For instances Amann et al. (2011) applies source-receptor matrices to describe the response of the air quality indicators to the precursor changes. Shih et al. (1998) used a locally linear approximation to the non-linear relationship between photochemical pollutants and their precursors, although this approach is not spatially heterogeneous. So far air quality integrated assessment model have not yet used the full capacities of the photochemical models when the integrated assessment model is run in optimisation mode. New and more complete reduction techniques, as well as faster photochemical air quality models need to be developed.

2.3 Energy-Economic Models

In Fig. 2.2, *Society* is the component that describes the human activity, which is later linked via "emissions" to the environmental factor *Air*. Society is modelled analysing the activity of energy-economic systems. Energy models rely on energy demand and supply, and both are characterised in terms of energy quantity and energy price. According to Connolly et al. (2010), they can be classified as:

- Simulation models: operate in small time-periods (e.g. year) to simulate the hourly operations of an energy-system in order to supply the energy demands.
- Scenario models: are long term models that resolve in a yearly time step.
- Equilibrium models: assess the behaviour of supply, demand and prices of one or several markets in equilibrium.

- Operation optimisation models: optimise the operation of the energy-system.
- Investment optimisation: optimise investments in new or available energy solution and technologies.
- Top-down models, also called aggregated models, are based on an economic approach. They use aggregated variables on consumption, prices and factor costs to calculate the demand of goods and services and the supply from the different sectors. The demand is set endogenously and is driven by macroeconomic market behaviour. Technology is represented by shares of the inputs of purchase and the technologies are not represented explicitly. Aggregated variables are in general more reliable and thus the models are more stable when extrapolations over longs periods of simulation are carried out (Nakata, 2004).
- On the contrary, bottom-up models adopt an engineering approach that reproduces technological potentials. They are based on detailed information about energy technologies and run independently from the market behaviour. The energy system is represented in a disaggregated manner between the processes, the energy carriers and the emissions, and considers the interconnections between them. They are used to assist technological choices studies, based on sectoral analysis. This approach neglects the relationships between energy related sectors and other non-energy related sectors. In this case the technologies are related to its energy consumption/production, its efficiency and cost (Nakata, 2004).

One can also distinguish between general equilibrium models and partial equilibrium models. The former simulate the factors of production, products and foreign exchanges. Partial equilibrium models, also named dynamic energy optimisation models, minimise the total cost of the energy system (Nakata, 2004).

Energy-economic models have been used since the 70's. Amongst the most used models, it is mentioned MARKet ALlocation (MARKAL) (Fishbone and Abilock, 1981), TIMES (Kanudia et al., 2005), PRIMES (Capros et al., 1999), POLES (Criqui et al., 1999) and GEM-E3 (Capros et al., 1997).

The MARKAL/TIMES family of models belong to the group of Techno-Economic models (TEMs), sometimes refereed to as E^3 since they are used to study the Energy-Economy-Environment interactions. The model belongs to the bottom-up class of models and it was developed at the Energy Technology Systems Analysis Programme (ETSAP) of the International Energy Agency (IEA).

The TIMES model is the most recent version of MARKAL, it expands the range of application of MARKAL and its flexibility. MARKAL/TIMES model

is one of the most applied models and is currently used in approximately 70 countries and by around 250 institutions (Connolly et al., 2010). It has been used in numerous studies and modelling approaches, such as the utilisation of hydrogen or fuel cells, the nuclear power, nuclear fusion, wind power or fuel usages. The EU policies on renewable energies, climate change, energy efficiency, and the "20-20-20" targets use MARKAL/TIMES as a technical support (Cen, 2012).

MARKAL/TIMES finds the "best" Reference Energy-System (RES), by minimising the total discounted cost, or the total discounted surplus over a planning horizon. The discounted cost is the total energy cost but taking into account the investment time preference of the investor. The selected RES is then the least-cost solution. The models are limited by policy and physical constraints. It can be applied at global, regional, national, state level or community scale. The calculations are run for time horizons of 20 to 30 years, periods of 1 to 5 years, which are divided in time slices, e.g. seasonal, weekly and hourly.

Figure 2.4 shows a generalised RES. The energy system flows start with the supply and availability of primary resources, undergo energy processing and conversion to be used by the end-use devices that serve the demand. Energy demand is disaggregated in sectors and in functions, for instance industrial refrigeration. The level of disaggregation depends on the user objectives and the availability of data.

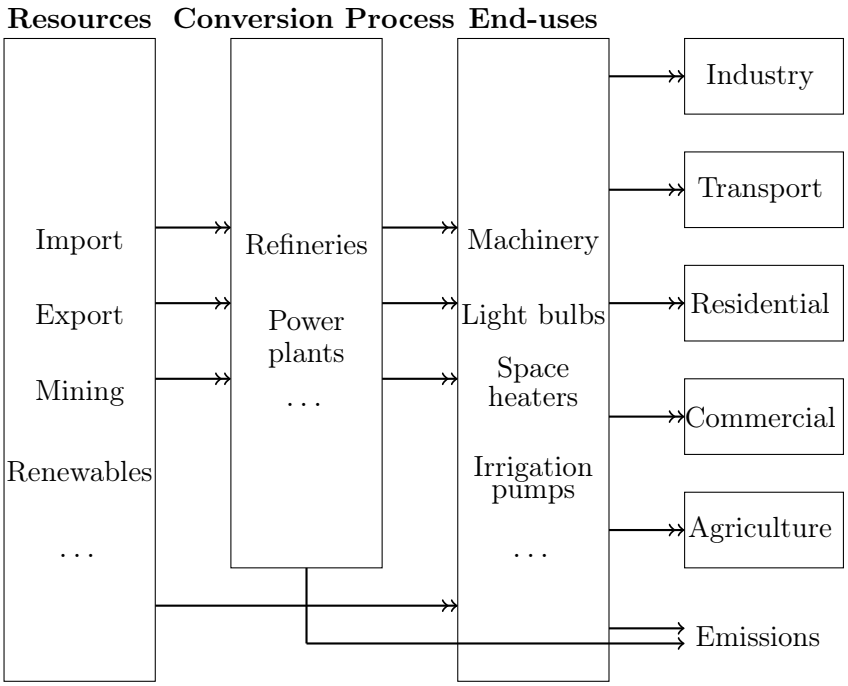

Figure 2.4: Example of a general reference energy system.

The energy-economic models include a catalogue of available technologies, which range from highly polluting intensive technologies to Best Available Technologies (BAT). The natural price relation is that the most polluting technologies are the cheapest and visa-versa. The effects of this price/efficiency relation can be explored using the model. In the same way it allows the assessment of the impacts of pollution mitigation measures. The model behaviour can be controlled introducing constraints as for instances in activity, capacity or rate of penetration of a technology. In this case the least-cost solution is still achieved but only after the constraints are met. The most interesting characteristic energy-economic models for the context of this work is the possibility to introduce constraints on pollutant's emissions forcing the model to choose less polluting technologies to achieve a given emissions level.

2.4 Air Quality Models

Air quality models describe the dynamics of a pollutant based on information about meteorology, topography and emissions. They are nowadays essential in air quality management and in scientific research, as monitoring studies only yield punctual concentrations, and are not sufficient to understand the atmospheric system as a whole. Furthermore it is not possible to evaluate strategies of pollution control based on monitoring data. In a simplified manner, air quality models are meant to relate emissions with ambient concentrations. This relation is driven mainly through emissions, meteorology, topography and chemistry (Russell, 1997).

Figure 2.5 shows the main components of a general air quality model. Emission values can be obtained from national inventories or in some cases they are calculated from aggregated values, which can be disaggregated according to land use or population density. One distinguishes two types of emissions, those coming from human activity called anthropogenic, and those coming from vegetation referred as biogenic. Chemistry modules might include heterogeneous and homogeneous reactions. The latter refers to reaction in which the compounds are all in the same phase, e.g. gaseous, and the former relates to reactants in more than one phase.

The first air quality modelling efforts begun in the 1930's with the Gaussian plume models. Over the past 40 years urban and larger scale air quality models have undergone major advancements, evolving from plume-rise and Gaussian models to Lagrangian and Eulerian grid models. In the 1980's a major step was made with the first developments of 3-D models. These models were multidimensional, and included aqueous phase chemistry representing anywhere from 5 to 100 additional species and 10 to 200 additional reactions (Jacob and Gottlieb, 1989; Pandis and Seinfeld, 1989).

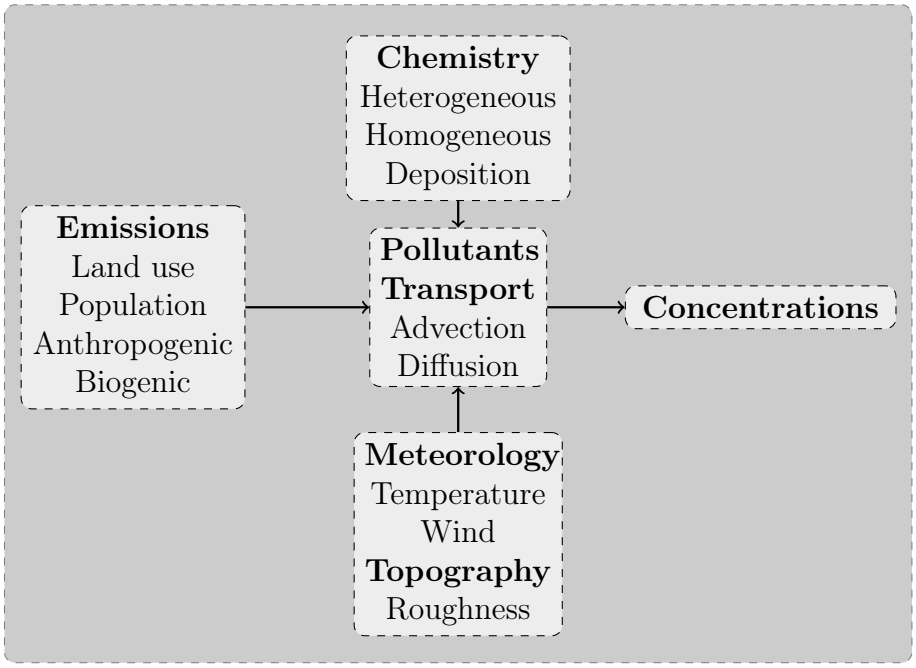

Figure 2.5: Schematic representation of an air quality model.

Currently, there is a large number of air quality models that have been used in various projects, some of them are not published in atmospheric reviews or modelling journals. Models differ in the numerical schemes they use to solve the differential equations and on the way they describe chemistry and physics. They generally focus on one of the phenomena scale they described, and vary in the approximations and parametrisations assumed. Despite the number of existing models many share a common aspect, they solve the transport Eq. (2.1):

$$\frac{\partial c_i}{\partial t} + \nabla \cdot \mathbf{U} c_i = \nabla \cdot D_i \nabla c_i + \mathbf{R_i}(c_1, \cdots c_i, T, t) + S(\mathbf{x}, t), \ \forall i \in \{1, 2, 3 \ldots, n\} . \tag{2.1}$$

In Eq. (2.1) c_i is the concentration average component of the pollutant i, n is the number of pollutants, $\mathbf{U}$ is the wind velocity vector, D_i is the molecular diffusivity of species, $\mathbf{R}$ is the rate of change of the species concentrations due to chemical reactions, which depends on time t, and can also depend on meteorological variables as temperature T, and $S(\mathbf{x}, t)$ is the emission rate at location $\mathbf{x}$.

Equation (2.1) represents the rate of change of concentration of pollutant i, first term, plus the convective transport term correspondent to the concentration that is transported in and out of a given volume of air. This is dependent on the pollutant's diffusion, the chemical production or depletion of the substance and on the pollutant's emissions. The behaviour of a gas in atmosphere is described by Eq. (2.1), however the atmosphere is turbulent,

thus $\mathbf{U}$ includes fluctuations.

Turbulence is generally described with the Reynold's decomposition, where $\mathbf{U}$ is the sum of an averaged $\overline{\mathbf{U}}$ and a fluctuation component, $\mathbf{U}'$.

$$\mathbf{U} = \overline{\mathbf{U}} + \mathbf{U}' \tag{2.2}$$

The random component $\mathbf{U}'$ provokes a turbulent diffusion causing the fluid to spread. Since $\mathbf{U}$ is turbulent the concentration resulting from Eq. (2.1) is also turbulent, and its random component is $c_i{}'$, with $\langle c_i{}' \rangle = 0$ by definition (Seinfeld and Pandis, 2006). The $^-$ refers to a temporal averaging, while the angle brackets $\langle\rangle$ relates to the average of a sample.

Averaging Eq. (2.1) over an ensemble of turbulent flow realizations and incorporating Eq. (2.2) yields:

$$\frac{\partial \langle c_i \rangle}{\partial t} + \nabla \cdot \left(\overline{\mathbf{U}} \langle c_i \rangle + \langle \mathbf{U}' c_i{}' \rangle \right) = \nabla \cdot D_i \nabla \langle c_i \rangle + \mathbf{R_i}(\langle c_1 \rangle, \cdots \langle c_i \rangle, T, t) + \langle S(\mathbf{x}, t) \rangle, \quad \forall i \in \{1, 2, 3 \ldots, n\} . \tag{2.3}$$

In Eq. (2.3) there are more than one unknown, c_i and $\langle \mathbf{U}' c_i{}' \rangle$ posing a closure problem for turbulent flows. This problem becomes even more complex if the chemical reactions are non-linear. Therefore solution of Eq. (2.1) is only known for extremely simplified conditions.

One very common approach to solve Eq. (2.3), is parametrizing $\langle \mathbf{U}' c_i{}' \rangle$, using the so called $\mathbf{K}$-theory:

$$\langle \mathbf{U}' c_i{}' \rangle = -\mathbf{K} \frac{\partial \langle c_i \rangle}{\partial \mathbf{x}}, \tag{2.4}$$

where $\mathbf{K}$ is the turbulent diffusivity tensor. In reality, molecular diffusion is much smaller than the turbulent diffusion therefore it can be neglected.

Replacing Eq. (2.4) in Eq. (2.3) yields:

$$\frac{\partial \langle c_i \rangle}{\partial t} + \nabla \overline{\mathbf{U}} \langle c_i \rangle = \nabla \cdot \mathbf{K} \nabla \langle c_i \rangle + \mathbf{R_i}(\langle c_1 \rangle, \cdots \langle c_i \rangle, T, t) + \langle S(\mathbf{x}, t) \rangle, \quad \forall i \in \{1, 2, 3 \ldots, n\} \tag{2.5}$$

Equation (2.5) is the advection-diffusion equation and it is solved with defined initial and boundary conditions.

There have been attempts of cataloguing the existing air quality models, as for instances the model documentation system (Moussiopoulos, 2009) developed at the Aristotle University of Thessaloniki and on the COST 728/732 Model Inventory (COST, 2007).

2.4.1 Classification of Air Quality Models

Air quality models can be classified according to several criteria, e.g. scale, transport frame of reference or type of application.

2.4.1.1 Transport Frame of Reference

According to their transport frame of reference, air quality models can be classified as Eulerian or Lagrangian. Both approaches are currently used in regional and urban scale studies. The main difference between them is that in Lagrangian models the reference frame follows the flow moving along with it. Contrarily in Eulerian models the frame is fixed in a grid, and the fluxes of all the grid cells are investigated. In this case the observer watches the dispersion of the plume as it moves.

Eulerian models Eulerian models, also called grid models, are the most complex type of models but also the most computer intensive. They represent the greatest part of photochemical air quality models. They investigate fluxes, as shown in Fig. 2.6, solving Eq. (2.5) via finite approximation for all the cells in the domain. The study area is divided vertically and horizontally into cells, which are connected with each other via advection and diffusion processes. The simulations evolve from initial conditions that are subject to boundary conditions and allow the variables to evolve in time. Input data, include emission fields; topography; meteorology such as wind direction and velocity, temperature or solar radiation; initial and background pollutant concentrations.

Lagrangian models Lagrangian models simulate the trajectories of a sample of air parcels, which follow the instantaneous flow. The pollutants concentration distribution is computed using a deterministic velocity, which corresponds to the average wind, and random velocity correspondent to the turbulent velocity. Using the trajectories of a large number of particles it is possible to calculate the concentration fields, Fig. 2.7.

Lagrangian models are nevertheless more limited when it comes to the incorporation of complex chemistry.

Comparing both categories of models In the Eulerian approach equation Eq. (2.5) is solved, this is a useful approach because the chemical reactions are directly applied in the governing equations. Nevertheless this approach is mathematically problematic, because it leads to a "closure problem", where there are less equations than variables. Additionally, for distances near the

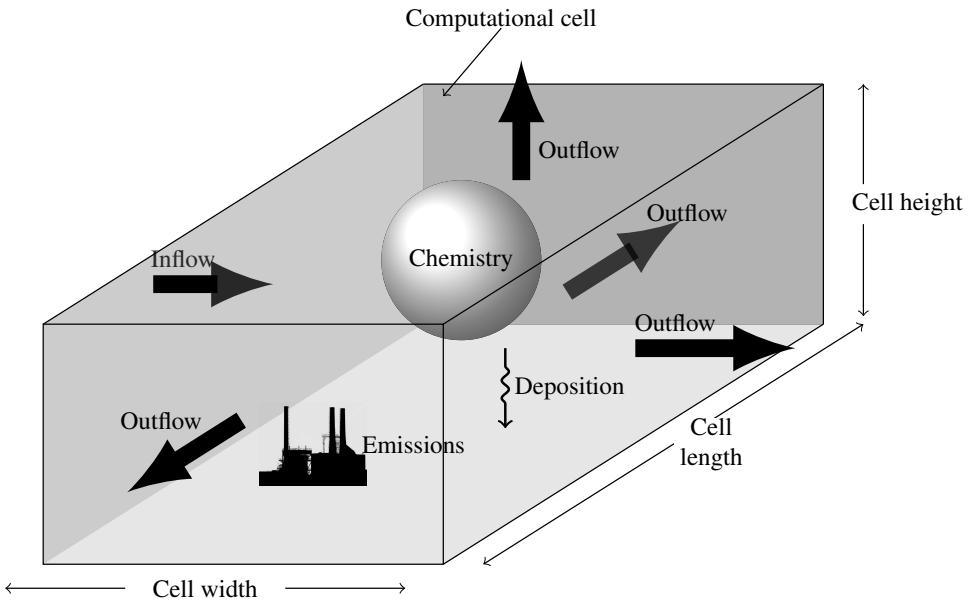

Figure 2.6: Simplified representation of an Eulerian cell, in which the main wind direction is represented by the inflow arrow and the wall of the cell are permeable. Inside the cell, chemical and physical can occur, such as photochemistry or dry deposition.

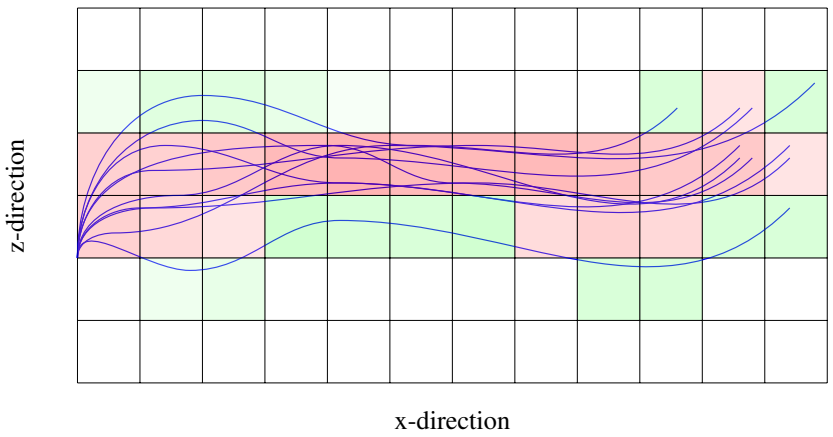

Figure 2.7: Generic representation of a 2-D Lagragian approach, during a time step, the lines represent the particles' trajectory. The coloured scale represents the concentration field, where red represents the highest concentration and green the lowest.

source this equation is not valid because the sources are defined in a grid and the turbulent diffusion in the near-source can not be captured.

On the other hand, the Lagrangian approach is not subject to these limitations. It uses the statistics of the groups of the Lagrangian particles, therefore the concentration values are subject to a statistical uncertainty, which should be accounted for. Mathematically, this approach is advantageous because it avoids the implicit numerical diffusion errors of the numerical schemes used in solving Eq. (2.5). However chemical transformations are more difficult to implement because non-linear reactions are not directly applicable, since they depend on the concentration which is not available at the particle level. In Lagrangian models particle trajectory is known, whereas in Eulerian models an homogeneous distribution inside the cells is assumed, thus Lagrangian models are known to perform better in the near-source region where turbulent diffusion dominates, (Hurley et al., 2005; Nguyen et al., 1994). A major advantage of Lagrangian models is the availability to reduce the calculation time by lowering the number of Lagrangian particles, however increasing the statistical uncertainty.

2.4.1.2 Application Type

Regarding the type of application one can distinguish four types of air quality models: regulatory, policy support, public information and scientific research, as defied by Moussiopoulos et al. (1996).

Regulatory models Air quality models for regulatory purposes are designed to model episodes of pollution, where pollution peaks occur, and long-term average spatially distributed concentrations for comparison with legislated values. AUSTAL2000 (Janicke and Janicke, 2004) is a good example of a regulatory model.

Policy support models On the other hand, policy support models are generally used to determine the impact of abatement measures. They simulate meteorological and pollution scenarios in which the conditions differ from the current status. Policy support models have been used in integrated studies, coupled with other models coming from different scientific and social fields. The EMEP model has been used for this purpose.

Forecasting models Forecasting models are used for public information and focus on the typical temporal evolution of the pollutants for short time periods. Their use has been growing as the need for forecasting of smog episodes became important. Public information might be crucial for people

who have respiratory problems, and therefore are more susceptible to air pollution. The LOTOS-EUROS model (Schaap et al., 2005) has been used for air quality forecasts.

Scientific research models In another way, models that are used in scientific research, normally involve detailed description of the dynamics of the air flows and of the complexity of the chemical reactions. This type of model has experienced a huge development in the last decades with the advancements in hardware. MM5-CAMx and WRF-chem are widely used models for scientific research.

Different applications demand different requirements. For instance forecasting models that need to provide fast responses are normally not as detailed as research oriented models. On the other hand, policy support models are generally used to predict future periods, 5 to 10 years in the future, and therefore have high uncertainties inherent to the time evolution of the input variables.

2.4.1.3 Scale

Air pollution is primarily an emission related phenomena, however weather plays a strong role in the concentrations distribution and in the production of secondary pollutants. The air quality models can be grouped according to the scale of the atmospheric processes. These are classified into Macro, Meso and Microscale.

Macroscale models In macroscale and global climate models, with a typical horizontal scale ranging from 1000 km to 10 000 km, the flows are mainly driven by synoptic processes, originated by the disequilibrium of the surface energy.

Mesoscale models Mesoscale models, few kilometres to ≈500 km, affect local to regional dispersion of air pollutants. They are able to simulate sea and land breezes and encompass both hydrodynamic and inhomogeneities on the energy balance, the latter caused by land-cover and the former due to roughness effect, for instance.

Microscale models Microscale phenomena, <1 km, are normally simulated with street canyon models and imply very complex flows that are strongly influenced by the surface characteristics.

The classification according to scale can have other nomenclature, such as local, urban, regional and global models. Where the global designation is related with macroscale and local with microscale. Regional models encompass mesoscale and also some macroscale phenomena, whereas urban models relate to mesoscale and microscale phenomena.

The phenomena which influence the pollutants motion happens at different scales thus the models simulate the phenomena for the scale which they have been designed. That is, a microscale model is able to capture molecular diffusion, however it can not capture the effects of fronts. In the same way microscale models can resolve buildings, whereas a mesoscale model simulates the effect of buildings by using the roughness lengths. The large scale models are not able to solve the local scale processes, nor is the inverse is true. Therefore in the larger the domains, less detail is possible (Aleluia Reis et al., 2009).

2.4.1.4 Other Types of Modelling Approaches

Other commonly mentioned types of models are: Gaussian models, puff models, receptor models, screening models and box models.

Gaussian models Gaussian models represent the first historically big development in air quality modelling. As the name indicates they assume that the concentration in a plume transported downwind has horizontal and vertical Gaussian distribution, as shown in Fig. 2.8.

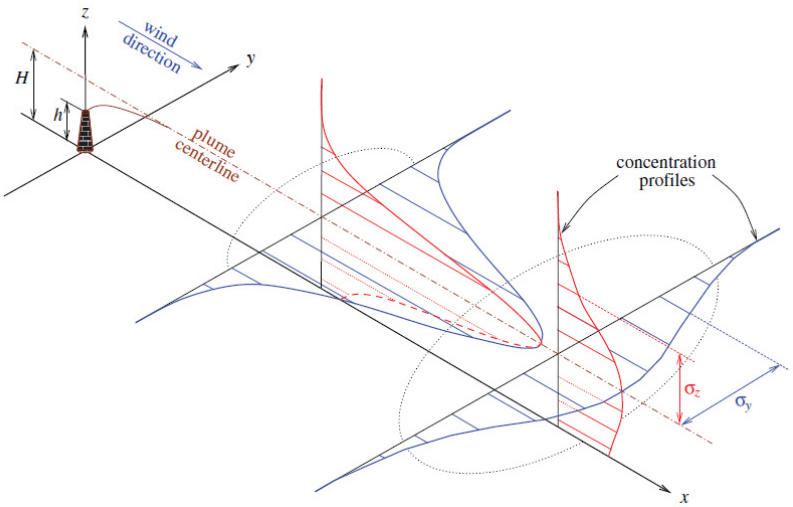

Figure 2.8: Schematic representation of a Gaussian plume, where the cross-sections are relative to the plume central axis, after (Stockie, 2011).

They simulate a continuous point source emitting a given pollutant in a

unidirectional wind. They are based on the analytical solution of the stationary classical diffusion equation, subject to a variety of approximations. This type of models are used in local and urban scale studies, to assess the impact of existing or potential sources. Examples of this type of models are PROKAS-V (Romberg et al., 1996), DISPERSION21 (Omstedtt, 1988), SYMOS97 (Srnensky, 1998), UDM-FMI (Olesen, 1995), STACKS (Erbrink and Bange, 1991) and PLUME (Turner, 1970).

Puff models Puff models represent an improvement of Gaussian plume models, they simulate the temporal evolution of a pollutant puff emitted at a given point in time. Contrarily to Gaussian plume models that describe a pollution source via a steady growing plume, the plume is seen as a series of "puffs" released over time. The puffs are independent of each other thus the plume responds to changing winds and terrain. The puffs expand due to the turbulent nature of atmosphere and the trajectory moves the puff through its central point. However, this models are limited, as they solve the diffusion equation with various approximations. Figure 2.9 shows a general visual representation of a puff model.

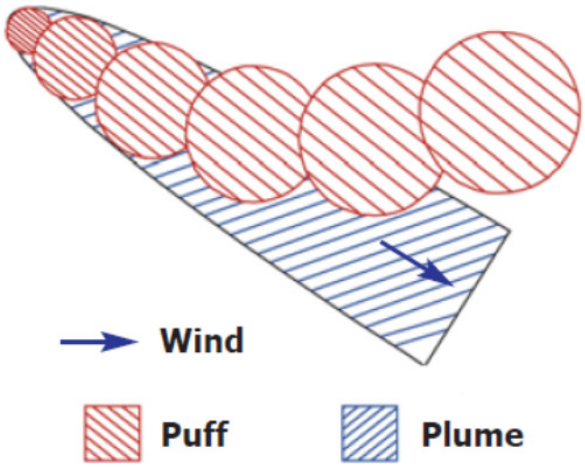

Figure 2.9: Schematic representation of a Puff model, showing the difference between plume and puff models, after (Environmental, 2011).

Receptor models Receptor models work in the reverse sense of general dispersion models. They start from the observed concentrations at the receptor point and search for the share contribution of the various source types. The emission's chemical composition is known and it is allocated to the sources. These are statistical models based on the mass balance equation. Known receptor models are Chemical Mass Balance Model (CMB) (EPA, 2005), Unmix (Norris et al., 2007) and Positive Matrix Factorisation (PMF) (Norris and Vedantham, 2008).

Screening models Screening models have been used for first level assessments, calculating average concentrations with low level of spatial and temporal resolutions, (Sokhi et al., 2008). They are advantageous because they require few input data and constitute a good tool to identify key problems which require further detailed study. Some of these models do not require meteorological data, ignoring local problems originated by the local effects of weather, (Mutchimwong, 2005). They are run in a few minutes providing quick and cheap answers. Examples of these models are DMRB (Department of the Environment and the Regions, 1999) and AERSCREEN (EPA, 2011).

Box models Finally, box models are 0-Dimension models which see the atmospheric domain of interest as a single "box", unlike eulerian model where the model is resolved on a grid. They assume uniform mixing inside the "box" and include emissions inside of the domain, advective inflow and and outflow. They allow, also, the simulation of entrainment of pollution from aloft due to the elevation of the mixing height during the day. These models compute the time series of the one volume "box" and allow the implementation of sophisticated chemical mechanisms (Arya, 1999). Commonly used box models are Air Force Dispersion Assessment Model (ADAM) (U.S, 2012), Photochemical Box model (PBM) (EPA, 1984) and OZIPR (Gery and Crouse, 1990).

Additionally two other types of model exist, hydrostatic or non-hydrostatic models. Hydrostatic models, e.g. ALADIN-CAMx (Morris et al., 2005), are those that assume a hydrostatic approximation. These models normally use pressure or sigma pressure vertical coordinates. Sigma coordinates are those which follow the terrain. This approach has disadvantages because hydrostatic approximation might not hold for high horizontal resolutions. On the contrary non-hydrostatic models such as EURAD-IM, (Hass, 1991), MM5-CAMx, (Grell et al., 1994) and WRF-chem (Skamarock et al., 2005), solve the complete vertical momentum equation, and normally use altitude or sigma altitude coordinates.

The wide number of air quality models available, and the various types of classifications provide a primary guidance when one needs to select the most appropriate model for a given application. The different models have different assumptions, as for instances different chemical schemes, therefore for the same case study different models might give different results. Hence it is advantageous to have several models available. This model classification has been used in the work to select a transport core calculator for the LEAQ air quality model, as explained in Chapter 3.

2.5 Emission Reduction Instruments

There are two main approaches considered in emission reduction strategies: Regulatory measures and market-based measures.

Regulatory instruments Regulatory measures, also called command and control measures, are those which intervene directly at the source implementing rules and regulations. These are legally supported through national or international regulations or treaties. Regulatory instruments control the use of certain standard devices, operational system designs and efficiency standards. They can be further subdivided into *normative*, when a standard is applied such as emission quotas and *informative*, when the consumer is informed about the energy efficiency of the product and decides based on it as for example labelling and certification (UNEP, 2007). In this case the emitter agent is obliged to meet the standards regardless of what the reduction cost might be. One of the disadvantages of these measures is that they might be inefficient due to the complexity of the technical logistics and the control it implies.

Market-based instruments Market-based instruments use economic mechanisms, they represent a "voluntary" participation of the emitters and offer financial incentives through price adjustments. They can be implemented in the form of emission taxes or tradeable emission credits. Just as the regulatory measures, market-based measures aim at reducing emission levels, but in this case the reductions can be cooperative. A major example of these measures are the Kyoto flexibility mechanisms, e.g. emission trading scheme via carbon credits, where "emission reductions", called *credits*, can be traded amongst countries to minimize the cost of reduction. In the European trading scheme, emission permits are attributed to a polluting agent such as a country or enterprise, which according to its efficiency will need to buy or sell its emission allowances. The sum of all the emission rights in the market should comply with the emission level objectives, limiting the amount of pollution.

Emission taxes promote the elimination of negative externalities such as social costs, by obliging the less efficient producers to pay a tax, whereas the products with less social costs do not pay tax. Taxes induce emission reduction through three mechanisms: reducing exchanges quantity, fostering technical replacement, promoting the development of more efficient technologies (Kübler, 2001). Other type of taxes are the incentive taxes, which stimulates the emitter to invest in less polluting technologies. This type of tax encourages to the principle of precaution.

Additionally, one can consider another class of less strict measures, the so-called support, information and voluntary action. These include the voluntary

labelling and certification, awareness rising and informational campaigns or detailed billing. The effect of these kinds of measures is more difficult to model. Since they do not depend directly on controllable variables, the cost effectiveness of these measures is very difficult to determine.

In conclusion there are several instruments to reduce emissions, and there is no single answer on how to tackle this problem. Regulatory measures that are very strict can lead to unsuccessful results due to the fact that meeting such strict limits leads to high reduction costs. On the other hand, market instruments, such as emission credit market scheme, although generally have proven to be effective, do not avoid certain problems of spatial heterogeneity in emissions. Probably the best solution would be a combination of several policy instruments.

The MARKAL/TIMES family of models can be used to examine the effectiveness of market-based instruments and the possible combinations between them. Emission reduction policies only analyse pollutant emissions but ignore the effect of those emissions on the quality of the air. Since the relations between emissions and air quality are not linearly related, a more complex modelling framework must be used. Technically it is possible to find the least-cost policy measures which relates to standard air quality ambient levels. This can be achieved by coupling economic models with air quality models. The level of complexity of the air quality model depends on the pollutants of interest and on the integrated assessment model running mode, optimisation or simulation.

Ozone is one of the most challenging pollutants because as a secondary pollutant, the control of concentration levels has to be done through its precursors. Moreover, the non-linear behaviour of the chemistry involved makes ozone pollution a complex problem.

Reducing ozone ambient levels continues to be a major focus of air quality research in the last decade in Western Europe (EEA, 2006, 2011). The European environment agency reports yearly on the continued exceeded ozone limits, both the long-term objectives and target values. However the reduction of ozone levels is far from being an easy-solving issue. As a secondary pollutant, ozone is not emitted and thus ozone control strategies must be done through the reduction of emissions of its precursors. However the ozone concentrations are a non-linear function of NO_x and VOC concentrations, (Diem and Andrew, 2001).

The non-linearities of ozone behaviour, specially with respect to NO_x, make the ozone control measures more complex. In other words a reduction of NO_x emissions does not necessarily lead to a reduction in ozone concentrations, depending if the ozone regime is NO_x- or VOC-sensitive. Figure 2.10 shows a general ozone isopleth which is a typical graph to represent the ozone behaviour as a function of its precursors.

Point A of Fig. 2.10 illustrates the NO_x-saturated regime, where a reduction of NO_x induces an increase in ozone concentrations. In this case a reduction of VOC emissions would be more effective.

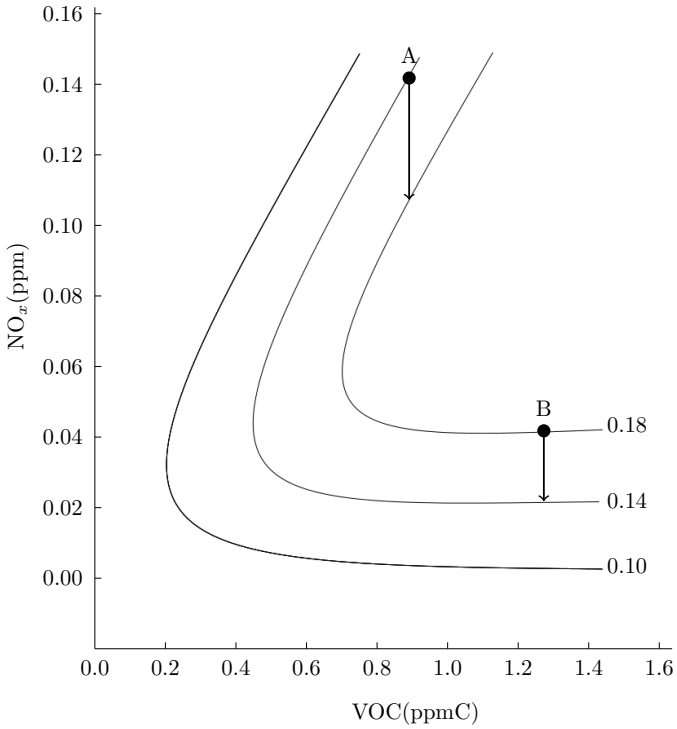

Figure 2.10: Ozone isopleths, in ppm, as a function of NO_x, in ppm, and VOC, ppmC.

Likewise point B of Fig. 2.10 represents the NO_x-limited regime where a reduction in NO_x lead to a reduction in ozone levels. Reducing NO_x emissions, is only effective in NO_x-limited regimes, which occur preferentially in rural areas and during the hottest months. Therefore spatial relations, as well as temporal factors such as seasonality and hours of the day, which relate to variations in temperature and radiation, also play a role in ozone formation.

This spatio-temporal heterogeneities of ozone must be taken into account, as they contribute to the non-linear problem. In transitional zones as for example in sub-urban regions in city borders, a reduction of both the precursors may be needed. Nevertheless reductions of NO_x in sub-urban areas may lead to a reduction of the local ozone, but also to an increase of urban ozone levels, leading to high exposure. Therefore ozone reduction strategies may be a compromise between different types of consequences (Diem and Andrew, 2001).

The complex relations that involve ozone formation/depletion together with its spatio-temporal variability emphasises the need for more comprehensive decision support tools. Moreover, approaches other than emission

reduction can be implemented, such as measures to lower the high urban atmospheric temperatures, caused by the urban heat island effect. This can be achieved via structural changes in urban planning such as the use of less absorbing materials and colours in construction, or the introduction of ozone-tolerant and low biogenic VOC emission plants.

Chapter 3

The Energy - Air Quality Integrated Assessment Model

Contents

3.1 Objectives and Concept

The Luxembourg Energy-Air Quality model (LEAQ, http://crteweb.tudor.lu/leaq/), developed by the *Centre de Recherche Public Henri Tudor*, is an air quality integrated assessment model designed for the Grand-Duchy of Luxembourg (Zachary et al., 2009) and (Zachary et al., 2011).

The LEAQ project arises from the necessity of linking energy with air quality levels in Luxembourg. Luxembourg is very small country, 2'586km^2, however with a high economic and demographic growth. From 1990 to 2007, the Luxembourg population grew by 27% and it's GDP increased by 4.7% from 2000 to 2006. Furthermore between the period of 1990 and 2007 the energy consumption in the country increased by 24%. These growing factors impose pressures on the environment mainly through the increase of energetic demand. For instances the rate of growth of the number of passenger cars per inhabitants with respect to the period from 1991 to 2007 was the highest in the EU (MDDI, 2010).

The LEAQ project is a follow up of the earlier work of Carlson et al. (2004) done for the Geneva region, applied to the Grand-Duchy of Luxembourg. This project presents a few enhancements in relation to the previous application namely the air quality model TAPOM-lite (Zachary et al., 2003) is enhanced

in this work. The techno-economic model, ETEM, evolved from MARKAL-Lite, has been redesigned for the Grand-Duchy of Luxembourg during the LEAQ project. Finally, a more detailed emission allocator scheme has been implemented.

Carlson et al. (2004) applied an air quality integrated assessment model in optimisation mode to the Geneva canton. The LEAQ model is based on the same integrated assessment architecture and operating mode. The goal is to built an integrated assessment policy support tool for Luxembourg, that is able to run both in simulation and optimisation mode. The model permits exploring possible long term policy measures for Luxembourg. On the assumption that LEAQ is run in simulation mode the outcome is the quantitative evaluation of a policy measure in terms of air quality and cost. Whereas in case it operates in optimisation mode the outcome will be the most cost-effective policy measure that satisfies the air quality standards, (Zachary et al., 2011). Therefore assessing efficient policy strategies to provide technical guidance to the decision makers aiming at a structured economic development. For these reasons the LEAQ project is focused on the optimisation operational mode. The ultimate goal is to apply the LEAQ model to other target regions or cities.

The LEAQ model aims at solving the following problem:

> *Find the optimal energy arrangement which complies with a given ambient ozone level standard.*

The LEAQ model has been assembled around two underlying philosophies:

Open-source The project has been built using only open-source software. This allows the LEAQ tool to be open for application and disclosure. Moreover open-source tools are easy to extend or adapt to other applications. As for example, the inclusion of more pollutants, the development of more detailed physics or the inclusion of new economic concepts.

Flexibility The LEAQ model has been designed for Luxembourg country however the project philosophy is that it should be flexible enough to be applied to other cities or regions. Therefore both sub-models must be able to treat different domain sizes and resolutions. This issue is more critical for the air quality model since the techno-economic model does not work on a spatial distributed basis.

3.2 The LEAQ Structure

The LEAQ model consists of two sub-models, the energy model ETEM and the air quality model, AUSTAL2000-AYLTP. The two models are coupled by an optimisation routine called OBOE. The structure and the components of the LEAQ integrated assessment model is represented in Fig. 3.1.

Figure 3.1 and Table 3.1 present the main components of the LEAQ model. The LEAQ model has four main modules (Aleluia Reis et al., 2011a):

1. The energy model ETEM which is itself an energy optimisation model, it minimizes the cost function and the optimal energy flows in the energy sector with emission and energy constraints, e.g. demand, operational, technological and seasonal variability.

2. An emission allocator module which uses hourly, weekly and monthly profiles as well as economic sectoral maps to disaggregate the emissions and prepares them in the input format of AUSTAL2000-AYLTP.

3. OBOE which uses an oracle, which is a program that obtains and delivers the information that OBOE needs, and a method Analytic Centre Cutting point Method (ACCPM) to solve an optimisation problem. In OBOE the sub-models are treated as "black boxes" by an oracle which delivers the required information to the optimizer (Babonneau et al., 2006).

4. The air quality model AUSTAL2000-AYLTP which simulates the transport of the air pollutants and the photochemical reaction of ozone. The result is a time series of spatially distributed pollutant concentrations.

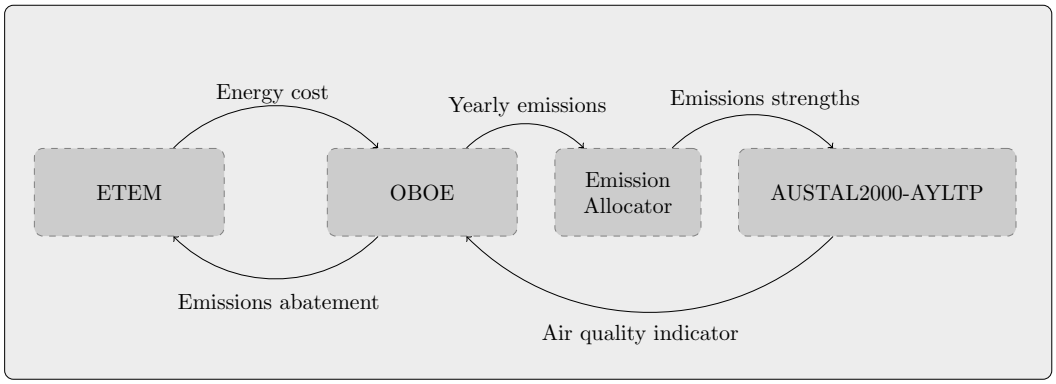

Figure 3.1: Overview of the integrated assessment LEAQ model, showing the two sub-models, ETEM and AUSTAL2000-AYLTP, their relation through the emission allocator, and the variables which are exchanged between them.

Table 3.1: Generic characteristics of the LEAQ modules.

	ETEM	OBOE	Emissions Allocator	AUSTAL2000-AYLTP
Inputs	Useful demand Energy technologies Emission factors Energy price	Air quality indicator Energy cost	Yearly Emissions Sectoral maps Sectoral temporal profiles	Topographical map Wind fields Pollutant emissions
Outputs	Energy system cost Energy composition Pollutant emissions	Emission abatement	Time series of emission strengths maps	Pollutant concentration map
Time Scale	Year	—	—	Hour or few minutes
Spatial scale	Country Region City	—	—	Domain size: hundreds of kilometres Resolution: hundred meters to kilometres
CPU time	Few minutes	< 1 sec	Few Seconds	from 3-100 min
Programming language	GMPL/ (GAMS)	C++	Ruby	C, Fortran

The two models, ETEM and AUSTAL2000-AYLTP, are connected by a common variable or by a module which "translates" the information from one model to the other. The model is started with a first guess of yearly emissions and then disaggregated spatially and temporally by the emission allocator, which in turn uses the emission time series to feed the air quality model in order to compute concentrations. This algorithm path assumes the LEAQ model is run in simulation mode. However in the optimisation mode, the sequence continues and the meta-model provides feedback to the energy model. The OBOE module checks if the air quality index breaches an air quality limit. In this context, the air quality limit can be a legislative value or a long term objective. In this work, the main focus is the ozone pollutant, due to its harmful effects on human health and vegetation. Additionally, its complex relation between the precursor emissions and the ozone formation represent a challenge in terms of ozone pollution policies. Therefore, the air quality indicator is based on ozone levels. However other pollutants which can be assumed to be non reactive, such as CO, SO_2 and primary PM, may be evaluated. The inclusion of reactive pollutants might be added, since the LEAQ framework is flexible, but it demands additional development efforts.

If the air quality index breaches a given limit, OBOE proposes new emission constraints. This procedure is repeated until the air quality levels satisfy the limit. Once the air quality compliance is assured, the constraint forces ETEM to choose less pollutant technologies, which normally leads to a raise in the cost. ETEM then optimizes the energy shares to arrive at the least-cost energy arrangement that complies with a given air quality objective.

3.2.1 The ETEM - Techno-Economic Model

The ETEM model (Drouet and Thénié, 2008), is a E^3 partial equilibrium model that follows a bottom-up approach and belongs to the MARKAL-TIMES family. The model was developed by the ORDECSYS company for the Geneva canton. This type of models have been widely used in policy support studies. Simões et al. (2008) has presented a study for CO_2 abatement policies using the TIMES model. In Changhong et al. (2006), the authors have expanded the study not only to CO_2 but also to NO_x and SO_2 reductions for the energy policy in China. A more recent work by Pietrapertosa et al. (2010) includes the pollutants NO_x, SO_2, PM and VOC.

In ETEM the supply of energy is arranged such that the total cost is minimum. A number of constraints, such as resource availability or emission levels, can be introduced in order to assure that the optimal solution is found in a realistic space domain and obeys to certain socio-economic and pollution restrictions. The total cost includes the cost of equipment investment, operation, salvage cost and the importation and exportation of primary energy.

The model is technology intensive and the information about each technology is stored in a dedicated database.

The ETEM model version designed for Luxembourg is referred to as the ETEM Luxembourg model. The ETEM Luxembourg has been developed for the LEAQ project, but not in the context of this thesis work. In the LEAQ integrated assessment framework, the role of ETEM Luxembourg is to furnish the representation of the technologies that best fits the energy demand of the Grand-Duchy of Luxembourg. Additionally it delivers the sectoral emissions associated to the activity of the installed technologies. These emissions feed the air quality model and serve as the "dialogue" variable between the sub-models of LEAQ.

ETEM was designed under the concept of integrated assessment modelling and therefore is ready to be coupled with other models or modules. Furthermore it is flexible allowing the incorporation of new features and different levels of detail of the energy systems. The implementation of ETEM Luxembourg has been done in GNU MathProg Language (GMPL), a subset of the AMPL language (Fourer et al., 1990).

3.2.1.1 The ETEM Luxembourg Structure

ETEM is defined by four main components: time, demand, the Reference Energy-System (RES) and the database of technologies.

Time Time concerns the time partition. The total time domain of ETEM is called time horizon and it starts from the base year to the end of the last year of the decision process. The time horizon is composed of several time periods which are typically of one to five years. Additionally, a year subdivision is defined, called time-slice. Some economic activities may vary according to season, as household heating, hour of the day, as lighting, day of the week such as traffic.

The model has been calibrated for the base year 2005, according to the socio-economic factors coming from the EU energy trends to 2030 report (EU, 2010b) and the socio-economic projections, from 2010-2060, report of the national institute of statistics and economical studies (STATEC, 2010a). The following years until the year 2030, are evaluated by the model. The time periods have the duration of one year which corresponds to 26 periods. The "decision years" correspond to the time that lasts from the base year to the end of the model evaluation.

Figure 3.2 represents the time-line of the ETEM Luxembourg application. The time slices are divided according to season into winter W, intermediate which includes spring and autumn I, and summer S. Additionally, a daily

division is assumed, distinguishing day, D, and night, N. These times slices are crucial for some types of technologies as for example photovoltaic power production in which the summer and day time slice will contribute significantly more to the yearly production.

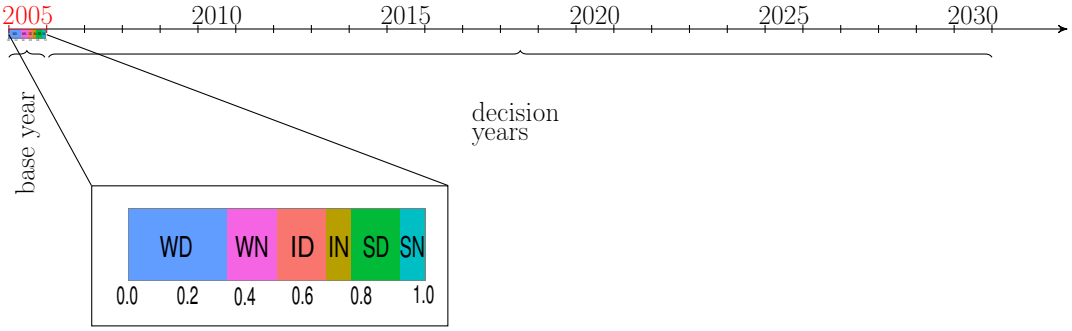

Figure 3.2: Time distribution in ETEM Luxembourg. The zoomed square shows the share of the time slices defined for each time-interval. The capital letters W, I, S, D and N, stand for winter, intermediate, summer, day and night respectively. After (Drouet, 2011).

Demand The demand in the energy services, for example demand in transportation, is the main driver of the ETEM model. Demands are, normally, projected using a base line year and information about demography growth, Gross Domestic Product (GDP), urban development plans and other type of socio-economic factors that may be available. In ETEM Luxembourg Demand D is projected for all the commodities s, at each time period t. Commodities are energy carriers, energy services, materials, monetary flows, and emissions, which are produced by a processes (Loulou and Labriet, 2008).

The demand is calculated according to the formula (Drouet, 2011):

$$D_s(t) = D_s(t = 2005) \times f_s^{\theta} \,, \forall s \in S = \{1, 2, \ldots, n_s\} \,, \tag{3.1}$$

where f_s is a social or economic factor of the type mentioned before, θ is the elasticity and n_s is the number of commodities. Elasticity is a parameter that measures the response of a variable to the change of other. In this case, it is the response of demand to the change in the socio-economic factor.

In ETEM Luxembourg, the demand is aggregated into seven economic sectors: imports/exports, secondary production of energy, agriculture, commercial/institutional, industry, residential and transport. The sector imports/exports does not have direct emissions associated, due to the fact that there is no production. Further division of sectors into sub-sectors is possible if enough details are available in the energy data and in the land-use maps. For example, residential sector has been divided in three sub-sectors, space heating, water heating and others.

As mentioned before, Luxembourg is a unique country, due to its small dimensions and its fast economical growth. Therefore in some sectors, some distinct characteristics are worth mentioning. The Luxembourg production sector, includes the production of energy and the transformation of energy. Most of Luxembourg's energy is imported, for instances 66% of the electricity has been imported in 2005. The national production is assured by thermal power plants 82%, co-generation, hydro-electric, wind, biomass and photovoltaic (MDDI, 2010).

The industry sector is dominated by metallurgy, mainly iron and steel. The production of chemicals is also considerable, others such as the production of clinker and flat glass have little importance.

The share of energy demand of the agricultural sector in Luxembourg is significantly low, 5% (Drouet, 2011), thus this sector has low level of detail in ETEM Luxembourg.

Transport is the sector most marked by the particularities of Luxembourg. Transportation is the highest final energy consumer in Luxembourg. Nevertheless, the numbers do not correspond to the real domestic consumption. The OCDE reports that, in Luxembourg, 75% of the oil is sold to non-national vehicles (OECD, 2010). The main reasons which contribute to this fact is that Luxembourg is a small and central country, positioned between three countries, and it's fuel prices are very competitive in comparison to its neighbouring countries. Therefore in the model the traffic sector has a dedicated sub sector for the road traffic commuters.

Reference Energy System The RES describes the relations between elements of an energy system: processes, commodities and flows. An energy system is composed of commodities which may be primary energy e.g. oil; energy services e.g. lighting; and emissions. The energy resources may be produced by a process or imported. The processes convert the commodities of type energy resources to a commodity of type energy services. In the same way, commodities of type energy services are transformed into the commodity emissions. Processes are technologies as for instances power plants or air conditioners. Finally the flows are the links between the commodities and the processes. Figure 3.3 shows schematically a RES where four commodities are represented — oil, electricity, space heating and carbon dioxide. In Fig. 3.3, the processes power plant, electric heater and oil furnace are connected to the commodities by the flows, which are represented by the horizontal lines. In this simplified example the processes "electric heater" and "oil furnace" compete with each-other, both will be available to meet the demand "space heating". The choice of the shares of activity and capacity of these two technologies is based on the cost and on the efficiency level. The latter due to constraints in emissions might force the model to choose the most costly technology. The

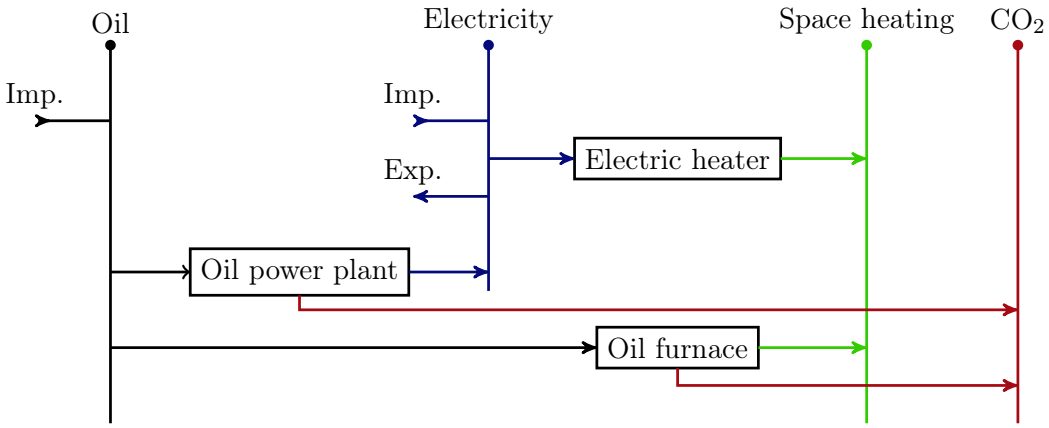

Figure 3.3: Simplified representation of the RES of ETEM Luxembourg for the commodity space heating, Source: ETEM Luxembourg technical report (Drouet, 2011).

total cost of a technology is evaluated taking into account the whole energy system and decision time. This means ETEM may decide to install for instance an oil power plant to produce electricity instead of buying imported electricity because it is less expensive in the long term (Drouet, 2011).

Database of technologies The database is a set of parameters which describe the energy system. It includes the model's general parameters such as time horizon and time periods, projection of future demands, energy prices, the future potential technologies, the emission factors of the technologies and the description of the technologies (Drouet, 2011). It contains also the database of the future generation of technologies. Table 3.2 describes all the types of parameters that compose the database.

The current status of the ETEM Luxembourg database includes the emission factors for the pollutants, NO_x and VOC. Others may be added if data is available. For a detailed description of the database please refer to the ETEM Luxembourg Technical Report (Drouet, 2011).

At the end of the simulation for the time horizon, ETEM outputs:

- the activity of processes, which corresponds to the main flows that are used to size the capacity. For instance, for a power plant the corresponding activity is electricity production. It is computed for all the processes, at all time periods and slices.
- The capacity for each time period and process. For a power plant it corresponds to the installed power.
- The production of each commodity for each time period and slice. Additionally the sum of production and importation is also computed and

Table 3.2: ETEM database parameters

Elements	Parameters	
	Type	Description
Processes	Technical	Efficiency, availability factors, commodity consumption per unit of activity, shares of fuel per unit of activity, technology life time
	Economical	Investment cost, operation cost
	Bounds	Investment capacity, total capacity, activity
Commodities	Technical	Efficiency of distribution, time-slices, demand projections
	Economical	Import and export cost
	Bounds	Production
Flows	Technical	Commodities that form a flow, share of the commodity in the flow,
	Economical	
	Bounds	Production and consumption of a flow by a process

it is defined as procurement.

- The consumption of a commodity for each time period and slice. The sum of consumption and exportation is called disposal and it is equally calculated.

- Pollutant emissions, NO_x and VOC, per economical sector.

The emissions in ETEM Luxembourg for the year 2005 were calibrated according to LRTAP and are presented in Table 3.3. The model is applied to the Grand-Duchy of Luxembourg and therefore it accounts only for the emissions that take place above the national territory.

Table 3.3: NO_x and VOC emissions, according to LRTAP (EEA, 2010b) for the base year 2005.

Source category	NO_x [t]	VOC [t]
1.A.1 Energy Industries	1335.97	152.80
1.A.2 Manufacturing Industries and Construction	3942.49	31.92
1.A.3 Transport	7966.67	2365.92
1.A.4 Other Sectors	570.43	211.87
1.A.5 Other (Not elsewhere specified)	70.74	26.74
1.A Fuel Combustion	13886.30	2789.25

3.2.1.2 Mathematical Formulation

The ETEM model is an optimisation problem of the linear form (Drouet and Thénié, 2008),

$$\min_{\mathbf{x}}\{\mathbf{c}'\mathbf{x} \mid \mathbf{A}\mathbf{x} = \mathbf{b}, \mathbf{x} \geq 0\}, \tag{3.2}$$

where $\mathbf{x} \in \mathbb{R}^n$ is the vector of ETEM decision variables, such as the investments in new technologies, the consumption and the production of installed technologies, $\mathbf{c}' \in \mathbb{R}^n$ is the transpose of the cost vector. The matrix $\mathbf{A} \in \mathbb{R}^{m \times n}$ and the vector $\mathbf{b} \in \mathbb{R}^m$ are the description of the energy system and its technical coefficients. Where n and m are the number of rows and columns of the matrix $\mathbf{A}$.

The constraint $\mathbf{A}\mathbf{x} = \mathbf{b}$ is the mathematical formulation of a linear system which describes the reference energy system of Luxembourg.

The model calculates the sectoral pollutant emissions $\mathbf{e} = e_{j,k,\sigma}$ for each pollutant $j \in J = \{\mathrm{NO_x}, \mathrm{VOC}\}$, at each time period $k = 1, \ldots, K$ and each emitter sector $\sigma \in \xi$. The sectoral emission vector $\mathbf{e} = e_{j,k,\sigma}$ is calculated using a linear relation between the fuel consumption of the sector technologies and emission factors $\mathbf{p}$.

In addition to the existing constraints of Eq. (3.2), an emission constraint $\bar{e}$ can be added and the objective function of the ETEM model then becomes,

$$\min_{\mathbf{x}}\{\mathbf{c}'\mathbf{x} \mid \mathbf{A}\mathbf{x} = \mathbf{b}, \mathbf{p}'\mathbf{x} = \mathbf{e} \leq \bar{\mathbf{e}}, \mathbf{x} \geq 0\}, \tag{3.3}$$

where $\bar{\mathbf{e}} = \bar{e}_{j,k,\sigma}$ represents the vector of yearly maximum sectoral emissions. By construction, it is ensured that Eq. (3.3) has an optimal solution and that the constraint $\mathbf{e} \leq \bar{\mathbf{e}}$ on sectoral emissions is an equality at optimality, i.e. when an optimal solution $x^\star$ is found, one has $\mathbf{e} = \bar{\mathbf{e}}$.

3.2.2 Emission Allocator Module

The Emission Allocator Module has been developed to "communicate" the coupling variable, emissions, between the two sub-models, ETEM and AUSTAL2000-AYLTP. Figure 3.4 shows the differences in temporal and spatial scale between the two sub-models. One of the challenges of the LEAQ model is dealing with these differences.

Figure 3.4 demonstrates that the sub-models domains do not overlap in the temporal dimension and do not match on the spatial resolution. Therefore the development of a module that could "translate" the "dialogue" variable — emissions — between the sub-modes was required.

The emission allocator was designed to receive land use fraction maps and temporal profiles in order to prepare the emission sources locations and

strengths for the AUSTAL2000-AYLTP model. This modules makes the connection between the yearly emissions proposed by the oracle and the air quality model, solving the spatial and temporal scale differences between the two models.

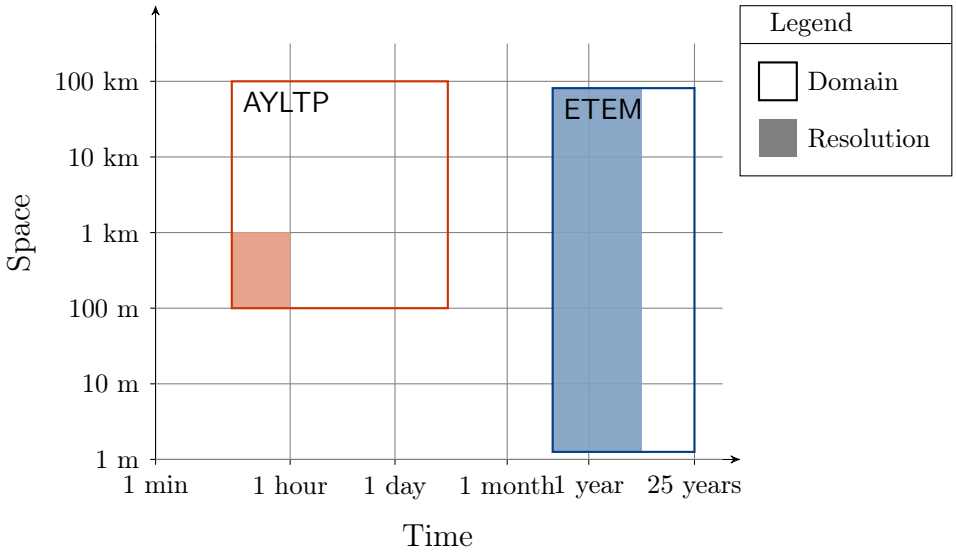

Figure 3.4: Space and time scale comparison between the ETEM and AYLTP in LEAQ. The squares compare the space/time domain of the models, while the filled areas compare the space/time resolution of the models, from Aleluia Reis et al. (2011a).

3.2.2.1 Temporal Allocation

The temporal domain takes the form of a day or several days that could form a pollution episode. An air quality episode is a period of abnormally high concentration of air pollutants, often due to low winds and temperature inversions, that can have damaging effects on human health and/or ecosystems.

The disaggregation of the annual emission values have been carried out according to temporal profiles. Several activities can be used as surrogates for monthly, daily and hourly load profiles. In this application the temporal profiles for Luxembourg have been provided by the GENEMIS project (Ebel et al., 1997). GENEMIS is a EUROTRAC-2 (A EUREKA Environmental Project) project which aims at supporting the generation of emission data, that can be used for the development of air pollution abatement strategies in Europe.

GENEMIS refers to SNAP sectors, which have been aggregated into the ETEM sectors according to Table 3.4.

A literature survey has also been carried out by Drouet and Aleluia Reis

Table 3.4: Correspondence with the SNAP - sectors, the SNAP - sectors signalised with "—" do not have a correspondence with the ETEM sectors.

Sector	SNAP Code	Designation
Production	1	Combustion in energy and transformation industries
Commercial/Institutional	2	Non-industrial combustion plants
Industry	3	Combustion in manufacturing industry
—	4	Production Processes
—	5	Extraction and distribution of fossil fuels and geothermal energy
—	6	Solvent and other product use
Transportation	7	Road transport
—	8	Other mobile sources and machinery
—	9	waste treatment and disposal
Agriculture	10	Agriculture

(2012), and the profiles found could be chosen alternatively according with the similarities with the Luxembourg situation.

As mentioned before, the load factors are mainly issued from the GENEMIS database, nevertheless some load factors have been selected from the survey. Specifically, the daily load profile of the sector "Commercial/Institutional" is given by Tsilingiridis et al. (2002) and the monthly and daily profiles of the residential sector are given by Tsilingiridis et al. (2002).

The time sectoral-scheduling function $h_\sigma(t)$ is calculated for all sectors σ as,

$$h_\sigma(t) = \frac{l_{m(t)} l_{d(t)} l_{h(t)}}{n_w(t)}, \forall \sigma \in \xi\,, \tag{3.4}$$

with

$$n_w(t) = \frac{\text{days in month} = \{28, 29, 30, 31\}}{7}\,, \tag{3.5}$$

where $l_{m(t)}$, $l_{d(t)}$ and $l_{h(t)}$ are the loads of the month, day and hour respectively at date t. The term $n_w(t)$ is the number of weeks in the month at date t. In the case of periods shorter than one hour, generally 10 minutes, AUSTAL2000-AYLTP divides the one hour values homogeneously.

The details relative to the treatment of biogenic emissions are presented in Chapter A.

3.2.2.2 Spatial Allocation

Emissions are distributed according to sectors, using a land use map. The high resolution land-use map, 20m grid resolution, has been obtained through the national land cover database, called OBS from 2007. The land use categories

have been aggregated into the economic sectors. Table 3.5 reports on the correspondence between the land-cover and the sectors.

Table 3.5: Correspondence OBS land-cover - sectors. Source: (Drouet and Aleluia Reis, 2012).

Sector	OBS class	Designation
Residential	UAD	Dense urban zone
Residential	UAA	Semi-urban zone with vegetation
Residential	UAS	Semi-urban zone without vegetation
Residential	UAL	Urbanisation along roads
Residential	UAH	Rural Housing
Comm./Institut.	UIA	Economic activity zone
Comm./Institut.	UPS	Socio-cultural buildings
Industry	UIL	Heavy industry
Agriculture	UAC	Agricultural buildings
Road transportation	UTR	Roads
Road transportation	UTS	Parking area
Rails transportation	UTF	Train station, Rails

The sectoral map has been subsequently aggregated to a lower resolution grid before it is passed to the air quality model. The resolution is predefined, usually 1 km, 500 m or 300 m, and must be the same for all sectors. The distribution uses a sectoral fraction $g_{k,\sigma}(s)$ of the total representation of the sector, σ, in the spatial domain of the of the ETEM model, for the time-period k. In this case it is the share of the total area of the sector in Luxembourg per cell.

The normalised spatial allocation function, g over the space $s \in S$ is defined such that:

$$\int_S g_{k,\sigma}(s)\mathrm{ds} = 1, k \in 1, \ldots, K. \tag{3.6}$$

In this application $g_{k,\sigma}$ is equal for all time periods k, but one can envision an extra module that calculates the land use for future periods and consequent feedback on the emission distribution. Zachary et al. (2009) present a first attempt to use LEAQ as a spatial planning tool.

The annual sectoral emissions are denoted $\mathbf{e} = e_{j,\sigma}$, where $j \in \mathrm{NO_x}$, VOC is the pollutant and σ is the sector $\in \xi$ expressed in tons per year. The space-time distributed emissions $e_j(t,s)$ are given by:

$$e_j(t,s) = \sum_{\sigma \in \xi} \left(h_\sigma(t) \times g_{k,\sigma}(s) \times e_{j,\sigma}\right), \forall j \in J, \forall t \in [0,T], \tag{3.7}$$

where T is the duration of the episode.

3.2.3 Oracle Based Optimisation Engine

OBOE is the module that solves the meta-model optimisation problem, based on an oracle. The oracle is a program that calls the sub-models at each query point to obtain the information about the models' response, and delivers it to OBOE. Accordingly, the ETEM model passes the total cost, the objective, to OBOE via the oracle. In other words, OBOE coordinates the iterative process that communicates between an optimisation program and an oracle to approximate the objective cost function.

OBOE solves a convex and non-differential optimisation problem, which means the components of the problem, the objective and the constraints, must be convex. A problem is convex if its objective function $f(x)$ is convex, geometrically it means that any line segment formed by two points of the convex function always lies on or above the graph. It is based on a cutting plane method, ACCPM (Babonneau et al., 2006), that uses the constraints of the problem, the objective and the sub-gradients to propose a new point. The next query point is proposed by minimising the distances between the planes, and thus placing the point in the analytic centre of the localisation set. The localisation set is the space that contains the optimal value, along with the admissible values.

The ETEM function is by construction convex, the objective in this problem is the cost and the decision variables are the NO_x and VOC emissions. OBOE, then, minimises the convex function in a constrained convex interval.

The oracle sends linear information about the problem whenever OBOE needs it. It can send information of two types (Drouet, 2006):

- the outer linear information to define the epigraph, which is area above the function, of the convex function, as illustrated in Fig. 3.5;
- the delineation of the set of admissible solutions.

OBOE sends a sequence of query points for the decision variables. If the query point is not feasible, i.e. is out of the space determined by the constraints, the oracle delivers a plane which separates the point from the realizable half-plane and excludes the other. The query point is the point for which both sub-models, ETEM and AUSTAL2000-AYLTP, are called (Carlson et al., 2004). This type of cut is called a feasibility cut.

If the query point is feasible, an optimality cut is undertaken, and thus the oracle delivers the value of the function and the derivative, or sub-gradient, at the point. In this way "designing" the epigraph of the objective function, Fig. 3.5. The intersection of the sequence of planes defines the localisation set (Drouet, 2006).

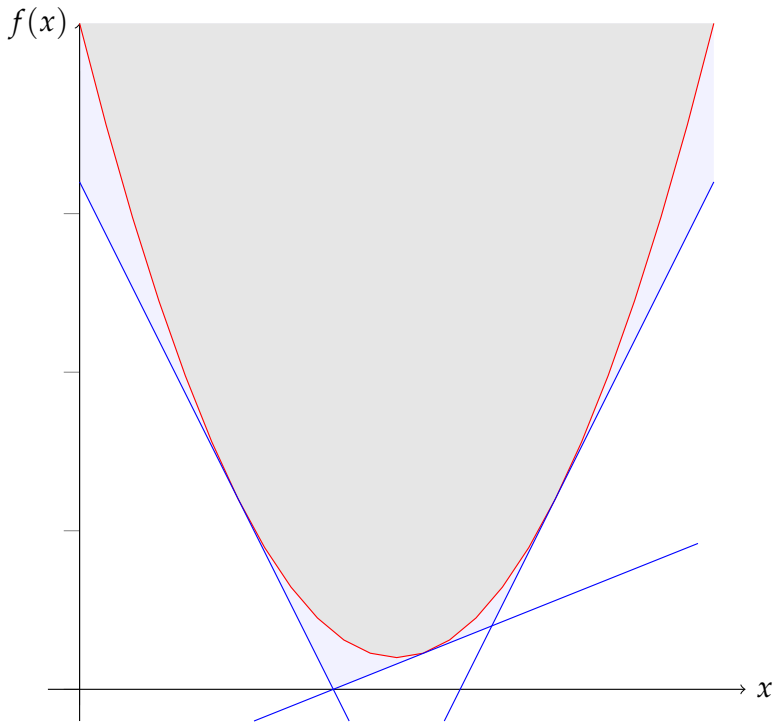

Figure 3.5: Outer linear information of a convex function. The most shaded part inside the parabola is the epigraph of the function, while the area limited by the blue lines represents the linear support that approximates the epigraph of the real function.

The method of ACCPM is efficient due to the use of planes which reduces the ensemble of location with precision and in a reasonable computational time. Moreover OBOE is the tool that permits coupling between two different sub-models in an optimization mode.

3.2.3.1 Mathematical Formulation

OBOE solves the following problem:

$$\min \{f(x)|x \in C \subset \mathbb{R}^n\}, \tag{3.8}$$

where $f(x)$ is the objective convex function and C is the convex feasible set. The epigraph is by definition all the points that lie above the function curve and is given by

$$\left\{(x,z)|z \geq f(x) \subset \mathbb{R}^{n+1}\right\}. \tag{3.9}$$

The oracle provides information about the form of $f(x)$, by performing optimality cuts, and about the form of C by feasibility cuts. Usually, C can be defined as a set of constraints, with the form $h_i(u) \leq 0$:

$$C = \{x|h_i(x) \leq 0, \forall i = 1, \ldots, m\}, \tag{3.10}$$

where m is the number of constraints.

The oracle sends the query point $u \in \mathbb{R}^n$, and depending on the type of cut, it returns (Babonneau et al., 2006; Drouet, 2006):

- if $u \in C$, an optimality cut: it returns a and c such that $a^T u' - c \leq f(x), \forall u' \in C$.
- if $u \notin C$, feasibility cut: it returns a and c such that $a^T u' - c \leq 0, \forall u' \in C$.

In other words, in one dimension the optimality cut represents a linear curve with

$$a = \frac{\partial f(u)}{\partial u}, \tag{3.11}$$

giving the inclination of the line and,

$$c = f(u), \tag{3.12}$$

yielding the intersection. In the case of a feasibility cut, for each non satisfactory constraint $h_i(u)$

$$a_i = \frac{\partial h_i(u)}{\partial u} \tag{3.13}$$

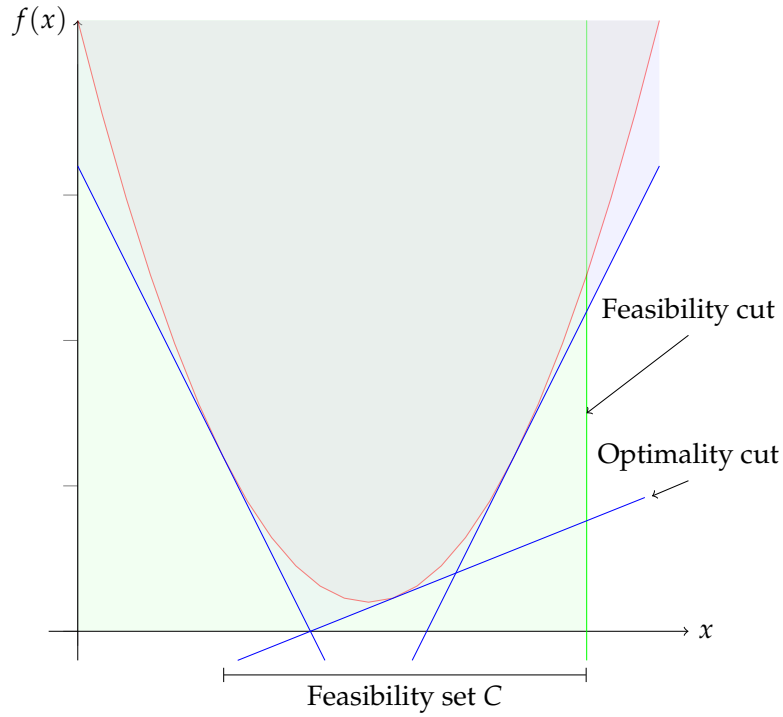

Figure 3.6: Feasibility and optimality cuts of for a one dimensional problem.

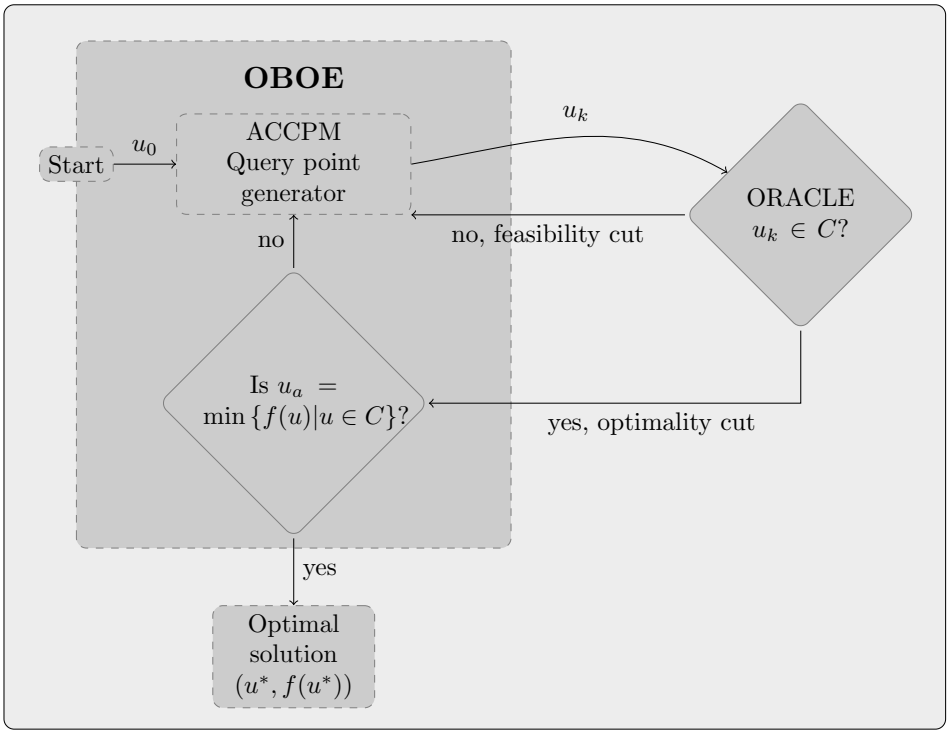

Figure 3.7: Schematic representation of the OBOE algorithm.

and

$$c_i = \frac{\partial h_i(u)}{\partial u} u - h_i(u)\,. \tag{3.14}$$

Figure 3.6 shows, visually, the difference between a feasibility and an optimality cut for a one dimensional problem.

In conclusion, Fig. 3.7 represents the algorithm above explained, in which ACCPM proposes a query point and the oracle delivers the optimality or the feasibility cut depending if the point belongs to the feasibility set. Iteration after iteration, OBOE continues to "cut" the localisation set until its size is small enough to be considered that an optimal solution is found. That is, until the "stop tolerance" is reached.

3.2.4 The Air Quality Model - AUSTAL2000-AYLTP

The AUSTAL2000-AYLTP is the air quality model that has been built to the LEAQ meta-model. The AUSTAL2000 model is the transport core calculator that has been adapted to receive a photochemical module, the AYLTP. The model that resulted from this implementation has been given the name AUSTAL2000-AYLTP model. In order to simplify the notation until the end of this chapter AUSTAL2000-AYLTP is referred as AYLTP.

In the current section it is explained how the selection of the transport core calculator was carried out. The enhancement of the air quality sub-model is the main goal of this work, and therefore its transport calculator model is explained in mode detail in Chapter 4.

Currently, there is a large number of air quality models that have been used in various projects. This fact hinders the survey of all the models available in order to select the model that best suits the goals of each framework.

Each framework has different goals and therefore requires a specific type of model. So far many developments have been made in the field of air pollution. Larger efforts have been put into developing scientific research oriented models, but also forecasting, regulatory and policy support models. Nevertheless few have been specifically developed for the coupling approach inherent to an integrated assessment modelling. Even more rare is to find studies where models have been run in its full mode in an optimisation environment, as it has been shown before, in Table 2.1 of Chapter 2.

In what concerns integrated assessment models which run in optimisation mode, the analysis of air quality is more direct for non-reactive pollutants, where the relation between emissions and concentrations can, more easily, be approximated to a linear relation. However, this is not true for secondary pollutants, such as ozone. The relation between ozone precursors, NO_x and VOC, is not linear. There are nowadays models that can simulate this relation with

acceptable accuracy. Nevertheless, such models demand high computational resources (Carnevale et al., 2008). The optimisation framework involves many evaluation runs and thus the integrated assessment structure must be built strategically.

In the known attempts of using integrated assessment air quality models in optimisation mode, it is typical to apply reduction techniques. The reason for this is that air quality models are generally CPU time intensive (Carnevale et al., 2008). For instances in the LEAQ framework, the air quality model is the most CPU intensive part, as seen in Fig. 3.1. Amongst the most used reduction techniques are linearisation, source-receptor matrices or model reduction.

Linearisation The linearisation technique has been used by Shih et al. (1998), where first a response surface — isopleth — is generated. An isopleth relates the ozone concentration levels to the NO_x and VOC emissions, they are useful to evaluate precursor emission reductions. Afterwards, a mathematical program approximates the response surface. This is a very fast technique that allows the incorporation into an optimised decision making model. Amann et al. (2011) assume a linear relationship between NO_x and VOC emissions and an ozone based air quality indicator.

Source-receptor matrices Source-receptor matrices, which are also a form of linearisation, store information about the contribution of emissions by a source to the concentration levels in a receptor point. They can be used in emission reduction policy studies, where they yield the change of concentration per change in emissions. Oxley et al. (2009) makes use of this technique to calculate the reduction in the concentration of SO_x, NH_3, NO_x and PMs. Nevertheless secondary aerosol chemistry has been ignored and uniform vertical mixing has been assumed to lighten the computational resources. Reis et al. (2005) and Carnevale et al. (2008) also applies this technique in an optimisation integrated assessment study. It has been also used in other policy studies, although not in an optimisation framework (Muller and Mendelsoh, 2006). However, source-receptor matrices are limited to the selected scenarios for which they have been simulated.

Model reduction This is a technique to reduce the order of the equation of the problem. It has been used earlier by Venkatram et al. (1994) who applied a methodology based on semi-empirical relations. Likewise, Carlson et al. (2004) used model reduction techniques in order to reduce the TAPOM models to its simpler form, the TAPOM-Lite, by assuming a first order relationship between the NO_x and VOC concentrations.

Carnevale et al. (2008) points out the need to develop innovative solutions that can reproduce the complex relations between ozone and its precursors, and at the same time simple enough to keep the uncertainties at a minimum level. It is important to define well the objectives of the work and the requirements of the LEAQ integrated assessment framework in order to select a good starting base for the development of the model.

3.2.4.1 Selection of an Air Quality Core Calculator

As mentioned before, LEAQ was designed to run in optimisation mode. At each iteration, the methodology needs the sensitivity of the air quality model, which is estimated by finite differences. Therefore the air quality model is evaluated $(n_v + 1) \times n_i$ times, where n_v is the number of decision variables plus a non perturbed run and n_i is the number of iterations. Hence the submodels are required to be fast.

Table 3.6 summarises the characteristics of the LEAQ air quality framework.

Table 3.6: LEAQ air quality problem definition.

Decision criteria	**Characteristics**	**Class**
Spatial scale	Luxembourg country	Urban to regional
Temporal Scale	Typical day, episodes	Day, hour
Problem definition	Calculation of air quality level for energy scenarios	Regulatory/policy support
Physical and chemical processes	Turbulence, dry deposition and photochemistry	Chemical transport models
IAM operating mode	OBOE	Optimisation

The selection of the air quality model followed the criteria of Table 3.6. It should respect the spatial and temporal domain and resolution of the integrated assessment objectives.

As ETEM has been applied to Grand-Duchy of Luxembourg, the air quality model needed to solve urban to regional phenomena. This is a particular case study, since Luxembourg, as mentioned before, is a country of very small dimensions but with important emission levels.

There exist a large number of air quality models, they differ in their type of application, transport reference or scale. An analysis of existing models, which potentially could fit the LEAQ requirements, has been undertaken. A series of queries has been carried out using the model documentation system

of the European Topic Centre on Air and Climate Change (EIONET, 2012). This model documentation system provides a structured search engine that can be used to group the models in the catalogue by their characteristics. The results of the queries are presented in Fig. 3.8.

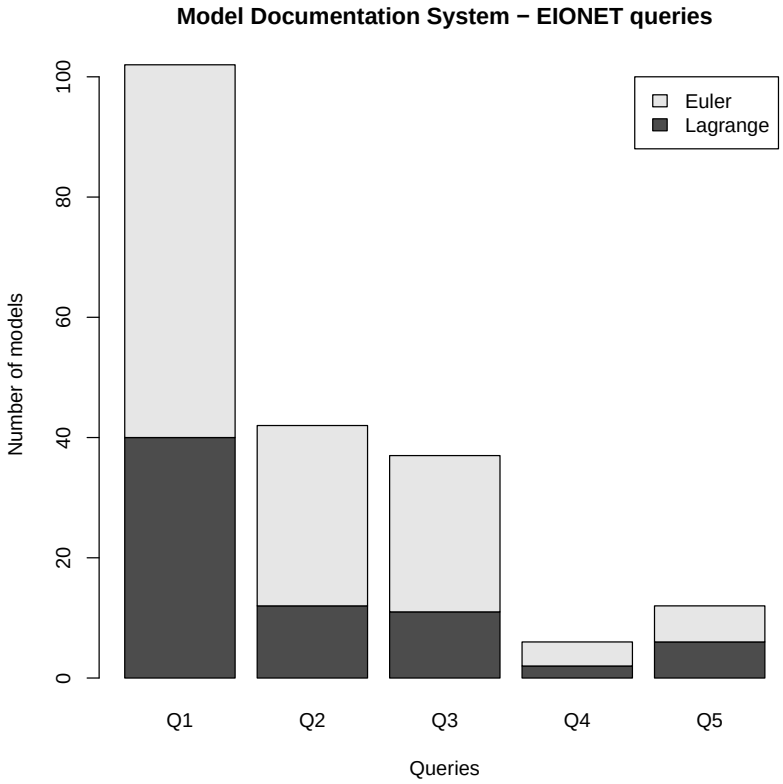

Q1	Queries for Lagrangian/Eulerian models
Q2	Queries calculation of tropospheric ozone
Q3	Queries the Q2 ∩ "Regulatory or policy support models"
Q4	Queries Q2 ∩ "local to regional scale" ∩ "up to 10 minutes CPU time"
Q5	Queries Q3 ∩ "local to regional scale" ∩ "multiple source" ∩ "calculates ambient levels" ∩ "up to 1 hour CPU time"

Figure 3.8: Model Documentation System of the European Topic Centre on Air and Climate Change (EIONET, 2012) queries.

The first query Q1 shows that there are more Eulerian models than Lagrangian. This is to some extent coherent with the direction of model usage in air quality modelling. Query Q2 is also in the line with the fact that it is less complex to implement chemistry in Eulerian models than in Lagrangian models. The third query shows that the great majority of photochemical models are used in regulatory or policy support applications.

On the other hand, query Q4 introduces a strong CPU constrain which reduces significantly the number of models. Analysing the selected models in

query four, it is found these models have been selected because of ambiguous information. For instances, EURAD-IM model is registered as "up to 10 min CPU time", but in a simulation that requires 16 processors. In the same way SILAM model takes less than 10 minutes but for a simple point source.

Finally query Q5 revealed a higher number of models. Likewise when the selected models were evaluated in more detail, seven have been immediately excluded because they are not available under an open-source license. From the remaining models, some had the same type of problems as mentioned before for query Q4, and two presented CPU times between 25 to 50 minutes which is still considered high. The ideal time would be around 10 min, although this is a rather ambitious value.

Additionally, it can also be noted that when the CPU constraint is applied, more Lagrangian models appear in proportion.

Conclusively the current existing models are not yet developed to the point of calculating fast spatially distributed concentrations.

A further model selection study, based on the scales of the LEAQ framework, has been carried out (Aleluia Reis et al., 2009) where a review on air quality models has been carried out in order to choose the most appropriate core model as a basis for the LEAQ air quality model. The review was based on the list provided by the Model Documentation System (EIONET, 2012) developed at the Aristotle University of Thessaloniki and on the COST 728/732 Model Inventory (COST, 2007). Two potential models have resulted from that evaluation, METRAS and AUSTAL2000. These models differ in their transport methods and in their application type. METRAS is a scientific research oriented Eulerian model, whereas AUSTAL2000 is a regulatory Lagrangian particle model.

First, the spatial and temporal scales as well as the resolution were evaluated. As presented in Chapter 2, models can be grouped by scale. Figure 3.9 shows a comparison between the local, urban and mesoscale models.

The LEAQ requirements do not fit inside any of the blocks in Fig. 3.9, but rather lies between the urban to mesoscale blocks. The spatial domain of AYLTP falls in the range of urban to mesoscale models, whereas the grid resolution is typical of a local to urban scale model. This is because of the reduced dimensions of the country, where a course resolution might not reveal enough detail in such a small domain. All these specificities called for a different selection approach of a core calculator.

The analysis of the criteria was made graphically in Fig. 3.10. The graph was constructed using the range of spatial domain and resolution found for each model. Only the open source models were included in this selection process. The models in which the information about the spatial and temporal scale was not available are not shown. In this analysis, it is assumed that

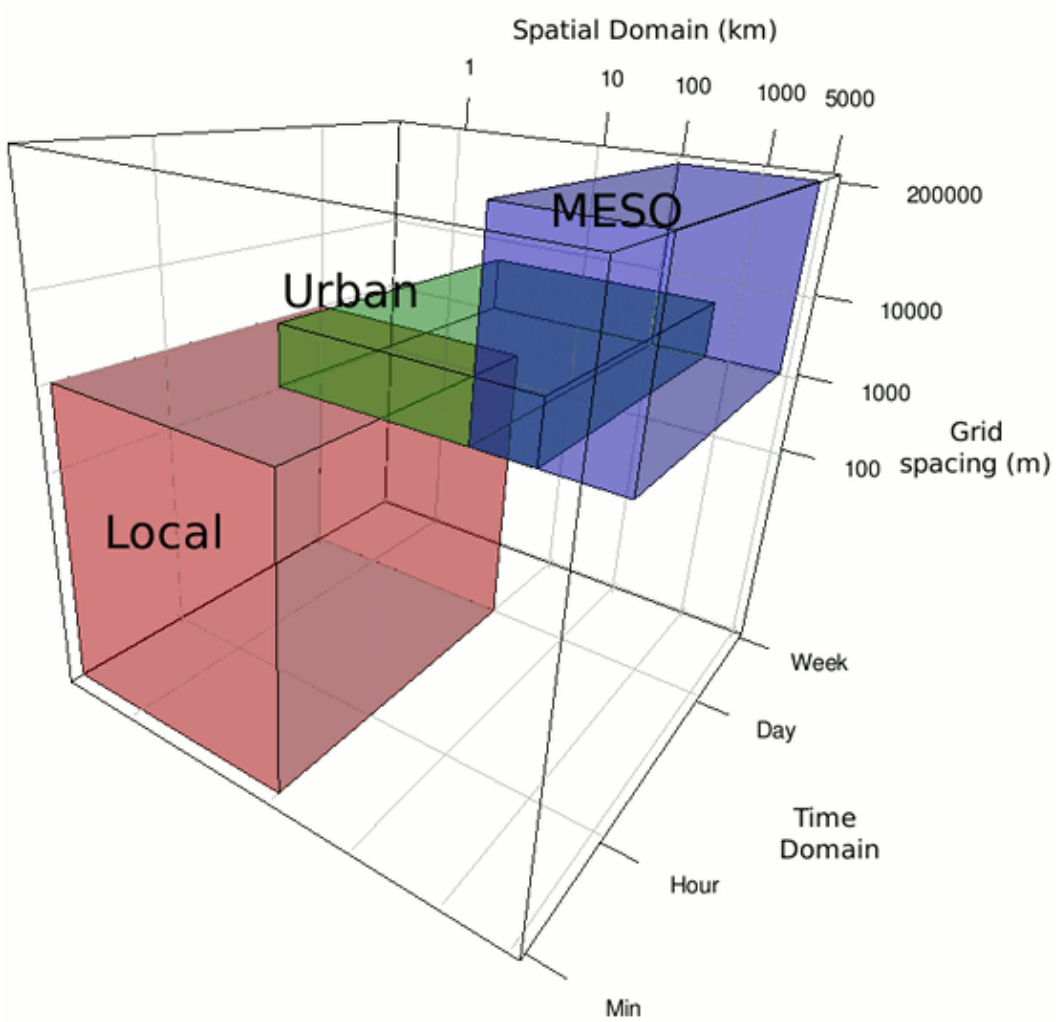

Figure 3.9: Schematic representation of air quality model scales: red represents local scale models, green urban scale, blue the mesoscale/regional.

for a constant CPU time, the grid spacing increases linearly with the spatial domain. Thus instead of a range box, a triangle is used to convey this relationship. The triangles show that the smallest grid spacing available for each model is in fact not applicable for all domain sizes, if one imposes the constant CPU constraint. In practice, imposing a CPU time constraint, the combinations of grid spacing and spatial domain available lie on the shaded area above the triangle's hypotenuse.

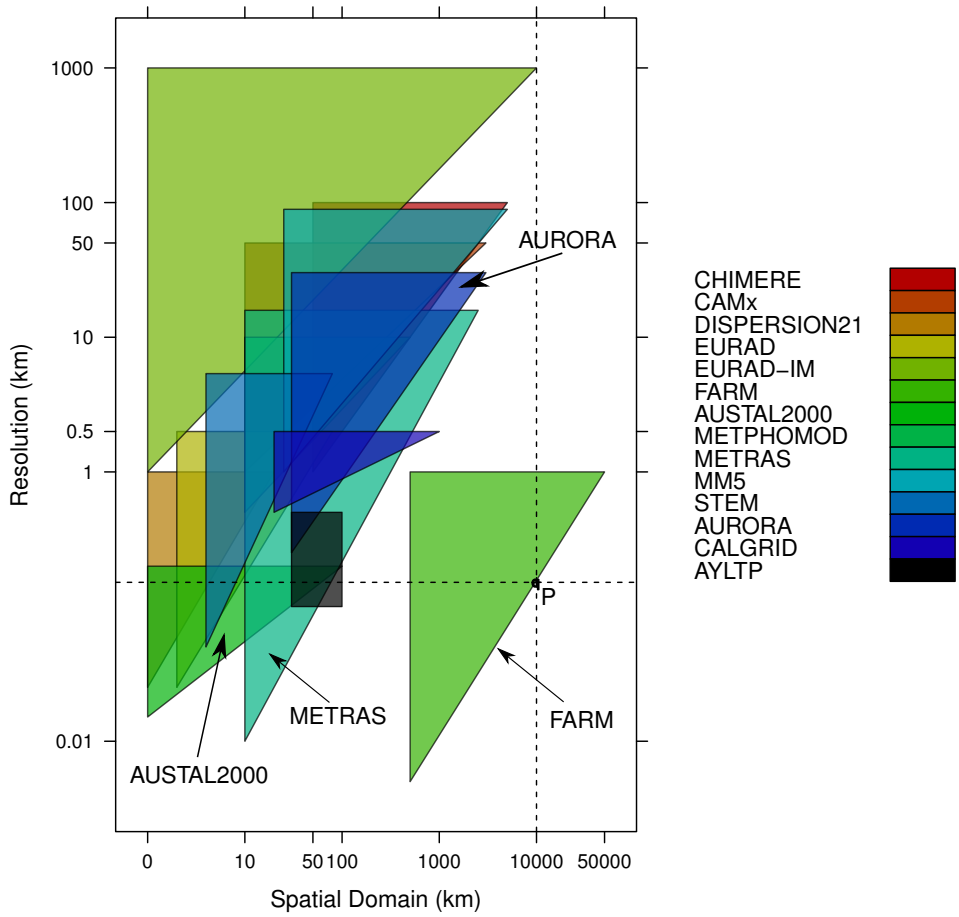

Figure 3.10: Compilation of model's spatial applications, where the back box represents AYLTP. The black point "P" represents an example of how for a certain domain, the grid spacing applicable lies on the shaded area above the horizontal line.

Taking the FARM model as an example, symbolised green triangle where the black point "P" lies in Fig. 3.10, and assuming a spatial domain of 10 000 km, the grid spacing applicable, in practice, would be the range from the horizontal line that crosses the black point up to the top of the shaded area. The same type of analysis can be carried out for grid spacing, i.e. for a certain desired grid spacing, the maximum domain size that can be applied lies on the point where the horizontal line crosses the triangle hypotenuse.

It can be observed that AUSTAL2000 and METRAS are the models that overlap the AYLTP box. Likewise the model AURORA also overlaps the AYLTP range. However the CPU time found for AURORA is considerably high (EIONET, 2012). As a result, AUSTAL2000 and METRAS were found to be the best suited to serve as a core calculator. Both models overlap the AYLTP range, although none of them can, for a fixed CPU time, run with the largest domain and the highest resolution. Therefore, an extended analysis on these two models was carried out. Both models fit the spatial prerequisites, the main difference between them is their fluid motion approach. AUSTAL2000 is a Lagrangian particle model while METRAS is an Eulerian model.

The METRAS model calculates atmospheric flows, mesoscale effects, transport of pollutants and deposition of species. It can handle a complex terrain and chemistry. AUSTAL2000, on the other hand, is a Lagrangian particle model, the official reference model of the German Regulation on air quality control. It simulates the trajectories of tracer particles instead of investigating the fluxes. This approach offers in general more flexibility and precision in modelling the physical processes involved (Janicke, 2002). It simulates the transport by the mean wind field, dispersion in the atmosphere, sedimentation of heavy aerosols, ground deposition and chemical conversion of NO to NO_2. The effect of turbulence on the particles is simulated by a random walk model.

Comparing the two models, METRAS model is more complete, including all the aimed features and rather complex chemical and deposition mechanisms. In contrast, ozone chemistry needs to be implemented in AUSTAL2000. The issue arising from this analysis is to decide between the simplification of the chemistry module of METRAS or the implementation of a simplified chemistry package for AUSTAL2000.

As previously mentioned CPU time is a key factor for this project. Flexibility is another important issue, as the LEAQ meta-model is meant to be applicable to any city. Hence, a flexible grid spacing is desirable. This point is important when one takes into account the availability of the different quality input information for each city, and the city's dimensions and terrain particularities. Furthermore METRAS is not under an open-source license, although it is available for research purposes. This is an excluding factor, since one of the LEAQ project main goals is to provide an open policy support tool.

AUSTAL2000 uses a faster methodology to calculate pollutant's transport, whereas numerical schemes, used in Eulerian models, are CPU expensive (Mathur et al., 2004). The particle approach yields more flexibility, because for a fixed grid spacing and spatial domain, it still allows the adjustment of the number of particles. This adjustment enables a compromise between statistical uncertainty and CPU time, tuning the number of particles.

The LEAQ integrated approach has inherently large uncertainties associ-

ated, which are propagated through all the modules of the LEAQ. Despite the attempt to include the most important factors influencing air quality, it is important to keep a compromise between CPU time and accuracy. Hence, phenomena are treated on a simple level. The air quality model is dependent on the energy model, which calculates the energy scenarios for a one year interval in a 30 year time horizon. Accordingly, certain assumptions and simplifications can be done.

In this sense, AUSTAL2000 better serves the purpose of this work. Its approach is faster and the model structure involves less parameters, thus is more readily adaptable and reduces the uncertainties in the parameters. Nevertheless, it has some disadvantages, mainly because the Lagrangian particle approach is less flexible when dealing with chemistry, because it does not deal with concentrations directly.

Chapter 4

The Air Quality Model

Contents

The necessity of a fast air quality model for LEAQ led to the choice of AUSTAL2000 as the transport core calculator. AUSTAL2000 had to be adapted to receive a photochemical module. The description of the AUSTAL2000 model will be given in this section.

AUSTAL2000 is the official reference model of the German Regulation on Air Quality Control (BMU, 2002). It is a well established Lagrangian particle open source model, available at `http://www.austal2000.de`.

The main answer provided by air quality models is the pollutant's concentration distribution. This can be achieved solving the advection-diffusion equation, either numerically as in Eulerian models, simulating trajectories like Lagrangian models or analytically as in Gaussian models.

Unlike in Eulerian models, in Lagrangian particle models the dispersion process itself is modelled in a coordinate system that moves with the mean wind velocity. The advection and diffusion of a representative sample of particles is simulated and applied to each particle independently.

A plume of air is composed of a large number of particles. The particles are tracers of gaseous pollutants or particulate mater, therefore in this chapter the term "particle" refers to the tracer particles, also called Lagrangian particles, and not to particulate matter, unless stated otherwise. Lagrangian models consider only a sample of particles to describe the fluid and that sample is considered representative of the whole plume. The particles have the same properties of the constituents of the plume and a single Lagrangian particle may carry information of several species, namely the mass of several pollutants.

The particles are transported according to the mean wind velocity and the turbulent velocity. The mean wind velocity is responsible for the displacement for the whole plume, whereas the turbulent velocity is responsible for the dispersion of the plume apart from the central line of the plume. In AUSTAL2000, the turbulent velocity is simulated using a random walk model. The details about the inputs of the model are described in Chapter B.

4.1 Model Concept

The evolution of a gas pollutant's concentration, c_i, is described, as mentioned in Chapter 2, by the advection-diffusion equation. For the ease of understating the term correspondent to the change of concentration due to chemical reactions is left out and it will be explained in detail in Chapter 5. In addition, this description starts with the advection-diffusion equation and not with the more general Fokker-Planck equation to which Lagrangian particles models apply. The advection-diffusion equation, considering there are no chemical reactions, reduces to:

$$\frac{\partial \langle c_i \rangle}{\partial t} + \nabla \cdot (\overline{\mathbf{U}} \langle c_i \rangle) = \nabla \cdot \mathbf{K} \nabla \langle c_i \rangle + \langle S(\mathbf{x}, t) \rangle \,, \ \forall i \in \{1, 2, 3 \ldots, n\} \ , \quad (4.1)$$

where i is the pollutant species, n is the number of pollutants, $\mathbf{U}$ is the wind velocity vector, $\mathbf{K}$ is the turbulent diffusivity tensor, and $S(\mathbf{x}, t)$ is the emission rate at location $\mathbf{x}$. The angle brackets $\langle\rangle$ relates to the average of a sample, while the bar $\bar{}$ refers to a temporal averaging.

Equation (4.1) is the fundamental equation of many air quality model. Considering only gas transport and no sources, Eq. (4.1) reduces to

$$\frac{\partial \langle c_i \rangle}{\partial t} + \nabla \cdot (\overline{\mathbf{U}} \langle c_i \rangle) = \nabla \cdot \mathbf{K} \nabla \langle c_i \rangle \,, \ \forall i \in \{1, 2, 3 \ldots, n\} \quad (4.2)$$

Which gives a concentration field, without the influence of sources, in the Eulerian representation.

4.2 Lagrangian Representation

The Lagrangian form of the equation of transport of the pollutants reads (Wilson and Sawford, 1996):

$$\frac{dc}{dt} = 0 \quad (4.3)$$

This equation represents the variation in time of pollutant's concentration in an elementary volume of air that follows the flow. In this way, the elemental volume, can be viewed as an individual parcel or air which moves with the flow. This is the basis of the Lagrangian representation in which the average pollutant concentration must be related with the distribution of particles.

The Lagrangian approaches simulate trajectories of a sample of Lagrangian particles which follow the flow (Wilson and Sawford, 1996), therefore by construction, the Lagrangian form of Eq. (4.2) is given by Eq. (4.4) expressed in the Lagrangian referential.

$$\frac{\partial \langle c_i \rangle}{\partial t} = \nabla \cdot (\mathbf{K} \cdot \nabla \langle c_i \rangle), \ \forall i \in \{1, 2, 3 \ldots, n\} \ . \tag{4.4}$$

where, $\mathbf{K}$ stands for the diffusivity coefficients. This equation describes the concentration in a reference system which follows the moving particle.

The Lagrangian approach is an alternative way to solve the continuity equation of air pollutants. In the Lagrangian representation, the transport of a particle from a given position x' at time t' to a future time t, can be described by its trajectory $X[x', t'; t]$. In Lagrangian models the pollutants concentration is directly related to the movement and position of the Lagrangian particles. As mentioned before, it follows an ensemble of particles thus the concentration refers to the statistics of the particles' ensemble. Accordingly it is related to the probability of the particle to be in the volume space $\mathbf{x} + d\mathbf{x}$ at time t given by the probability density function, (Seinfeld and Pandis, 2006):

$$\int_V \psi(\mathbf{x}, t) d\mathbf{x} = 1 \ . \tag{4.5}$$

Accordingly, the probability density function $\psi(\mathbf{x}, t)d\mathbf{x}$, which describes the probability of the particle to be in $\mathbf{x}$ at time t can be given by, (Seinfeld and Pandis, 2006):

$$\psi(\mathbf{x}, t) = \int_V P(\mathbf{x}, t|\mathbf{x}', t')\psi(\mathbf{x}', t')d\mathbf{x}' \tag{4.6}$$

In Eq. (4.6), $P(\mathbf{x}, t|\mathbf{x}', t')$ represents the probability that the particle, which is at $\mathbf{x}'$ at time t' will be at $\mathbf{x}$ at time t. The second function in Eq. (4.6) refers to the probability that the particle was previously at $\mathbf{x}'$ at time t', which is integrated for all the possible previous positional points.

Considering a n_p number of particles that share the same $\psi(\mathbf{x}, t)$ function, the concentration is then expressed in terms of the sum of all density functions, (Seinfeld and Pandis, 2006).

$$\langle c(\mathbf{x},t)\rangle = \sum_{p=1}^{n_p} \psi_p(\mathbf{x},t) \tag{4.7}$$

The general formula for the average concentration, in number of particles per volume (Seinfeld and Pandis, 2006),

$$\langle c(\mathbf{x},t)\rangle = \int_V P(\mathbf{x},t|x_0,t_0)\,\langle c(\mathbf{x}_0,t_0)\rangle\,d\mathbf{x}_0 + \int_V \int_{t_0}^{t} P(\mathbf{x},t|\mathbf{x}',t')S(\mathbf{x}',t')dt'd\mathbf{x}'\ , \tag{4.8}$$

where $S(\mathbf{x}',t')$ is the particles' source. The term $P(\mathbf{x},t|\mathbf{x}',t')$, also called transition probability density, can be determined by modelling the velocity field. In differential form Eq. (4.8) yields the Fokker-Planck equation which is a more general form of the classical diffusion equation, describing both turbulent and classical diffusion.

The description of the AUSTAL2000 model that follows, is entirely based on the Verein Deutscher Ingenieure (VDI) guidelines for environmental meteorology part 3 (VDI, 2000) and 8 (VDI, 2002), unless cited otherwise.

4.3 Transport Algorithm

In AUSTAL2000 the pollutant's motion in the atmosphere is modelled using a Markov process. A Markov process is a type of random walk where the stochastic behaviour of a particle after a point in time is independent of its behaviour before this point. The particle's transport is undertaken in time steps τ, normally of the order of seconds. The transport from position x_t at time t, to the position $x_{t+\tau}$ at time $t+\tau$, is given by:

$$\mathbf{x}_{t+\tau} = \mathbf{x}_t + \tau\,[V + u' + Ua]\,, \tag{4.9}$$

where V is the mean wind velocity, u' is the turbulent velocity and Ua is referred to as additional velocity. This additional velocity refers to processes such as buoyant rise or sedimentation velocity.

The turbulent velocity u' is simulated using a Markov chain process.

Smith (1968) proposed a Markov process where the $u'_{t+\tau}$ can be expressed in terms of it's previous turbulent velocity $u'(t)$ and of a random term, by:

$$u'(t+\tau) = R_L(\tau)u'(t) + u'', \tag{4.10}$$

where $R_L(\tau)u'(t)$ is the Lagrangian autocorrelation function and u'' is a random variable (Arya, 1999; VDI, 2000).

The autocorrelation function expresses the correlation of the turbulent velocity in time. A common form of the Lagrangian autocorrelation function is given by (Arya, 1999):

$$R_L(\tau) = \exp\left(-\frac{\tau}{T_L}\right), \tag{4.11}$$

where T_L is the Lagrangian time scale, which is the time that the particle retains the value of a stochastic quantity. It represents the time scale of large eddies present in the flow which are responsible for the correlation of the turbulent velocity values at distinct times.

When τ is zero the autocorrelation function yields unity, contrarily if τ tends to infinity then $R_L(\tau) = 0$. Likewise, in the Markov model in Eq. (4.10), for large values of τ/T_L, $\tau \gg T_L$, $R_L \approx 0$, therefore the turbulent velocity reduces to the random component u''.

Other equations have been proposed for the form of R_L, however it has been shown that the Lagrangian time scale has more influence on the diffusion than the form of R_L (Arya, 1999; VDI, 2000). The Lagrangian time scale T_L is given by the integral of R_L:

$$T_L = \int_0^\infty R_L(\tau) d\tau. \tag{4.12}$$

In AUSTAL2000 the turbulent velocity u' is simulated by a Markov process, according to:

$$u'_{t+\tau} = \Psi(\mathbf{x}_t) \cdot u'_t + w\,, \tag{4.13}$$

where Ψ is a parameter of the random process that represents the autocorrelation coefficient which depends on $\mathbf{x}_t$, and w is a random variable.

The random fluctuation part of Eq. (4.10) is assumed to have zero mean and it is composed of a purely random component $\Lambda(\mathbf{x_t}) \cdot \mathbf{r}$ and a drift velocity W.

$$w = W(\mathbf{x}_t) + \Lambda(\mathbf{x_t}) \cdot \mathbf{r} \tag{4.14}$$

Summarising, the turbulent velocity u is then given by:

$$u'_{t+\tau} = \Psi(\mathbf{x}_t) \cdot u'_t + W(\mathbf{x}_t) + \Lambda(\mathbf{x_t}) \cdot \mathbf{r}, \tag{4.15}$$

where Ψ, W and Λ are parameters of the random walk model, and $\mathbf{r}$ is a vector of random numbers.

The vector $\mathbf{r}$ has the distribution density $p(\mathbf{r})$, which is assumed to be normal:

$$\int p(\mathbf{r}) d^3\mathbf{r} = 1. \tag{4.16}$$

The random vectors are independent from each other and therefore:

$$\int \mathbf{r} p(\mathbf{r}) d^3\mathbf{r} = 0 \tag{4.17}$$

$$\int \mathbf{r}\mathbf{r} p(\mathbf{r}) d^3\mathbf{r} = \mathbf{I}\,, \tag{4.18}$$

where $\mathbf{rr}$ is a dyadic product of two vectors.

The random walk parameters,Ψ, W and Λ, are related with the physical fields:

- $\mathbf{K}$, diffusion tensor;
- Σ, variance of the turbulent velocities;
- $\mathbf{V}$, mean wind field.

The relations between the model parameters and physical parameters $\mathbf{K}$, Σ and $\mathbf{V}$ have been deduced by Janicke (2000). Accordingly,

$$\Psi = (2\mathbf{I} - \tau\Phi) \cdot (2\mathbf{I} + \tau\Phi)^{-1} \tag{4.19}$$

$$\Phi = \Sigma \cdot K^{-1} \tag{4.20}$$

$$\Omega = \Sigma - \Psi \cdot \Sigma \cdot \Sigma^T \tag{4.21}$$

$$W = \frac{\tau}{2}(\mathbf{I} + \Psi) \cdot (\nabla \cdot \Sigma) \tag{4.22}$$

The component Φ represents the reciprocal Lagrangian time scale T_L and $\mathbf{I}$ is the identity matrix. Additionally, Λ is given by the Cholesky decomposition of the tensor Ω:

$$\Omega = \Lambda \cdot \Lambda^T\,, \tag{4.23}$$

where the superscript ^{T} represents the transpose matrix.

The Cholesky decomposition implies that Ω must be a symmetrical positively definite tensor. This constraint influences the choice of τ according to:

$$|\tau\Phi(\mathbf{x})| < 2. \tag{4.24}$$

The drift velocity W is the mean value of the stochastic velocity increment used in the particle algorithm. It prevents systematic errors in the calculation of concentrations assuming inhomogeneous turbulence or when τ is spatially variable. By allowing τ to be a function of space the computational demands are reduced. In this case, W has the following form:

$$W = \frac{1}{2}(\mathbf{I} - \Psi) \cdot [\nabla \cdot (\tau(\mathbf{x})\Sigma)] + \tau(\mathbf{x})\Psi \cdot (\nabla \cdot \Sigma)\,. \tag{4.25}$$

The details about this derivation are given in Janicke (2000).

4.4 Concentration and Dry Deposition

In the previous section it has been shown how the particles are transported. The particles carry the pollutant's mass, and their position, which is a result of transport along the average time interval, yields the concentration. The derivation from mass to concentration is explained hereafter.

Concentration The concentration distribution in space and time is modelled as mean values in discrete cell volumes and time intervals.

For each source s, at the beginning of each averaging time Δt, the initial mass of a pollutant q is allocated to the particles according to

$$m_{0,q}(s) = \frac{E_{s,q}(s, \Delta t)\Delta t}{n_p(s)} \tag{4.26}$$

where $n_p(s)$ is the number of particles released per averaging interval Δt by a source and $E_{s,q}$ is the source emission strength in mass per time.

During the transport, the particles mass can vary due to two reasons, when they contact with the ground surface and by chemical reactions. When a particle is in contact with the ground surface it may transfer mass, this phenomena is called deposition. Each particle carries the following information:

- position $\mathbf{x}$;
- turbulent velocity u';
- mass of pollutant m_q, where q is the pollutant;
- velocity Ua.

The concentration is calculated for every grid cell of a counting grid. The grid is usually identical to the calculation grid on which meteorological and other model parameters are defined. The grid cell indices are i, j, k, for the averaging time interval Δt where, $i \in \{1, ..., n_x\}$, $j \in \{1, ..., n_y\}$ and $k \in \{1, ..., n_z\}$, with n_x, n_y, and n_z is the number of cells in x,y and z directions respectively.

The averaging time is much larger than the time step τ used to move a particle on the order of seconds, typically ten minutes or one hour. The concentration is given as a function of the mass of all the particles that cross cell volume V_{ijk}, during the averaging interval.

Hence $c_{i,j,k,q}$, for a given averaging time interval, is given by:

$$c_{i,j,k,q} = \frac{\sum_{n=1}^{n_p} \int_{\Delta t} \lambda_{ijk,n}(t) m(t) n, q \, dt}{V_{ijk}\Delta t}, \tag{4.27}$$

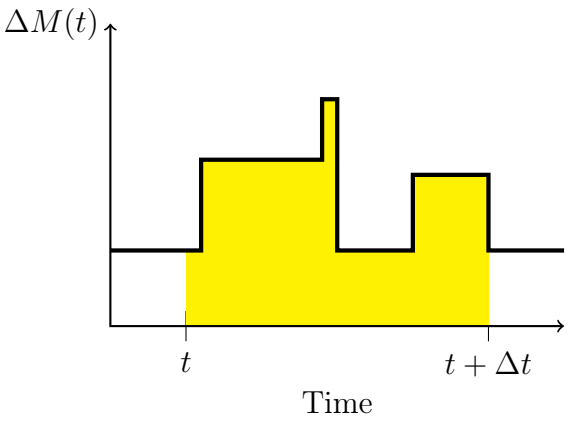

Figure 4.1: Schematic example of mass contribution $\Delta M(t)$ of all particle which cross a cell during the time interval $[t; t + \Delta t]$.

where n_p is the number of particles and

$$\lambda_{ijk,n}(t) = \begin{cases} 1 & \text{if particle } n \text{ crossed } V_{ijk} \text{ during } \Delta t, \\ 0 & \text{otherwise.} \end{cases} \tag{4.28}$$

Figure Fig. 4.1 shows the mass contributions in one cell. During the time interval Δt there has been several contributions to the total mass, these are due to particles which enter the cell during the time step, the peak in Fig. 4.1 is the moment when more particles are in the cell.

As it has been mentioned before, the models are approximations of the real phenomena and are based on assumptions. The degree to which a model can describe the reality can be evaluated. The accuracy of the model results depends mainly on:

- the quality of the input data, which is normally the most important source of inaccuracy and uncertainty;
- the model assumptions;
- the model implementation, such as algorithm and numerical schemes, discretisation, and particle sample size.

AUSTAL2000 automatically calculates the sampling error associated with the use of a limited number of Lagrangian particles, the details of this calculation are presented in Section B.2 of Chapter B.

Dry deposition Dry deposition is the process by which a particle looses mass by adsorption to the ground surface when a contact exists. It is modelled

by assuming that a fraction of the mass, pd_q, is deposited on the ground surface, according to:

$$m_q{}' = (1 - pd_q)m_q, \tag{4.29}$$

where $m_q{}'$ is the mass after the impact with the ground surface. When a particle contacts with the ground surface it is reflected back following the vector normal to the ground surface, and it is transported until it has deposited all its mass.

For heavy aerosols, sedimentation which is the process of gravitational settling is accounted for. It increases deposition and depends on the aerodynamic diameter of the aerosol. As a simulation particle can move downwards only with one single settling velocity, for the case of particulate matter calculations, the Lagrangian particles can only hold the information for particles of the same size, e.g. PM_{10}, $PM_{2.5}$.

The velocity at which a gas deposits on a surface depends on the type of surface and on the pollutant species. Deposition velocities have been derived empirically (VDI, 2000).

The deposition $d_{i,j,k,q}$ over a surface of area A takes the form

$$d_{i,j,k,q} = \frac{\sum_{n=1,l}^{np} \int_{\Delta t} \delta(t - t_{i,j}^{l}) pd_q m_{p,q}\, dt}{A\Delta t}, \tag{4.30}$$

where δ is the Dirac delta function and $t_{i,j}^{l}$ is the time at which a particle contacts with the surface. One particle can touch a surface l times. The Dirac delta function takes the value of unity when $t = t_{i,j}^{l}$, and otherwise is zero.

4.4.1 Turbulence

The Lagrangian representation of equation Eq. (4.4) (Seinfeld and Pandis, 2006; Wilson and Sawford, 1996) is of the form:

$$\langle c(\mathbf{x}, t)\rangle = \int_V P(\mathbf{x}, t|x_0, t_0)\, \langle c(\mathbf{x}_0, t_0)\rangle\, d\mathbf{x}_0\,, \tag{4.31}$$

The probability function $P(\mathbf{x}, t|x_0, t_0)$ is solved using the random walk process, given by the turbulent velocity equation Eq. (4.13), which depends only on the properties of the turbulent wind field. Therefore, it is important to describe the turbulent structure of the atmospheric boundary layer. The boundary layer can be characterised by means of atmospheric stability classes.

Previously in Eqs. (4.15) and (4.19) to (4.22), it is shown how the turbulent velocity is related to the diffusion coefficients $\mathbf{K}$ and the variance of the turbulent wind velocity fluctuations Σ. The determination of $\mathbf{K}$ and Σ

is dependent on the characterization of the atmospheric boundary layer and based on scaling and stratification parameters. In the following sections the atmospheric boundary layer characteristics and the scaling and stratification parameters are presented and described.

4.4.1.1 Atmospheric Stability

The classification of atmospheric stability into classes is commonly used for the parametrisation of turbulent diffusion in the boundary layer.

The atmospheric boundary layer, also called planetary boundary layer, plays a very important role in air pollution. The motion processes that occur in the boundary layer determine the dispersion of the emitted pollutants. This layer is characterised by strong variations of wind velocity, temperature and gas concentrations. Its structure is variable, as the physical and thermal properties will determine its depth, the transport, the diffusion properties and the energy dissipation. Its height is variable, specially over land, ranging from tens of hundreds of meters to kilometres. The height of the boundary layer is generally referred as the mixing height. Figure 4.2 shows a schematic representation of the atmospheric boundary layer, where the potential temperature is given by:

$$\Theta = T \left(\frac{p_0}{p} \right)^{\frac{R}{c_p}} . \tag{4.32}$$

In Eq. (4.32), T is the air temperature, p is air pressure, p_0 is the air pressure at 1000 hPa, R is the gas constant for dry air and c_p is the specific heat of dry air at constant pressure. The potential temperature is the temperature of a given parcel of air if it was brought dry adiabatically from pressure p to p_0.

The atmospheric boundary layer is further characterized by sub-layers, as shown in Fig. 4.2, such as the viscose, Ekman and the Prandtl layers, characterized hereafter. The viscous layer lies between the surface and the roughness length z_0, only molecular diffusion is present in this layer and turbulent diffusion is nonexisting. At the roughness height z_0 the mean wind velocity is assumed to be zero. The Prandtl layer, also called surface layer, occupies the lower part of the boundary layer, generally 10% of its height z_i. In this layer the temperature and wind velocity variations with height are strong, however the turbulent flows may be approximate to constant in relation with height. The wind direction preserves its near surface direction. The Ekman layer is characterised by weaker variations of wind and temperature. The wind direction and velocity adjusts to the geostrophic values of direction and speed. The atmospheric boundary layer represents only the lower part of the troposphere.

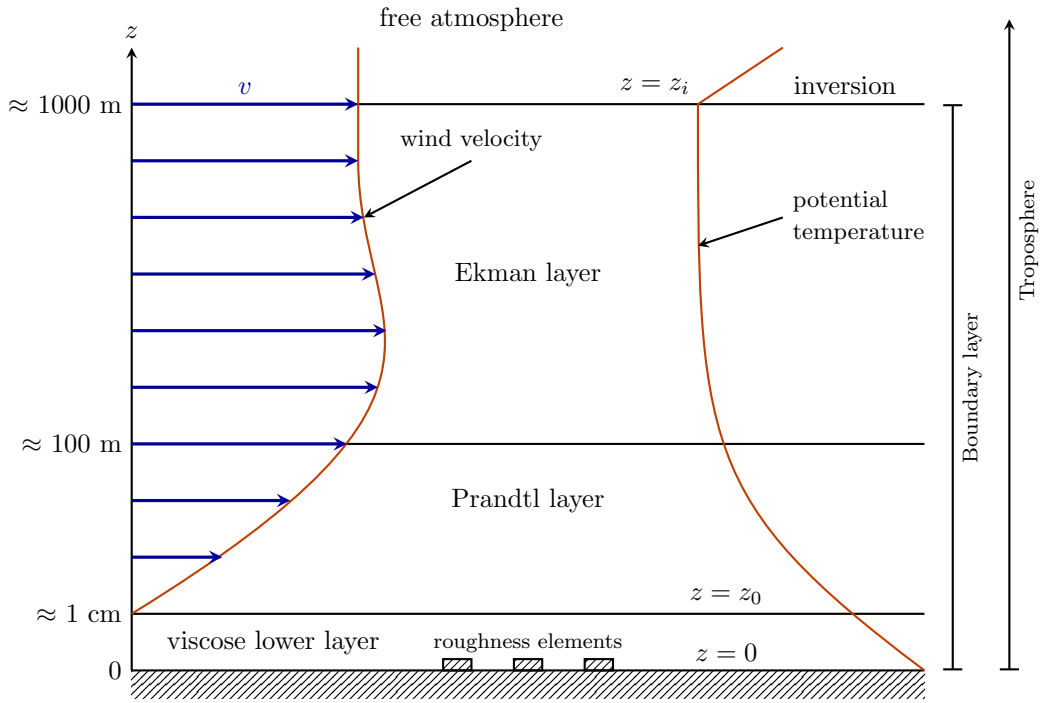

Figure 4.2: General scheme of the atmospheric boundary layer. It depicts the several sub-layers. The wind and temperature profiles are those of an unstable layer and show the strong variations of the meteorological variables. After Arya (1999).

The German classification for atmospheric stability is based on the Klug/Manier classes (VDI, 2000), presented in Table 4.1. The stability of the atmosphere can be understood by inferring what would happen to the points in Fig. 4.3 if one would try to displace them.

Table 4.1: Klug/Manier stability classes

Klug/Manier	Atmospheric stability
I	very stable
II	stable
III/1	stable to neutral
III/2	neutral to unstable
IV	unstable
V	very unstable

A stratified atmosphere is called stable if an air parcel tends to return to its initial position when lifted. As opposed, in an unstable situation the air parcels will keep moving further away from the initial position. The atmosphere is considered neutral if no buoyancy force acts on the displaced air parcel, in this case the parcel remains where it was displaced (Arya, 1999).

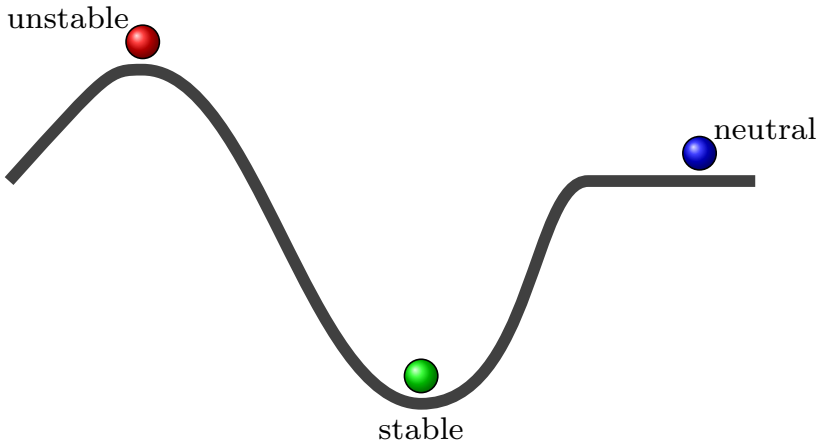

Figure 4.3: Atmospheric stability states.

4.4.1.2 Scaling Parameters

Scaling parameters which can be used are the characteristic temperature Θ_*, the convective scaling velocity w_* and the friction velocity u_*. These parameters are used in the calculation of the variance of the turbulent velocities.

The friction velocity, also known as the shear-stress velocity, is useful to express shear stress in velocity units in order to compare the velocity flow with the velocity related to shear between two layers of that flow.

$$u_* = \sqrt{\frac{\tau_s}{\rho}}\,. \tag{4.33}$$

In Eq. (4.33), τ_s is the shear stress at the surface and ρ is the air density.

The characteristic temperature is given by:

$$\Theta_* = \frac{-\overline{(w'\Theta')}_0}{u_*}, \tag{4.34}$$

where $\overline{(w'\Theta')}_0$ is the heat flux at the ground, i.e. $z = z_0$. When strong ascending forces prevail, as in the case of unstable atmosphere, the convective scaling velocity is used:

$$w_* = \left(\frac{g}{\bar{\Theta}}\overline{(w'\Theta')}_0 z_i\right)^{\frac{1}{3}}, \tag{4.35}$$

where $\bar{\Theta}$ is the time average potential temperature and g is the gravitational acceleration.

4.4.1.3 Stratification Parameters

Stratification parameters help to characterise the relation of the vertical temperature gradients with turbulence. In the atmospheric boundary layer, the production of turbulence may be caused by thermal or mechanical forces, such as wind blowing over a terrain. The vertical temperature differences provoke ascending forces that generate turbulent movements. Likewise, the wind shear adds to the turbulence in the surface layer.

The flux Richardson number Ri_f , is equal to the ratio between the production of turbulent kinetic energy by buoyancy over the production by shear stress, in Eq. (4.36).

$$Ri_f = \frac{g}{\bar{\Theta}} \frac{\overline{w'\Theta'}}{\overline{w'u'}\frac{\partial \bar{u}}{\partial z}}. \tag{4.36}$$

The flux Richardson number Ri_f is dimensionless and can be used to provide a measure of stability.

The Monin-Obukhov similarity theory is widely applied to characterise the surface layer (Jacobson, 2005). The Monin-Obukhov length L is the height at which turbulence driven by buoyancy is dominant over the mechanically produced turbulence, in Eq. (4.37).

$$L = -\frac{u_*^3}{\kappa \frac{g}{\bar{\Theta}} \overline{(w'\Theta')}_0}, \tag{4.37}$$

where κ is the von Karman constant, $\kappa = 0.4$.

The parameters Ri_f and L relate with atmospheric stability according to Table 4.2. The roughness length is the height at which the wind speed is

Table 4.2: Ri_f and L relation with atmospheric stability.

Ri_f	L	Atmospheric stability
> 0	> 0	Stable
< 0	< 0	Unstable
$= 0$	$L \to \infty$	Neutral

assumed to be zero. It gives information on the ground surface characteristics and it affects the intensity of mechanical turbulence at the ground surface.

AUSTAL2000 converts the information of stability classes and roughness lengths according to Table 4.3.

Table 4.3: L in meters as a function of of stability class and z_0.

Klug/Manier	Roughness length z_0 in meters								
	0.01	0.02	0.05	0.10	0.20	0.50	1.00	1.50	2.00
I	7	9	13	17	24	40	65	90	118
II	25	31	44	60	83	139	223	310	406
III/1	99999	99999	99999	99999	99999	99999	99999	99999	99999
III/2	-25	-32	-45	-60	-81	-130	-196	-260	-326
IV	-10	-13	-19	-25	-34	-55	-83	-110	-137
V	-4	-5	-7	-10	-14	-22	-34	-45	-56

4.4.1.4 Vertical Velocity Profiles

The velocity profiles are used to calculate the scaling parameters, with the use of the stratification parameters. The vertical wind and temperature gradients are given as functions Φ_m and Φ_h by Eqs. (4.38) and (4.39):

$$\frac{\kappa z}{u_*}\frac{\partial \bar{u}}{\partial z} = \Phi_m(\zeta) \tag{4.38}$$

$$\frac{\kappa z}{\Theta_*}\frac{\partial \bar{\Theta}}{\partial z} = \Phi_h(\zeta)\,, \tag{4.39}$$

where the Monin-Obukhov length is used in combination with the height above the ground z, as a length dimensionless parameter:

$$\zeta = \frac{z}{L}\,. \tag{4.40}$$

Vertical profile functions have been formulated experimentally in several works. The functions for Φ_m and Φ_h have been proposed by Dyer and Hicks (1970) and are applicable to the Prandtl layer.

$$\Phi_m = \begin{cases} 1 + 5\frac{z}{L} & \text{if } \frac{z}{L} > 0, \\ \left(1 - 15\frac{z}{L}\right)^{-\frac{1}{4}} & \text{if } \frac{z}{L} < 0. \end{cases} \tag{4.41}$$

$$\Phi_h = \begin{cases} 0.74 + 5\frac{z}{L} & \text{if } \frac{z}{L} > 0, \\ 0.74\left(1 - 9\frac{z}{L}\right)^{-\frac{1}{2}} & \text{if } \frac{z}{L} < 0. \end{cases} \tag{4.42}$$

Sequentially, further works have been carried out and extrapolated to the entire boundary layer (VDI, 2002), for heights above the roughness length, Eq. (4.43).

$$\Phi_m(\frac{z}{L}) = \begin{cases} \left(1 - 15\frac{z}{L}\right)^{-\frac{1}{4}} & \text{if } \frac{z}{L} < 0, \\ 1 + 5\frac{z}{L} & \text{if } 0 \leq \frac{z}{L} < 0.5, \\ 8 - 4.25 + \frac{L}{z} = \left(\frac{L}{z}\right)^2 & \text{if } 0.5 \leq \frac{z}{L} < 10, \\ 0.7585\frac{z}{L} & \text{if } \frac{z}{L} > 10. \end{cases} \tag{4.43}$$

By rearranging Eq. (4.38),

$$\frac{\partial \bar{u}}{\partial z} = \frac{u_*}{\kappa}\frac{1}{z}\Phi_m\left(\frac{z}{L}\right), \tag{4.44}$$

and integrating Eq. (4.44) from z_0 to z, the mean wind velocity $\bar{u}$ is given as a function of u_*, $\frac{z}{L}$ and z_0,

$$\bar{u}(z) = f\left(u_*, \frac{z}{L}, z_0\right). \tag{4.45}$$

The *TA Luft* function f is described in detail in VDI (2002). The parameter u_* is obtained by solving Eq. (4.45) for a given wind speed at a given height.

Boundary layer height The boundary layer height z_i is another important parameter for the determination of the Lagrangian model turbulence parameters, $\mathbf{K}$ and Σ. It may be given as a function of the stability classes, according to Table 4.4.

Table 4.4: z_i as a function of Klug/Manier stability class

Klug/Manier	z_i in meter
I	as defined in Luft (2002)
II	as defined in Luft (2002)
III/1	800
III/2	800
IV	1100
V	1100

4.4.1.5 Turbulence Parametrisation

As mentioned before in Section 4.3, the standard deviation of the wind fluctuations Σ are required by the Lagrangian particle model Eqs. (4.20) to (4.22). It is explained hereafter how the $\sigma_u, \sigma_v, \sigma_w$, which are the diagonals of the matrix Σ, are calculated using the scaling parameters. They can be described by the boundary layer parameters, in the direction of the mean wind α,

$$\sigma_{u\alpha} = \left[(a_{ud}u_*)^3 + (b_{ud}w_*)^3\right]^{\frac{1}{3}}, \forall \alpha \in \{u, v, w\}, \tag{4.46}$$

where a_{ud} and b_{ud} are coefficients which have been determined experimentally and are found in the dedicated literature. In the case of "neutral" to "unstable" atmospheric stability classes, the standard deviation of the wind components are given by VDI (2002):

$$\sigma_u = \left[(2.4u_*)^3 + (0.59w_*)^3\right]^{\frac{1}{3}} \exp\left(-\frac{z}{z_i}\right), \tag{4.47}$$

$$\sigma_v = \left[(1.8u_*)^3 + (0.59w_*)^3\right]^{\frac{1}{3}} \exp\left(-\frac{z}{z_i}\right), \tag{4.48}$$

$$\sigma_w = \left\{\left[(1.3u_* \exp\left(-\frac{z}{z_i}\right)\right]^3 + \left[(1.3\left(-\frac{z}{z_i}\right)^{\frac{1}{3}}\left(1 - 0.8\frac{z}{z_i}\right)w_*\right]^3\right\}^{\frac{1}{3}}. \tag{4.49}$$

Likewise, for stable atmospheric conditions $w_* = 0$, these equation reduce to:

$$\sigma_u = 2.4u_* \exp\left(-\frac{z}{z_i}\right), \tag{4.50}$$

$$\sigma_v = 1.8u_* \exp\left(-\frac{z}{z_i}\right), \tag{4.51}$$

$$\sigma_w = 1.3u_* \exp\left(-\frac{z}{z_i}\right). \tag{4.52}$$

Lagrangian time scales The Lagrangian time scale is a mean to quantify the time that a particle remains correlated with its previous type of motion. They are necessary for the determination of the diffusion coefficients. Kolmogorov (1941) suggested a theory for small-scale motions with high Reynold's numbers. It relies on the fact that energy is transferred from larger to smaller eddies, and that for small scales the turbulent kinetic energy is dissipated into heat due to viscosity.

Based on Kolmogorov's theory, a relation between variance of the turbulent velocities exists, for the lower part of the convective layer:

$$T_{Ld} = \frac{2\sigma_{u\alpha}^2}{C_0\varepsilon}, \forall\alpha \in \{u, v, w\}, \tag{4.53}$$

where C_0 is the Kolmogorov constant, and ε is the dissipation rate of turbulent kinetic energy.

The Kolmogorov constant values can be found in literature and depend on the atmospheric stability and on the direction. Additionally, ε for neutral to

unstable stability classes, is given by (VDI, 2002):

$$\varepsilon = \max\left\{\frac{u_*^3}{\kappa z}\left[\left(1-\frac{z}{z_i}\right)^2 + 2.5\kappa\frac{z}{z_i}\right] + \frac{w_*^3}{z_i}\left[1.5 - 1.3\left(\frac{z}{z_i}\right)^{\frac{1}{3}}\right], \frac{u_*^3}{\kappa z}\right\}. \tag{4.54}$$

In the case of stable conditions ε is given by:

$$\varepsilon = \frac{u_*^3}{\kappa z}\cdot\left(\Phi_m - \frac{z}{L}\right), \tag{4.55}$$

where Φ_m is given by Eq. (4.41).

Diffusion coefficients The diffusion coefficients relate to the variances of the turbulent speed and the Lagrangian time scale, according to, (VDI, 2002):

$$K_u = \sigma_u^2 T_{Lu}, \tag{4.56}$$
$$K_v = \sigma_v^2 T_{Lv}, \tag{4.57}$$
$$K_w = \sigma_w^2 T_{Lw}. \tag{4.58}$$

K_u, K_v, K_w stand for the diffusion coefficients and T_{Lu}, T_{Lv} and T_{Lw} for the Lagrangian time scales.

4.4.2 Diagnostic Wind Field

The wind field model, TALdia, is a diagnostic wind field, which is part of the AUSTAL2000 model. It is used to calculate the wind fields in the case of a complex terrain. Diagnostic wind field models provide three dimensional stationary wind fields for a given meteorological situation. Diagnostic wind models are considered to perform well with sufficiently accuracy and in a reasonable computationally time (Moussiopoulos et al., 1988). They use as input data, usually a time series of observed data. The diagnostic wind field model is initialized by a homogeneous wind field. This diagnostic procedure then adjusts the wind field locally such that the normal component at boundary surfaces (for example the ground) vanishes and that the divergence vanishes in every grid cell in order to yield an incompressible flow field.

The wind field is calculated on the Arakawa-C grid. In this grid, the velocities are defined at the grid faces, for instances the x-component of the velocity is given as an average value over the face of the cell which has the normal vector parallel to the x axis. The advantage of this type of grid is that the divergence can be easily calculated for every grid cell.

The wind field calculation follows these steps, for a simulation with terrain but without the inclusion of buildings (Janicke, 2009):

1. An approximately homogeneous incoming flow field is generated and the coordinate system is adjusted according to the terrain. This provides an estimation of the wind filed based on observations.

2. The flow is adjusted to the terrain profile, accounting for the atmospheric stability the surface roughness, and a divergence-free wind field is created.

3. The logarithmic vertical profile of the Prandtl layer is imposed.

4. Finally, the diagnostic wind field is generated by removing the divergence for the second time.

TALdia generates the vertical velocity profiles and the turbulence parameters that the Lagrangian model requires, Σ and $\mathbf{K}$. The turbulence parameters are determined as a function of the meteorological parameters: atmospheric stability, surface roughness and wind velocity.

The characteristic boundary layer parameters used are:

- friction velocity u_*;
- Monin-Obukhov length L;
- boundary layer height z_i.

These meteorological parameters are given at a reference point, the anemometer which has been selected for the study.

The advection and diffusion algorithms have been analysed individually, with the objective of a better understanding of the model transport algorithms. Each of the processes have been isolated and compared with the analytical solutions. This analysis is presented in Chapter C.

Chapter 5

Ozone Photochemistry

Contents

Photochemistry is the underlying chemical mechanism that occurs under the influence of light. Tropospheric ozone is formed as a result of a series of gas-phase reactions of volatile organic compounds and nitrogen oxides in the presence of sunlight. Therefore the formation of ozone in the troposphere is the result of photochemical processes.

In order to assess ozone, O_3, control strategies, the O_3 concentrations must be analysed in relation to its precursors, NO_x and VOC. Ozone precursors are primary pollutants of which the sources are identifiable and known, therefore their emissions can be reduced by controlling the factors which contribute to emissions, such as efficiency of production processes (Kumar et al., 2008). However, this is not the case of ozone itself which is formed via photochemical reactions between NO_x and VOC.

The complete reaction system that leads to atmospheric ozone production includes hundreds of different species and thousands of reactions. Alternatively and for practical reasons, the chemistry of photochemical models generally include approximately 50 to 100 compounds and 100 to 200 chemical reactions, (Russell, 1997). Nevertheless the ozone formation can be understood with a simplified VOC-NO_x mechanism.

The NO_2, NO and O_3 cycle, described by Eqs. (5.1) to (5.3), starts with

the photolysis of NO_2:

$$NO_2 + h\nu \rightarrow NO + O \ (\lambda < 424\,nm) \tag{5.1}$$
$$O + O_2 + M \rightarrow O_3 + M, \tag{5.2}$$

where M represents a molecule which is able to absorb the excess vibrational energy stabilising the O_3 formed, normally it is NO_2 or O_2 (Mazzeo et al., 2005).

Equation (5.2) is the only significant source of ozone in the atmosphere (Seinfeld and Pandis, 2006). However O_3 is rapidly consumed in the oxidation of NO to regenerate NO_2:

$$O_3 + NO \rightarrow NO_2 + O_2 \tag{5.3}$$

In case no other compound is present, this cycle will reach an equilibrium and there will not be enough ozone to result in an ozone episode. The competition between NO_x and VOC for the hydroxyl radical (OH) is the key factor in breaking the NO_x cycle. In Fig. 5.1 the VOC-NO_x chemistry is simplified to hydrocarbons (RH)-NO_x reactions, in which RH are a group of VOC. Figure 5.1 shows the two types of regimes which define different ozone behaviours, defined as NO_x-saturated, also called VOC-limited, and NO_x-limited.

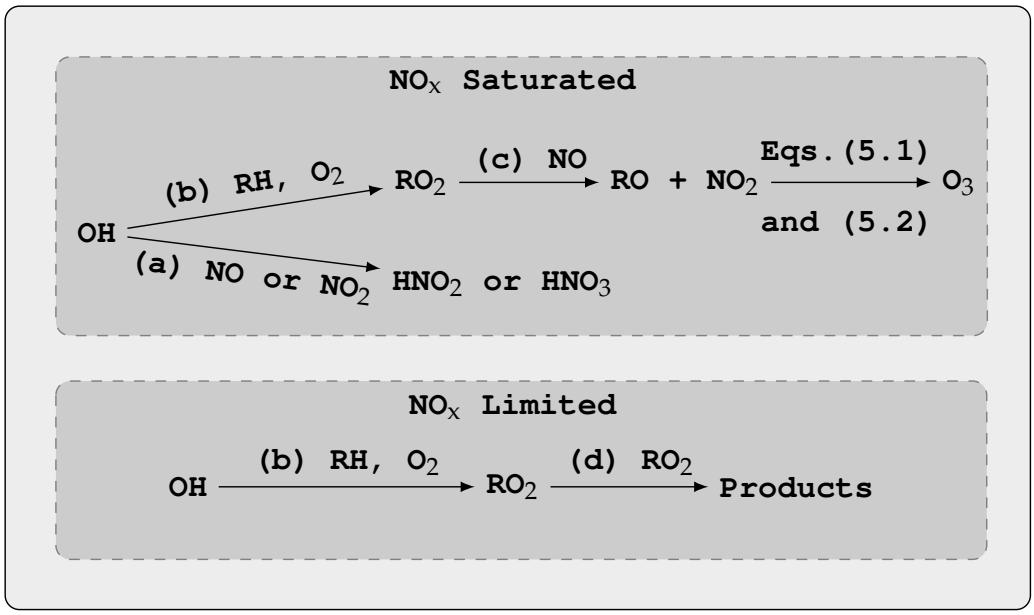

Figure 5.1: Generalized NO_x-VOC mechanism of ozone formation, inspired in Pearson (2001).

In urban areas, typically NO_x-saturated, where the large volume of road traffic produces high NO_x concentrations, OH-NO_x reaction dominates, represented by reaction (a) in Fig. 5.1. The consumption of NO_x will make

its concentration decrease and the VOC/NO_x ratio increase thus making the reaction with RH, reaction (b) in Fig. 5.1, more probable. Thus this NO_x reduction will form more alkyl peroxy radicals (RO_2) through reaction (b), however in this regime NO_x is still in excess in relation to the RO_2 and reaction (c) will tend to occur instead of (d). Via reaction (c) NO is oxidized to NO_2 by RO_2, leading to ozone production through Eqs. (5.1) and (5.2), thus increasing ozone. Therefore, in this regime a reduction in NO_x leads to an increase in ozone levels.

Contrarily, in sub-urban and rural areas, where the NO_x emissions are typically lower, the ratio VOC/NO_x is higher. Consequently OH tends to react with RH through reaction (b). Thus the atmospheric ozone build up will depend on the competition between (c) and (d). When NO_x is decreased the ratio VOC/NO_x will increase thus the quantity of NO relative to RO_2 will decrease and reaction (d) is more probable than (c), reducing ozone levels. This is characteristic of NO_x-limited regimes, where a decrease in NO_x causes a decrease in ozone concentrations. In the same way, it can be said that in this regime increasing NO_x leads to an increase in ozone. This is the reason why ozone is typically higher in rural areas.

There is a value of the ratio VOC/NO_x for which OH will react equally with NO_x and VOC. This value depends on the VOC composition, as the OH reaction varies with the different VOC species (Seinfeld and Pandis, 2006). This regime is often referred as transitional, and it typically occurs at the borders of the cities in sub-urban zones.

AUSTAL2000 does not include a chemical module to calculate the ozone concentrations. The implementation of such a photochemical module into AUSTAL2000 has required code adaptations and the development of a methodology to model ozone photochemistry. Details of the code adaptations and modifications are presented in Chapter E.

It has been shown how the transport and diffusion terms of the advection-diffusion equation Eq. (5.4), previously presented in Chapter 4, are solved in AUSTAL2000-AYLTP.

$$\frac{\partial \langle c_p \rangle}{\partial t} + \nabla \cdot \left(\left\langle \bar{U} \right\rangle \langle c_p \rangle \right) = \nabla \cdot \left(\mathbf{K} \nabla \langle c_p \rangle \right) + \boxed{R_p(\langle c_1 \rangle, \cdots \langle c_p \rangle, T, t)} + \langle S(\mathbf{x}, t) \rangle \ , \quad \forall p \in \{1, 2, 3 \ldots, n\} \, . \tag{5.4}$$

The second term on the left hand side, highlighted by a red box, represents the change of the species concentration due to the photochemical reactions. In this chapter, the methodology to model this term avoiding a high computational burden is presented.

Hereafter, the NO_x and O_3 concentrations are expressed in ppm and the VOC in ppmC, unless specified otherwise.

5.1 Quasi-Linear Production Rates

As it has been explained the photochemical processes involve a large group of species and reactions. Hence photochemistry is, generally, modelled using a limited number of pollutants and reactions. Despite this fact, chemistry is generally one of the most CPU time expensive part of air quality models. This is the reason why model-reduction techniques are often applied in integrated assessment studies (Amann et al., 2011; Carnevale et al., 2008; Kalachev and Field, 2001; Reis et al., 2005; Shih et al., 1998).

The calculations of chemical reactions vary in complexity, ranging from first order reactions to very elaborated reactions chains. These reactions are described by chemical mechanisms which have been developed both for Eulerian and Lagrangian model approaches (Moussiopoulos et al., 1996). However, in Lagrangian models, the incorporation of higher order chemical reactions is very complex (Alessandrini and Ferrero, 2009; Nguyen et al., 1994; Seibert and Frank, 2004; Sportisse, 2007; VDI, 2000).

Lagrangian models deal with the mass fractions of the Lagrangian particles and not, directly, with concentrations thus higher order chemical mechanisms can not be directly applied. This is in contrast to first-order reactions which can be carried out within every particle individually and independent of the other particles. Accordingly, the photochemistry in AUSTAL2000 has been treated using quasi-linear reaction rates. It must be noticed here that these are rates of production, or depletion i.e. negative production, of a pollutant restricted to a given set of conditions and not a reaction rate of a stoichiometric reaction.

In this work, a set of initial conditions, defined by meteorological variables and initial concentrations, is simulated by a box model. The initial and the resulting final concentrations are then used to calculate the production rates, which are stored in a Look-up Table (LUT). The LUT is incorporated within AUSTAL2000, which reads the LUT based on the initial conditions, retrieves the correspondent production rates and uses them to affect a mass of the Lagrangian particle.

Ozone exhibits a non-linear behaviour, as it is the result of the interaction of many species and meteorological variables. Chang and Rudy (1993) states that despite that, it is possible to assume that under a certain number of restricted conditions a linear production rate holds. Shih et al. (1998) has adopted a similar approach using a local linear approximation to the non-linear behaviour of ozone photochemistry.

The previous air quality model prototype, TAPOM-Lite (Zachary et al., 2003), applied a Quasi-Steady State Assumption (QSSA) in order to reduce the ozone chemistry to only three species, O_3, NO_x and VOC. The QSSAs are widely used model reduction methodologies (Sportisse, 2007). This as-

sumption is based on the differences of the time scales of the reactions. The gas phase reaction dynamics reduction is achieved by distinguishing the behaviour of chemical kinetics (Djouad and Sportisse, 2003; Kalachev and Field, 2001; Zachary et al., 2003). This method assumes that the fast reaction rates can be assumed to be zero, since the intermediate species involved in the fast reaction, have a very short time of existence compared to the species involved in the slow reactions (Sportisse, 2007).

The ozone photochemical dynamics can be characterized by two sets of chemical species, the ones which have a fast time scale, T_f, as opposed to a slow time scale, T_s.

The ratio between both scales $\epsilon = \frac{T_f}{T_s}$ is used to scale the species concentration c,

$$\frac{\partial c}{\partial t} = f(c) \tag{5.5}$$

$$\epsilon \frac{\partial c_f}{\partial t} = f_f(c_f, c_s) \tag{5.6}$$

$$\frac{\partial c_s}{\partial t} = f_s(c_f, c_s), \tag{5.7}$$

where c_f and c_s are the fast and the slow species concentrations, and f_f and f_s represent the fast and slow chemical dynamics, respectively.

The quasi-steady state assumption applies (Sportisse, 2007):

$$0 = f_f(c_f, c_s) \tag{5.8}$$

$$\frac{\partial c_s}{\partial t} = f_s(c_f, c_s)\ . \tag{5.9}$$

Equation (5.8) means that the rate of production of and depletion of intermediate species, fast species, are considered equal (Zachary et al., 2003). This method has been applied by Zachary et al. (2003) in order to reduce the ozone photochemistry to the study of three main species, O_3, NO_x, and VOC.

In this framework, the photochemical module has also been reduced to these three species, to investigate the asymptotic levels of ozone pollution. However in this case, the photochemical mechanism is not reduced, because it is pre-simulated by a box model. The box model, uses the levels of O_3, NO_x, and VOC restricted by a set of meteorological conditions, e.g. temperature, relative humidity and zenith angle, to solve the Carbon Bond CB-IV chemical mechanism (Gery et al., 1988) over a stipulated interval. The meteorological variables used to set the conditions of a given production rate are: temperature T, relative humidity RH and the zenith angle θ. The resulting concentrations of O_3, NO_x, and VOC are used to calculate a production rate for each pollutant. The rates are stored in a LUT and the LUT is attached

to AUSTAL2000-AYLTP, which "searches" for the closest condition, fixed by T, RH, θ and the pollutants concentrations, in the table and receives the correspondent production rates. The rates are used in AUSTAL2000-AYLTP to affect the masses of the Lagrangian particles.

The box model, OZIPR (Gery and Crouse, 1990) has been used to calculate the production rates for the LUT. The calculation of the production rates is based on six variables: O_3, NO_x and VOC concentrations, temperature, relative humidity and zenith angle.

The AYLTP module calculates the reaction rates Ks_p, for each pollutant p,

$$\frac{\partial c_p}{\partial t} = Ks_p. \tag{5.10}$$

For each of the model variables, intervals of values have been set. The intervals have to be selected using probable values of each variable. However, this model is designed as a policy support tool and its purpose is to respond to strong variations of the variables which might occur in a mid-long term, e.g. 20–30 years. Therefore, selection of the intervals must also reflect this fact.

OZIPR has then been run for all possible combinations of values of the selected intervals of each variable. The resulting concentrations have been stored in the LUT and used to calculate the reaction rates, Ks, for all the reactive pollutants $p \in \{NO_x, \text{VOC}, O_3\}$, according to

$$Ks_p(c_p(t), \Omega) = \frac{c_p(t + \Delta t; c_p(t), \Omega) - c_p(t)}{\Delta t}, \Omega = \{T, RH, \theta\}, \tag{5.11}$$

where c is concentration, t is the time, Δt is the time averaging interval and Ω is a tuple of the meteorological variables: temperature T, relative humidity RH and zenith angle θ. The final concentration $c_p(t+\Delta t, c_p(t), \Omega)$ is calculated by OZIPR and is dependent on the concentrations of the pollutants and the meteorological conditions. The rates resulting from all the possible combinations of variables are stored in the LUT. The LUT is then attached to AUSTAL2000-AYLTP.

The transport core calculator, AUSTAL2000 queries the LUT at each cell, i, j, k, of the space E and at each time t, based on the conditions in the cell, that are given by $T(t)_{i,j,k}$, $RH(t)_{i,j,k}$, $\theta(t)_{i,j,k}$ and the three reactive species concentrations $c(t)_{p,i,j,k}$.

The rates are applied in AUSTAL2000-AYLTP to update the masses as follows:

$$m'_{p,i,j,k}(t) = m_{p,i,j,k}(t) + Ks_p(c_p(t), \Omega)\Delta t V, \forall (i, j, k) \in E, \tag{5.12}$$

where $m'_{p,i,j,k}(t)$ is the mass resulting from the photochemical reaction, and V is the cell volume. The upgraded mass, $m'_{p,i,j,k}(t)$, is then equally distributed over all the particles of the cell i, j, k. This approach assumes that the rates are steady during the time interval Δt. The Lagrangian particles are afterwards moved, by AUSTAL2000, to the next time interval carrying the photochemical transformed mass.

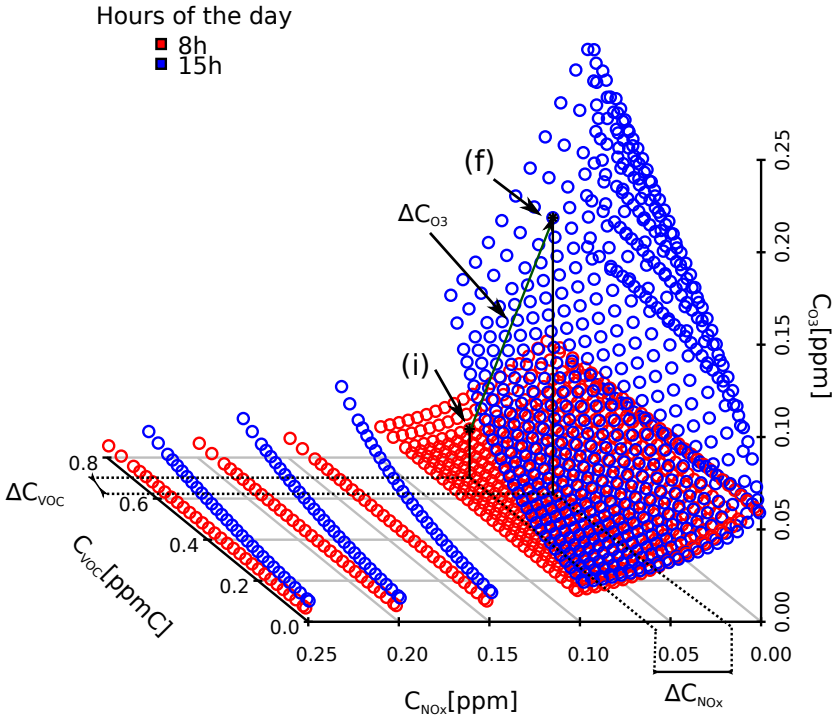

Figure 5.2: Subset of the look-up table for two different hours, 8 and 15 hours of the day, where the ozone concentration, $[O_3]$, is represented as a function of the NO_x and VOC concentrations, $[NO_x]$ and $[VOC]$ respectively. In this plot the temperature and the relative humidity are fixed and do not vary. Point **(i)** represents an initial point at 8:00, and **(f)** represents the resulting ozone concentration (ppm) 7 hours later. The ΔNO_x, ΔVOC and ΔO_3 are used to calculate the production rates according to Eq. (5.11).

Figure 5.2 represents a 3-D subset of the look-up table for two different hours of the day, in this case only dependent on the NO_x and VOC concentration. The model performs a search on the initial point *(i)*, and retrieves the equivalent reaction rate a time interval after *(f)*. In Fig. 5.2 the time interval is defined as seven hours to ease the visualization. Generally, the time interval for the calculation of the table is set to 10 minutes or one hour. The production rates are calculated using the information of *(i)* and *(f)* according to Eq. (5.11).

The surface is discrete and not equally distributed, this happens because

the look-up table is limited in size, mainly due to memory constraints. At the time of the query, if the values of the variables may not correspond to ones of the records in the table, the values are replaced by the closest values existent on the LUT. The implementation of the look-up table is an important factor to reduce the calculation time, because AUSTAL2000-AYLTP does not have to solve the CB-VI chemical mechanism but instead reads values from a file.

5.2 OZIPR — Calculation of The Look-up Tables

The look-up table is indexed according to six variables, such as the precursors' concentrations, temperature, relative humidity and zenith angle, and yields the resulting O_3, NO_x and VOC production rates.

The reaction rates have been computed with the Ozone Isopleth Package for Research (OZIPR) photochemical box model, developed by U.S. Environmental Protection Agency (EPA) as an urban pollution model (Souza, 2011).

Box models are by design simple. They require as input: the pollutants' initial concentrations, the meteorological conditions and the definition of a chemical mechanism which describes the photochemical process. The model simulates an homogeneous air column and that does not expand horizontally. OZIPR is able to receive chemical mechanisms with a high level of complexity. This model is therefore adequate to perform several simulations for various NO_x and VOC concentrations. Moreover, it has been used in several air pollution control studies (Kumar et al., 2008; Milt et al., 2009; Shiu et al., 2007).

The inputs to the model are:

- VOC speciation, which is the split of the individual VOC species in the VOC mixture;
- initial concentrations of the pollutants;
- meteorological data: temperature, relative humidity, location and date which are necessary for the calculation of the zenith angle;
- chemical mechanism.

The model uses the location and the date to calculate the zenith angle and to retrieve the photolysis rates from a set of representative values (Zahng and S., 1999). In this study a mid July day has been selected as the day to represent a typical summer day. It is worth noting that the zenith angle is, actually, represented by the variable "hour of the day". The use of "hour of

the day" is less misleading since during one day the solar angle can take the same value in the morning and in the afternoon. Hence using directly "hour of the day" variable facilitates the indexing of the results in the LUT.

5.2.1 Chemical Mechanism: CB-IV

There are currently several reaction schemes for simulating the dynamics of photochemical reactions (Dodge, 2000; Moussiopoulos et al., 1996). The chemical Carbon Bond Mechanism version 4, CB-IV, (Gery et al., 1989) has been used in the present work. CB-IV is a widely used chemical mechanism, considered as a standard since more than 20 years (Kumar et al., 2008; Thomas et al., 2008). It has been validated with environmental chamber experiments (Gery et al., 1988), and it has been proven to be a good compromise between chemical accuracy and computational cost (Zahng and S., 1999). It is based on a condensed method to simulate the VOC reactions, it has a lumped structure mechanism where organic species are grouped according to reactive elements based on the types of carbon bonds in each species. The groups are organic species, which are represented explicitly as the cases of formaldehyde, ethene or isoprene; single bounded carbon atoms such as paraffins; carbon-carbon double bond as olefins and molecular surrogates e.g. toluene and xylene (Maurizi, 2008). This mechanism contains over 80 reactions and 30 chemical species, the list of all the reactions is detailed in Section D.1 of Chapter D.

5.2.2 The VOC's Speciation for Luxembourg

OZIPR has been prepared to carry on the VOC's speciation according to the Emission Database for Global Atmospheric Research (EDGAR) profiles for Luxembourg (Olivier et al., 2001). This data consists of the VOC partition according to the species groups defined in the EDGAR database per SNAP sector.

The VOC EDGAR species fractions are, afterwards, converted into CB-IV groups, using the CB-IV molar split which has been used by Visschedijk et al. (2007) and Markakis et al. (2010). The VOC speciation is important since different VOC species react differently with the hydroxyl radical OH, and therefore affect the ozone cycle. Each country might exhibit a different partition of VOC species, because they differ in the composition of their industrial parks. Additionally, biogenic VOC, depend on the vegetation species, thus the autochthonous plant species of each country may change the VOC speciation.

5.2.3 Analysis of the OZIPR model results

OZIPR is the model used to generate the LUT. An analysis of OZIPR's behaviour has been carried out in order to understand how should the outcomes of OZIPR be stored in the LUT.

The LUTs contain thousands of data thus the visual data analysis is very troublesome. On the other hand it is important to have a deep knowledge of the OZIPR responses, in order to understand the LUT. Therefore three different simulation cases have been prepared and analysed. All the cases represent a daily evolution with a constant temperature of 25°C and a constant relative humidity of 45%. The initial concentrations of the simulations subject to analysis are described in Table 5.1.

Table 5.1: The initial concentration of NO_x and VOC for the three cases subject to analysis.

Simulation case	NO_x [ppm]	VOC [ppmC]
1	0.050	0.010
2	0.001	0.160
3	0.050	0.300

The cases have been chosen from a larger sample of cases and are representative of three different ozone situations. They represent different initial concentrations, in order to analyse diverse evolution curves. The first case represents a low VOC concentration and a moderate NO_x concentration, in case 2 the VOC concentration is extremely high and the NO_x levels are almost vestigial. Whereas case 3 represents a moderate NO_x and moderate VOC concentration situation. The cases have been simulated from 6h00 to 21h00, and their different initial concentrations are expected to yield different daily profiles for the pollutant's concentrations.

The time series of the ozone production rates has been plotted to analyse their temporal behaviour according to the different time step simulations. Figure 5.3 shows the one hour and 10 minutes ozone rates over the simulation period, as well as NO_x, VOC and O_3 resulting concentrations. The one hour curves follows the 10 minutes curves. For the case 1 and 3 the one hour rates catch well the ozone rate peak, however for case 2 the averaging implicit to the calculation of longer time steps, is not able to catch the ozone's rate peak completely.

The curves show that the precursors are consumed as ozone concentration builds up until it reaches a peak. After the peak, the photolysis reactions slow down, due to lower income solar radiation, and the depletion of ozone by NO is higher than the production of ozone. Figure 5.3 (b) and (c) shows that for

high values of VOC the ozone peak is achieved later, although the peaks are higher. In Fig. 5.3 (b), ozone remains at the peak concentration, this happens because there is no more NO_x in the system to consume ozone.

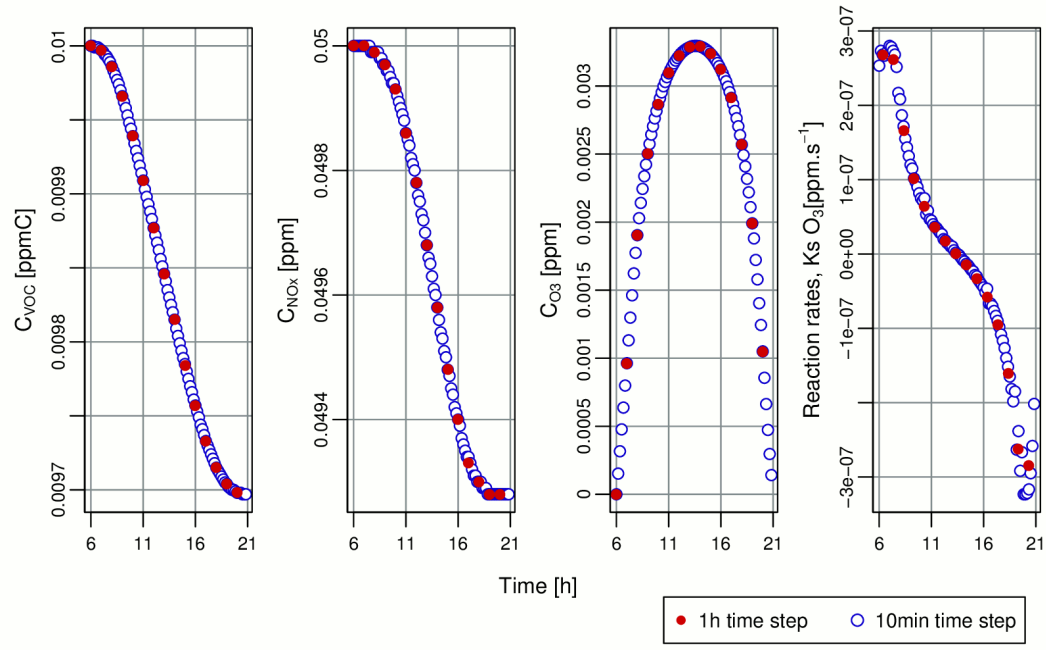

(a) Simulation case 1

Figure 5.3: One day time series, from 6h00 to 21h00, of the evolution of VOC, NO_x, O_3 concentration and ozone production rates for 1 hour and 10 minutes simulations. Ks is the reaction rate.

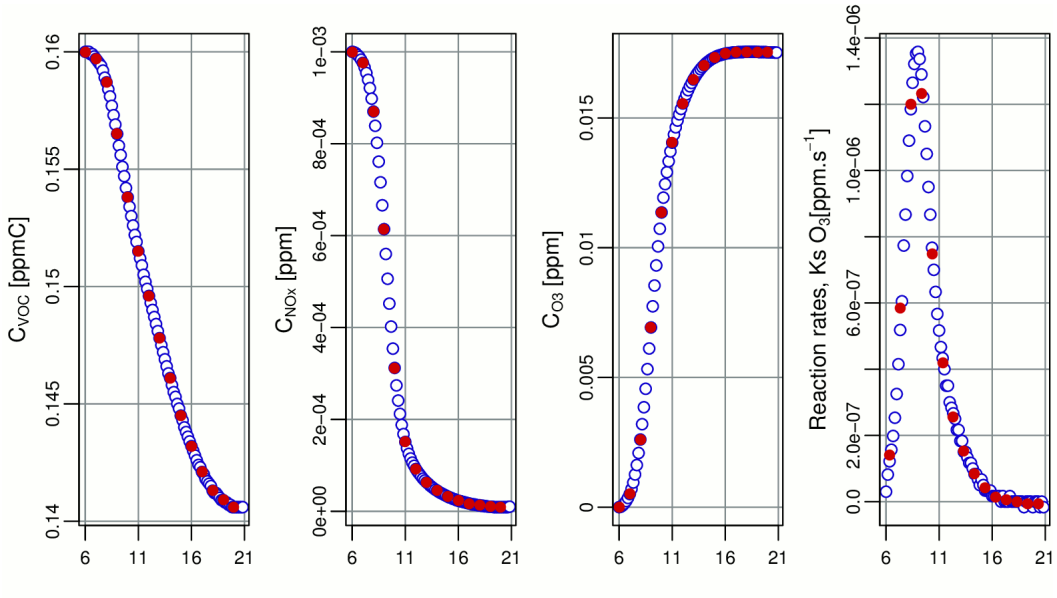

(b) Simulation case 2

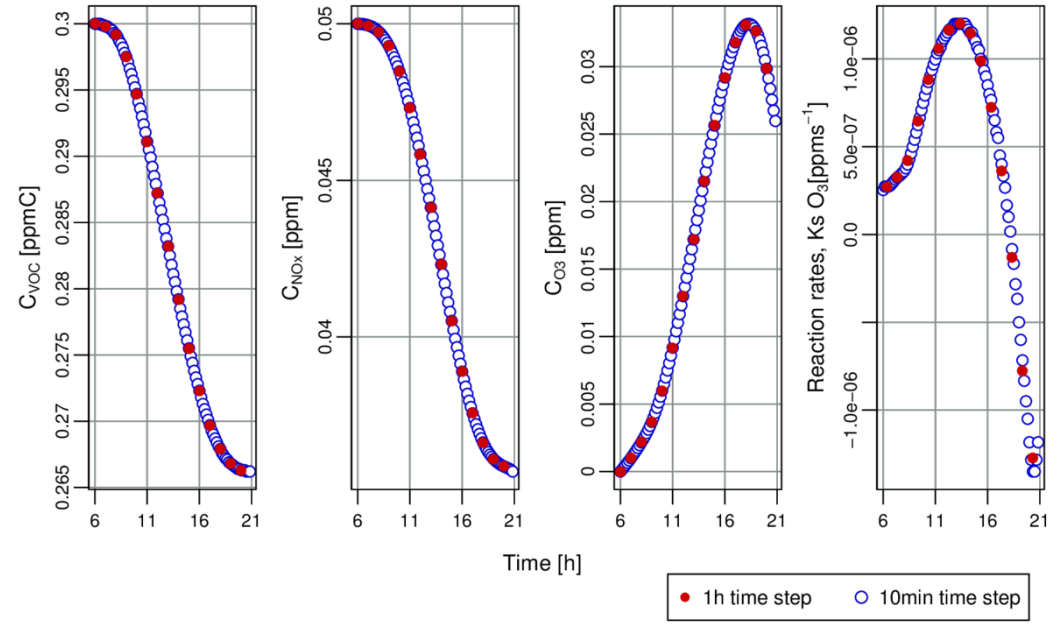

(c) Simulation case 3

Figure 5.3: One day time series of the evolution of VOC, NO_x, O_3 concentration and ozone production rates for 1 hour and 10 minutes simulations. Ks is the reaction rate.

The same analysis has been carried out for the ozone precursors. The 10 minutes and one hour time steps are compared in Fig. 5.4 for NO_x and Fig. 5.5 for VOC.

In Figs. 5.4 and 5.5, it is visible that the 10 minutes production rates present an oscillatory behaviour. This behaviour can be attributed to the numerical method used by OZIPR to calculate the concentration. The method used is the Gear method, Sandu et al. (1997) has carried out an investigation of chemical integrations methods and concluded that Gear's method performs better using larger iterations steps (Tonnesen et al., 1998). On possible way of reducing this oscillations in the future when using a LUT with a 10 minutes time step, is to lower the tolerance allowed for the error in one time step (Finlayson, 2003; Gery and Crouse, 1990).

The rates vary around the hour time step values, and exhibit the same general trend. The 10 minutes time step is too small to achieve a more stable daily profile. However, it must be noticed that the NO_x and VOC production rates have magnitudes of the order of 10^{-8} to 10^{-9} thus these variations do not have a great impact on the final concentrations.

This has not been the case of the ozone rates, which have been presented before, that are in a range of values of the order of 10^{-6} to 10^{-7} and do not exhibit an unstable behaviour.

Figures 5.4 and 5.5 show that OZIPR is specially unstable for the 10 minutes time steps, for the cases 1 and 2. These are the cases where the differences between NO_x and VOC initial concentrations are larger.

The results of OZIPR demonstrate that the 10 minutes time step do not assure a stable tendency on the precursors' production rates. The one hour time step has proven to have a better behaviour, hence the 10 minutes time step LUTs has not been consider further in the AUSTAL2000-AYLTP simulations. Furthermore, a study about the influence of the initial concentrations in OZIPR simulations has been carried out and it is presented in Section D.2 of Chapter D.

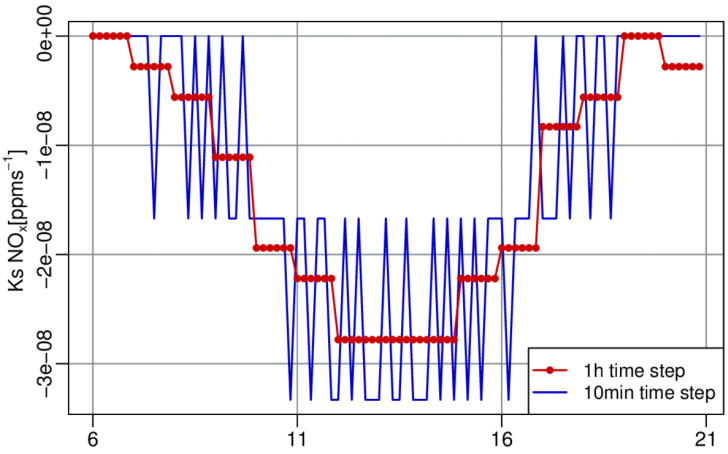

(a) Simulation case 1

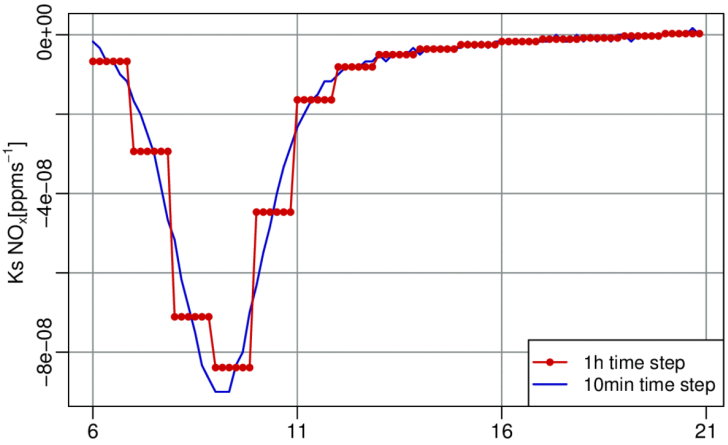

(b) Simulation case 2

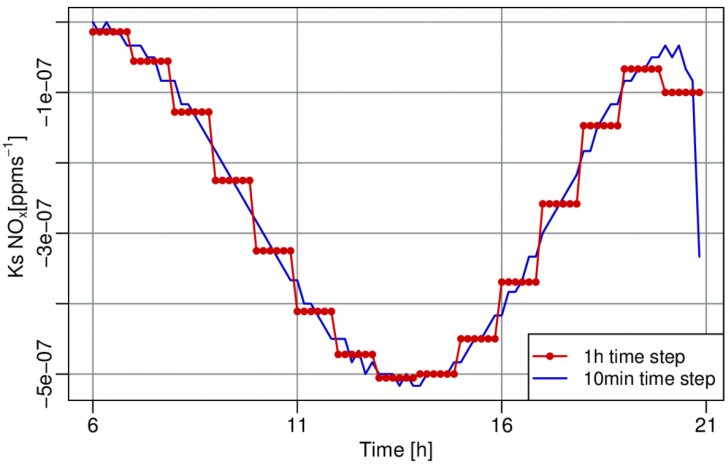

(c) Simulation case 3

Figure 5.4: One day time series, from 6h00 to 21h00, evolution of NO_x production rates for 10 minutes and 1 hour simulations. Ks is the reaction rate.

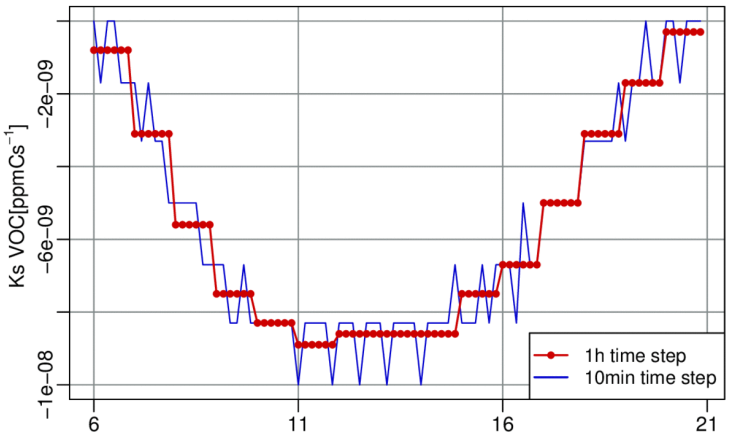

(a) Simulation case 1

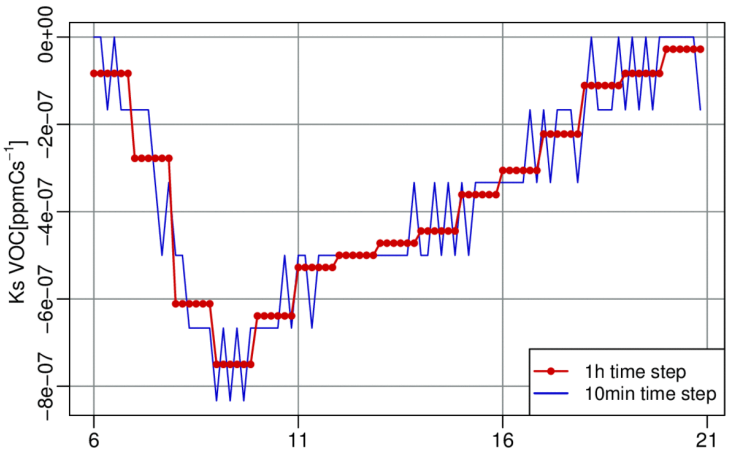

(b) Simulation case 2

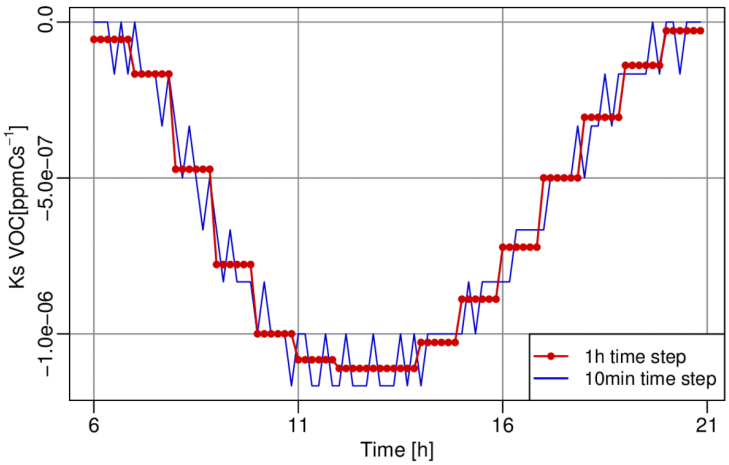

(c) Simulation case 3

Figure 5.5: One day time series, from 6h00 to 21h00, evolution of VOC production rates for 10 minutes and 1 hour simulations. Ks is the reaction rate.

5.3 Characteristics of the Look-up table

The LUT is where all the reaction rates are stored, it is calculated previously and independently from AUSTAL2000-AYLTP. The dimensions of the LUT are defined by the user. It is run for a given application, and it is dependent on the location since the VOC speciation and the zenith angle vary according to the region. For this study the LUT has been built specifically for the region of Luxembourg. Hence, for applications other than this one, the more different the characteristics of the VOC composition and the latitude of the region are, the less appropriate is to use the LUT which is presented here. The intervals of the variables must also be adjusted to the typical ranges of the variables of the region.

A LUT with two different time steps, has been prepared and it is presented in Table 5.2. The range of values in the LUT is purposely high, because policy support models need to be able to respond to strong changes in the emissions and therefore high values are included.

Table 5.2: Initial set of conditions used in the LUT generation and the number of entries for the 1 h and the 10 minutes time steps.

O_3	0.001	0.005	0.01	0.015	0.02	0.025	0.03	0.035	0.04
	0.045	0.05	0.055	0.06	0.065	0.07	0.075	0.08	0.085
	0.09	0.095	0.1	0.15	0.2				
NO_x	0.001	0.01	0.015	0.02	0.025	0.03	0.035	0.04	0.045
	0.05	0.055	0.06	0.065	0.07	0.075	0.08	0.085	0.09
	0.095	0.1	0.15	0.2	0.25				
VOC	0.01	0.02	0.05	0.075	0.1	0.125	0.15	0.175	0.2
	0.225	0.25	0.275	0.3	0.325	0.35	0.375	0.4	0.425
	0.45	0.475	0.5	0.525	0.55	0.575	0.6	0.625	0.65
	0.675	0.7	0.75	0.8					
T [°C]	20	21	22	23	24	25	26	27	28
	29	30	31	32	33	34	35	36	37
RH [%]	10	20	30	40	50	60	70	80	90
Time step					1 h				10 min
Total size					37 192 932				231 127 506

To realize the coverage of the LUT in terms of concentrations, the shape of the ozone concentrations in the one hour LUT have been plotted and are presented in Fig. 5.6(a). Similarly, the ozone rates are also presented in Fig. 5.6(b). Figure 5.6 shows the range of ozone concentrations and production rates which is represented in the one hour time step LUT. It is possible to observe that the highest values of ozone are restricted to low concentra-

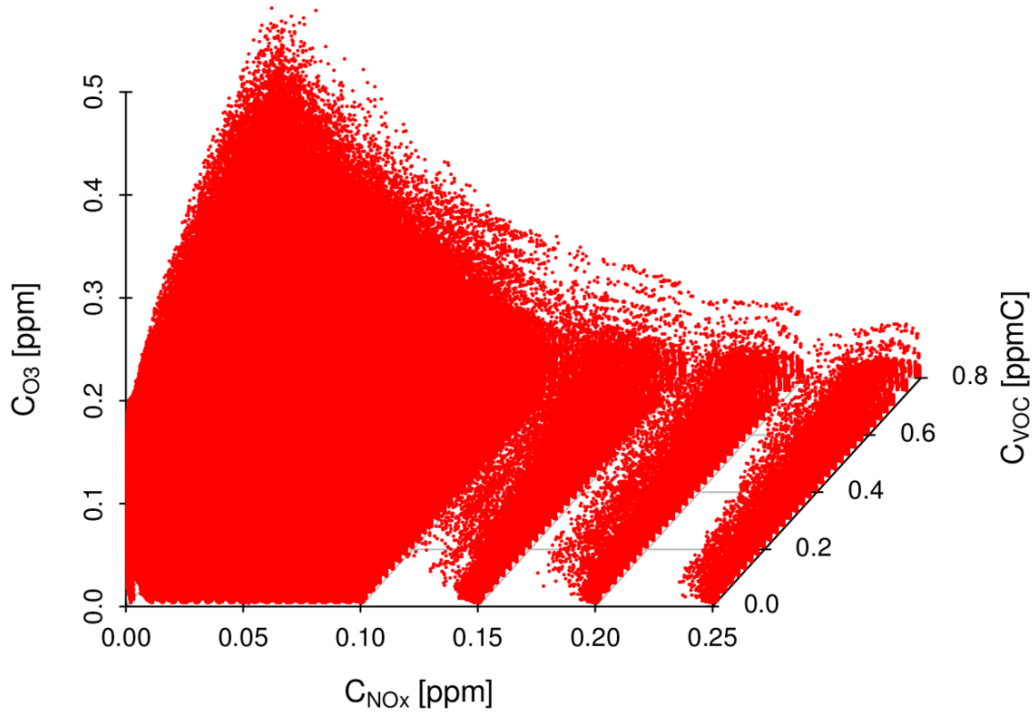

(a) O_3 concentrations.

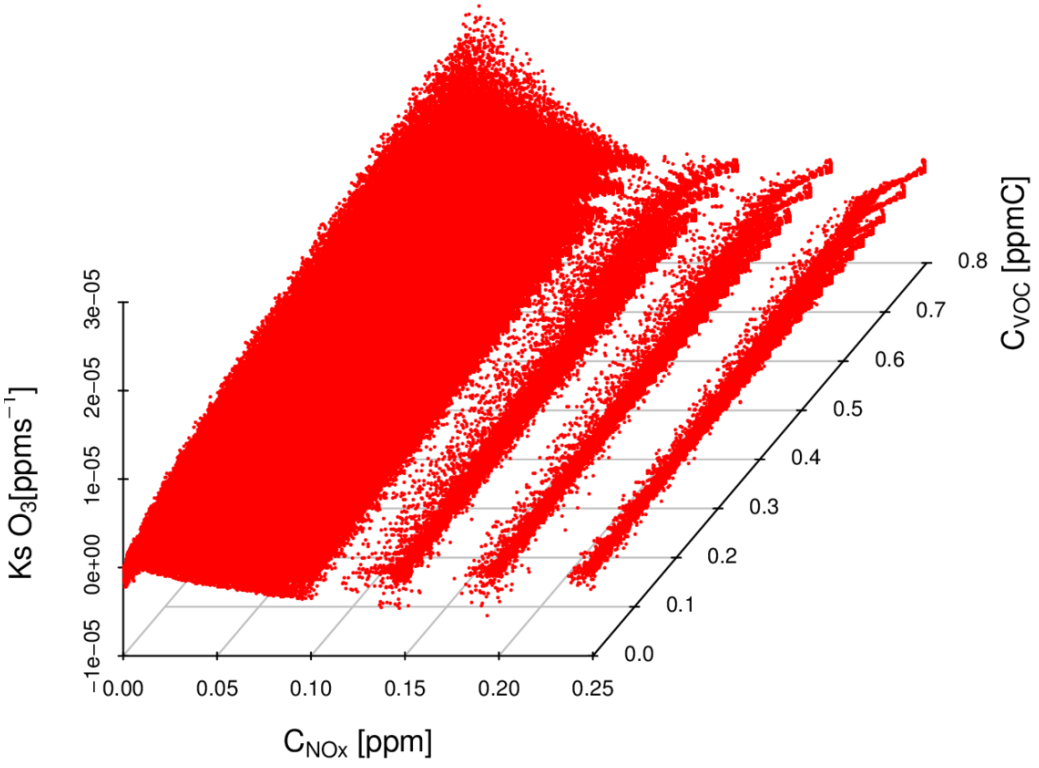

(b) O_3 production rates.

Figure 5.6: One hour LUT frequency of O_3 concentrations (a) and production rates (b), as a function of NO_x and VOC concentrations. The plot represents a random subset of 100 000 values from the LUTs.

Table 5.3: Computational time for the LUT calculation.

	Calculation time [hour]		Number of
	1h	10 min	concurrent CPUs
LUT 1	6.1	7.3	18

tions of NO_x and for high VOC concentration values. Likewise, the highest ozone reaction coefficients are found in the lower NO_x concentration area, and augment with the increasing VOC concentrations. This behaviour is due to the high NO_x regions tendency to consume ozone in the oxidation of NO to NO_2.

The generation of the LUT, carried out with OZIPR, is a pre-requisite of the AUSTAL2000-AYLTP model, since the LUT is an input of the model. This procedure in only undertaken once, however it is the most time consuming stage of the model input preparation. The calculation time of the LUTs presented in Table 5.3, it is the overhead time of the study case stage, i.e. it is only required at the beginning of the study, and therefore does not account for the model ruining time. The LUTs have been calculated from 6h00 to 21h00.

5.3.1 The Relations Between the LUT Variables and the Production Rates

The LUT is connected to AUSTAL2000-AYLTP via a file which contains a huge number of sorted reactions rates. However it is important to understand and to know the LUT functional relations with its variables and their shapes in order to better understand the results of the model. Hence an analysis of the LUT response to its variables has been undertaken. The results for the one hour LUTs are presented hereafter.

In order to visualise the influence of each variable of the LUT in both ozone concentration and coefficients, the meteorological variables have been fixed. In this case, temperature has been set at 27°C, relative humidity at 50% and the hour at 15h00.

The relationship between the ozone production rates and its precursors' rates is presented in Fig. 5.7(a) for NO_x and in Fig. 5.7(b) for VOC.

Figure 5.7 shows that the ozone rates have an inverse relationship with its precursors' rates. That is, the higher ozone rates are found for the lower NO_x and VOC rates. The response is expected since the production of ozone leads to the consumption of its precursors. This relation is more clear in the case of NO_x than in the case of VOC where the values show a wider spread. The reason for this is that the NO_x concentrations tend to be more limiting.

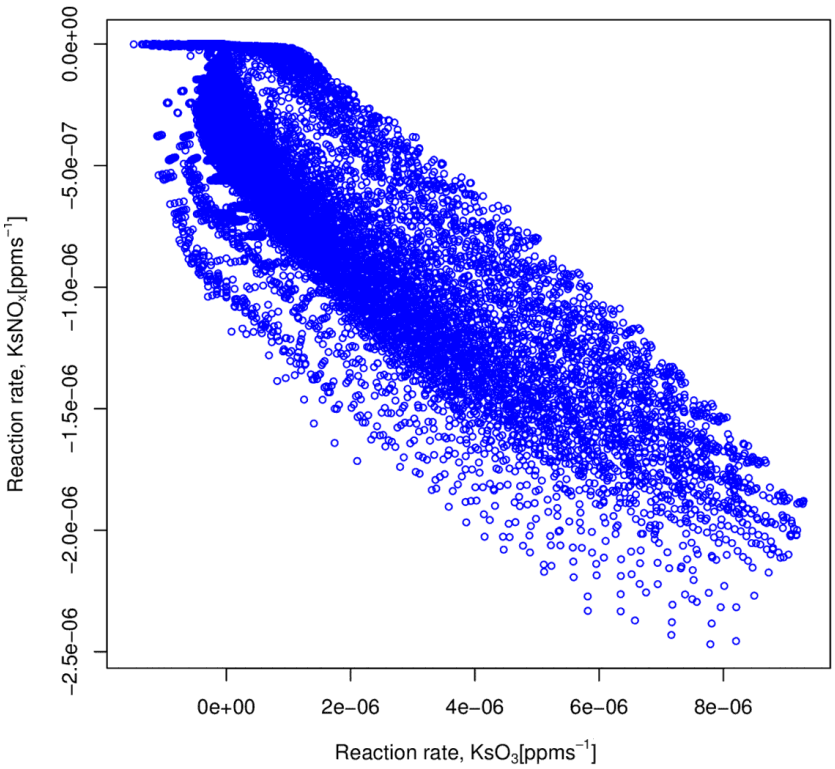

(a) NO_x production rates, $KsNO_x$, as a function of ozone production rates, KsO_3.

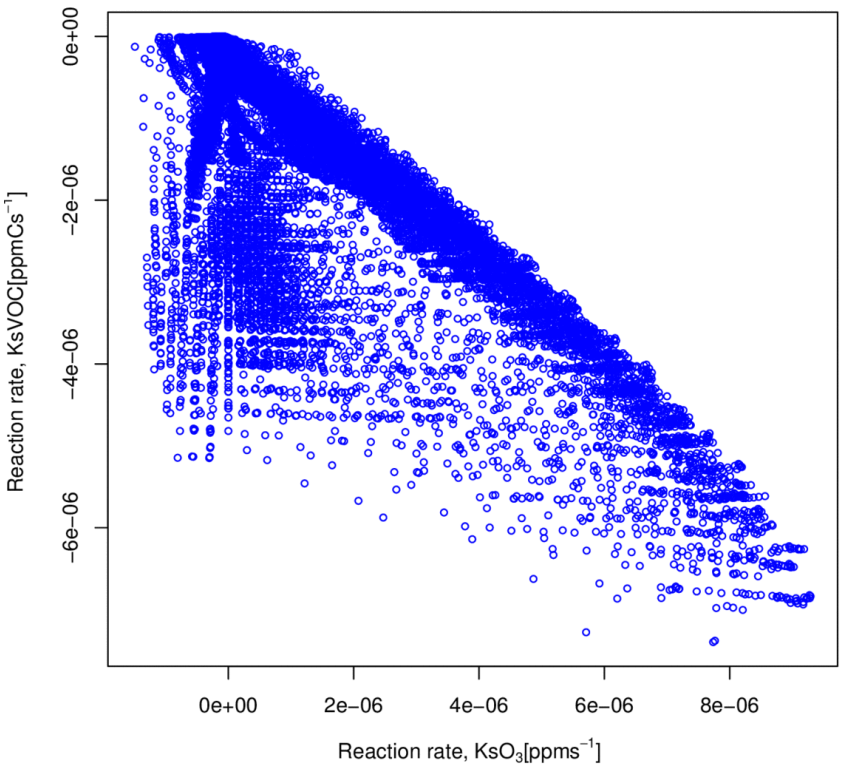

(b) VOC production rates, $KsVOC$, as a function of ozone production rates, KsO_3.

Figure 5.7: NO_x production rates, $KsNO_x$, and the VOC production rates $KsVOC$, as a function of ozone production rates, KsO_3.

5.3.2 Relations Between the LUT Meteorological Variables and the Production Rates

In this section follows an analysis of the relation of each meteorological variable on ozone production. Meteorology influences photochemical reactions, this influence is represented in this study by three variables: temperature, T; zenith angle, θ; and relative humidity, RH.

Temperature accelerates gaseous chemical reactions due to the increase of the frequency of collisions between molecules. Additionally, high temperatures are strongly related to clear skies, and thus to strong solar radiation, which is crucial for the generation of ozone. Likewise, the solar zenith angle is an indicator of the quantity of sun light that might be available to photolysis, it depends on the date and the latitude (Walcek and Yuan, 1994). Relative humidity is important to regulate the amount of hydroxyl radicals OH available for the photochemical reactions and is associated to cloud coverage (Karatzas and Kaltsatos, 2007). These meteorological variables plus NO_x, VOC and O_3 concentrations are used to compute reaction coefficients.

The relation of temperature and the ozone rates is presented in Fig. 5.8(a) for a fixed hour, 15h00 and relative humidity 50%.

The influence of temperature is visible, for higher values of temperature the ozone rates show higher values. Additionally, it shows a wider amplitude of rates with increasing temperature. This is coherent with the fact that temperature accelerates chemical reactions.

It can be observed that the graph is not continuous, this is due to the fact that the initial condition values are also not continuous. This effect is more clear for the meteorological variables since they are kept constant during the whole day simulation.

Additionally, as it has been observed before, the results show that a high number of ozone rates are found close to zero.

The relation of ozone with relative humidity is not as clear as for temperature. However, Fig. 5.8(b) reveals that ozone rates are higher for higher values of relative humidity, at a fixed temperature, 27° C, and hour, 15h00. For higher values of relative humidity, more H_2O is available for the reactions which lead to ozone, especially the high availability of OH.

The influence of the zenith angle, here represented by the hour index, is presented in Fig. 5.8(c), for a constant relative humidity of 50% and a temperature of $27°C$.

The highest ozone rates are found at noon when the solar radiation is very strong. In the late afternoon, around 18h00 to 20h00 the ozone rates are more negative. The reason for this is that these are the hours with a lower solar radiation income, when no more ozone is produced but instead it is consumed

in the oxidation of NO.

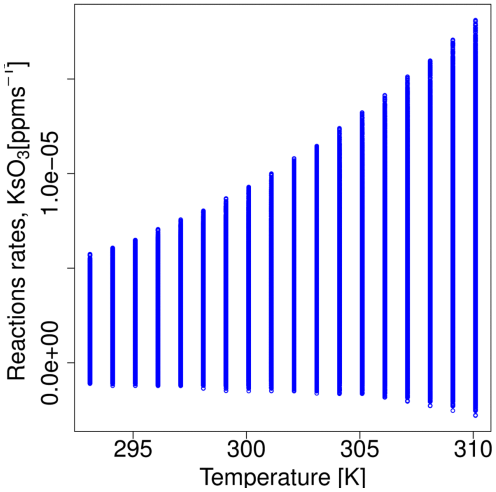

(a) The reaction rate KsO_3, as a function of temperature.

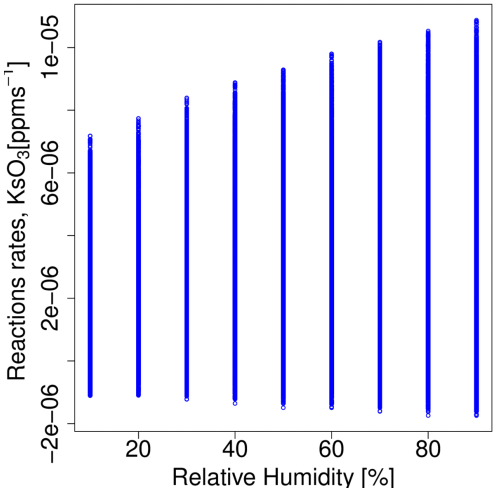

(b) The reaction rate KsO_3 as a function of relative humidity.

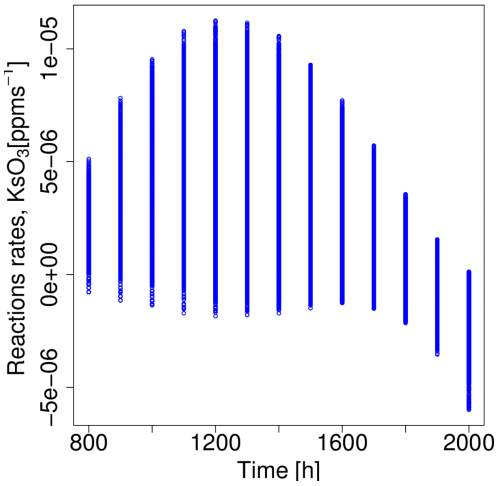

(c) The reaction rate KsO_3 as a function of daytime.

Figure 5.8: Ozone production rates KsO_3, as a function of temperature (a), relative Humidity (b) and hour of the day (c).

Chapter 6

Validation of the Air Quality Model

Contents

The stage that follows the development of an enhanced model is its application and evaluation. In this chapter, the simulation application of AUSTAL2000-AYLTP is described and the results are discussed and presented.

6.1 Modelling Application

The main focus of this work is Luxembourg's Grand-Duchy model application. The LEAQ model aims at assessing ozone control strategies for the country of Luxembourg. This strategy is undertaken through the ozone precursors emissions which are calculated by the ETEM Luxembourg model, Section 3.2.1. The ozone levels do not depend solely on the emissions of its precursors, meteorology and topography also play an important role. Hence, the characteristics of the country of Luxembourg, such as topography, demography and climate, influence the wind fields and the distribution of emission sources, and consequently the concentration levels of the pollutants.

Luxembourg is a small country crossed by tributary rivers and mainly consisting of forests, cultivated land and pastures. It is surrounded by three other countries, Belgium on the west side, Germany on the east and France on the south. Its topography, presented in the Digital Elevation Model (DEM) Fig. 6.1, is marked by a hilly region on the northern part, called *Oesling*, which belongs to the high plateau of the *Ardennes*. The rest of the country is relatively flat with river valleys, representing almost two-thirds of the country. The river *Moselle*, the *Sûre* and the *Our* create a natural boundary with Germany. The river *Sûre* crosses the country in the north from west to east until it joins the *Moselle*, and is Luxembourg's longest river.

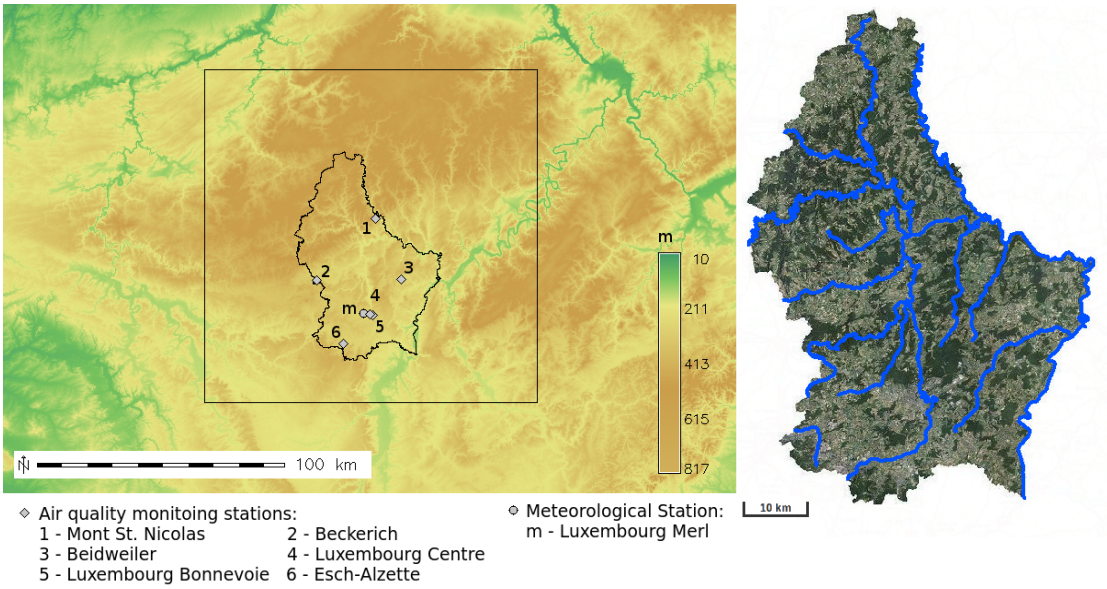

(a) The DEM of the Luxembourg region **(b)** Rivers of Luxembourg.

Figure 6.1: (a) The DEM, in meters, of the Luxembourg region containing the meteorological station of Merl and the air quality monitoring stations. The black square represents the calculation domain. (b) Zoom over Luxembourg country, detailing the rivers which cross the country (ACT, 2012).

Figure 6.1 presents the six air quality monitoring stations which measure ozone in Luxembourg. Their characteristics are presented in Table 6.1.

The capital, Luxembourg city, is the largest city, which is located in the south of the country. Other important residential centres are the cities of Esch-sur-Alzete, Dudelange, and Differdange, all located in the south. These are also important industrial centres.

Luxembourg is characterised by a west European continental climate, with a temperate climate in which extreme whether conditions are rare. The winters are moderate and the summers are cool, with average temperatures varying approximately from 0 °C to 20 °C. On the other hand, the precipitations

Table 6.1: Luxembourg's ozone air quality monitoring stations.

Stations' Characteristics	Type of station	Coordinates (in decimal degrees)		Altitude [m]
		latitude	longitude	
Beckerich	background	49.737	5.850	295
Beidweiler	background	49.727	6.305	319
Esch-Alzette	industrial	49.510	5.977	292
Lux. Bonnevoie	traffic suburban	49.603	6.138	280
Lux. Centre	traffic urban	49.610	6.127	280
Mont St. Nicolas	background	49.943	6.176	515

levels are high, even in summer. The sunniest months are encompass between May and August (SGL, 2012).

Luxembourg is generally not considered a problematic country in what concerns air quality. Despite this fact, the levels of some pollutants, as it is the case of nitrogen dioxide NO_x, have not undergone significant reductions during the last decade (EEA, 2011). The EEA reports on NO_2 annual averages breaching the limit value, $40\,\mu g\,m^{-3}$, which has been established in 2010. Additionally, the hourly limit, $200\,\mu g\,m^{-3}$, has also been exceeded in some occasions, mainly in the city of Luxembourg heavily influenced by the dense traffic volume. Nitrogen dioxide is a precursor of ozone, and as such, its high levels are, most probably, at the origin of the ozone peaks registered in Luxembourg. Although the frequency and magnitude of ozone episodes is not extremely high, e.g. the alert threshold, $240\,\mu g\,m^{-1}$, has never been exceeded, the pre-alert and the information threshold, $160\,\mu g\,m^{-3}$, has been breached several times (EEA, 2011).

Figures 6.2 and 6.3 present the historical annual averages of both NO_x and O_3 for air quality monitoring stations of Luxembourg which monitor ozone.

The relationship between NO_x and ozone is visible in Figs. 6.2 and 6.3, the stations where the values of NO_x are higher, Luxembourg Centre registering the highest, correspond to the stations where the lowest values of ozone have been registered. Luxembourg Centre is an urban traffic station and therefore is expected to present lower values of ozone and higher values of NO_x due to vehicle traffic. The station Luxembourg Bonnevoie is a suburban traffic station and therefore the NO_x values are lower than in Luxembourg Centre, accordingly the ozone values are higher. The station of Esch-sur-Alzette is an industrial type of station, it reveals high levels of NO_x, however lower than the values found in the capital's stations, due to the lower volume of traffic. Despite the high levels of NO_x, found in Esch-sur-Alzette, the annual average ozone levels are rather high. The station of Elvange, closed in 2006 and located close to Beckerich, was a rural background station, on the other hand

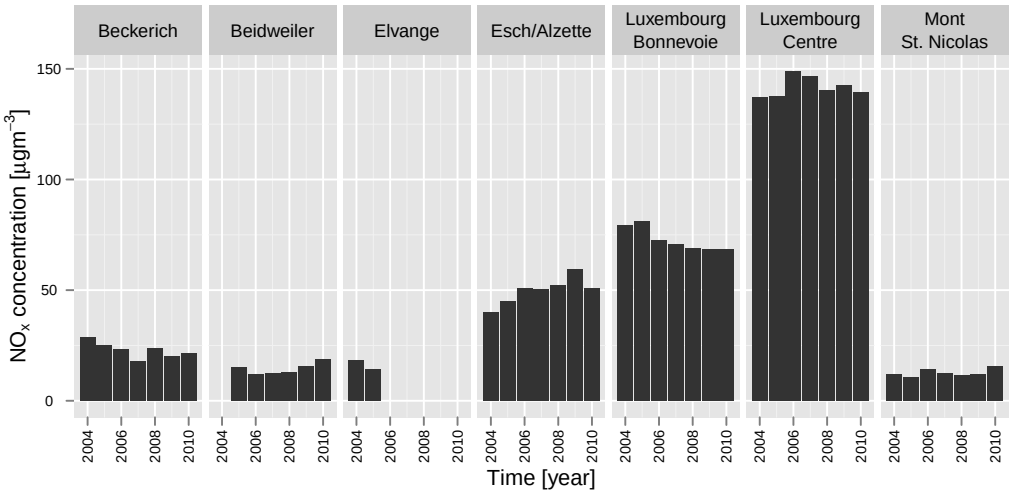

Figure 6.2: Annual average concentration of NO_x for the years 2004 to 2010, and the air quality monitoring stations Elvange, Luxembourg Centre, Luxembourg Bonnevoie, Esch/Alzette, Beckerich, Beidweiler and Mont St. Nicolas. Based on the *AirBase* data (EEA, 2012a).

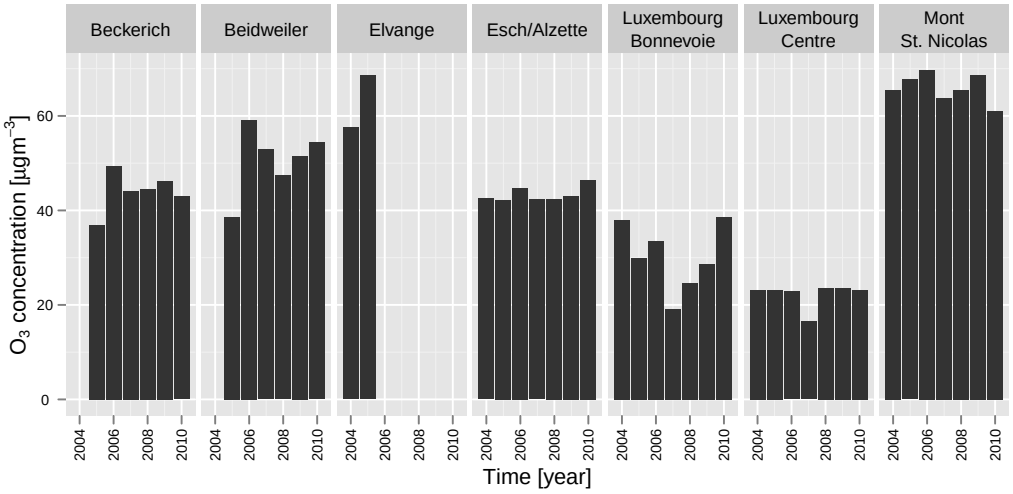

Figure 6.3: Annual average concentration of O_3 for the years 2004 to 2010, and the air quality monitoring stations Elvange, Luxembourg Centre, Luxembourg Bonnevoie, Esch/Alzette, Beckerich, Beidweiler and Mont St. Nicolas. Based on the *AirBase* data (EEA, 2012a).

two other background stations, Beckerich and Beidweiler, started to work in 2005. Mont St. Nicolas, rural background station which is nowadays called Vianden, is the station that registers the highest values of ozone, followed by Beidweiler and Beckerich.

Table 6.2: Ozone exceedances to the hourly information threshold value of $180\,\mu g^3\,m^{-1}$, for the period of 2004 to 2010.

Station name	Number of exceeded days	Number of hours exceeded
Elvange	9	36
Luxembourg Centre	0	0
Luxembourg Bonnevoie	2	2
Esch-sur-Alzette	4	9
Beckerich	4	14
Beidweiler	8	28
Mont St. Nicolas	22	74

Table 6.2 shows the number of exceeded hours and days of the ozone information threshold, during the period of 2004 to 2010. The background stations naturally register more ozone exceedances, due to the lower influence of near NO_x sources. Luxembourg Centre does not register any exceedances, during this period, due to the high levels of NO_x found in this area. However, the suburban station of Luxembourg Bonnevoie has exceeded this threshold twice. In the south, Esch-sur-Alzette, a very industrialised region has registered 4 days over the $180\,\mu g^3\,m^{-1}$.

6.1.1 Modelling Domain

The air quality simulation has been carried out with the AUSTAL2000-AYLTP model. The modelling system is composed of AUSTAL2000 transport model and AYLTP chemical module, and it has been applied to the region of the Luxembourg Grand-Duchy. The three main pollutants which are important in photochemical reactions, such as O_3, VOC, and NO_x, have been considered.

The air quality simulation domain is 130 km by 130 km with a regular resolution of 5 km by 5 km. The calculation domain is represented by the black square in Fig. 6.1. The model is run with 19 vertical layers, up to 1500 meters, and concentrations are evaluated for the near-ground layer, up to 3 meters.

The terrain information is given to the model by a DEM, which has been provided by Shuttle Radar Topography Mission (SRTM) (CGIAR, 2012), with

a resolution of 77.85 m. The terrain is displayed in Fig. 6.1. The roughness length map has been prepared according to the land-use and then converted into roughness classes defined by the German Technical Instructions on Air Quality Control (*TA Luft*), so that it can be read by AUSTAL2000 (Janicke, 2009).

6.1.2 Meteorology

The diagnostic wind model, Taldia, used by AUSTAL2000, requires the wind speed and direction of only one meteorological station of the domain. This is a limiting factor, since the wind field is only based on one station, the one close to Luxembourg city. The station which has been used is Luxembourg Merl, indicated by point *m* in Fig. 6.1. This station is situated in Luxembourg city, and it has continuous measurements of wind speed and direction, temperature, and relative humidity.

Figure 6.4 shows the temporal evolution of the wind speed and direction, temperature and relative humidity in the station of Luxembourg Merl for the day 19th of July 2006, (ASTA, 2010).

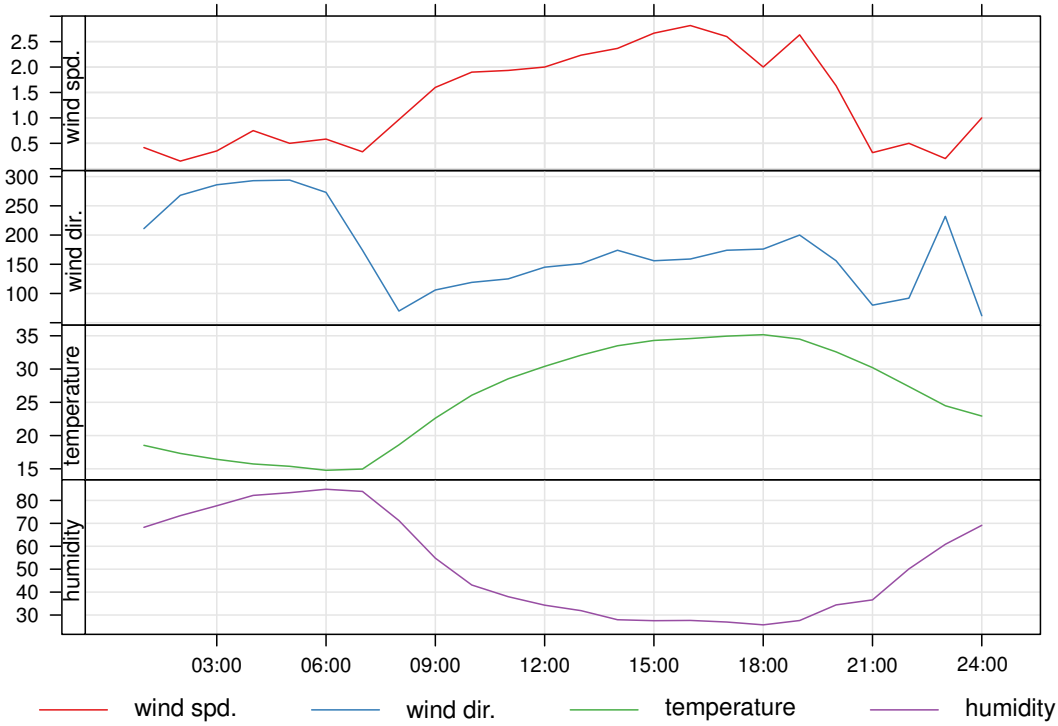

Figure 6.4: Temporal evolution of the temperature, wind speed and direction and relative humidity for Luxembourg Merl meteorological station of the day 19th of July 2006. The data which has been used in this work has been provided by *Administration des Services techniques de l'Agriculture*, ASTA (2010).

It can be observed that the temperature reached 35 °C and the wind direction changes from north-west to south. Additionally relative humidity decreased strongly in the morning.

Concerning, the atmospheric stability, no data was available at the time of this study. It is assumed that the atmospheric conditions are stable, because that is the atmospheric stability conditions which better agree with the NO_x concentration measurements at the Luxembourg centre station, the station close to the meteorological station. Setting the atmospheric stability to be stable limits the vertical transport of the pollutants and therefore it is related to high concentrations on the ground layer. Hence, for the future, more realistic data regarding atmospheric stability should be considered.

6.1.3 Emissions

The emissions used in this study are provided by the ETEM Luxembourg model, and the European Monitoring and Evaluation Programme (EMEP) emission database (CEIP, 2012). The biogenic VOC emission data has been provided by the AUTH (Poupkou et al., 2010). The EMEP web base contains the national emissions aggregated by SNAP sectors on an European grid of 50 km by 50 km originally in a Lambert Azimuthal Equal Area projection. This data is prepared with the officially reported emissions and receive an extra correction for filling gaps in the data. The emissions from ETEM Luxembourg have been calibrated for the year 2005 using the energy consumption data from STATEC (2010b), and have been complemented with United Nations Framework Convention on Climate Change (UNFCCC) (UNFCCC, 2010) and EEA (EEA, 2010c), when no data were available.

The ETEM emissions are only energy related, however not all emissions are energy related, e.g. use of solvents, therefore not all the SNAP economic sectors have a correspondence to the ETEM sectors. The correspondence between the SNAP sectors and the ETEM Luxembourg energy sectors has been presented previously in Table 3.4 in Chapter 3. Thus the SNAP sectors 4, 5, 6 and 9 have been included in the domain.

Figure 6.5 shows the EMEP grid and the domain of the emissions represented by all the shaded areas. Each of the four outer areas, is treated a less aggregated source, AUSTAL2000 allows flexible definition of sources and, it is more convenient to define four big squares with less detail instead of an emission grid. This techniques improves the CPU memory requirements with the caveat of having less detail in this area. The emissions in these areas are averaged by sector taking into account the contribution of each cell that overlaps the area. The inner squared shaded areas, in Fig. 6.5, is the area where the emissions are defined on a higher resolution, 1 km by 1 km.

The EMEP emissions are allocated by the emission allocator according to

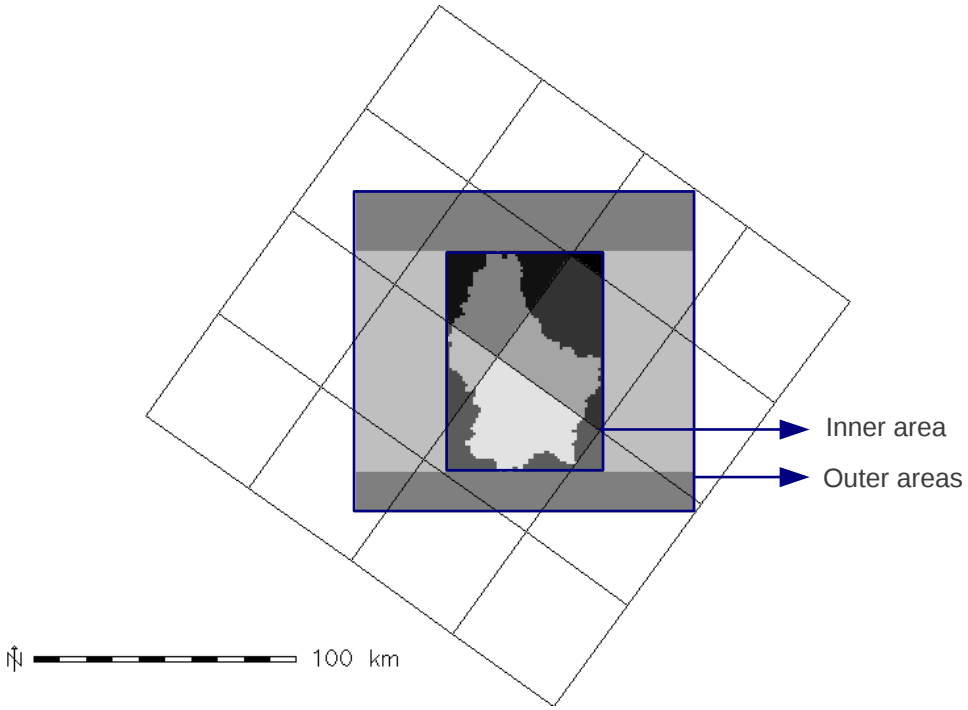

Figure 6.5: EMEP Emission domain set-up on UTM 31N projection. The EMEP information is represented by the grid and all the shaded areas have been attributed with emissions. The inner area has a resolution of 1km by 1km.

the land-use, as explained in Chapter 3. The emissions on cells of the EMEP grid which overlap the territory of Luxembourg, are allocated according to the LEAQ emission allocator for the sectors of ETEM, and the values given by ETEM are subtracted to the emissions of EMEP. The remaining is allocated to the area outside Luxembourg which is encompassed by the EMEP cell. The emissions on the inner area but which are not inside Luxembourg, have a resolution of 1 km by 1 km although the emission values are distributed equally and not according to the land-use.

Figures 6.6 and 6.7 present the sectoral emissions of NO_x and VOC respectively, both from EMEP and ETEM. Concerning the pollutant NO_x, the greatest contribution comes from the road transport sector, followed by industry and energy production sectors. The load of road transport NO_x emissions is very important in Luxembourg due to the central location of the country and the very competitive prices of fuel which attract the mid-long range routes of goods.

On the other hand, regarding the VOC emissions, the biogenic emissions represent the largest share, followed by SNAP 6, which refers to solvent and other product use, generally one of the most important sources of VOC. Additionally, road transport has a significant weight on the total VOC emissions, followed by SNAP 4 concerning the production processes sector.

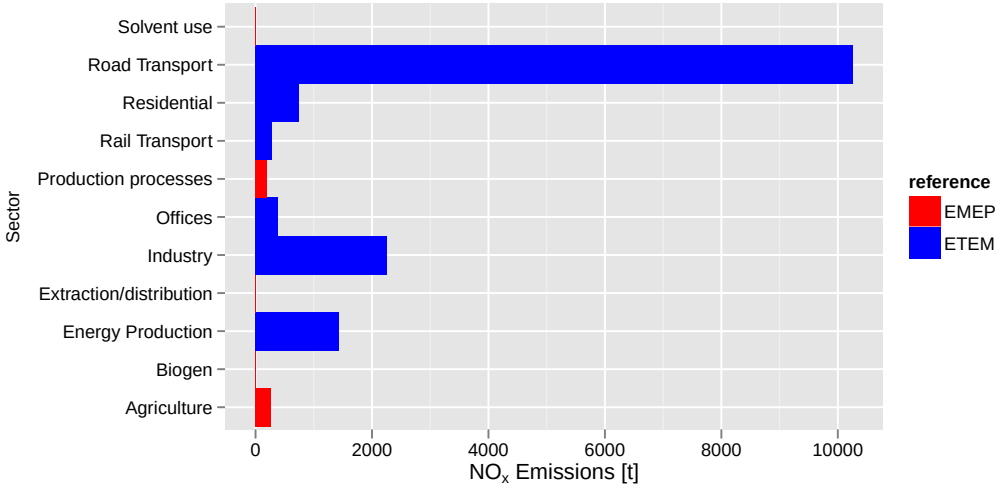

Figure 6.6: Sectoral annual NO_x emissions for 2006 from both ETEM and EMEP.

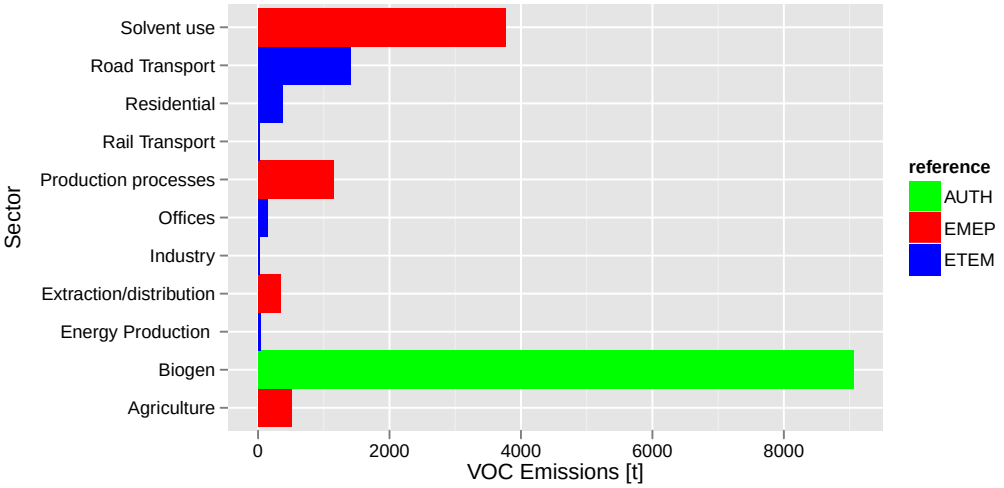

Figure 6.7: Sectoral annual VOC emissions for 2006 from ETEM and EMEP and AUTH.

The emissions allocator module, takes an average emission height for all sources. The source height which has been used in this applications is 20 meters, which was found to be a compromise between the industrial, energy production and road traffic sectors, which are the greatest emitter sectors. A further development of the emissions allocator module should include a specific source height for each sector.

6.2 AUSTAL2000-AYLTP Results

The results of NO_x and O_3 have been analysed and compared with measurements and with another air quality model, the LOng Term Ozone Simulation - European Ozone Simulation, LOTOS-EUROS model (de Leeuw et al., 1990). The VOC concentrations have not been analysed due to lack of measurement data, thus evaluation of the results is not possible. The chosen day for the simulation is the 19th of July 2006, which corresponded to a generalised ozone peak, over $180\,\mu g\,m^{-3}$, that has been registered in all monitoring stations with the exception of Luxembourg centre. In some of the stations the concentration remained high for several days, although not above the information threshold $180\,\mu g\,m^{-3}$. The background concentrations have been calculated using the background stations of Beckerich and Beidweiler. The station Mont St. Nicolas has not been used due to the fact that it is situated at a high altitude, Table 6.1. At high altitudes, the ozone concentrations are, generally, higher because the depletion by NO_x is less accentuated, and there is more intrusion of ozone from the stratosphere. The additional concentration load has been subtracted to the measured values of both stations and the average of the difference is set as the background concentration.

In what concerns the number of particles, the simulation has applied at least 63 000 000 particles as defined in Janicke (2009). The time step used is one hour.

Figure 6.8 presents the resulting ozone daily average over the calculation domain. The results show coherence, in terms of the spatial distribution, the prediction results show that in the three rural background stations, Beckerich, Beidweiler and Mont St. Nicolas, the average concentration is higher, with the station of Mont St. Nicolas being in the highest concentration zone, as it happened on that day. The results show border effects at the upwind limits of the calculation domain, due to the non existence of pollutants outside of the calculation area. The southern stations, both stations of Luxembourg city and the industrial station of Esch-Alzette, show lower ozone daily averages as it was expected. This is related to the NO_x ozone relation, but also to the fact that this stations are located upwind. Thus the high speed wind from the south has transported the ozone across the upper part of the calculation

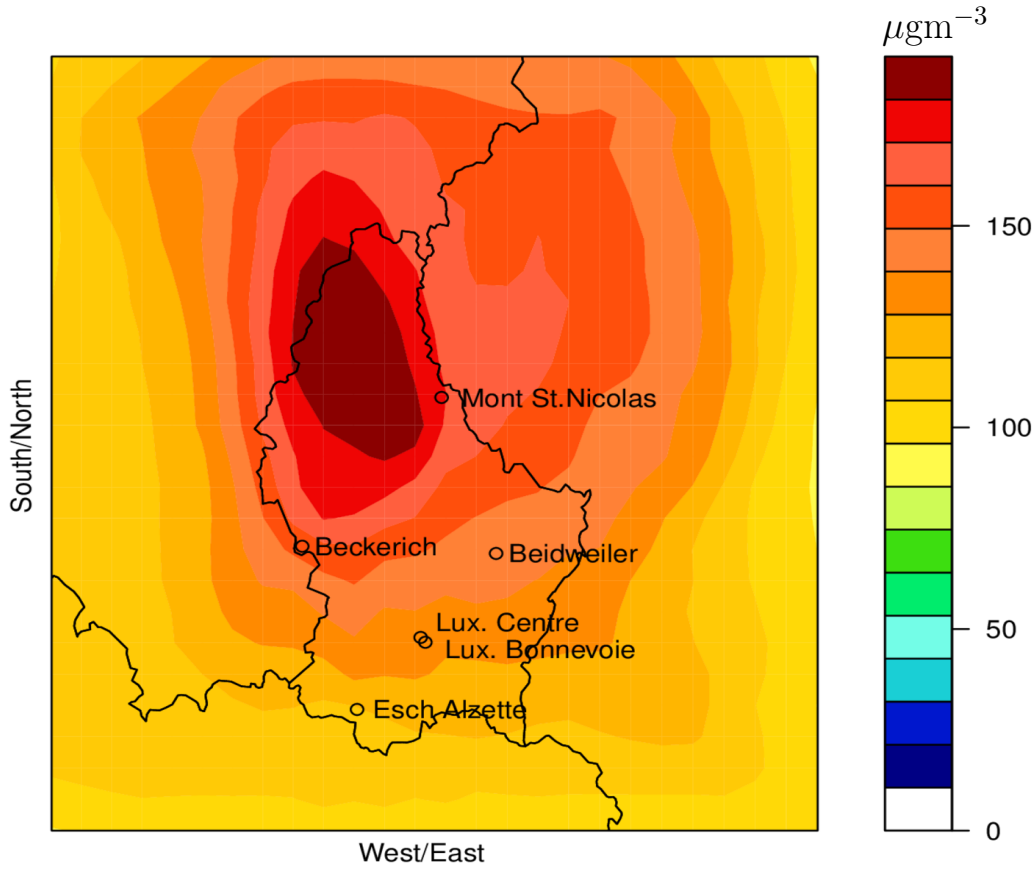

Figure 6.8: AUSTAL2000-AYLTP ozone daily average over the calculation domain, for July 19^{th} of 2006.

domain and there is no advection in through the border. Luxembourg Centre and Bonnevoie, are located in the same concentration level zone although the measurements in Luxembourg Bonnevoie show that the levels have been higher than in Luxembourg Centre.

The hourly spatial profile of the concentrations is important to understand if the model behaves consistently in terms of the temporal evolution of the pollutants. Figures 6.9 and 6.10 show the ozone and the NO_x concentration fields, respectively, for the 24 hours of the simulation.

Figure 6.9 shows that the highest ozone concentrations are found from 2pm to 4pm, the hours of higher incoming solar radiation. The ozone peak is found at 4pm near the region of Beckerich. This is the expected behaviour since the reactions which lead to the formation of ozone are depended on sunlight. Regarding the pollutant NO_x the highest concentrations are found near the city of Luxembourg, along the highway which leads to the city, and in Esch-Alzette where the industrial activity is high. The NO_x concentration peak is found at 10am in the region of Esch-Alzette. However from 2pm until 7pm the dispersion of NO_x concentration is more pronounced, due to the increase of the wind speed. The NO_x concentrations found, are generally high. This is because of the stable atmospheric conditions used in this simulation, which have been calibrated for the station of Luxembourg centre, where the meteorological station is located.

The ozone concentrations build up progressively in the morning, from 6am on. The influence of the NO_x concentrations from Luxembourg city and Esch-Alzette during the morning period is visible presenting lower ozone values where higher NO_x values are found. From 1pm until 2pm a high concentration area builds up on the north-east of Luxembourg city when NO_x is advected to less populated areas with large regions of forest. At 15pm an ozone hotspot is seen near the station of Beckerich. The advection of the of ozone through the domain in the direction of the north-west border is visible. The influence of the wind speeds is noticed during the day, being more pronounced from 12pm to 20pm, where even during the hours of higher photochemical production the wind advects the pollutants though the north and north west out of the domain. During night, the wind speed is lower and a region of higher ozone values remains in the north. It would be expected that, during night, ozone would be depleted by NO_x, since the NO_x concentrations remain high in the regions where ozone is found. In order to understand this in more detail, the reaction rates must be analysed.

The distribution of the hourly O_3 reaction rates is presented, in Fig. 6.11. In the first hour, the reaction rates are not calculated since their calculation involves the knowledge of the precursor concentrations, which are known at the end of the previous time step. The results of the O_3 reaction rates are coherent with the concentrations which have been predicted, in Fig. 6.9.

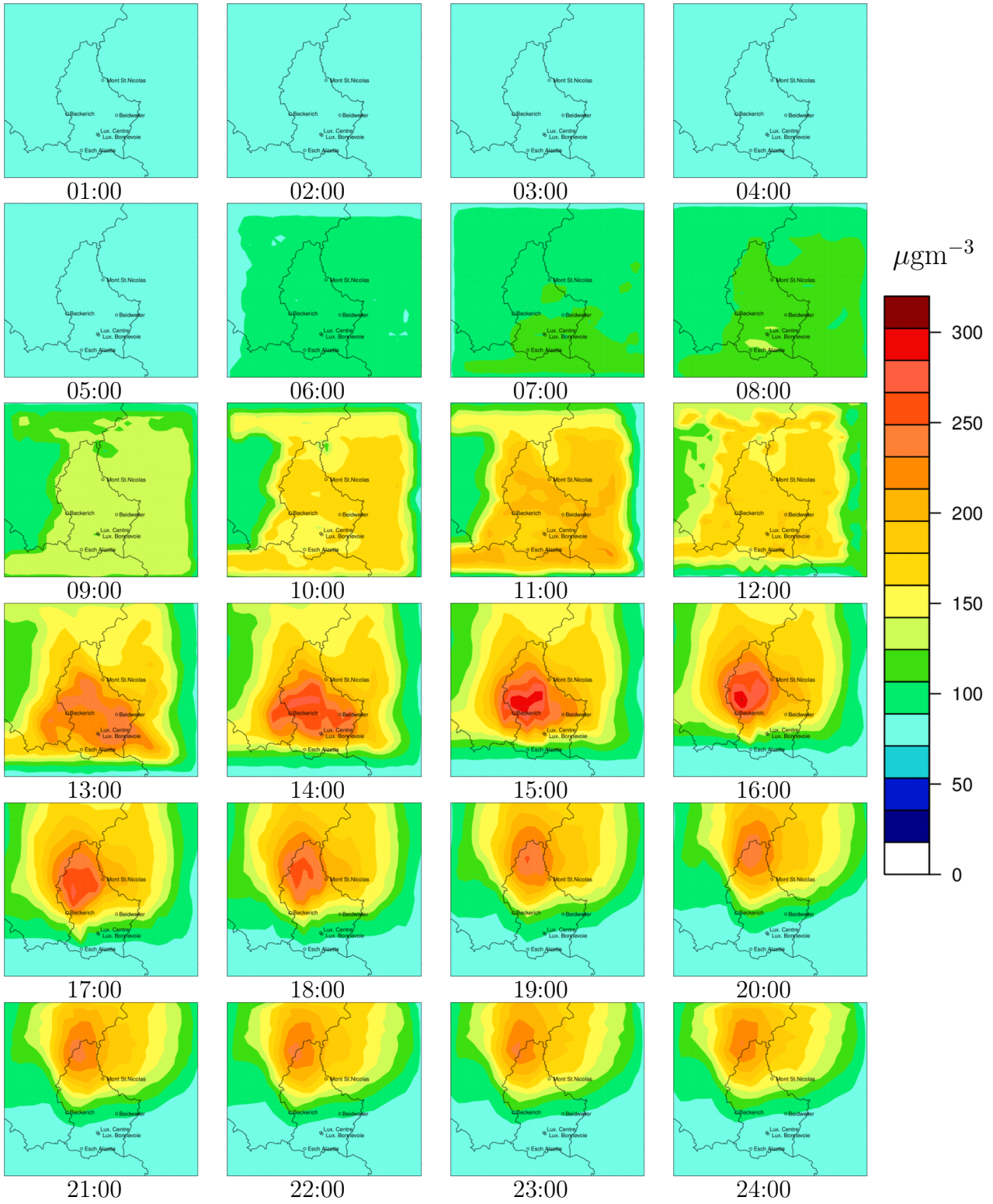

Figure 6.9: Spatial and hourly distribution of the predicted O_3 concentrations, by AUSTAL2000-AYLTP on July 19^{th}, 2006.

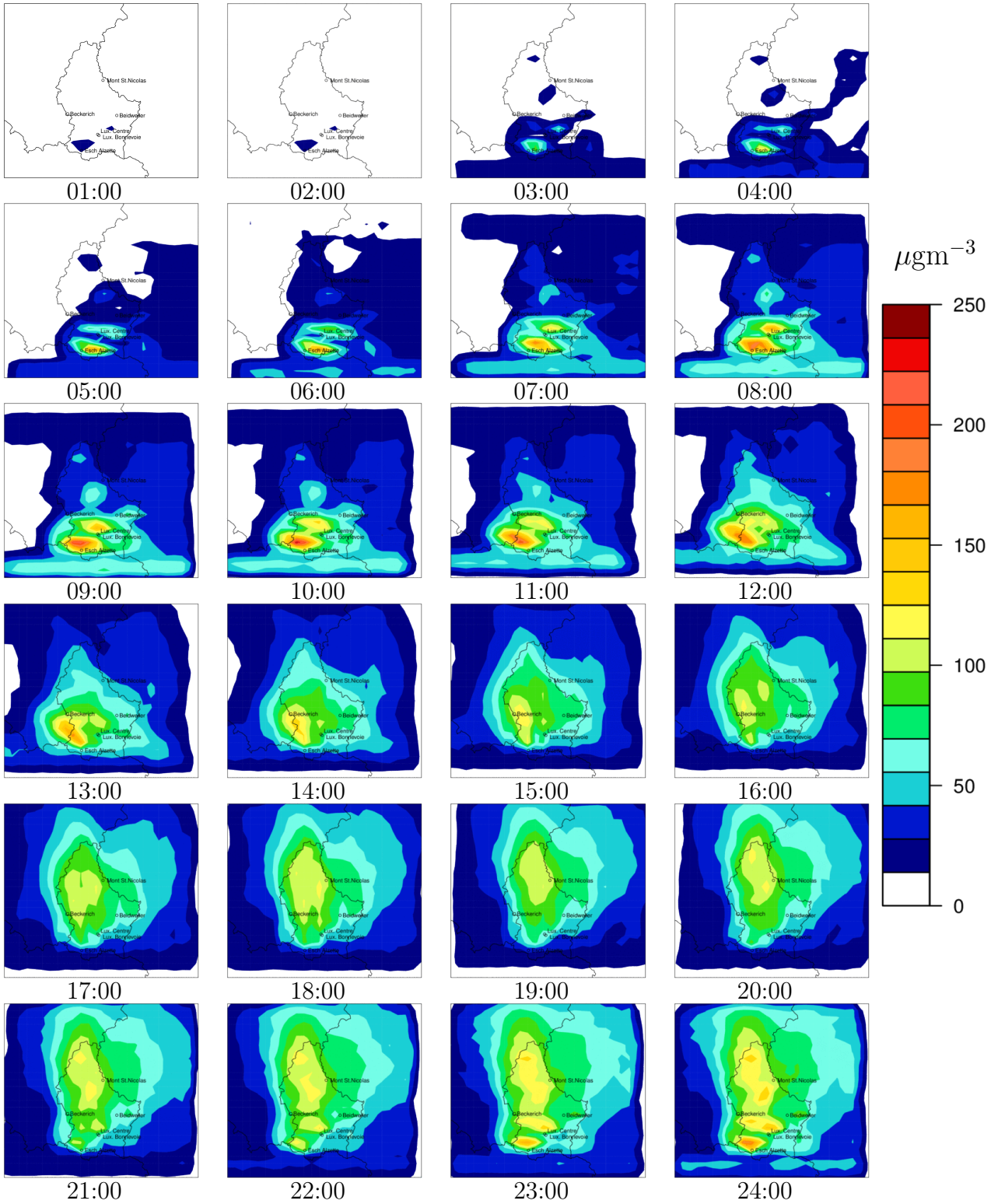

Figure 6.10: Spatial and hourly distribution of the predicted NO_x concentrations, by AUSTAL2000-AYLTP on July 19^{th}, 2006.

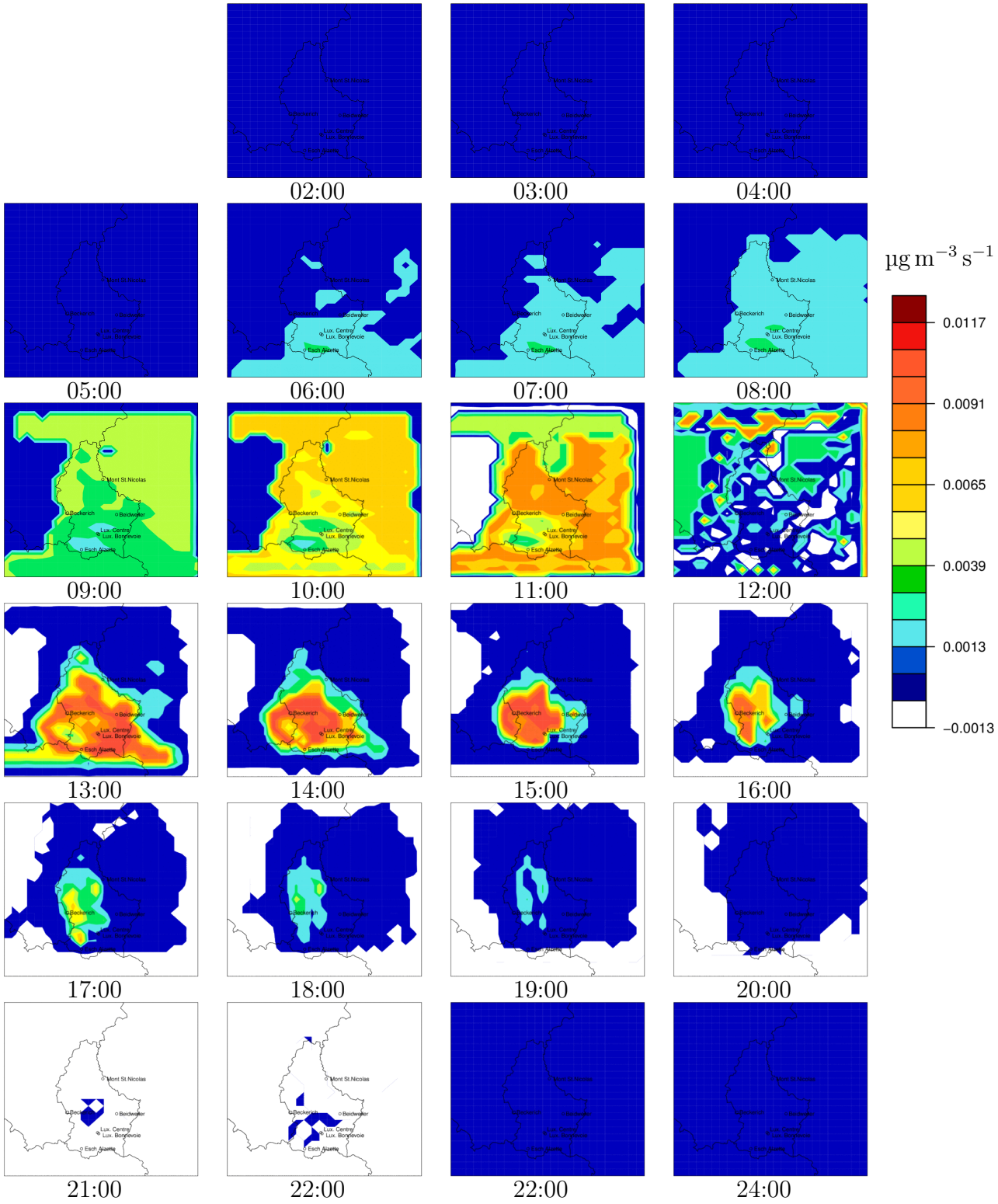

Figure 6.11: Spatial and hourly distribution of the predicted O_3 rate reactions, by AUSTAL2000-AYLTP on July 19^{th}, 2006.

During dawn, until 5am, there is nor ozone production nor destruction of ozone, as the reaction rates are zero. They start to be positive from 6am on, presenting higher values on the south and south-east of the domain. From the beginning of the simulation until 8am the highest rates are found in the regions where NO_x is present. This situation inverts at 9am, when the highest NO_x regions show the lowest ozone reactions rates, until 2am. Therefore, the NO_x-ozone relationship is present, although there is no ozone depletion, that is no negative reaction rates in the regions of higher NO_x concentration, with the exception of mid-day. At mid-day the regions with higher NO_x concentrations show no ozone production or a negative ozone rate. However, from 1pm until 9pm, the rates are positive in regions where NO_x concentrations are high. This can happen if the concentrations of VOC are also very high. The same happens at night, where in the highest NO_x concentration areas, the negative reaction rates only appear at 9pm. This is the reason why ozone concentrations do not decrease significantly at night in regions where NO_x is also high. Generally, the reaction rates daily profiles behave as expected, that is the highest ozone reaction rates are found in during the hours of higher solar radiation, specifically from 1pm to 4pm.

6.3 Model Evaluation

Assessing the ability of air quality models to approximate natural behaviours is of great importance. The EEA dedicates high relevance to model evaluation and quality assurance. Accordingly, the EU supports the development of model evaluation standards. Amongst these are the COST Action 728 (COST728, 2012) and 732 (COST732, 2011) on standardization of model evaluation, the ACCENT framework (ACCENT, 2012), on benchmarking good practises for air quality assessment. Other well know initiative is the Forum for Air Quality Modelling in Europe FAIRMODE, aiming at granting harmonised approaches for benchmarking and to provide good practises for scientific research on the field of air quality modelling.

In this work the results of the AUSTAL2000-AYLTP model simulation are compared with the observed data in the six air quality monitoring stations on the Luxembourg territory that measure ozone. Both the simulation results for NO_x and O_3 are evaluated, however no measurement data was available for VOC and therefore the simulation results can not be evaluated.

Model results can be evaluated qualitatively and quantitatively. Model evaluation is carried out by comparing model results with measurements or via model inter-comparison, or both.

6.3.1 Qualitative Evaluation

A qualitative evaluation consists in evaluating visually the the general behaviour of the model. The evaluation has been carried out comparing AUSTAL2000-AYLTP with both measurements and a chemical transport model, LOTOS-EUROS.

LOTOS-EUROS is regional Eulerian grid model for the whole of Europe. It has been developed and maintained by the Institute of Environmental Sciences, TNO, the National Institute for Public Health and the Environment, the Royal Netherlands Meteorological Institute and the Netherlands Environmental Assessment Agency. The LOTOS-EUROS is a well established and validated model (Stern et al., 2008; Timmermans et al., 2010; Vautard et al., 2012), the simulation results have been kindly granted by TNO. The LOTOS-EUROS data has a time resolution of one hour and a spatial horizontal resolution of 0.125° longitude by a 0.0625° latitude, corresponding to $\approx$ 6 km to 7 km by $\approx$ 6 km to 7 km.

The emissions used in the LOTOS-EUROS simulation are the TNO European emission dataset (Kuenen et al., 2011). They are not the same as the emissions for AUSTAL2000-AYLTP, because the TNO European emission dataset is not completely open and free. This fact constrains the model comparisons, as the differences in the results might differ greatly if the emissions are very distinct. Despite the fact that the model resolution is not the same used in the AUSTAL2000-AYLTP applications and that the emission used in the TNO model are not known, model inter-comparison has been carried out. The model inter-comparison is important, to assess the difference between using AUSTAL2000-AYLTP and a scientific research state of the art model.

Figure 6.12 presents the AUSTAL2000-AYLTP's and LOTOS-EUROS's simulation results as well as the observed data on the six air quality monitoring stations of Luxembourg. The discontinuities on the observed values in Fig. 6.12 are due to the existence of non valid measurements at the stations.

Generally, Fig. 6.12 shows a better agreement for the background stations, namely Beckerich, Beidweiler and Mont St. Nicolas. Additionally, Fig. 6.12 reveals that AUSTAL2000-AYLTP over-predicts the ozone peak concentrations in the overall stations.

On the other hand, the station of Luxembourg Centre is the one where ozone concentration is more poorly predicted. For the station of Beckerich, AUSTAL200-AYLTP predicts well the morning rising of the concentration, the peak is predicted two hours before than the observed peak. However, AUSTAL200-AYLTP predicts the ozone afternoon decrease before the measured descending slope. For this station, AUSTAL200-AYLTP predicts relatively well the peak behaviour and the magnitude of the peak. The LOTOS-

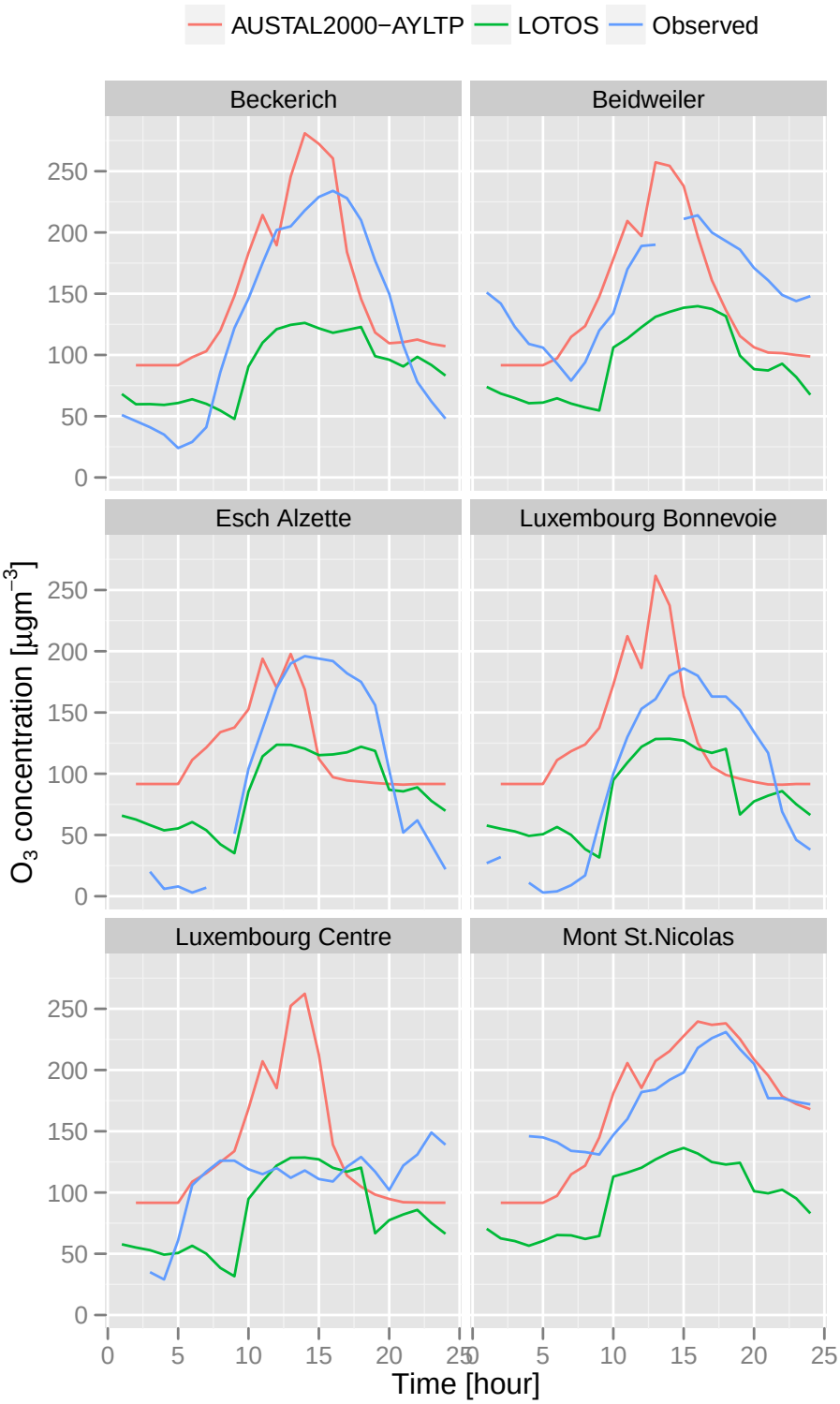

Figure 6.12: Comparison of ozone hourly results of AUSTAL2000-AYLTP and LOTOS-EUROS with measurements in the six monitoring stations of Luxembourg, for July 19^{th}, 2006.

EUROS model underestimates the ozone concentrations.

In what concerns the station of Beidweiler AUSTAL200-AYLTP overestimates the ozone concentrations, although generally follows the behaviour of the observed values. Nevertheless, the ozone peak is predicted 2 hours before the real peak and the ozone concentrations fall steeply after the peak. This fact is attributed to the strong east-southern wind observed during the day, which advected the ozone in the north/north-west direction. This decreasing behaviour around 3pm is observed in most of the stations, with the exception of Mont St. Nicolas, which is the station that presents a better prediction. This is the station which is situated downwind and in the area of higher ozone production, as shown by Fig. 6.9. In this case LOTOS-EUROS also underestimates the ozone peak and the ozone values in general.

The urban station of Luxembourg Centre and the suburban station of Luxembourg Bonnevoie are poorly predicted by AUSTAL200-AYLTP. In both stations, the ozone peak is over predicted, and the daily behaviour of ozone in these stations is inadequately predicted. Additionally, the station of Esch-Alzette presents a morning build up of ozone concentrations, however due to the southern winds the peak falls very quickly slightly before 3pm. The peak falls before on this station due to the fact that this is the most southern station. A similar behaviour can be observed for the other two southern located stations. As there is no feeding of polluted air from outside the computational domain, the concentration falls, as the wind advects the polluted air mass to the north/north-west. The LOTOS-EUROS model predicts, generally, better, although under-predicting the ozone peaks. This is due to the fact that LOTOS-EUROS is a regional model, and it is calculated for the whole of Europe, hence these stations are not located near the border of the LOTOS-EUROS domain.

Figure 6.13 presents the results for NO_x on the ozone monitoring stations of the Grand-Duchy of Luxembourg. The non-continue curve of the measured NO_x, at Esch-Alzette, is due to falling of the measuring device. For the same reason there are no measurements available in Luxembourg Bonnevoie station.

The typical NO_x daily pattern, is a two hump curve, with the two major peaks, one in the morning and another in the afternoon, corresponding to the traffic commuting hours of the working days, the simulation day corresponds to a Wednesday. NO_x is overestimated in the background stations, especially in Beckerich and Mont St. Nicolas, however it is well predicted in Luxembourg centre and Esch-Alzette. This is due to the fact that NO_x concentrations in Luxembourg centre have been calibrated adjusting the atmospheric stability to stable conditions. The use of stable atmospheric conditions is also the reason why the concentration is high in the background stations. The stable atmospheric conditions suppress vertical motion thus the polluted air masses arrive very concentrated at the background sites.

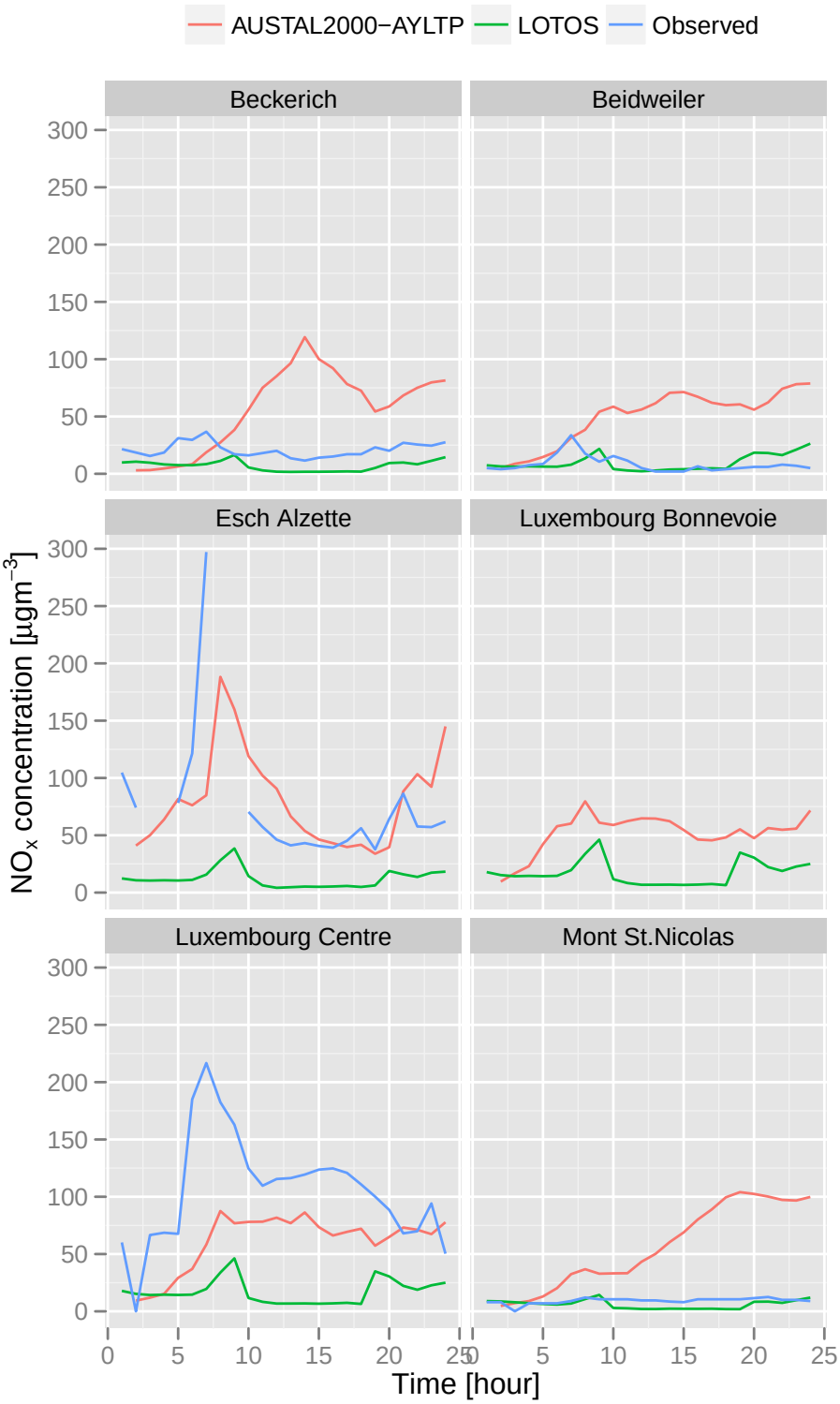

Figure 6.13: Comparison of NO_x hourly results of AUSTAL2000-AYLTP and LOTOS-EUROS with measurements in the six monitoring stations of Luxembourg, for July 19^{th}, 2006.

Regarding the Luxembourg Bonnevoie station, no valid NO_x concentration data was available for this day, nevertheless both models follow the same pattern. Unlike AUSTAL2000-AYLTP, LOTOS-EUROS well predicts the NO_x concentrations at the background stations, and it performs poorly for Luxembourg Centre and Esch-Alzette. The lower NO_x concentrations found for this stations might be related to the lower resolution of the emission sources or to lower resolution of the LOTOS-EUROS model.

Figures 6.14 and 6.15 present the scatter plots representing the AUSTAL2000-AYLTP predicted values versus the observed measurements, both for O_3 and NO_x, respectively.

The results are in agreement with the conclusions of the previous analysis of Figs. 6.12 and 6.13. The stations which show a better agreement are Beckerich and Mont St. Nicolas, furthermore the background stations present better agreement for ozone. However, the stations in Luxembourg city are not adequately predicted, especially Luxembourg Centre station.

Nevertheless, analysing Fig. 6.14 the model presents the same a general positive trend, as it can be seem by the growing blue line, although fail in some cases to predict on the magnitude of the concentration values.

In what concerns the NO_x predictions, Fig. 6.15 shows poorer agreement between predicted and measurement data than for ozone. However, the results for Luxembourg Centre and Esch-Alzette stations are considered relatively good. As it has been mentioned before, Fig. 6.15 shows that NO_x values are overestimated in the background stations.

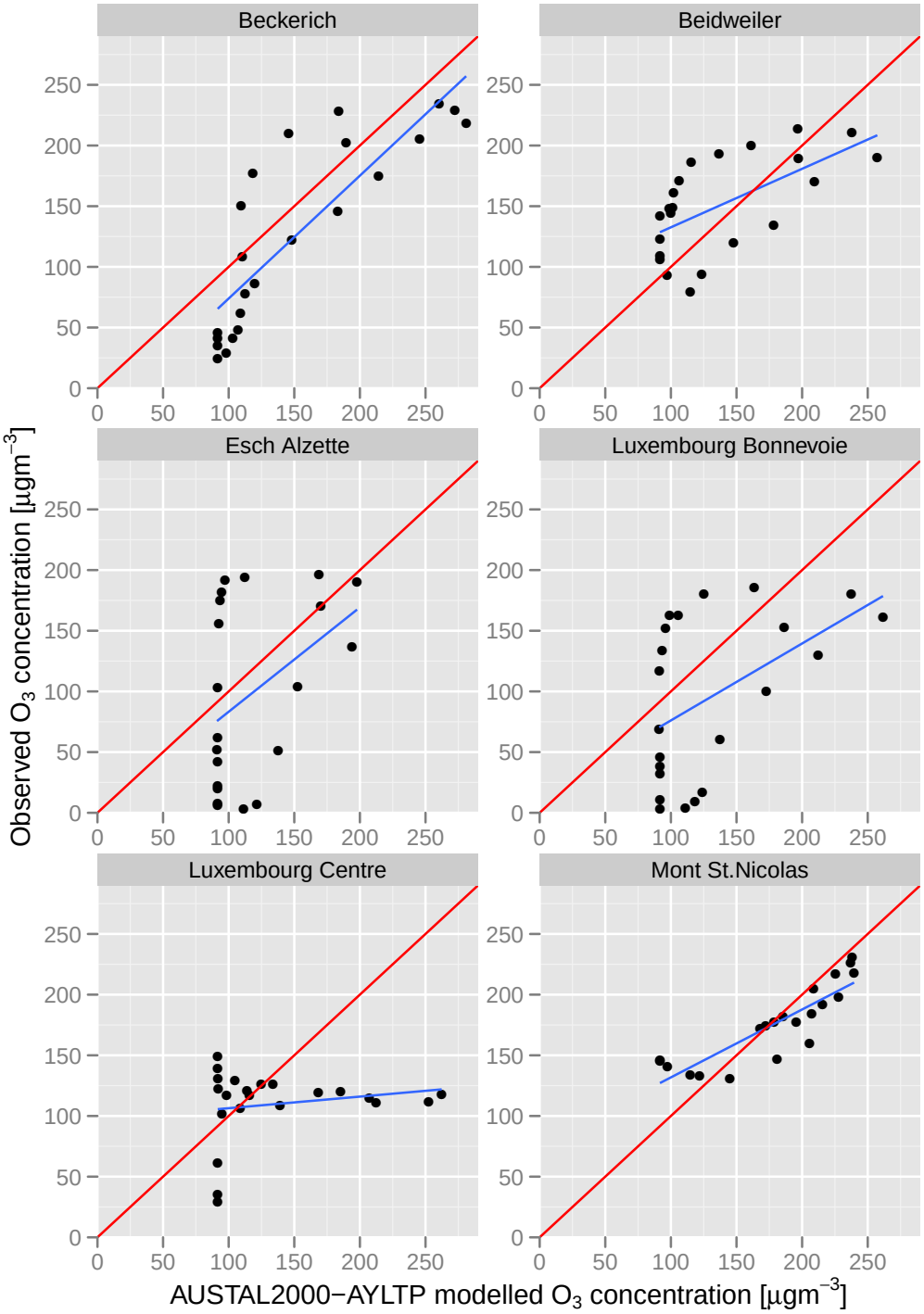

Figure 6.14: Scatter plots of ozone predicted concentrations against observations. The red line represents the ideal correlation between observed and predicted data. The blue line represents the simulations' results agreement.

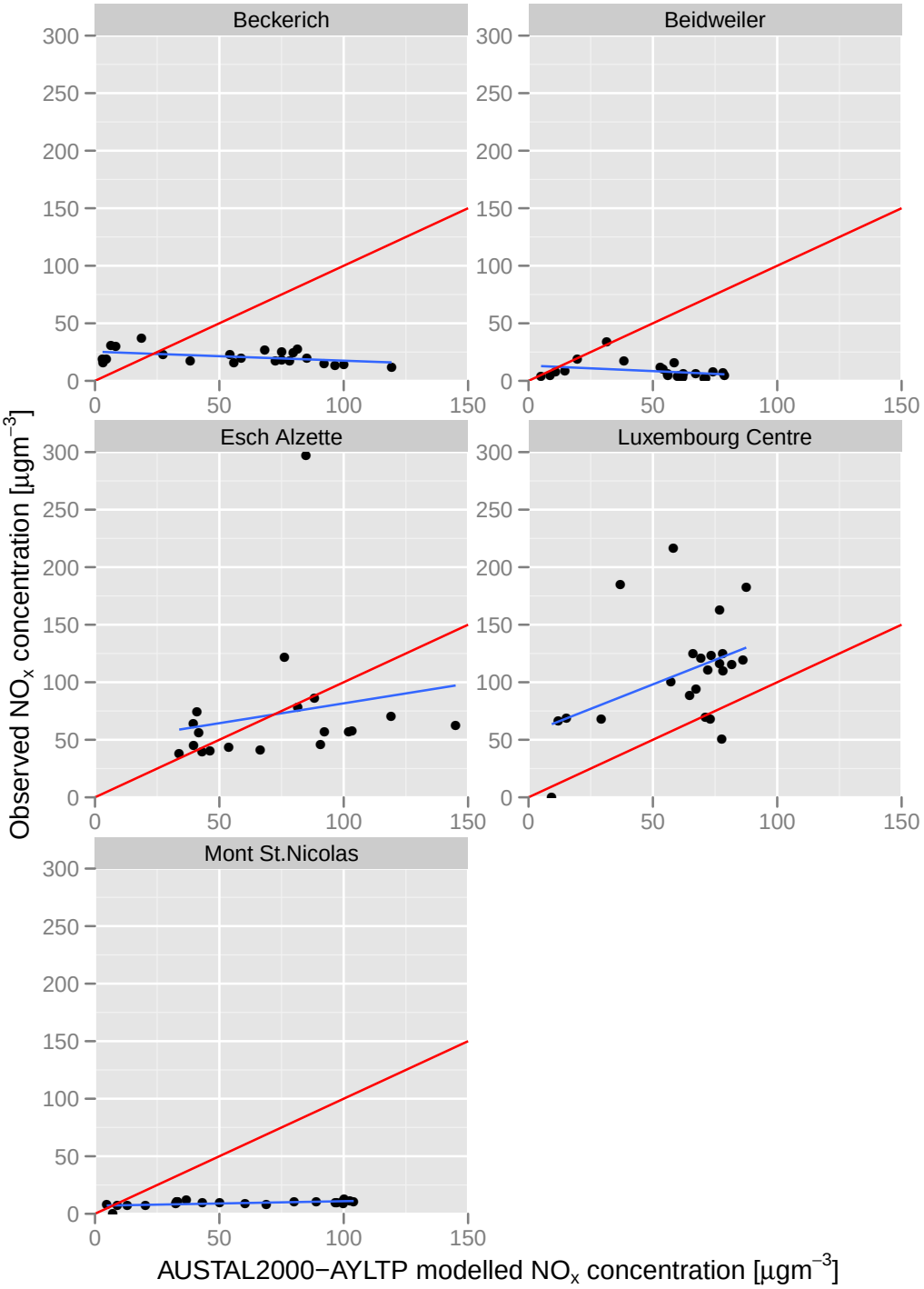

Figure 6.15: Scatter plots of NO_x predicted concentrations against observations.The red line represents the ideal correlation between observed and predicted data. The blue line represents the simulations' results agreement.

6.3.2 Model Inter-comparison

Air quality models differ in many ways, such as the transport frame of reference, the chemical schemes or model parameterisations and approximations. Model inter-comparison is useful for model evaluation because it is important to understand the capacity of the AUSTAL2000-AYLTP model in comparison with the existing air quality models.

In Fig. 6.16 the predictions of both models are compared against each other. It can be observed that AUSTAL2000-AYLTP model shows a good agreement with the LOTOS-EUROS predictions. The Luxembourg Centre station presents a better agreement with LOTOS-EUROS results than with measurements. Fig. 6.16 shows that AUSTAL2000-AYLTP predicts higher ozone concentrations than LOTOS-EUROS.

Moreover, in terms of NO_x predictions, the models show a poor agreement for all the stations. This is in agreement with the previous analysis of Figs. 6.13 and 6.15, which shows that results for NO_x in the city of Luxembourg are better represented by AUSTAL2000-AYLTP, whereas in the background stations LOTOS-EUROS performs better.

The qualitative evaluation has revealed that AUSTAL2000-AYLTP well predicts the ozone concentrations in the background stations, especially in Mont St. Nicolas and Beckerich stations. On the other hand, the AUSTAL2000-AYLTP results for Luxembourg Centre station present a poor agreement with the observed data. Regarding the prediction of NO_x, the Esch-Alzette and Luxembourg centre are the stations which are better modelled by AUSTAL2000-AYLTP model. LOTOS-EUROS on the other hand poorly predicts the NO_x concentrations for the non background stations, while the NO_x concentrations at the background stations are generally well represented by LOTOS-EUROS in terms of the magnitude of the values. In order to analyse deeply the model results a quantitative evaluation has been undertaken.

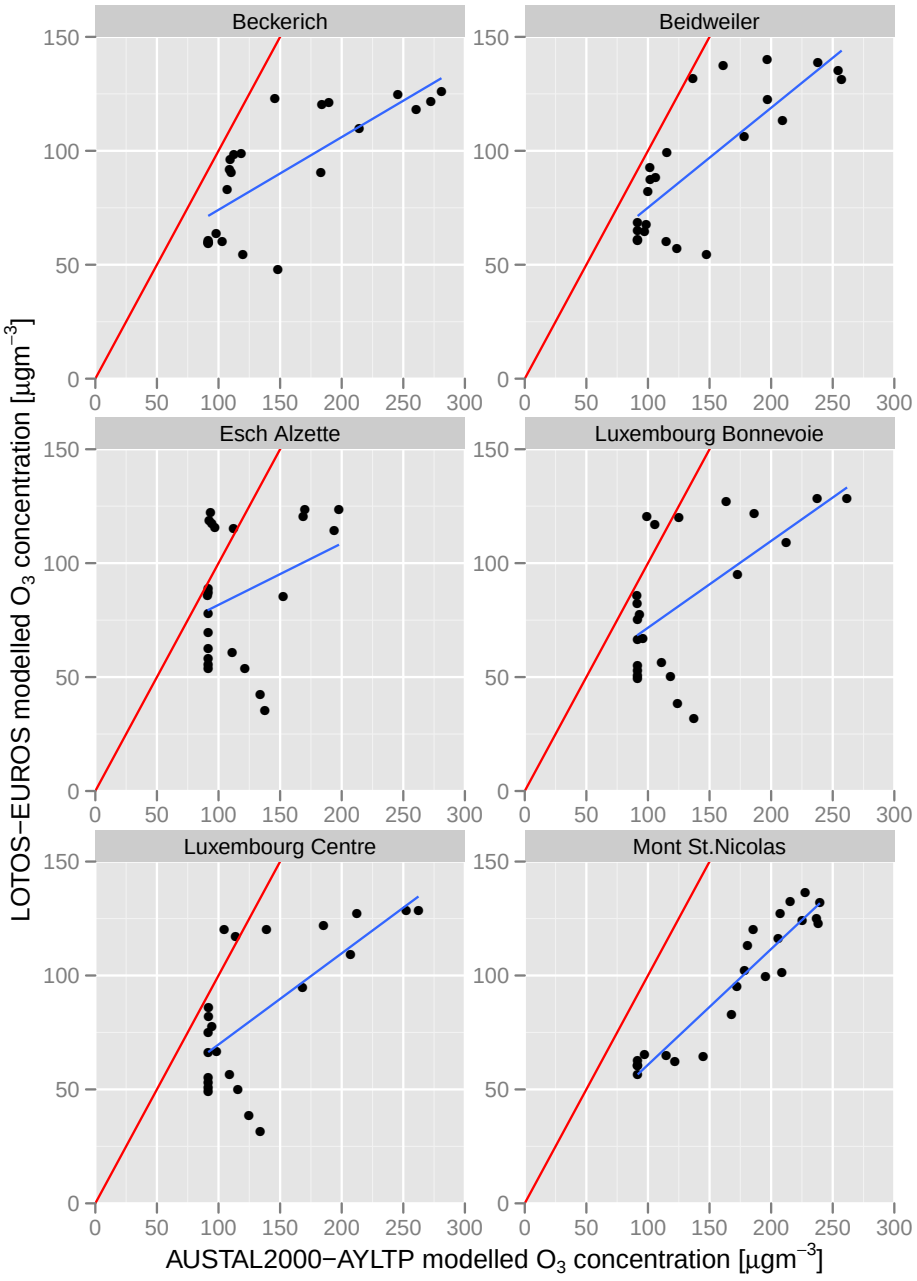

Figure 6.16: Scatter plots of ozone predicted concentrations against LOTOS-EUROS predictions.

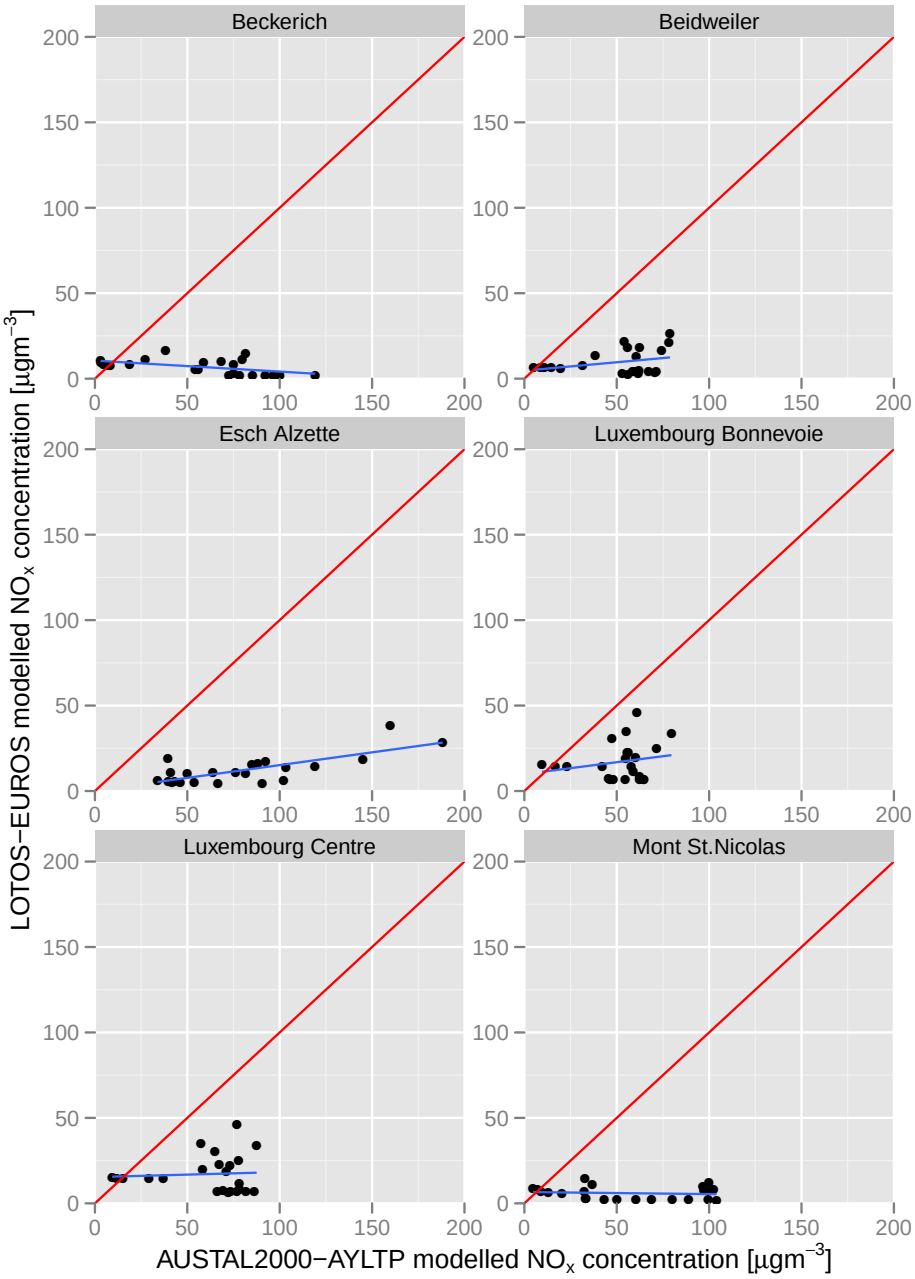

Figure 6.17: Scatter plots of NO_x predicted concentrations against LOTOS-EUROS predictions.

6.4 Quantitative Evaluation

The Taylor diagram provides concise information about the quantitative model performance. It relates the correlation coefficient, the normalized standard deviation and the normalized centred Root Mean Square (RMS) difference.

The Taylor diagram in Fig. 6.18 shows the models' agreement with the observed values. The observations are represented by the black dot on the x axis, the closer the models are of this value the better are the predictions.

Generally, the analysis of the Taylor diagrams is coherent with the qualitative analysis. Figure 6.18(a) shows that LOTOS-EUROS model predictions present a lower RMS difference, which would be expected since the magnitude of the perditions of LOTOS-EUROS is lower compared to the AUSTAL2000-AYLTP. LOTOS-EUROS presents a very good agreement with the observed data, showing correlations between approximately 0.8 and 0.9, except for the station of Luxembourg Centre. In this station both models perform poorly.

On the other hand, AUSTAL2000-AYLTP also shows a good agreement, with the exception of the Luxembourg Centre station. As discussed before, the background stations show better results in terms of correlation. The region of Beckerich is where AUSTAL2000-AYLTP performs better, in terms of predicting the magnitude and behaviour of the ozone concentrations, showing a lower RMS difference than the LOTOS-EUROS model predictions. However, Mont St. Nicolas is the stations which presents a better correlations coefficient.

In what concerns the NO_x perditions, Fig. 6.18(b), the results are not satisfactory for both models, with the AUSTAL2000-AYLTP predicting very poorly except for the stations of Luxembourg centre and Esch-Alzette. It must be noted that the results of some stations are not presented in this diagram. This has been done purposely in order to ease the visualization, since some results have negative correlations. Additionally, there are no measurements for the Luxembourg Bonnevoie stations, and therefore the comparison is not possible to be carried on. The stations of Beckerich and Beidweiler present negative correlations and a high RMS difference, 37.6 and 25.6 respectively. The station of Mont St. Nicolas presents a positive correlation, 0.61, but it has a RMS difference of 33.3. In the case of LOTOS-EUROS, the prediction of NO_x for Mont St. Nicolas presents a negative correlation. Generally, the LOTOS-EUROS estimations present a lower normalized RMS difference, as expected since the magnitude of the predicted values is very low.

The discrepancy between observed and modelled results is more pronounced than what it would be desired, and it happens in many model application studies, mostly attributed to poor quality and availability of the emission and meteorological data (Dennis, 2010). Models' results strongly depend on

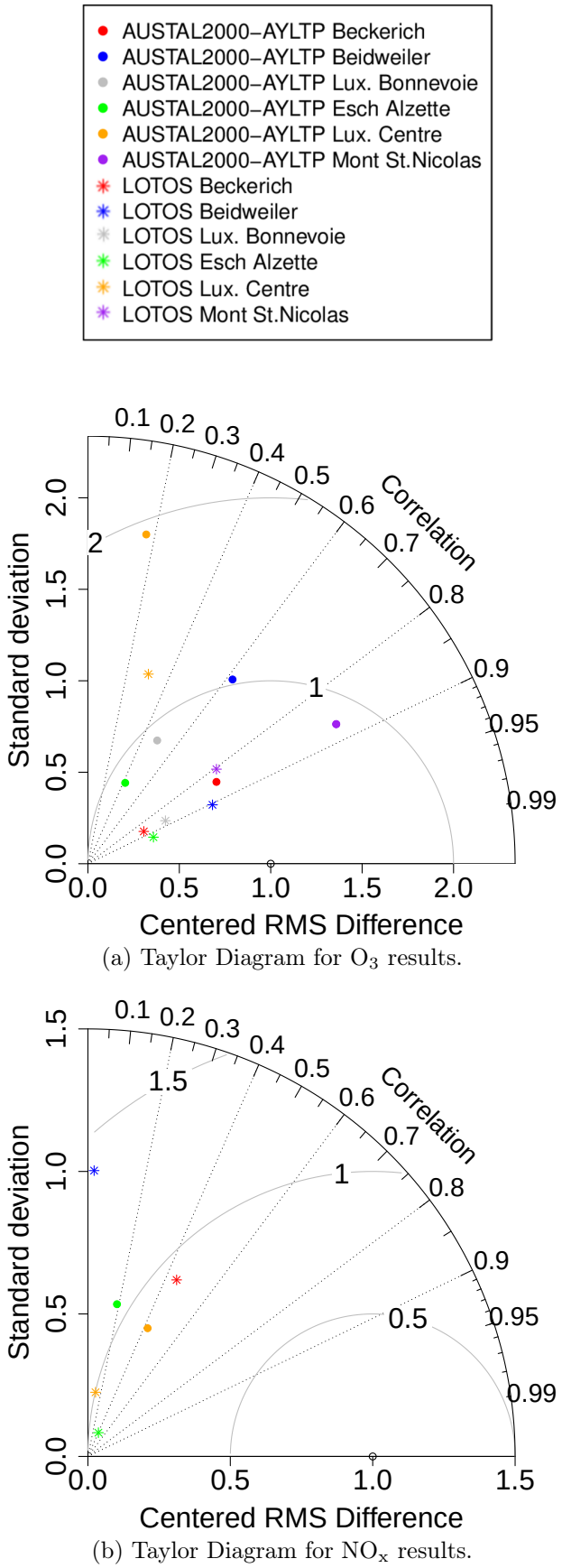

(a) Taylor Diagram for O_3 results.

(b) Taylor Diagram for NO_x results.

Figure 6.18: The Taylor diagram for both AUSTAL2000-AYLTP and LOTOS-EUROS models and the observed O_3 measurements, indicated by the black outlined point in the x axis.

the input data quality. In this application the poorly results found for NO_x can be attributed to the stable atmospheric conditions and to the fact that the wind field can only be based on one meteorological station. The meteorological station is located close to Luxembourg Centre, and the NO_x have been calibrated for the Luxembourg Centre station adjusting the atmospheric stability conditions to stable. However, this suppresses the vertical motion of pollutants and the polluted air masses remain very concentrated as they are advected away from the sources.

Field data, in general, has a drawback for the validation of pollutants' concentrations, because the comparison of point measurements with an average 5 km by 5 km grid cell rises doubts about the representativeness of the measurements (Dennis, 2010).

Concluding, the model produced explicable results, and it is able to respond to the relationship between NO_x and O_3, and reproduces the typical daily ozone profiles in function of the higher solar radiation hours. Although the NO_x-O_3 is visible, it would be expected that there would be more intensive depletion of O_3 by NO_x. This can be explained if the VOC concentrations are also very high. However, the lack of VOC measurement data limits this analysis.

Furthermore, the reaction rates show comprehensible results not just in what concerns the spatial distribution but also in its temporal relationship with solar radiation. Moreover, the AUSTAL2000-AYLTP results are comparable to those of LOTOS-EUROS and to the observed concentrations. The results of the validation are considered satisfactory.

It is worth to emphasise that AUSTAL2000-AYLTP has been built for an integrated assessment framework, and therefore it is not a scientific research model nor a forecast model, but a policy support model. Dennis (2010); Moussiopoulos et al. (1996); Sportisse (2007) point out that these models should be evaluated and applied according to their specific application and not outside the model objectives. In the case of AUSTAL2000-AYLTP, a policy support model is required to respond to strong variations on the initial conditions, as strong variations in the emission values. Hence, air quality policy support models should be judged in their objective frameworks. In the next chapter, AUSTAL2000-AYLTP is integrated in LEAQ and the results are analysed and discussed.

Chapter 7

The Luxembourg Energy and Air Quality Model

Contents

The ultimate goal of the LEAQ project is to provide technical guidance for air quality, with the focus in ozone pollution, control strategies. The objective is to find the most cost-efficient control strategy, which could be applied by the Luxembourg's authorities in order to comply with a given quality threshold in a mid range term. This can be answered solving an optimization problem. In the LEAQ framework, this task is undergone by OBOE.

The optimisation problem minimises the discounted total energy cost while respecting an air quality restriction as follows:

$$\min_{\hat{\mathbf{e}}} \{\gamma(\hat{\mathbf{e}}) : p(\hat{\mathbf{e}}) - \hat{p} \leq 0\}, \tag{7.1}$$

where $\hat{p}$ is the air quality indicator target. $\gamma(\hat{\mathbf{e}})$ is the cost function issued from ETEM and $p(\hat{\mathbf{e}})$ is the chosen air quality indicator, calculated with AUSTAL2000-AYLTP. The discounted cost is the total energy cost but taking into account the investment time preference of the investor. In the following section, it is explained how ETEM and AUSTAL2000-AYLTP are used in the coupling of both models.

7.1 Coupling Methodology

The LEAQ integrated assessment model couples an energy model ETEM with the air quality model AUSTAL2000-AYLTP. The details of the coupling are presented in this section.

7.1.1 Energy System Cost

To calculate the energy system's activities and investments, ETEM solves a partial equilibrium, which contrary to a general equilibrium, is a condition of an economic equilibrium when only a part of the market is considered, here the energy market. The demand in energy services is fixed, so it does not adjust according to the energy price, i.e. an increase or a decrease in the price of energy does not impact the level of demand in energy services. It minimises the discounted total cost of the energy system of the country, i.e. investment costs, activity costs and purchase costs of energy commodities. The model is driven by the demand in energy services in transportation, in industry, in residential, in the commercial/institutional sector and in agriculture. To meet this demand, the model provides the optimal energy activities and investments over the time horizon. The model solves an optimisation problem of the linear form and computes the optimal value of the objective function

$$\gamma(\hat{\mathbf{e}}) = \min_{\mathbf{x}}\{\mathbf{r}'\mathbf{x} \mid \mathbf{A}\mathbf{x} = \mathbf{b}, \mathbf{m}'\mathbf{x} = \mathbf{e} \leq \hat{\mathbf{e}}, \mathbf{x} \geq 0\}, \tag{7.2}$$

where $\mathbf{x} \in \mathbb{R}^n$ is the vector of the decision variables, e.g. technology investments and activities, $\mathbf{r} \in \mathbb{R}^n$ is the cost vector and the constraint $\mathbf{A}\mathbf{x} = \mathbf{b}$ describes the structure of the reference energy system, the characteristics of the technologies and of the energy resources.

In addition, the model calculates the annual emissions $\mathbf{e} = e_{q,\mu}$ (expressed in $\mathrm{t\,yr^{-1}}$) of the pollutants $q \in \{\mathrm{NO_x}, \mathrm{VOC}\}$ for each sector $\mu \in \xi$. The emission vector is obtained by multiplying the fuel consumption with the associated emission factor which is a component of $\mathbf{m}$. The emissions are constrained by the upper bounds $\hat{\mathbf{e}}$ representing the annual sectoral emissions maximum.

The aggregated annual sectoral emissions $\hat{e}_{q,\mu}$ are distributed per sector according to the spatial allocation functions and the time profile functions.

7.1.2 Air Quality Indicator

As described in Chapter 4, the air quality model is based on AUSTAL2000, an atmospheric dispersion model for simulating the dispersion of air pollutants in the ambient atmosphere (Janicke, 2000). It is called AUSTAL2000-AYLTP

and is an augmented version integrating a fast photochemical calculator to simulate the ozone production.

Using the emissions strengths $e_{q,k}(t,s)$, AUSTAL2000-AYLTP computes the concentrations of pollutants at every time step t over the region S. The dispersion modelling provides the expected values of the concentrations $\bar{c}(s,t)$ and the associated errors $\sigma_s(s,t)$, as discussed in Section B.2 of Chapter B.

An air quality indicator is calculated as the Accumulated Ozone exposure over a Threshold AOT. As defined in the Directive 2008/50/EC, the AOT is a measure of the ozone concentration exceedances over a certain threshold measured during the day, from 8:00 to 20:00, e.g. AOT_{40} corresponds to the accumulated ozone exposure over a threshold of 40 ppb (EU, 2008a).

The expected value of AOT_i is defined as:

$$E[AOT_i] = \alpha \int_S \int_{t_1}^{t_2} \max(0, (\bar{c}(s,t) - i))\, \mathrm{d}t\mathrm{d}s, \tag{7.3}$$

where $\alpha = (|S| \cdot |t_2 - t_1|)^{-1}$. t_1 and t_2 are respectively at 8:00 and 20:00 of the day, and $|S|$ is the surface of the region S.

Taking into account the air quality model sampling error from Eq. (B.1), using the 95% upper limit of the confidence interval of the concentrations levels, an upper limit of the AOT can be calculated as follows:

$$U[AOT_i] = \alpha \int_S \int_{t_1}^{t_2} \max(0, (\bar{c}(s,t) + 1.96\sigma_c(s,t) - i))\, \mathrm{d}t\mathrm{d}s. \tag{7.4}$$

This confidence interval does not include all types of uncertainty and only contains the uncertainty related with the air quality model sampling error. Other uncertainties can arise from both model formulation and application such as uncertainties on the input data, on the model assumptions and parameters or on the model resolution and boundaries. However a complete uncertainty study is out of the scope of this work.

The air quality indicator can be generalised as a function of $\hat{\mathbf{e}}$, which is the input of the emission allocation transformation and, consequently influences the input of the air quality model. Here, the air quality indicator is given as $p(\hat{\mathbf{e}}) = E[AOT_i]$ or $U[AOT_i]$.

7.1.3 Implementation

The optimisation problem, Eq. (7.1), is non-differentiable, and can be solved by a cutting-plane method, such as ACCPM (Goffin and Vial, 1993), as explained in Section 3.2.3. The oracle-based optimisation engine OBOE implements such a method and provides convenient framework using an oracle (Babonneau et al., 2006). An oracle is a program which calculates the

information required by the optimiser and gives a reply under the form of an inequality, called "cut". The oracle returns either an optimality cut, to support the objective function, or a feasibility cut, to define an outer space of the feasible set.

Figure 7.1 presents schematically the algorithm and the communication between the models, where the threshold is defined at the beginning. ϵ is the perturbation applied to the emissions to calculate the sensitivity of AUSTAL2000-AYLTP, as defined in Eq. (7.5).

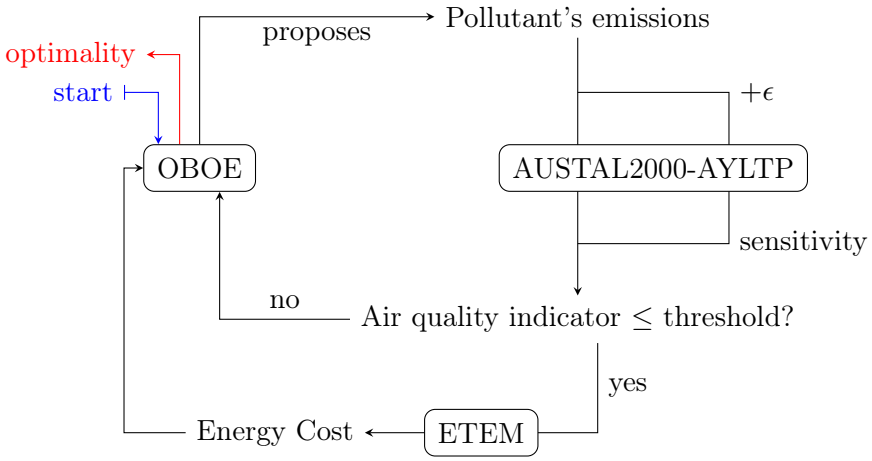

Figure 7.1: Algorithm scheme and information exchange between the models. Where ϵ is the perturbed emission value and the limit is defined as an air quality objective for the defined time horizon.

At a query point, the optimality cuts (O) and the feasibility cuts (F) are defined by three components:

- the objective function value (O) or the sub-space defined by the constraint (F);
- the sub-gradients, as defined hereafter;
- a cut indicator: 0 (O) or 1 (F).

Concerning ETEM, the gradient values of the objective function $\delta\gamma$ at the query point $\hat{\mathbf{e}}$ are equal to the optimal dual value of the constraints $\mathbf{e} \leq \hat{\mathbf{e}}$, in Eq. (7.2). The linear program solver provides these dual values as an output of the ETEM model.

The sub-gradient values, related to AUSTAL2000-AYLTP, required by the feasibility cut, cannot be obtained analytically because $p(\hat{\mathbf{e}})$ results from a call to the model AUSTAL2000-AYLTP. An estimation of the sub-gradients can be calculated by finite difference:

$$\delta p(\hat{\mathbf{e}}) \approx \frac{p(\hat{\mathbf{e}} + \epsilon) - p(\hat{\mathbf{e}})}{\epsilon}, \tag{7.5}$$

where $p(\hat{\mathbf{e}} + \epsilon)$ is a vector of the values of the perturbed air quality indicator.

At each iteration, the optimiser proposes a new query point chosen as the analytic centre of a localisation set, built from the generated cuts and containing all admissible solutions. This localisation set is shrinking as the iterations proceed, and when a stopping criterion is attained, the optimal solution is found as the last query point. This cutting plane method has been proven to converge in Nesterov (1995).

The resolution algorithm is the following:

1. Define a starting query point $\hat{\mathbf{e}}_{\mathbf{n=0}}$;
2. Evaluate the AQ indicator $p(\hat{\mathbf{e}}_{\mathbf{n}})$:
   (a) Allocate $\hat{\mathbf{e}}_{\mathbf{n}}$ during the episode and over Luxembourg,
   (b) Run AUSTAL2000-AYLTP,
   (c) Compute $p(\hat{\mathbf{e}}_{\mathbf{n}})$;
3. If $p(\hat{\mathbf{e}}_{\mathbf{n}}) > \hat{p}$ then generate a feasibility cut:
   (a) Evaluate the components of $\mathbf{p}(\hat{\mathbf{e}}_{\mathbf{n}} + \epsilon)$,
   (b) Calculate $\delta\mathbf{p}(\hat{\mathbf{e}}_{\mathbf{n}})$,
   (c) Define the cut as $[p(\hat{\mathbf{e}}_{\mathbf{n}}) - \hat{p}, \delta\mathbf{p}(\hat{\mathbf{e}}_{\mathbf{n}}), 0]$

   else generate an optimality cut:
   (a) Run ETEM with bounds on emissions=$\hat{\mathbf{e}}_{\mathbf{n}}$,
   (b) Get the optimal objective value and the dual values of bounds,
   (c) Define the cut as $[\gamma(\hat{\mathbf{e}}_{\mathbf{n}}), \delta\gamma(\hat{\mathbf{e}}_{\mathbf{n}}), 1]$
4. Send the generated cut to OBOE;
5. Get the next query point $\hat{\mathbf{e}}_{\mathbf{n+1}}$ from OBOE;
6. If the stopping criterion is met then stop, else $n = n + 1$ and go to 2.

In this thesis work, two case studies have been evaluated. One, where only the Luxembourg's national emissions have been considered - the Luxembourg country study case; and another where the emissions from the surrounding countries have been included. The former included two scenarios: scenario 1, using the NO_x national emissions as coupling variable; scenario 2, using the emissions from the region of Luxembourg as a coupling variable.

7.2 The Luxembourg Country

This study case has been simulated to determine the optimal NO_x emission levels from Luxembourg to comply with drastic air quality limits after 2020, by simulating a typical three-day episode in the worst meteorological case scenario.

ETEM Luxembourg describes the Luxembourg energy sector from 2005 to 2030. The base years 2005–2012 are calibrated with the national energy balance, according to the National Institute for Statistics and Economic Studies of the Grand-Duchy of Luxembourg (Drouet, 2011). The coupling variables limit the total annual NO_x emissions during the period 2020–2030, imposing maximum emission bounds in ETEM. It must be noted that ETEM only provided the energy related emissions, and only includes the emissions of the Luxembourg Grand-Duchy territory, as emission reduction measures can only be controlled unilaterally at a national level.

In this case study, AUSTAL2000-AYLTP was set to simulate a three-day episode during summer, from the 16th to the 19th of July. Additionally to the energy-related emissions, biogenic VOC emission data are also taken into account, using data from the Aristotle University of Thessaloniki. The spatial domain is a 20×24 horizontal grid with a resolution of 5 km, 15 vertical layers up to 1500 m and with the near-ground vertical layer of 20 m. This layer height has been chosen for the coupling simulation due the averaging source height. In this sense, a more averaged ground layer compensates the averaging of the source height. The time step is set to one hour.

The AQ indicators, expected and upper AOT_1, are calculated for the last day of the episode from 8:00 to 20:00 over Luxembourg as defined in Section 7.1.2.

7.2.1 Convex Optimization approach Limitations

One major requirement of the oracle-based optimisation method is the convexity of the optimisation problem. The objective function, assimilated to ETEM Luxembourg, is convex by construction because when the emissions bounds $\hat{\mathbf{e}}$ decrease, the total energy cost increases and vice versa.

The convexity of the feasible set, where the solution lies, is more difficult to establish because the response of the air quality is not convex: an increase in NO_x emissions could result in the production or in the destruction of ozone, depending on the VOC/NO_x ratio. A convex surface implies that, if two points of a given 3D surface are connected by a straight line, this line only intercepts the 3D surface at maximum two points. Nevertheless, in practice, a pseudo-convex response can be obtained by restricting the search domain of

the coupling variables. This search domain can be determined by exploring the response surface of the air quality model. Hence, two response surfaces for two different meteorological conditions have been analysed. One where realistic meteorological conditions are used, and another one representing a worst case scenario where meteorological conditions are favourable to originate ozone episodes. The worst case scenario is a highly unlikely scenario, however it is relevant in terms of policy support. If an energetic strategy is found for the worst case scenario then the most probable less aggravating meteorological conditions are also in compliance.

Figure 7.2 shows two surfaces of AOT_1 in function of the total emissions of NO_x and VOC during a three-day episode.

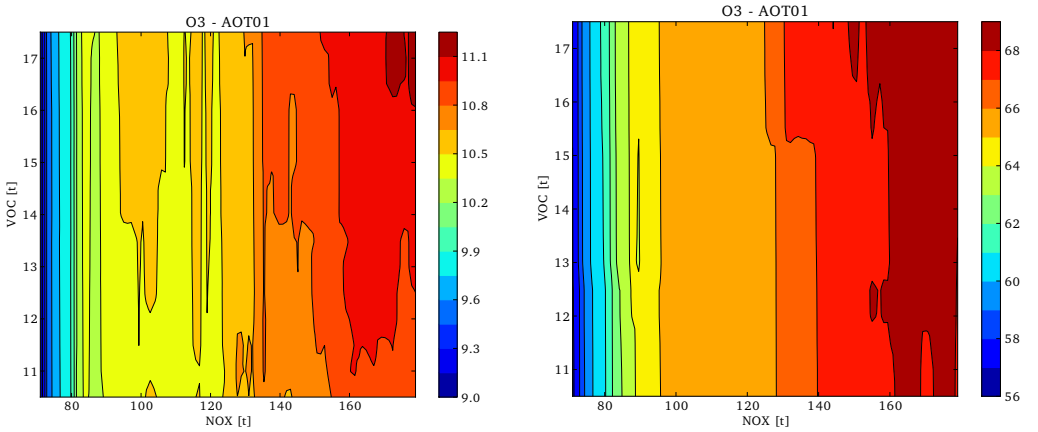

(a) Real meteorological conditions

(b) Favourable meteorological conditions for ozone production

Figure 7.2: The air quality indicator $E[AOT_1]$ surface, in $\mu g\,m^{-3}$, as a function of the total NO_x and VOC emissions, in t during a three-day episode, using AUSTAL2000-AYLTP with two meteorological conditions.

They compare the air quality model outputs when using two conditions: using real meteorological conditions, and using stable atmospheric conditions, e.g. low constant wind speed, $0.7\,m\,s^{-1}$, constant wind direction, constant high temperature, 37 °C, constant relative humidity, 55%. The stable meteorological conditions can also be seen as the most favourable meteorological conditions to produce ozone. It can be noticed in Fig. 7.2 that the air quality response surface is smoother with stable meteorological conditions. These conditions remove the "chaotic"-like behaviour of the ozone's response observed with realistic conditions Fig. 7.2(a), mainly provoked by changes in wind direction and velocity. However it must be noticed that this is a theoretical exercise, to obtain a more suitable response for the optimizer, and it is an unrealistic scenario. Additionally, it also ensures that the air quality indicator is achieved for less critical meteorological conditions.

The surface graphs also show that the domain of interest is rather NO_x-

sensitive than VOC-sensitive. Since the ozone concentrations vary mainly with the increase of NO_x. Thus, the coupling variables are the NO_x emissions, which better control the impact on the air quality indicator.

Two scenarios have been simulated. In the first, scenario 1, the coupling variable is the total Luxembourg NO_x emissions. In the second scenario, scenario 2, the coupling variables are the NO_x emissions from the transport sector, the residential sector and the other sectors. In this case, only the impacts from the energy policy implemented in Luxembourg are considered. The impacts on the ozone concentrations in the surrounding countries are excluded, but also the impacts in Luxembourg induced by the energy policies of others countries.

For each scenario, the optimisation problem in Eq. (7.1) is solved for different values of the threshold AOT_1, $\hat{p} \in \{40, 45, 50, 55, 60, 65, 70, 75, 80\}$. An iteration takes about 9 min to be completed on a computer machine 4×quad-core AMD 800 MHz CPU, which is a satisfactory time for an iteration of OBOE. This means that the objectives of a reasonably fast air quality model have been achieved, given that the sensitivity of the air quality model is calculated in parallel. The air quality model runtime is on average 5 min. ETEM Luxembourg is written in GAMS (Rosenthal, 2011) and is solved with the MOSEK solver in 3 min.

The convergence is obtained after a number of iterations depending on the choice of the starting point, but in practice this number remains rather stable. In this study case, in order to evaluate the number of iterations, the starting point is fixed as the middle point of the interval of the possible values for NO_x and the stopping criterion is set to 10^{-5}. Figure 7.3 plots the number of iterations to converge for each scenario case according to the threshold. The figure shows that the number of iterations does not vary with the air quality indicator, but rather increases with the number of coupling variables, as is the case of scenario 2. In scenario 1, the average number of iterations is 15.75 (i.e. 2h20) while, in scenario 2, the average number of iterations is 23, (i.e. 3h30). In only 4 runs, the number of iteration exceeded 40 iterations (i.e 6h).

7.2.2 Scenario 1 - National NO_x emissions

Figure 7.4 gives the relative objective values, by comparing the discounted total energy costs with the minimum cost, obtained when no emission constraints are imposed. In the most drastic scenario, the total energy cost is multiplied per almost 2.6 in comparison of the minimum cost. With expected AOT_1, no additional cost is observed when the threshold is greater or equal to 70ppb.

Figure 7.5 plots the values of the expected and upper limit of AOT_1 for each query point, i.e. the national NO_x emissions, encountered during the

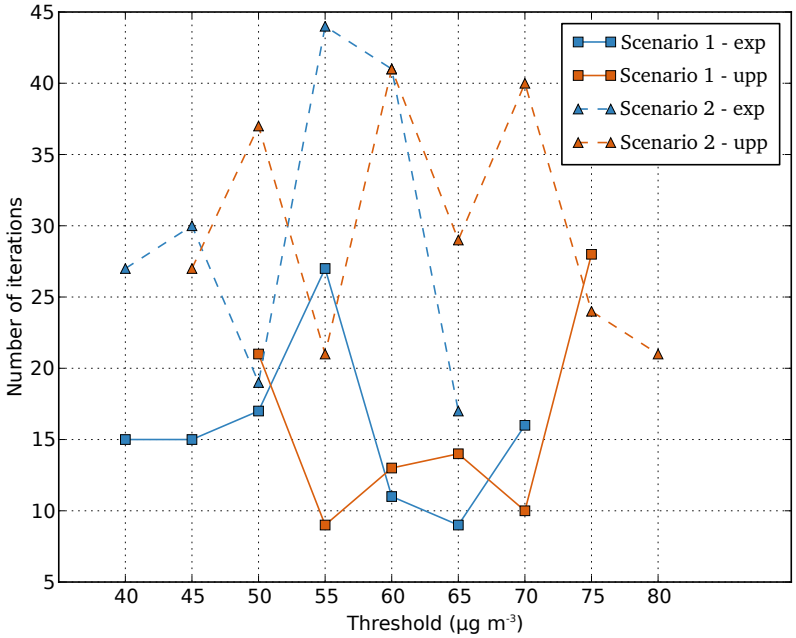

Figure 7.3: Number of iterations for each AQ indicator threshold. The "exp" abbreviation stands for expected AOT and "upp" stands for upper limit AOT, as defined in Eq. (7.4).

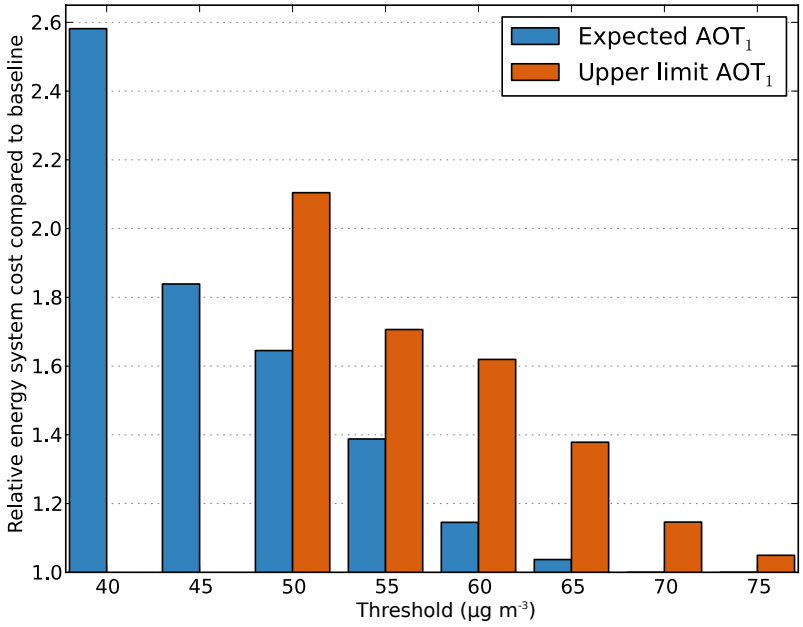

Figure 7.4: Scenario 1 — Relative energy system cost. For threshold smaller than 50, no optimal solutions have been found for upper limit AOT_1.

optimization process. The optimal solutions can be retrieved easily from this graph, at the intersection of the curve function and the horizontal line located at the threshold level. The figure highlights these optimal emissions for each run. The shapes of the functions are almost monotonously increasing, and have a very flat part between 100 t and 180 t. In the case of threshold values greater than 70 ppb for the expected AOT_1 and greater than 80 ppb for the upper limit, the solution is the maximum possible of NO_x emissions: 180 t. The points in Fig. 7.5 mark optimal solution for a given threshold, the three last dots, for NO_x national emissions of 180t, are displaced because this is maximal level of NO_x emissions, which does not produce such high AOT_1 levels. Therefore, theoretically, it is possible to comply with an expected AOT_1 of 70, 75 or 80, without implementing any additional measure.

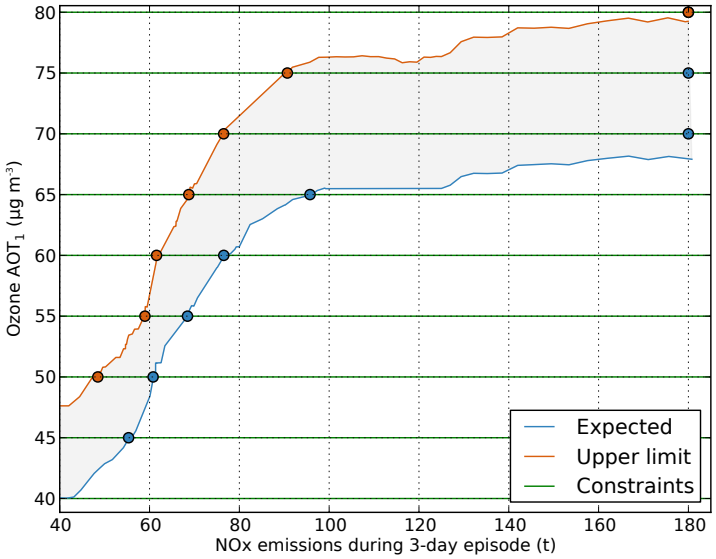

Figure 7.5: Scenario 1 — The curves are the expected and the upper limit, that is including the air quality model sampling error, of AOT_1 (ppb) as a function of the NO_x emissions. The points mark the optimal solutions, i.e. the optimal NO_x emissions, at each threshold denoted on the y-axis.

Figure 7.4 and Fig. 7.5 show that for a very low threshold limit the model does not have a solution when the upper limit AOT_1 is selected, that is when including the air quality model uncertainty. This occurs because the restrictions on emission are too strong and the demand in energy services cannot be met by the technologies catalogued by ETEM Luxembourg. In this case, if policy makers wish to attain this limits with 95% confidence, reducing only the energy related emissions would not be enough. The use of "end-of-pipe" technologies, e.g. treatment of air pollution streams, may help to achieve the lower pollution objectives. However "end-of-pipe" are not structural measures

and do not improve energy efficiency, thus should be used only as last resort.

7.2.3 Scenario 2 - Sectoral NO_x Emissions

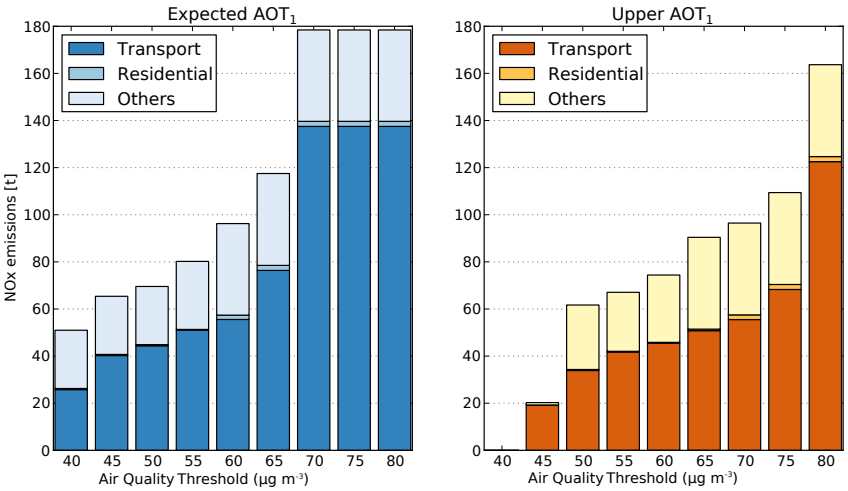

Figure 7.6: Scenario 2 — Optimal sectoral NO_x emissions. When the threshold is equal to 40 ppb and the indicator is upper limit AOT_1, no optimal solution has been found.

Figure 7.6 plots the optimal solutions for each threshold and for the two AQ thresholds with and without uncertainty. Results are detailed per sectors. The most impacted sector is the transport sector where the emission reductions are cheaper and faster to implement. Then comes the residential sector and finally the other sectors, where industry is the big emitter but without many emission reduction alternatives. The energy model contains, for some sectors, backstop technologies, i.e. non pollutant technologies which can substitute any others technologies but with a very high price. They can be seen also as "end-of-pipe" measures that could be implemented, however in this study the real costs of this measures have not been estimated, they are included as being very expensive, so that the OBOE can find a feasible solution. These clean technologies allow the solver to find an optimal solution even with a low emission limit of 20 t as is the case for the threshold 45 ppb using the upper limit AOT_1.

7.3 The Luxembourg Region

The Luxembourg region study case has been carried out after the study case for Luxembourg country. It is an attempt to include transboundary concentrations which contribute to the ozone levels in Luxembourg. The simulation of this case is important to understand the impact of transboundary pollution

in the territory of Luxembourg. Nevertheless, in this case, the calculation is much longer due to the inclusion of significant number of sources which imply more particles in the domain. The application set up is the same used in the AUSTAL2000-AYLTP validation, explained in Chapter 6. Therefore the coupling is carried out using only one coupling variable: the total NO_x emissions.

Like in the previous study case, in this study case the objective is to determine the energy-related NO_x emission levels from Luxembourg which comply with a given air quality limit after 2020.

The scenario has been undertaken with the annual NO_x emission limit from ETEM Luxembourg. However, contrary to what has been set for the study case of Luxembourg country, all emissions over the calculation domain are considered: the energy-related emissions from ETEM Luxembourg, the non-energy anthropogenic emissions from the EMEP model and the biogenic emissions, as listed in Figs. 6.6 and 6.7 of Chapter 6. The first category of emissions is controlled by the coupling model, while the two others categories are kept fixed, since they can not be controlled solely by the Luxembourgish decision makers.

The set-up of ETEM Luxembourg is identical to the previous study case, the coupling variable is a bound limit to the annual NO_x emissions during the decision period.

The emission allocator module took into account the EMEP emissions, covering the whole domain, using the same methodology as in Section 6.1.3.

In this study case, AUSTAL2000-AYLTP simulates one day in summer, the 19th of July. In comparison to the study case of Luxembourg country, the calculation domain has been augmented: The spatial domain is a 26 $\times$26 grid with an horizontal resolution of 5 km, 15 vertical layers up to 1500 m and are evaluated on the ground layer of 20 m height. The time step is also equal to one hour.

In this study case, three different air quality indicators of ozone have been considered: daily average, AOT_{40} and AOT_{80}. In the previous study case - the Luxembourg country, while the emissions were not covering the whole domain, AOT_1 was a reliable indicator to indicate the ozone production. In this case, this is no longer valid since the emissions cover the complete calculation domain. The air quality indicators have been calculated from 8:00 to 20:00 over the Luxembourg territory.

7.3.1 Air quality indicator surface response

In this study case, the response surface from AUSTAL2000-AYLTP is more realistic, considering only the combination of annual NO_x and VOC emissions

which are plausible for ETEM Luxembourg. That is, the emissions levels are produced by a set of technologies from the ETEM database, if a strong constraint is imposed on NO_x emissions, the chosen cleaner technologies would also emit less VOC emissions in most cases, since the emission of these two pollutants is associated.

Figure 7.7 depicts the response surfaces for the air quality indicators, respectively, ozone daily average, AOT_{40} and AOT_{80}.

To calculate these surface response plots, 850 random points, representing emissions levels, have been chosen in the interval of the surface plot and submitted to ETEM as bounds to the energy system. Then, ETEM calculates the corresponding emissions, in one of the following manners:

- keep the NO_x and VOC emissions if they both constrain ETEM;
- keep the emission level of the constrained pollutant and return the emission level calculated by ETEM for the other pollutant.

The higher level detailed sectoral emissions, also issued from ETEM, are then allocated in time and space, and serve as inputs to the AUSTAL2000-AYLTP model. Finally, the air quality indicators for ozone, daily average, AOT_{40}, AOT_{80}, are calculated from the emission levels.

The figures show that the emissions representing the possible future choice of technologies yield an air quality indicator response surface which is non convex. As mentioned before, a convex 3D surface implies that, if two points of the surface are connected by a straight line, the line only intercepts the surface at maximum two points. For instance in Fig. 7.7(a), if one draws a horizontal line at 1500t VOC emissions, from 15 000t to 20 000t NO_x emissions, the line would be out of the surface, since there is a region where the O_3 average concentration goes down after having achieved a local maximum.

There is a "tail" for very low emission levels, it corresponds to the introduction of backstop technologies, which are clean but very expensive. In this case the surfaces are restrained to the realistic combinations of the pollutants emissions and therefore the surface is not large.

Given that the non energetic emissions are also taken into account, the minimum value of the air quality indicator is already high, hence the range of the O_3 values is rather small. From Figure 7.7, it can be seen the indicators are rather NO_x-sensitive, as in the study case of Luxembourg country, because for a same level of NO_x emission, different levels of VOC yield the same air quality indicator value. Therefore, as in study case of the Luxembourg country, only the NO_x emissions are defined as the coupling variable.

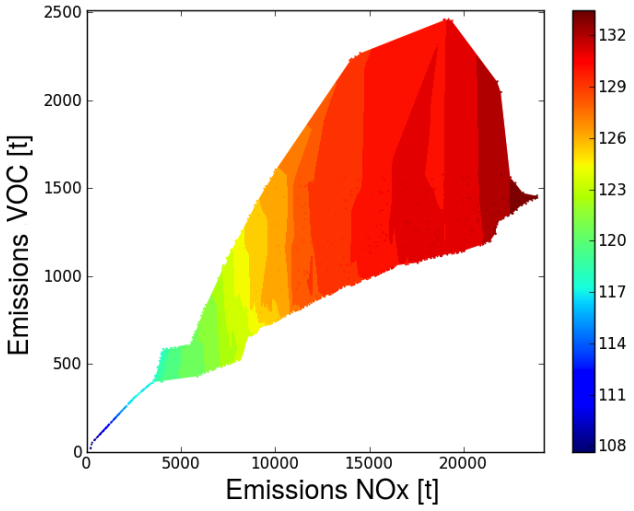

(a) Ozone daily average in $\mu g\,m^{-3}$.

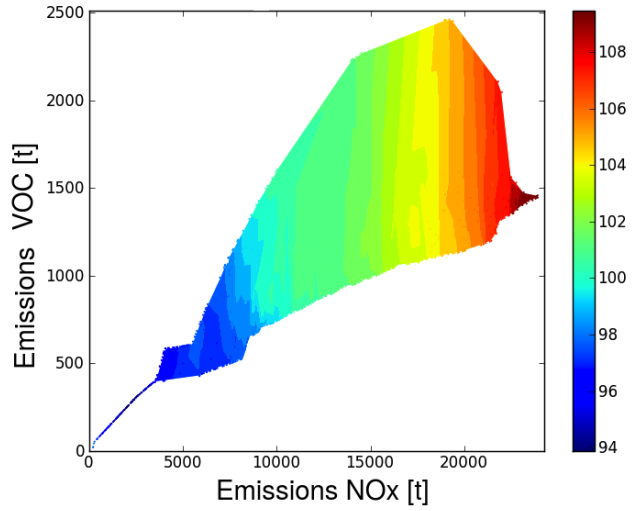

(b) Ozone AOT_{40} in $\mu g\,m^{-3}$.

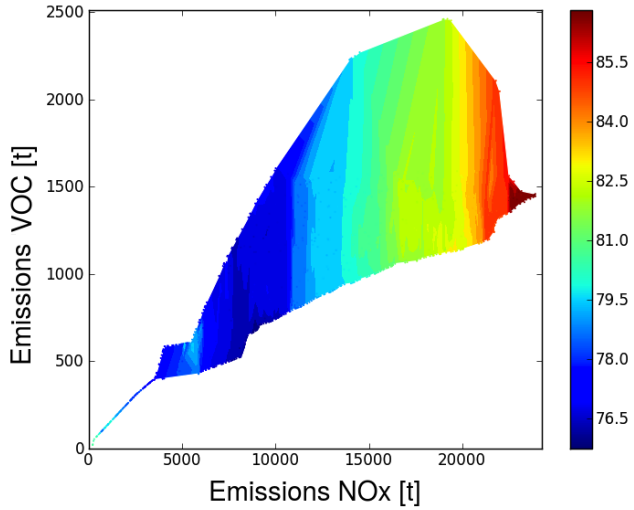

(c) Ozone AOT_{80} in $\mu g\,m^{-3}$.

Figure 7.7: Ozone indicators, Ozone daily average (a), Ozone AOT_{40} (b), Ozone AOT_{80} (c), as a function of annual NO_x and VOC emission [t]. The colored surface covers the plausible emissions for ETEM.

7.3.2 Results

The optimisation problem, Eq. (7.1), is solved for the air quality indicators and threshold showed in Table 7.1.

Air quality indicator	Thresholds [$\mu g\,m^{-3}$]
Daily average	110, 115, 120, 125, 130
AOT_{40}	100, 105
AOT_{80}	80, 85

Table 7.1: Coupling parameters for the Luxembourg region study case.

An iteration ran in 1 h20, which is eleven times longer than in the study case of Luxembourg country, on the same computer machine. The longer time is due to the new set-up of AUSTAL2000-AYLTP, a bigger domain and a larger number of emission sources.

The convergence of the coupling model is obtained in a comparable number of iterations with the previous study case.

As mentioned before, the coupling variable is the annual NO_x emissions. The VOC emissions are provided by ETEM, imposing only the NO_x emissions limit to the energy system.

Figure 7.8 shows the air quality indicator as a function of NO_x, the curve is built from the encountered points during the coupling process. The optimal solutions are marked by a circle.

Figure 7.8(a) presents the result for the ozone daily average. The curve is globally increasing monotonous. Optimal solutions have been found for five thresholds. The solutions for the lower threshold 110 and 115 $\mu g\,m^{-3}$ are very low, respectively 867 t and 1825 t of NO_x. These levels are very drastic and demand for the introduction of backstop technologies and a very high energy system cost, 600 times and 400 times the baseline energy system cost respectively. These two solutions cannot represent a realistic energy policy.

Figure 7.8(b) presents the result for the ozone AOT_{40}. The curve is increasing monotonous from a limit of 4000 t of NO_x. For lower emissions, the AOT_{40} has a different regime. The search interval for this indicator started from 4000 t. Two thresholds, 100 and 105 $\mu g\,m^{-3}$, have been established and the optimal solutions have been found and are presented in Fig. 7.8(b).

Figure 7.8(c) presents the result for the ozone AOT_{80}. The curve is also increasing monotonous from a limit of 10 000 t of NO_x. For lower emissions, the AOT_{80} follows different precursors sensitivity regimes. Therefore, the search interval for this indicator started from 10 000 t. Solutions have been found for two thresholds 80 and 85 $\mu g\,m^{-3}$.

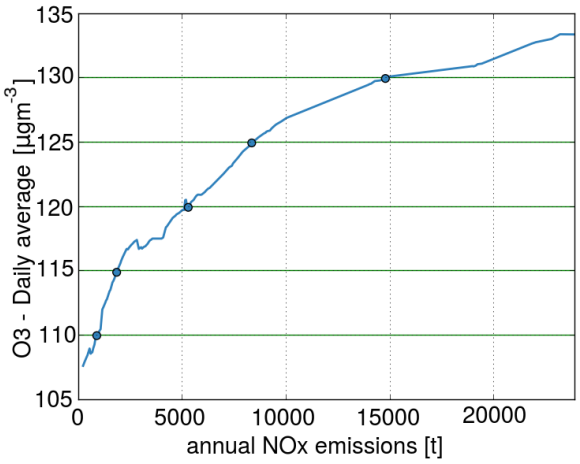

(a) Ozone daily average in $\mu g\,m^{-3}$, as a function of annual NO_x emission in t.

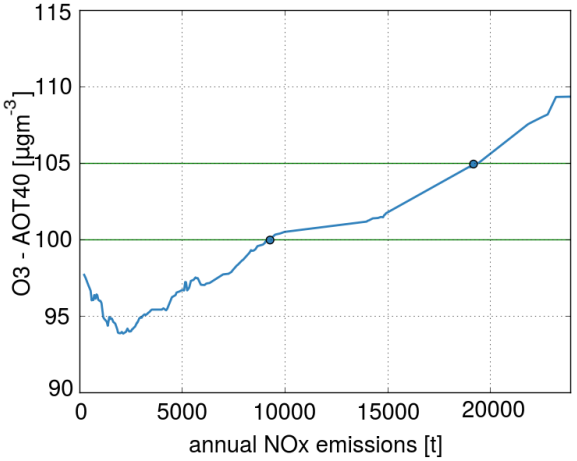

(b) Ozone AOT_{40} in $\mu g\,m^{-3}$, as a function of annual NO_x emission in t.

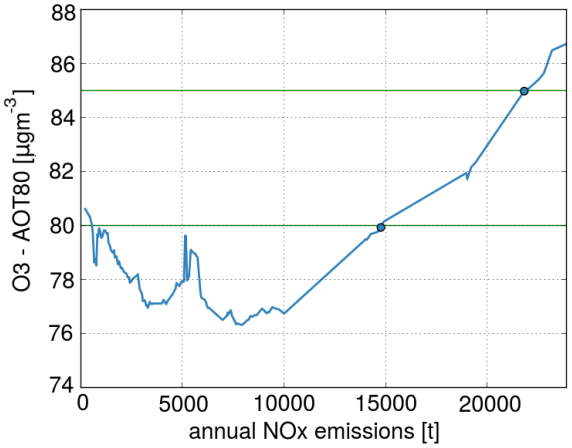

(c) Ozone AOT_{80} in $\mu g\,m^{-3}$, as a function of annual NO_x emission in t.

Figure 7.8: Ozone indicators, Ozone daily average (a), Ozone AOT_{40} (b), Ozone AOT_{80} (c), as a function of annual NO_x and VOC emission [t]. Optimal solutions are signaled with a circle.

Figure 7.9 compares the energy system costs for the different air quality indicators and thresholds, where DAVG is the ozone daily average.

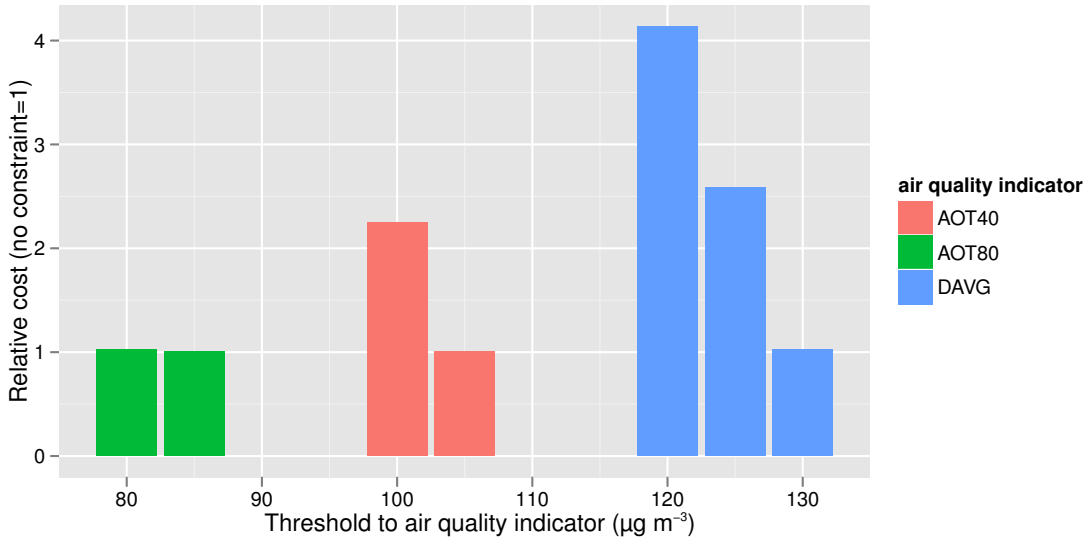

Figure 7.9: Relative ETEM cost per air quality indicator and threshold. Where DAVG is the ozone daily average air quality indicator.

Naturally, the less strict ozone thresholds have a lower energy system cost. For instances, to keep the ozone daily average at $120\,\mu g\,m^{-3}$ during a typical summer day with meteorological conditions very favourable to ozone pollution episodes, in the decade 2020—2030, would cost approximately four times more than the current reference scenario.

AOT_{80} is not advisable to be chosen as a controllable air quality indicator, since the AOT_{80} is very strict thus is very difficult to reduce AOT_{80} levels. In fact, with these emissions levels, in the period 2020 to 2030, it will be very difficult to avoid high AOT_{80} levels.

As a conclusion, the analysis of the Luxembourg region study case, has revealed that the Luxembourg ozone levels are highly dependent on the neighbouring country emissions. This is shown by the introduction of the EMEP emissions and the augmentation of the domain which did not allow the setting of very low air quality limits, as shown in Fig. 7.9. The transboundary nature of air pollution is well known, however for a country of the size of Luxembourg, this factor becomes even more crucial. Therefore it is extremely costly for Luxembourg to establish air quality policies without a common effort at regional and European levels. Additionally, the introduction of non energy-related sectors, has added other emissions which can not be controlled though energy policies in Luxembourg. The results of this study suggest that energy policies must be accompanied by other types of policies, such as "end-of-pipe" measures. For instances, the replacement of less polluting products

and composts or more efficient waste treatment plants could be implemented together with structural measures. It must be taken into account that this is a theoretical exercise, since the meteorological scenario used is very improbable.

Chapter 8

Conclusions

This work can be divided in two major parts: firstly the conceptualization and development of the model AUSTAL2000-AYLTP; and secondly, the validation and model inter-comparison of AUSTAL2000-AYLTP and its simulation within the LEAQ framework.

The review of the integrated assessment models for air quality policy has revealed that the majority of models are used in simulation mode. There is only a few number of integrated assessment models for air quality policy which operate in optimization mode. Photochemical air quality models demand great efforts in terms of data collection and treatment, as well as in computer resources. Optimization approaches, such as the one described here, imply that the air quality model is evaluated several times, thus it is impractical to use air quality models in their full working mode.

Several model reduction and emulation techniques are frequently applied in integrated assessment frameworks for practical reasons. This work is an attempt to develop a model which can be used in its full mode within an optimization framework. The design of an air quality model for this kind of context implies approximations and simplifications.

The application of economical structured planning policies is, generally, carried out in the mid-long term, e.g. 30 years. The meteorology, which drives the air quality models, is rather a short term, e.g. day, hour. Therefore the uncertainties associated with the prediction of the meteorology for the economical periods is very high. Hence simplifications are acceptable and a balance between accuracy and CPU time has been sought.

A review on existing air quality models which could adequately be used in the LEAQ model has been carried out. It revealed that there is no specific model which could serve all the requirements of the LEAQ approach. AUSTAL2000 has been chosen because it is a flexible, fast and open source model. It has been used as the transport core calculator, accordingly a photochemical module was necessary and has been developed and implemented. The photochemical module is based on a pre-tabulated quasi-linear reaction rate approach. It is a simplified approach which prevents the Lagrangian transport model to increase significantly the CPU time. The AYLTP module presents a reasonable trade-off between accuracy and CPU time and the amount of input data.

Furthermore, the pre-calculated reaction rates are stored in a Look-up Table (LUT), which is then assessed by AUSTAL2000. The use of Look-up tables increases the speed of the calculation since the model does not calculate the rate directly but instead it reads it from a file. The additional time caused by the implementation of the LUT is acceptable and allows the incorporation of the air quality model with LEAQ. The use of LUTs represents however an approximation since it can not include all the possible values. The AYLTP approach is fast and has proven to be adequate for the LEAQ integrated framework, however it assumes a constant production rate during one hour, which represents an average rate, based on one hour average concentrations.

The reaction rates are calculated by the OZIPR model, which is a well established box model, developed by EPA. The OZIPR simulations have been analysed for two different time steps. The one hour rates were found to be more appropriate to use in the air quality simulations. The reaction rates have been calculated with the OZIPR model using the CB-IV chemical mechanism. Although the CB-IV mechanism is well established and has proven to give good results, one must keep in mind that it is still a simplified representation of reality.

The considered ozone precursors, NO_x and VOC, are widely accepted as the most important precursors in ozone production. Nevertheless, both NO_x and VOC represent groups of pollutants and not single ones. Furthermore additional pollutants, such as CO which can also influence ozone concentration, have not been considered and might be taken into account in the future.

It is impossible to store all the possible initial conditions under which ozone could be generated. Therefore, the LUT only contains a subset of those possible conditions. When the initial conditions do not correspond to any of pre-tabulated values, these are approximated to the nearest value in the table. An interpolation can be implemented in the future, such as interpolation in multiple dimensions (Press et al., 2007).

An emission allocator has been developed specifically to convert the annual emission data into a temporal emission series which can be read by AUSTAL2000. The module is fast and does not present a problem in terms of the CPU time of the whole optimization. The allocator creates a spatial matrix of emissions. This is the most straight forward approach, because a great amount of emission data is provided in a grid form. Also this is the simplest way to automatize the the spatial allocation of emissions. However, the transport calculator AUSTAL2000 can handle a more detailed emissions source definition. For instances, the road network could be represented in the model as a series of line sources, accordingly, the big industries can be represented as point sources. This would give a more accurate representation of reality. Additionally, a spatial varying emissions source height, would be more realistic than an average 20 meters height for all sources. Additionally,

a study about how this assumption affects the final results can be developed in the future.

The temporal emissions profiles which have been used in the emission allocator have been around for many years, although still widely used in many European countries because it is the only available data. It is important to develop more detailed and up-to-date temporal profiles studies for Luxembourg as they might affect the prediction of the pollution peak hours. Additionally, emission inventories and emission factors, which have a great influence on the air quality models results, are normally considered to have high uncertainties. Studies and efforts must be taken in order to improve emission data.

The model has well reproduced the connections between ozone and NO_x and the relation with the solar radiation hours. The comparison of the model results with monitoring data reveals that Luxembourg air quality is strongly connected with transboundary pollution. This is visible due to the fact that the upwind stations show a steep decline in ozone concentrations in the hours of higher wind speed. This occurs because there is no transport of pollutants from outside through the model's boundaries. It was expected that Luxembourg would be highly dependent on transboundary pollution, due to the reduced dimensions of the country and the fact that ozone precursors can be transported for long distances.

The stronger winds during day time advect the pollutants through the domain in the direction north/north-west. The hours of stronger winds coincide with the ozone peaks in the downwind stations, and the decrease of the ozone concentrations on the upwind stations. Therefore the wind conditions affect the concentrations in the upwind stations, south of the domain, which results in an underestimation of the ozone concentrations. Accordingly, Kübler (2001) has concluded that the meteorological conditions can mask the effects of the ozone precursors on the concentrations of ozone.

AUSTAL2000-AYLTP presents good agreement with measurements and with the LOTOS-EUROS model for background stations, showing a better agreement with observed values than with LOTOS-EUROS modelled values. Concerning the NO_x emissions the predictions show a good agreement with the Luxembourg urban traffic station and the Esch-Alzette industrial station. This is due to the fact that the atmospheric stability conditions have been adjusted for the city Luxembourg meteorological station. However the establishment of these atmospheric conditions, and the fact that the wind field model only takes one station is the reason for very high concentrations in the background stations. Additionally, the lack of VOC concentration measurements limits the analysis, as well as the lack of atmospheric stability data. A further study with more complete VOC and meteorological data should be considered. Moreover, a study about the influence of the assumption of a stable atmosphere, could be further developed, using for example sensitivity

analysis.

The presented results demonstrate the technical functioning of the complete model chain of LEAQ, and tackle the major scientific issues. Further refinement and sensibility tests are required for a more complete model validation. In particular, application of a lager emission area, considerably larger than Luxembourg country, and a more realistic specification of the atmospheric stability should be envisioned. Likewise, sensitivity tests with respect to the applied source height and the spatial and temporal resolution of the concentration are to be considered in the future.

When comparing modelling results with measurements it must also be considered that there is always a representativeness error when comparing a point measurement with a 5km $\times$ 5km grid cell, the point measurement might not be representative of the average of the cell.

The comparison with LOTOS-EUROS is important to understand the performance of AUSTAL2000-AYLTP with a state-of-the-art model, however this analysis is restricted by the fact that the models have been run with different emission data and different resolution.

The process of model validation of AUSTAL2000-AYLTP is still at the beginning, model validation is a long process and the model has to be evaluated in different conditions, for instances other locations and other dates and longer time episodes. A dedicated air quality model for an integrated assessment optimization model has been developed, and despite the need for continuous and further validation, it can be used in any optimization framework.

The implementation of AUSTAL2000-AYLTP in LEAQ has been carried out in two study cases: one including only the Luxembourg country national emissions; and a second one for the Luxembourg region including also the neighbouring countries emissions. It has been shown that the model must be used with restrictions, since the optimization approach obliges the air quality surface function to be convex. The methodology used by OBOE is appropriate to find an optimal solution when there are many decision variables, e.g. NO_x and VOC sectoral emissions. This represents an advantage in relation to the existing, and most common, optimizations approaches. However, the convexity requirement limits the air quality model use, and therefore the use of a most favourable scenario to pollution production case scenario is necessary.

The effects of the hourly varying meteorology introduce a chaotic-like behaviour in the ozone response due to the changes in wind velocity and direction. OBOE requires a constant response in order to find the optimal solution. The most favourable scenario to pollution production case scenario, which corresponds to a constant meteorology, is then used. If the solution is found for the worst case scenario than it can be assured that the uncertainties of an average or typical scenario are also covered.

The model has potential for improvement, however the inclusion of new features and modules might significantly augment the CPU time and therefore interfere with its primary objective. One important remark is that this model, like others, should be evaluated according to its objective and used only for its purpose. In this sense a policy support model can not be evaluated as a forecast model. The inclusion of more influencing factors might provide more information about the response of the air pollutants, however they can also generate more uncertainties in the input data, the model approximations and the code implementation. Furthermore, the fact that OBOE requires a convex function limits considerably the expansion of the air quality model. In future studies, other optimization approaches might be considered such as meta-heuristic methods which include the iterative search algorithm applied by Oxley et al. (2003), or genetic algorithms as used in Reis et al. (2005). An important advancement, in terms of OBOE's methodology, would be to develop a spatial optimization. This would allow the application of a less aggregated ozone air quality indicator and therefore the application of more realistic meteorological conditions. However, the use of spatial air quality models is very important for the calculation of ozone, since the VOC/NO_x ratio is highly spatially dependent, and therefore the ozone concentrations as well.

Luxembourg is a small country, hence the energy system has less flexibility in terms of options than other countries where the economy provides higher variety and options of choice for the shares in the energy system. Moreover, a high share of the traffic sector consumption of fuel is related with "tank tourism", that is fuel which is bought in Luxembourg but consumed outside. This practise leaves few options to control the national emissions. Additionally, the establishment of very rigorous thresholds become extremely expensive or even impossible, since the pollution levels are highly dependent on the neighbouring countries' emissions. The results of the study case for the Luxembourg region, and also of the model validation, prove this fact. In this case the emissions from the neighbouring countries have been added and the establishment of lower thresholds has proven to be complex, since it can not be achieved controlling only the Luxembourg's national emissions. The transboundary pollution implicates global and regional policies because the effects of the policy of one country on another are not negligible. An action at one location may imply a change elsewhere, which makes the coordination of the policies necessary, but also difficult to succeed.

The model uncertainties have been taken into account in the decision support. However these are based only on the sampling error of the air quality model. A full uncertainty study of the LEAQ model, and of both sub-models AUSTAL2000-AYLTP and ETEM Luxembourg, may be considered in the future to understand the greatest sources of uncertainty and the way it is

propagated through the LEAQ model.

Concluding, ozone air quality policies must be integrated at regional and European levels. Additionally, "end-of-pipe" emission control solutions might be combined with structural planning of the energy system. "end-of-pipe" technologies only reduce the emissions at the emission exit and so do not foster reduction of primary resources consumption. They must not be considered as long term solutions by themselves, but complementary solutions to a more structured energy planning.

The LEAQ model, as well as its two major sub-models, are a policy support model. ETEM is a typical policy support model, and not a forecast model. It is not possible to predict the energy system, as it depends on macroeconomic factors which are unpredictable. The techno-economic models are based on trends, and therefore they are adequate to orient policy makers by drawing scenarios. Future developments of this work might include the simulation of LEAQ using different macroeconomic scenarios, in order to provide policy makers with more complete technical support.

Finally, the LEAQ tool, can be enhanced to include other factors in the decision, such as the health impact by poor air quality, in the population. This can be undertaken using an air quality indicator based on ozone, other pollutants or an aggregated indicator. Zachary et al. (2011) presents an approach that includes the impact by poor air quality, based on ozone, in the objective function. Additionally, LEAQ could be developed to be used as a spatial planning tool, in order to assess not only which measures should be taken, but also where they should be implemented.

Appendix A

The Luxembourg Energy-Air Quality Model Details

A.1 Biogenic Emissions

Biogenic emissions have been provided by the Laboratory of Atmospheric Physics of the Aristotle University of Thessaloniki (AUTH). Its is delivered from the model for European Biogenic Volatile Organic Compound emissions for the year 2003 (Poupkou et al., 2010). The year 2003 was an abnormal year in terms of temperature, which has a strong influence on the emission of biogenic VOC. This year was marked by a long heat wave in Europe, nevertheless it was the only time series available. However it is a good surrogate for the purpose of LEAQ, since it is interesting to test the model for a worst case meteorological scenario. Therefore, two scenarios have been developed for this study:

- a typical year
- a heat wave year

Both scenarios are useful to study the repercussions of energy pollution under "normal" and "worse case" scenarios. The "heat wave" scenario was carried out using the data as it was, since 2003 represented a good extreme event in terms of biogenic VOC emissions. The "typical year" scenario was built replacing the five hottest months, April to September, by their average.

The data has been provided in the European grid, in which Luxembourg is represented in 8 cells in the Lambert conformal conic projection Fig. A.1.

The portion of Luxembourg in each cell is calculated and used to weight the total emission value of the cell. Then the total annual emissions from biogenic sources per cell and the total of the country is computed. The monthly and hourly shares are also calculated to build the national biogenic emissions temporal profiles on winter months, October-March, and summer months, April-September. The emissions are afterwards allocated using Luxembourg's land use map. Only the forested areas are selected, i.e. the total emissions per cell are divided by the number of recorded forest cells.

The total annual emissions for both scenarios are presented in Table A.1.

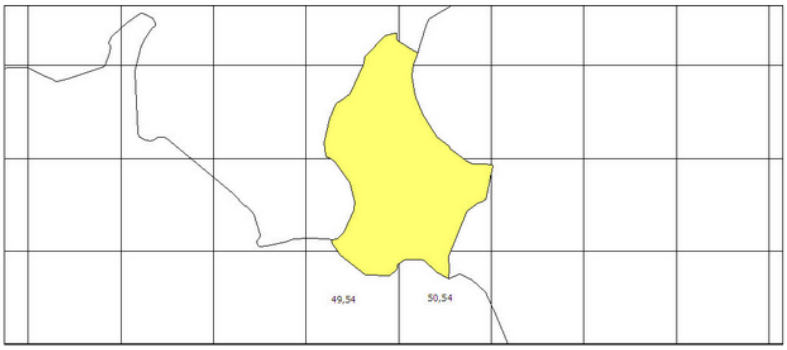

Figure A.1: Luxembourg in the European grid, 30km x 30km. Image ceded by AUTH.

Table A.1: Biogenic annual emissions in ton.

	VOC [t]
Typical year	8.657
Heatwave year	9.052

Appendix B

AUSTAL2000 Technical Details

B.1 AUSTAL2000 Input Data

AUSTAL2000 computes the dispersion of the pollutants over a complex terrain and for a time series. Figure B.1 presents a schematic representation of the transport and emissions of the Lagrangian particles, as well as the grid and source definitions. The input of the model might be directly specified by the user, as for example in the case of the grid structure, or given by a pre-processor, in the case of the temporal-spatially distributed emissions or the meteorological parameters.

The model requires as input:

- digital elevation model (DEM);
- meteorological data, such as wind speed and direction time series at the anemometer and the Monin-Obukhov length or atmospheric stability class;
- emission strengths, position and geometry of the sources;
- surface roughness length average value or map;
- grid definition.

Digital elevation model The digital elevation model is needed for the calculation since the inhomogeneities of the terrain affect the dispersion of pollutants. Therefore three-dimensional wind fields are calculated according to the terrain.

Meteorological data The meteorological data is prepared by a pre-processor model, which delivers the mean wind velocity and the necessary information to calculate turbulence to the Lagrangian particle model. The pre-processor model TALdia calculates the meteorological data at different heights from the ground.

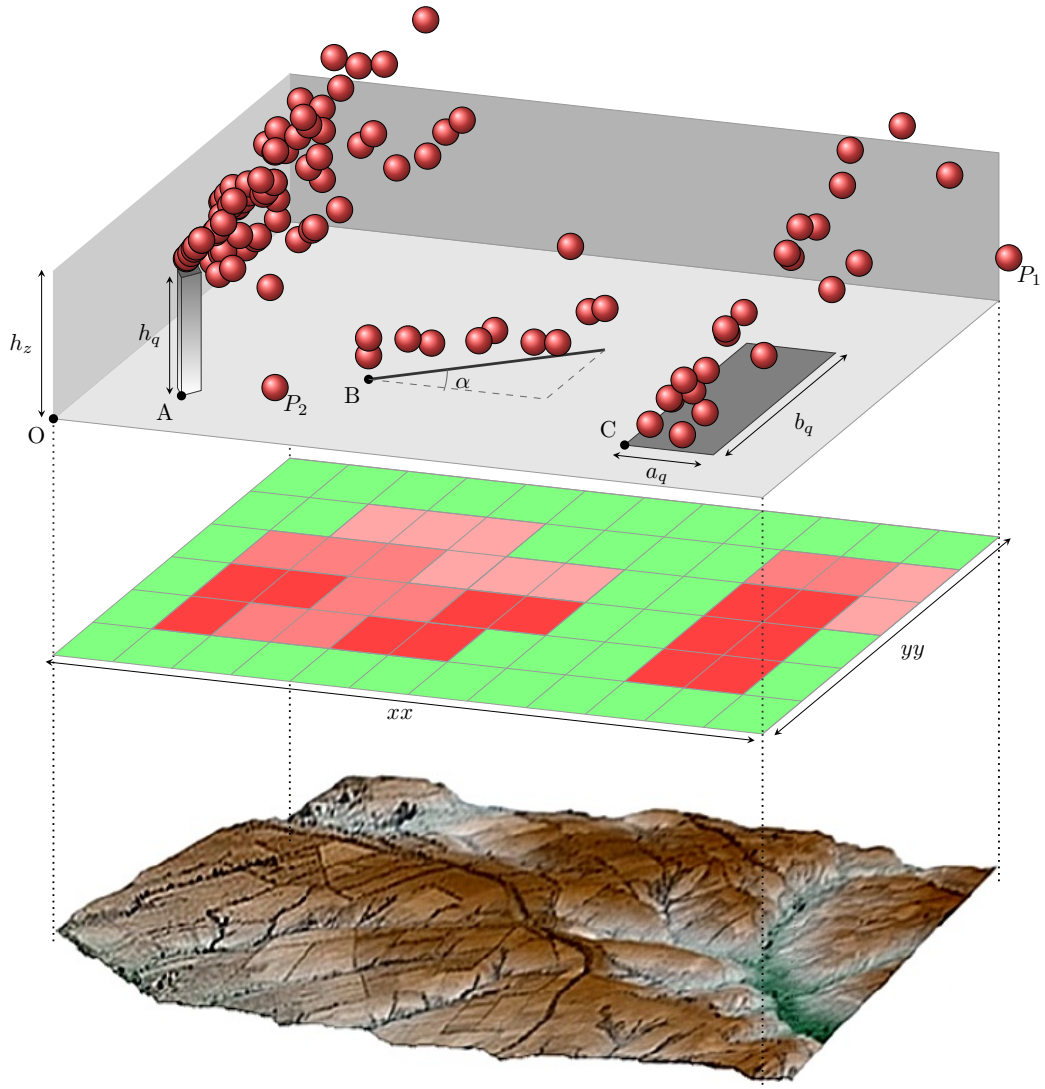

Figure B.1: Representation of transport and emission of the Lagrangian particles. The model source and the digital elevation model are represented. The middle horizontal grid shows a schematic concentration distribution. The domain size is defined by xx and yy and h_z. Points A, B and C indicate the lower left corner of the volume, line and area sources, respectively. a_q and b_q represent the extension of the source in x an y coordinates. Likewise h_q represents the height of the source. The sources can be rotated according to an α angle. The point O is the origin of the calculation domain, which must be completely inside the digital elevation model. P_1 represents a particle that leaves the domain and P_2 a particle that hits the ground.

Emission The emissions' geometry, strength and time series must be defined. Source's geometry can be represented by points, lines, areas or volumes as shown in Fig. B.1. Sources are defined by their lower left corner, represented by points A, B and C of Fig. B.1, and can be rotated according to an α angle. As shown in Fig. B.1 the source extension in x, y and z coordinates must defined for line, area and volume sources.

In the context of LEAQ, the emission allocator module converts the annual emissions into a time series matrix, in which each matrix value represents the emission strength of an area source, as explained in Chapter 3.

Roughness length value or map The roughness length z_0 can be given as a single value or as a map, from which the model calculates an average value. The z_0 is used to help calculate the vertical turbulent diffusion.

Grid definition The grid is defined by the user, it must be positioned inside the digital elevation model. The horizontal mesh must have the same grid spacing in y and x direction, whereas the vertical layers can be defined at any desired height. A particle that leaves the calculation domain is no longer considered for calculation, as represented by particle P_1 in Fig. B.1.

B.2 Statistical error

The number of Lagrangian particles used in the simulations is naturally finite, and much smaller than the number of "particles" in reality. Therefore, the results of the calculation of concentration have a sampling error associated with it. This error can be reduced by increasing the number of particles in the simulation. However, this increases the computational time. The reduction of the sampling error might also be achieved by augmenting the cell volume and the averaging time, nevertheless this increases the discretisation error.

As mentioned before, the turbulent velocities in AUSTAL2000 are simulated using a random velocity. The same simulation repeated with different sequences of random values will yield different concentrations distributions. Hence the method originates a sampling error ϵ_c, which is calculated by AUSTAL2000 for every time step Δt and for every cell of the domain, according to:

$$\varepsilon_c = \frac{\sigma_c}{\bar{c}}\,, \tag{B.1}$$

with the average concentration $\bar{c}$

$$\bar{c} = \frac{1}{n_g}\sum_{g=1}^{n_g} c_g\,, \tag{B.2}$$

where n_g is the number of groups with the same random sequences, c_g is the group concentration and the concentration variance is given by:

$$\sigma_c^2 = \frac{1}{n_g - 1} \sum_{g=1}^{n_g} (c_g - \bar{c})^2 \ . \tag{B.3}$$

Appendix C

Analysis of Advection and Diffusion Algorithms

C.1 Advection

Advection is the transport by the mean wind; the wind propagates the gases and the particles and their bulk motions are called advection (Jacobson, 2005). The transport by the mean wind field has been isolated and tested against the analytical solution of Eq. (C.1).

$$\frac{\mathrm{d}\bar{x}}{\mathrm{d}t} = \bar{u}. \tag{C.1}$$

The test case consists of a instantaneous release of a tracer pollutant, in a constant velocity wind field. The rate of emission particles is such that there is only one particle in the domain. AUSTAL2000 is run with the option "TRACE" which keeps track of the particle's trajectory. The details of the study case are presented in Table C.1.

Table C.1: Parameters of the study case

Symbol	Description	value
	Domain size in m	$2500 \times 500 \times 10$
	Time domain in hours	24
	Time of release	02h05
	Wind direction in °C	270
	Source position (x,y,z)	(200,250,5)
$\bar{u}$	Mean wind speed in x direction in $\mathrm{m\,s^{-1}}$	0.015
$\bar{v}$	Mean wind speed in y direction in $\mathrm{m\,s^{-1}}$	0.0
$\bar{w}$	Mean wind speed in z direction in $\mathrm{m\,s^{-1}}$	0.0
Δt	Average time interval in s	600
z_0	Roughness length in m	0.0
σ_u, σ_v, σ_w	Standard deviation of u, v and w in $\mathrm{m\,s^{-1}}$	0.0

The analytical solution of Eq. (C.1) yields

$$x(t) = x(t_0) + \bar{u}(t - t_0), \tag{C.2}$$

where t_0 is the previous time step.

The results of the analytical solution and of AUSTAL2000 simulation are presented in Fig. C.1.

Both the results of the analytical solution and of AUSTAL2000 simulation, presented in Fig. C.1, match. In the two cases the particles reach position $x = 1392.5$ at the same time $t = 86400$. AUSTAL2000 horizontal's transport solution shows a correct behaviour.

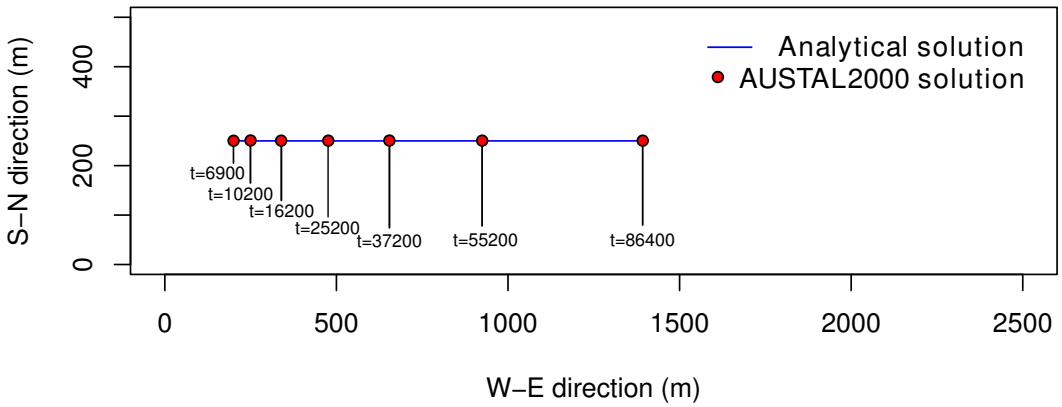

Figure C.1: Trajectory results of the AUSTAL2000 and of the analytical solution.

C.2 Diffusion

Diffusion is the process through which particles move, randomly, from regions of higher concentration to regions of lower concentration. One distinguishes two types of diffusion: molecular diffusion and turbulent diffusion (Jacobson, 2005). Molecular diffusion can be further subdivided into small scale and large scale motions. Small scale motion is characteristic of the molecules which are above the absolute zero temperature, $-273\,^{\circ}\mathrm{C}$. Whereas, the motion driven by particles which are large enough to collide with each other and move due to their kinetic energy, is called the Brownian motion. Turbulent diffusion, on the other hand, is the mixing caused by eddies, and is much more effective than molecular diffusion.

In atmospheric modelling, the molecular diffusion is normally neglected because the effects of turbulent diffusion are more important. Hence the Lagrangian diffusion equation, including a source S, is the following, expressed in the Lagrangian referential, (Seinfeld and Pandis, 2006):

$$\frac{\partial \langle c \rangle}{\partial t} = \nabla \cdot (\mathbf{K} \cdot \nabla \langle c \rangle) + S(\mathbf{x}, t), \tag{C.3}$$

where c is concentration, t is time and $\mathbf{K}$ is the diffusivity tensor.

The AUSTAL2000 diffusion results have been simulated for a homogeneous diffusion case and compared with the Gaussian analytical solution of the diffusion equation for isotropic turbulence and an instantaneous point source presented by Seinfeld and Pandis (2006).

C.2.0.1 Isotropic Atmospheric Diffusion for an Instantaneous Source

A simple homogeneous diffusion case has been set up, in a squared, flat terrain domain. The wind velocity is set to zero, thus only the effect of turbulent diffusion is driving the particles.

The simplest boundary layer model (Blm) of AUSTAL2000 has been chosen, i.e. Blm=0.1 as defined in the AUSTAL2000 user guide (Janicke, 2009). The Lagrangian time scales $T_{u,v,w}$ are given as follows:

$$T_u = T_v = 100, \tag{C.4}$$

$$T_w = 10\frac{z_0}{u_*} \tag{C.5}$$

and the diffusion coefficients K_u, K_v, K_w are calculated according to Eqs. (4.56) to (4.58), and u_* is the friction velocity. The parameter values are summarised in Table C.2.

Table C.2: AUSTAL2000 parameter values for the study case

Symbol	Description	Value
	Domain size in m	1200×1200×1
	Time domain in h	1
τ	time step in s	τ=5.00
Δt	time average in s	Δt=100
u_*	friction velocity in $\mathrm{m\,s^{-1}}$	u_*=0.20
z_0	roughness length in m	z_0=0.20
σ_u, σ_v, σ_w	standard deviations of the u, v and w in $\mathrm{m\,s^{-1}}$	σ_u=σ_v=0.30
		σ_w=0.00
σ_u^2, σ_v^2, σ_w^2	variance of the u, v and w in $\mathrm{m^2\,s^{-2}}$	σ_u^2=σ_v^2=0.09
		σ_u^2=0.00
T_u, T_v, T_w	Lagrangian time scale in s	T_u=T_v=100
		T_w=10.0
K_u, K_v, K_w	diffusivity coefficients in $\mathrm{m^2\,s^{-1}}$	K_u=K_v=9.00
		K_w=0.00

The problem parameters are kept constant through out the simulation. The standard deviation of the velocity w has been set to zero in order to have a strictly 2-dimensional diffusion problem. The diffusion equation in AUSTAL2000 is given by Eq. (4.15). The drift velocity is zero in the case of homogeneous turbulence, hence Eq. (4.15), for this particular case, is given by:

$$\mathbf{u_{t+\tau}} = \Psi(\mathbf{x}_t) \cdot \mathbf{u}_t + \Lambda(\mathbf{u}_t) \cdot r \ . \tag{C.6}$$

Likewise, the position is given by:

$$\mathbf{x}_{t+\tau} = \mathbf{x}_t + \tau \left[\mathbf{u_{t+\tau}}\right] \ . \tag{C.7}$$

Solving Eqs. (C.6) and (C.7) using the parameter values of Table C.2 and Eqs. (4.19) to (4.22) of the Lagrangian particle model, yields:

$$K = \begin{bmatrix} K_u & 0 \\ 0 & K_v \end{bmatrix} = \begin{bmatrix} 9.000 & 0.000 \\ 0.000 & 9.000 \end{bmatrix}$$

$$\Sigma = \begin{bmatrix} \sigma_u^2 & 0 \\ 0 & \sigma_v^2 \end{bmatrix} = \begin{bmatrix} 0.090 & 0.000 \\ 0.000 & 0.090 \end{bmatrix}$$

$$\Phi = \Sigma \cdot K^{-1} = \begin{bmatrix} 0.010 & 0.000 \\ 0.000 & 0.010 \end{bmatrix}$$

$$\Psi = (2\mathbf{I} - \tau \cdot \Phi) \cdot (2\mathbf{I} + \tau \cdot \Phi)^{-1} = \begin{bmatrix} 0.905 & 0.000 \\ 0.000 & 0.905 \end{bmatrix}$$

$$\Omega = \Sigma - \Psi \cdot \Sigma \cdot \Psi^T = \begin{bmatrix} 0.016 & 0.000 \\ 0.000 & 0.016 \end{bmatrix}$$

Applying the Cholesky decomposition, to solve $\Lambda.\Lambda^T = \Omega$, it gives:

$$\Lambda = \begin{bmatrix} 0.128 & 0.000 \\ 0.000 & 0.128 \end{bmatrix}$$

These are the solutions of the input parameters of AUSTAL2000 model. The study case has been simulated with 3 different numbers of Lagrangian particles, i.e. 100, 1000, 10'000. The average results are presented in Figs. C.2 to C.4.

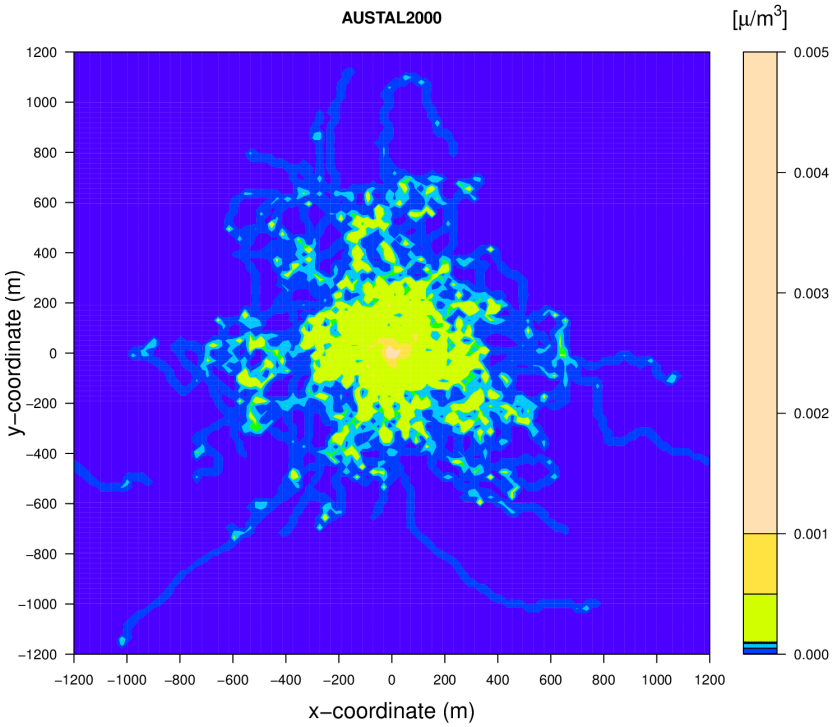

(a) Spatial distribution of average concentration.

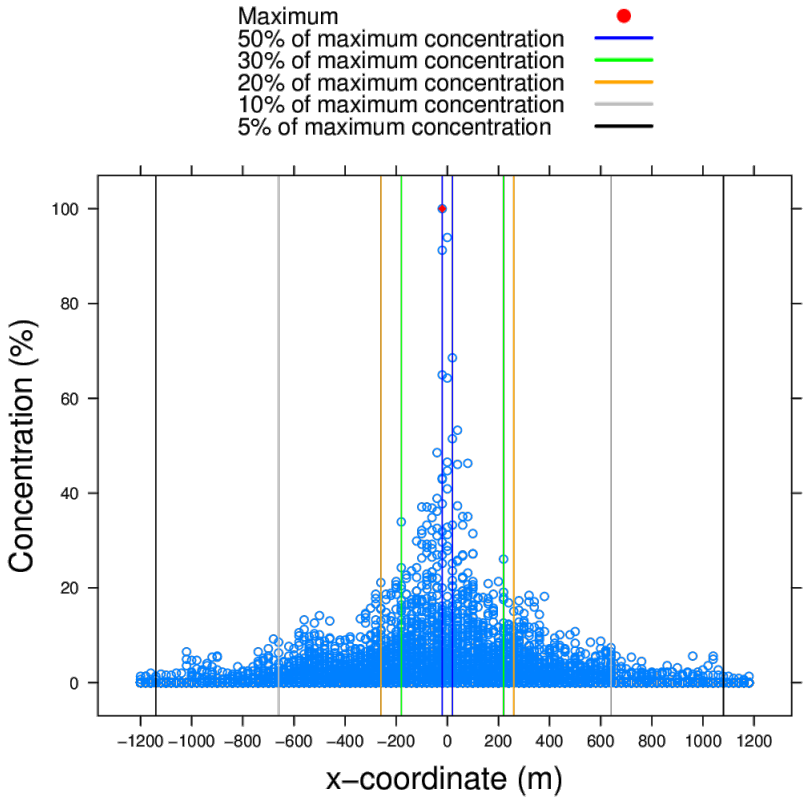

(b) Average concentration distribution over x-coordinate.

Figure C.2: AUSTAL2000 diffusion results using different 100 trace particles, after one hour.

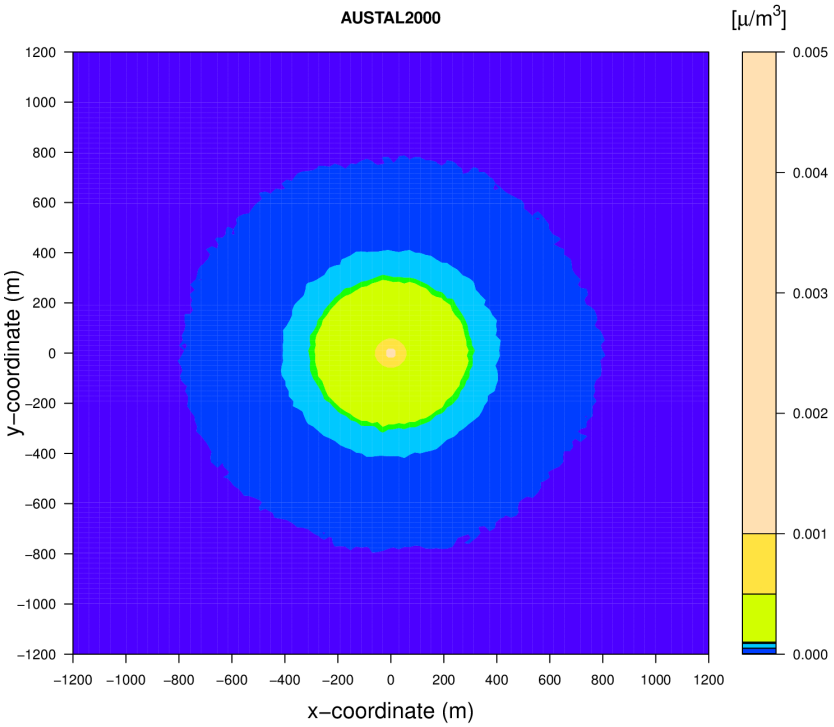

(a) Spatial distribution of average concentration.

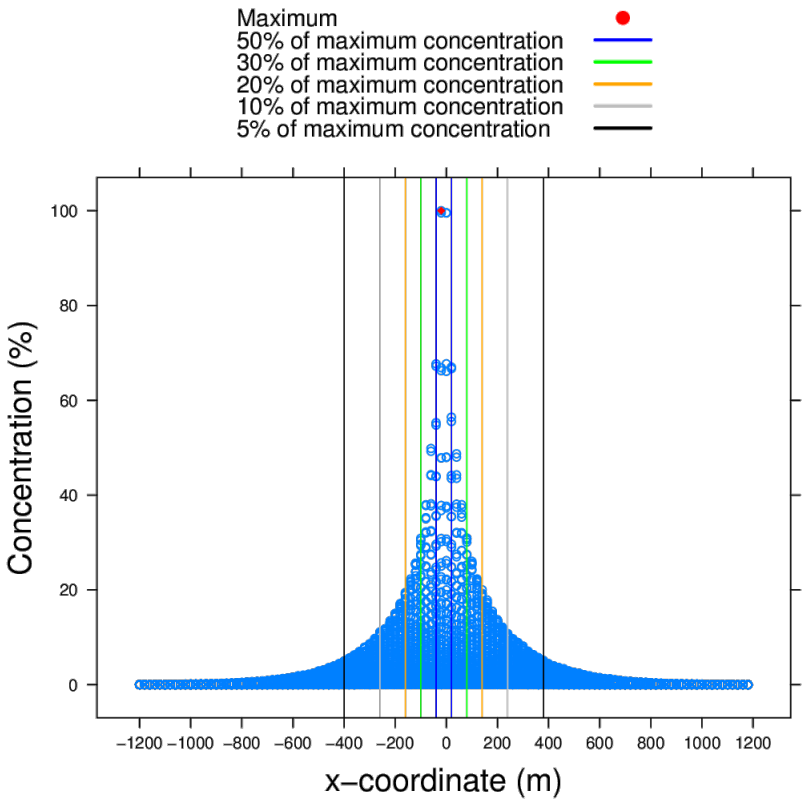

(b) Average concentration distribution over x-coordinate.

Figure C.3: AUSTAL2000 diffusion results using 1'000 trace particles, after one hour.

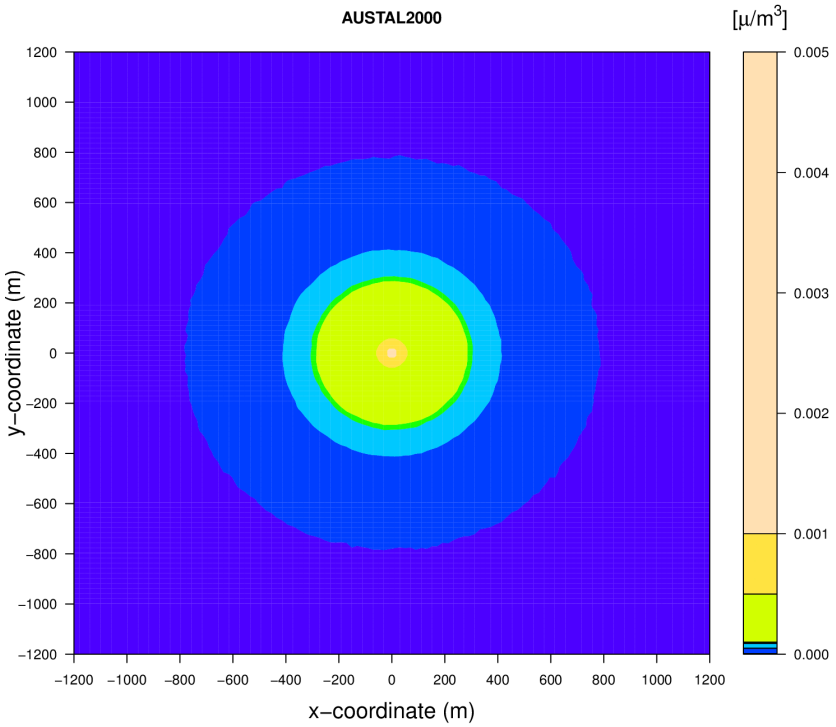

(a) Spatial distribution of average concentration

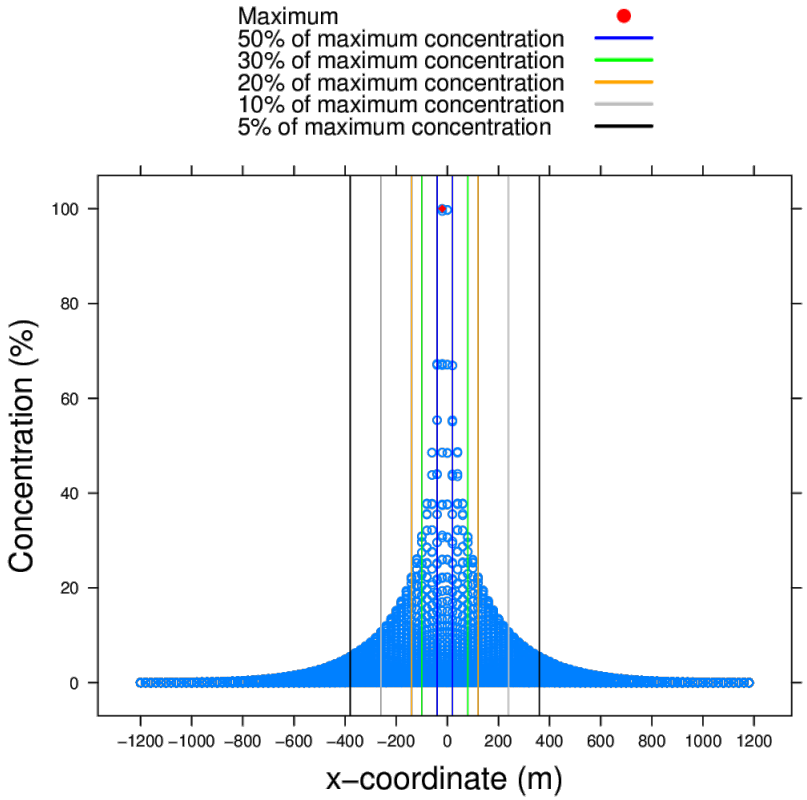

(b) Average concentration distribution over x-coordinate

Figure C.4: AUSTAL2000 diffusion results using 10'000 trace particles, after one hour.

The results show, in Fig. C.2, that for a small number of trace particles, i.e. 100, the spatial distribution is neither symmetric nor continuous. The diffusion results should show a symmetric result since the standard deviations of the u and v have been set to the same value. One hundred particles are not sufficiently representative of the diffusion process.

On the other hand, when the number of particles is larger, the results show a continuous and symmetric dispersion process, as shown in Figs. C.3 and C.4. The results of the simulation using 1'000 or 10'000 particles do not differ considerably, it can be concluded that 1'000 particles already yield a representative result. Nevertheless it can be seen that diffusion zone lines are more clearly defined in the case of the 10'000 particles. Their dispersion over the x axis shows that the 5% of the maximum concentration is reached slightly before in the case of the simulation with 10 000 particles.

Theoretically, one can state that the simulation with more particles is the most accurate, because it has a smaller associated sampling error, without a comparison with a similar real case or a theoretical estimate it is not possible to confirm this fact.

C.2.0.2 Comparison with the Gaussian solution

Another way to solve the diffusion equation is analytically. A reasonable assumption to solve the diffusion equation is that the probability distribution function of the velocity **u** has a Gaussian shape, (Seinfeld and Pandis, 2006). Moreover, it is assumed that the the velocity **u** is independent of x, depending only on time t and that $u(t)$ behaves according to a stationary random process. The derivation of this equation if explained in Seinfeld and Pandis (2006) and Arya (1999). Additionally, an instantaneous source at location $(x, y) = (0, 0)$ is assumed, as well as homogeneous and stationary turbulence. The derivation of the solution for Eq. (C.3) used the method of separation of variables, thus:

$$\langle c(x, y, z, t)\rangle = c_x(x, t)c_y(y, t)c_z(z, t)\,, \tag{C.8}$$

Therefore, when analysing only x and y directions, it can be assumed:

$$\langle c(x, y, t)\rangle = c_x(x, t)c_y(y, t)\,. \tag{C.9}$$

Equation (C.3) is solved using the following conditions,

$$\langle c(x, y, 0)\rangle = S\delta(x)\delta(y) \tag{C.10}$$

$$\langle c(x, y, t)\rangle = 0 \quad x, y \to \pm\infty \tag{C.11}$$

The concentration at (x, y) and at time t, is then given by:

$$c(x, y, t) = \frac{S}{2\pi\sigma_x\sigma_y} \times \exp\left[-\frac{1}{2}\left(\frac{x^2}{\sigma_x^2} + \frac{y^2}{\sigma_y^2}\right)\right]\,, \tag{C.12}$$

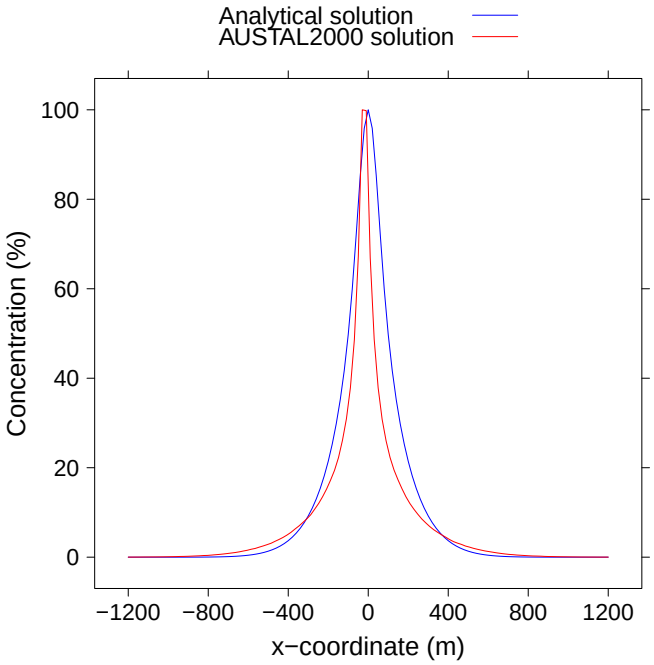

Figure C.5: Analytical and AUSTAL2000 solution Eq. (C.13) diffusion results.

where S is the source strength and σ_x and σ_y are the dispersion parameters in x and y direction. The detailed derivation of Eq. (C.12) is given by Arya (1999); Jacobson (2005); Seinfeld and Pandis (2006).

Additionally, solving Eq. (C.3) using the Fourier transform yields (Arya, 1999; Jacobson, 2005; Seinfeld and Pandis, 2006):

$$c(x,y,t) = \frac{S}{4\pi t\sqrt{K_u K_v}} \times \exp\left[-\frac{1}{4t}\left(\frac{x^2}{K_u} + \frac{y^2}{K_v}\right)\right] . \tag{C.13}$$

Equations (C.12) and (C.13) are equivalent if $\sigma_x^2 = 2K_u t$ and $\sigma_y^2 = 2K_v t$. This fact relates the plume dispersion variances of the Gaussian solution and the diffusivity coefficients.

The study case has been solved with Eq. (C.13), and the results are shown in Fig. C.6. The comparison between both solutions is presented in Fig. C.5. The analytical solution shows an area of bigger concentration accumulation near the source. The 5% of the maximum concentrations occurs around 400 meters, which is very close to the AUSTAL2000 solution with 10 000 particles. On the other hand, the last diffusion zone is wider in the AUSTAL2000 simulation, around 800 meters, compared to 600 meters of the analytical solution. The 20% of the maximum concentration is found on the range of -200 to 200 meters for the analytical solution while the AUSTAL2000 solution is found before that range.

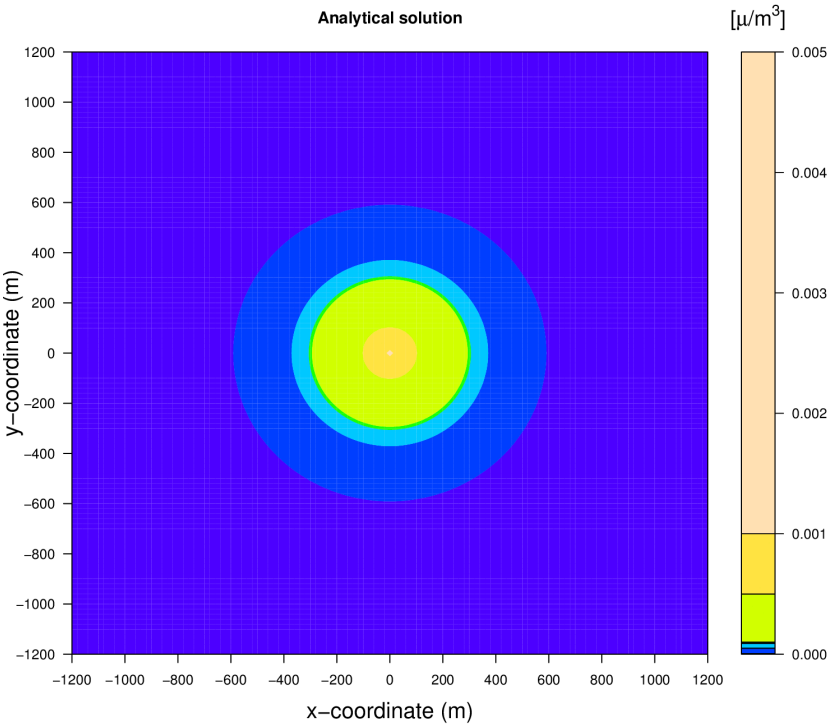

(a) Spatial distribution of average concentration

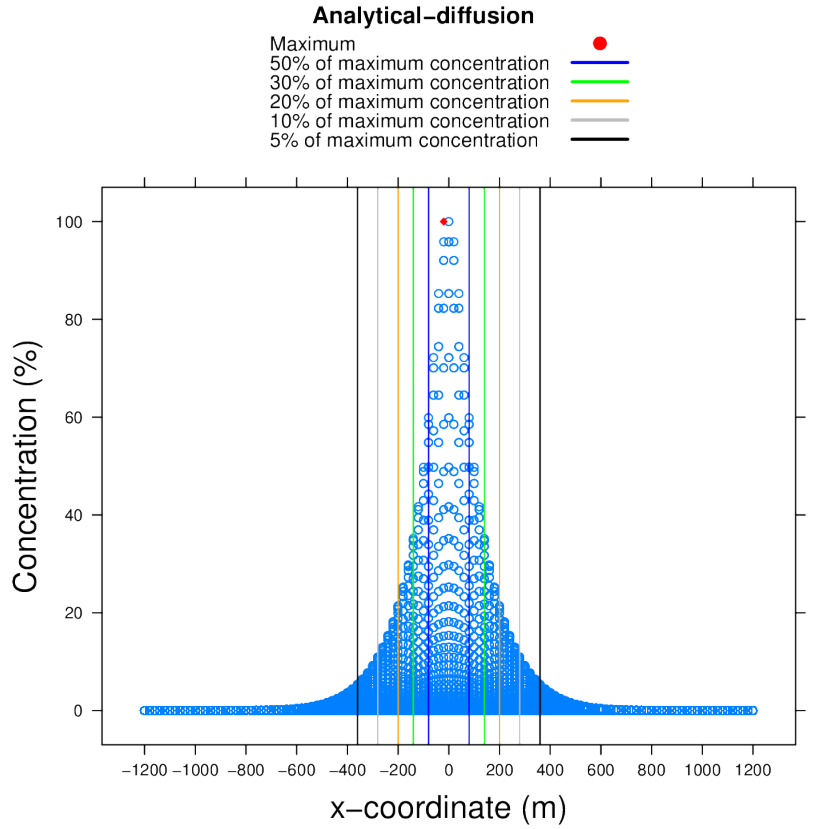

(b) Average concentration distribution over x-coordinate

Figure C.6: Analytical solution of Eq. (C.13) diffusion results.

Appendix D

Look-up Table — Further Considerations

D.1 CB-IV Mechanism Reactions

CB-IV mechanism reactions

```
{ 1}          NO2  =  NO +  O
{ 2}       O       =  O3
{ 3}  O3  +   NO   =  NO2
{ 4}  O   +  NO2   =  NO
{ 5}  O   +  NO2   =  NO3
{ 6}  O   +   NO   =  NO2
{ 7}  O3  +  NO2   =  NO3
{ 8}          O3   =  O
{ 9}          O3   =  O1D
{10}         O1D   =  O
{11}  H2O +  O1D   =  2.0*OH
{12}  O3  +   OH   =  HO2
{13}  O3  +  HO2   =  OH
{14}  NO3          = 0.89*NO2 + 0.89*O +  0.11*NO
{15}  NO3 +  NO    =  2.0*NO2
{16}  NO3  + NO2   =  NO + NO2
{17}  NO3  + NO2   =      N2O5
{18}  N2O5 + H2O   =   2.0*HNO3
{19}  N2O5         =   NO3  +    NO2
{20}  NO  +  NO    =   2.0*NO2
{21}  NO   + NO2 + H2O =   2.000*HONO
{22}  OH   + NO    =   HONO
{23}  HONO         =   OH    +      NO
{24}  OH  +  HONO  =   NO2
{25}  HONO + HONO  =   NO    +      NO2
{26}  OH   + NO2   =   HNO3
{27}  OH   + HNO3  =   NO3
{28}  HO2  + NO    =   OH     +     NO2
{29}  HO2  + NO2   =   PNA
{30}  PNA          =   HO2      +   NO2
{31}  OH   + PNA   =   NO2
{32}  HO2   +HO2   =   H2O2
{33}  HO2 +  HO2 + H2O  =   H2O2
{34}  H2O2         =  2*OH
{35}  OH  +  H2O2  =   HO2
{36}  OH +   CO    =   HO2
{37}  FORM + OH    =   HO2     +    CO
```

```
{38}  FORM        =  2*HO2  +       CO
{39}  FORM        =   CO
{40}  FORM + O     =   OH        +  HO2   +      CO
{41}  FORM  +NO3   =   HNO3      +  HO2    +     CO
{42}  ALD2 + O     =  C2O3    +    OH
{43}  ALD2 + OH    =   C2O3
{44}  ALD2 + NO3   =   C2O3    +    HNO3
{45}  ALD2        =  XO2 + 2*HO2 + CO + FORM
{46}  C2O3 + NO    =  NO2 + XO2 + FORM + HO2
{47}  C2O3 + NO2   =   PAN
{48}  PAN         =   C2O3 +       NO2
{49}  C2O3 + C2O3  =  2*XO2 +  2*FORM + 2*HO2
{50}  C2O3 + HO2   =  0.79*FORM + 0.79*XO2 + 0.79*HO2 + 0.79*OH
{51}  OH          =   XO2    +   FORM  +     HO2
{52}  PAR  + OH   =  0.87*XO2 + 0.13*XO2N + 0.11*HO2 + 0.11*ALD2 +
                     0.76*ROR + -0.11*PAR
{53}  ROR        =  1.1*ALD2 + 0.96*XO2 + 0.94*HO2 + -2.10*PAR +
                     0.04*XO2N + 0.020*ROR
{54}  ROR        =   HO2
{55}  ROR  + NO2  =
{56}  O    + OLE  =  0.63*ALD2 + 0.38*HO2  + 0.28*XO2 + 0.3*CO  +
                      0.2*FORM +  0.02*XO2N + 0.22*PAR +  0.2*OH
{57}  OH   + OLE  =  FORM + ALD2 + XO2 + HO2 + -1*PAR
{58}  O3   + OLE  =  0.5*ALD2 + 0.74*FORM + 0.33*CO + 0.44*HO2 +
                    0.22*XO2 + 0.1*OH + -1.00*PAR
{59} NO3 + OLE = 0.91*XO2 + 0.09*XO2N + FORM + ALD2 + -1*PAR + NO2
{60} O   + ETH = FORM + 0.7*XO2 + CO + 1.7*HO2  + 0.3*OH
{61}  OH   + ETH  =  XO2 + 1.56*FORM + HO2 + 0.22*ALD2
{62}  O3   + ETH  =  FORM + 0.42*CO +  0.12*HO2
{63} OH + TOL = 0.08*XO2 + 0.36*CRES + 0.44*HO2 + 0.56*TO2
{64}  TO2  + NO   = 0.9*NO2 + 0.9*HO2 + 0.9*OPEN
{65}  TO2        = CRES  +  HO2
{66}  OH   + CRES = 0.4*CRO + 0.6*XO2 + 0.6*HO2 + 0.3*OPEN
{67}  NO3  + CRES = CRO   +      HNO3
{68}  CRO  + NO2  =
{69}  OPEN       = C2O3   +     HO2    +     CO
{70}  OPEN + OH   = XO2 + 2*CO + 2*HO2 + C2O3 + FORM
{71}  OPEN + O3   = 0.03*ALD2 + 0.62*C2O3 + 0.7*FORM + 0.03*XO2 +
                   0.69*CO + 0.08*OH + 0.76*HO2 + 0.2*MGLY
{72}  OH   +XYL   = 0.7*HO2 + 0.5*XO2 + 0.2*CRES + 0.8*MGLY +
                    1.1*PAR + 0.3*TO2
{73}  OH  + MGLY  = XO2  +  C2O3
{74}  MGLY       = C2O3  + HO2  + CO
{75}  O  + ISOP   = 0.6*HO2 + 0.8*ALD2 + 0.55*OLE + 0.5*XO2 +
                    0.5*CO + 0.45*ETH  + 0.90*PAR
{76}  OH  +  ISOP  = XO2 + FORM + 0.67*HO2 + 0.13*XO2N + ETH +
                     0.4*MGLY + 0.2*C2O3 + 0.2*ALD2
{77}  O3  +  ISOP  =   FORM  + 0.4*ALD2 + 0.55*ETH + 0.2*MGLY + 0.1*PAR +
                       0.06*CO + 0.44*HO2  + 0.1*OH
{78}  NO3 +  ISOP  =   XO2N
{79}  XO2  + NO    =   NO2
```

```
{80}  XO2N + NO    =
{81}  XO2  + XO2   =
{82}  XO2 +  HO2   =
{83}  NR           =   NR
```

CB-IV mechanism reactions

D.2 Influence of the OZIPR Initialization

In order to analyse the initial concentrations, the same three cases have been simulated, from 6h00 to 21h00, but hourly, i.e. the simulation has not been run constantly from 6h00 to 21h00, but from 6h00 to 7h00, from 7h00 to 8h00 and so on. This allows the study of the importance of the OZIPR initial concentrations, which is important for the storage of the data in the LUT.

Figure D.1 presents the results of the ozone concentrations and rates for the hourly simulation.

The results show that the initial point, in green in Fig. D.1, of every hourly simulation, with a time step of 10 minutes, is unnatural to the time series. OZIPR presents a problem to stabilize the ozone initial concentrations. The same problem has been noticed before in previous studies (Souza, 2011).

Therefore, the simulation have not been carried out hour to hour but continually to avoid the ozone concentration initialisation caveat. The resulting concentrations are grouped according pre-defined intervals of concentrations and stored in the LUT. Also the first two values of the 10 minutes simulations of the run have not been considered in order to avoid this problem.

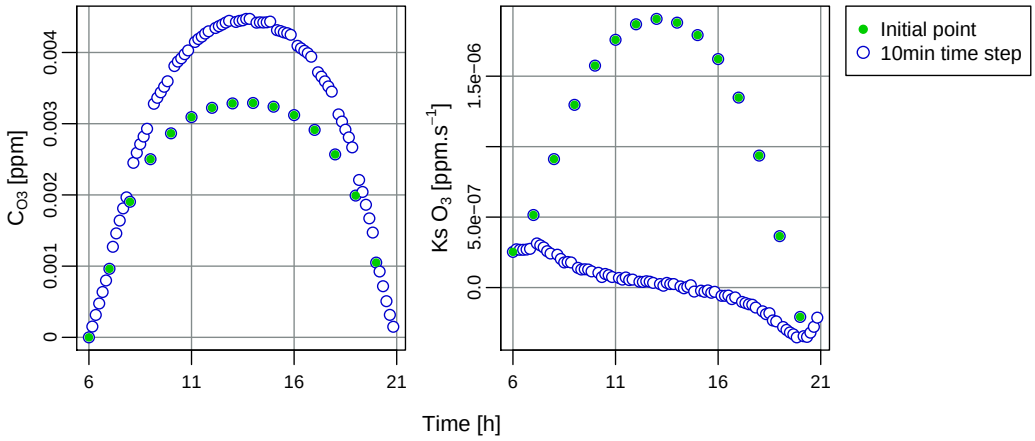

Simulation case 1

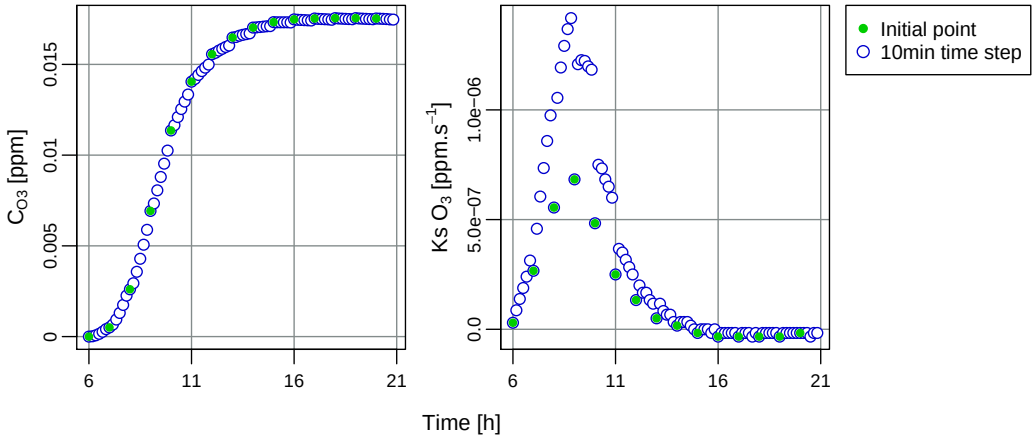

Simulation case 2

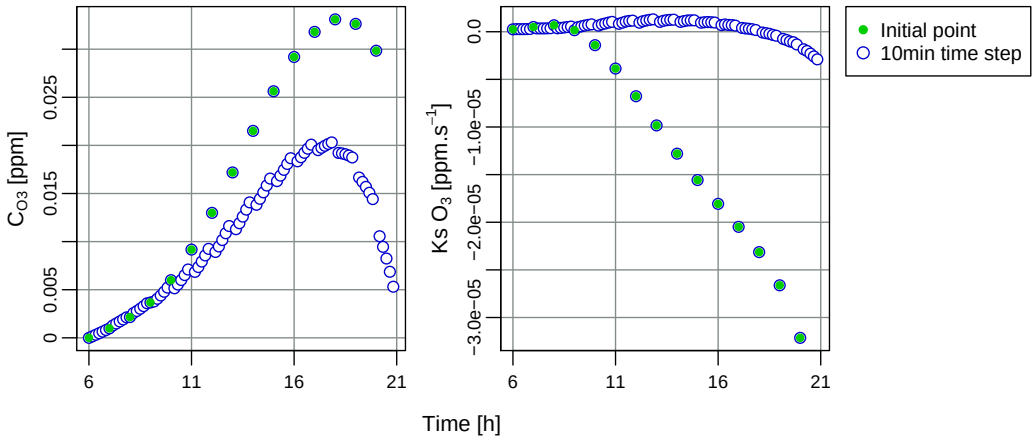

Simulation case 3

Figure D.1: One day time series of ozone rates, simulated hour by hour with 10 minutes time step. The green dots highlight the initial points of each hourly simulation.

D.3 Verification of the Photochemical Module

In order to verify that the photochemical module has been correctly implemented, a set of verification tests have been carried out.

First, all the AUSTAL2000 verification tests provided by Janicke (2009) have been carried out for a non reactive pollutant, in order to assure that the core of the AUSTAL2000 has not been affected by the implementation of the photochemical module. These are a set of tests which are provided directly by the AUSTAL2000 program package with the objective of verifying that the program correctly implments the model described in VDI (2000) The results of the verification testes for AUSTAL2000-AYLTP have given the exact same results as the ones for AUSTAL2000, therefore the implementation of AYLTP did not affect the transport core calculator. Additionally, three verification tests for the implementation of the AYLTP module have been undertaken:

1. Test 1: A simple one cell box, of dimensions $200 \times 200 \times 200$ meters with periodic boundary conditions has been set up. A release of 100 g/s of NO_x in the first 10 minutes of an one hour time series with 10 minutes time interval.

2. Test 2: The same set up of test 1 but assuming a decay of NO_x concentrations, with the reaction rate $Ks_{NO_x} = -0.015 \mu g \cdot m^{-3} \cdot s^{-1}$. The decay has been applied from the third time interval on.

3. Test 3: Extends the test 2 to the three reactive species instead of one, with the ozone reaction rate $Ks_{O_3} = 0.48265 \mu g \cdot m^{-3} \cdot s^{-1}$, the NO_x reaction rate, $Ks_{NO_x} = -0.00376 \mu g \cdot m^{-3} \cdot s^{-1}$ and the VOC reaction rate $Ks_{VOC} = -0.00099 \mu g \cdot m^{-3} \cdot s^{-1}$. The rates have been applied from the third time interval on.

The results of the verification tests 1 and 2 are presented in Fig. D.2.

The use of periodic boundary conditions, i.e. the particles which leave the domain through one of the boundaries enter it through the opposite boundary, is assured that no particle is lost and therefore no mass is lost. Theoretically, test 1 is expected to stabilise at a concentration of $7500\,\mu g\,m^{-3}$ The concentration stabilises at the expected concentration on the second time interval. The particles are released though out the whole time interval and not at the beginning, therefore not all the particles are in the domain during the whole first time interval. As a result, the first time interval concentration is smaller than in the following time intervals. For the following tests this value is already known from test 1 and therefore it is assumed as the theoretical value. The results of test 3 are shown in Fig. D.3, demonstrate an agreement with the

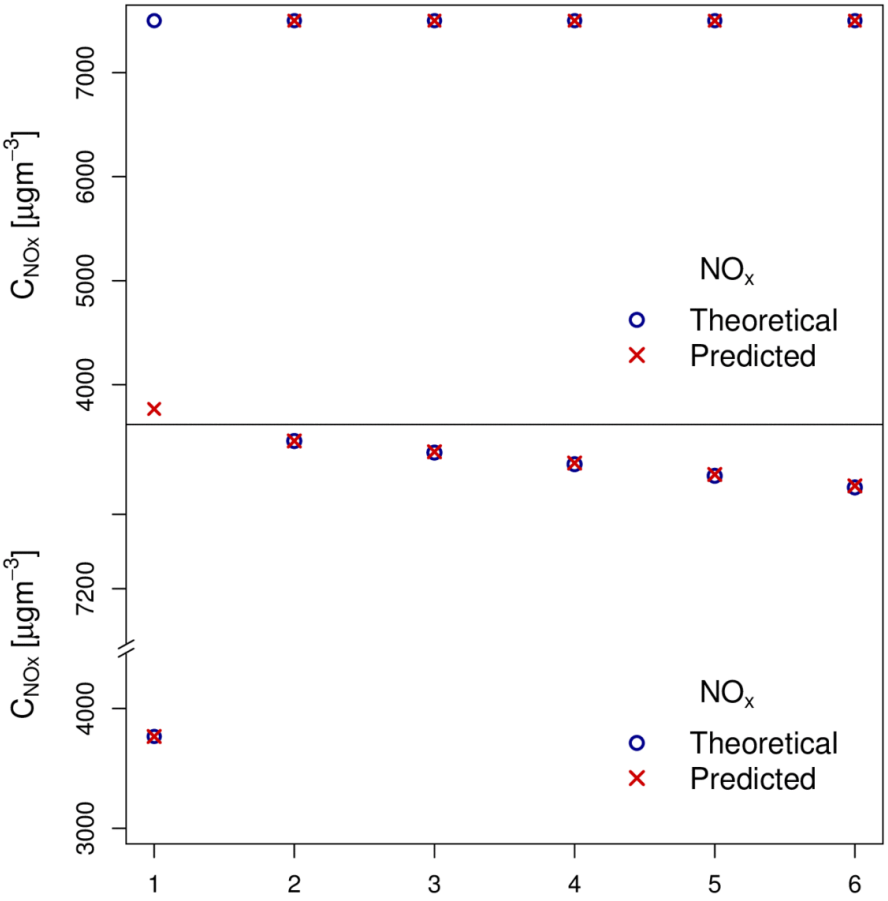

Figure D.2: Verification tests 1 and 2, AUSTAL2000-AYLTP resulting concentrations of NO_x and VOC.

theoretical concentrations resulting from the application of the rates through Eq. (D.1), here applied directly to concentration:

$$c_{p,i,j,k}(t+\Delta t) = c_{p,i,j,k}(t) + K s_p(c_p(t),\Omega)\Delta t, \quad \forall p\,, \forall (i,j,k) \in S\,, \quad \text{(D.1)}$$

Therefore it is concluded that the AYLTP photochemical module has been correctly implemented in AUSTAL2000-AYLTP.

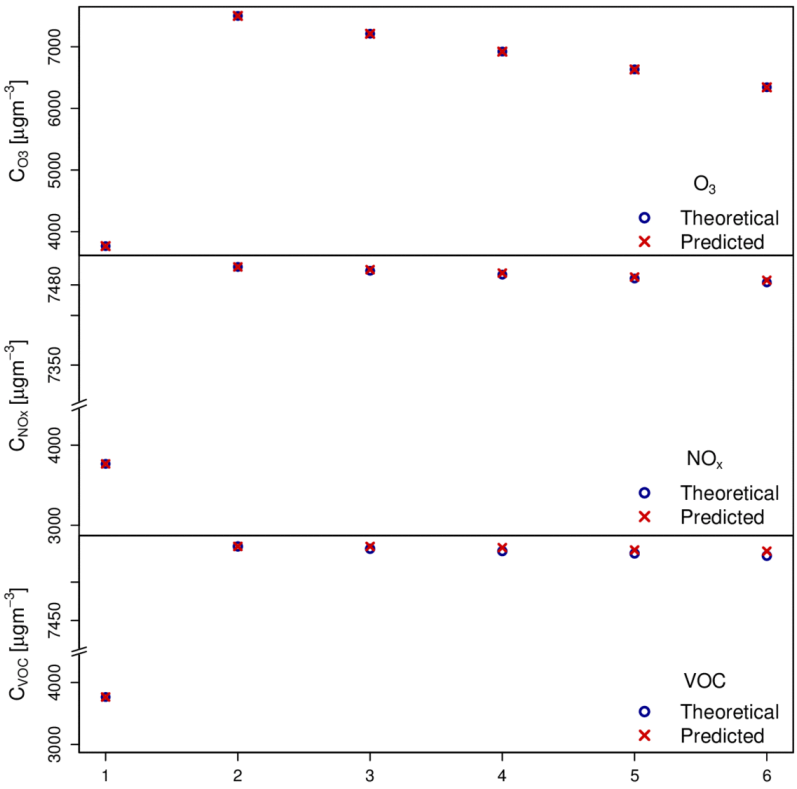

Figure D.3: Verification test 3, AUSTAL2000-AYLTP resulting concentrations of NO_x, VOC and O_3.

The small differences in Figs. D.2 and D.3 between the theoretical and predicted values can be attributed to the precision errors for small rates.

Appendix E

Modications of AUSTAL2000 Model

The implementation of the photochemical module AYLTP into AUSTAL2000 has required code changes. The main modifications are the following:

- Include of the pollutants: VOC and O_3.
- Increase of the allowed number of grid cells.
- Increase the buffer size for reading input files.
- Increase memory allocation size.
- Read LUT parameters from the AUSTAL2000 input file.
- Initialize and copy of the production rates', concentrations' and number of particles' tables.
- Write the production rates and concentrations.
- Read LUT and retrieve the production rates.
- Apply the production rates.
- Count the number of particles in each grid cell.
- Store concentrations.

Figure E.1 is a schematic representation of the AUSTAL2000 code locations where the modifications have been undertaken. Further details can be found in Aleluia Reis et al. (2011a).

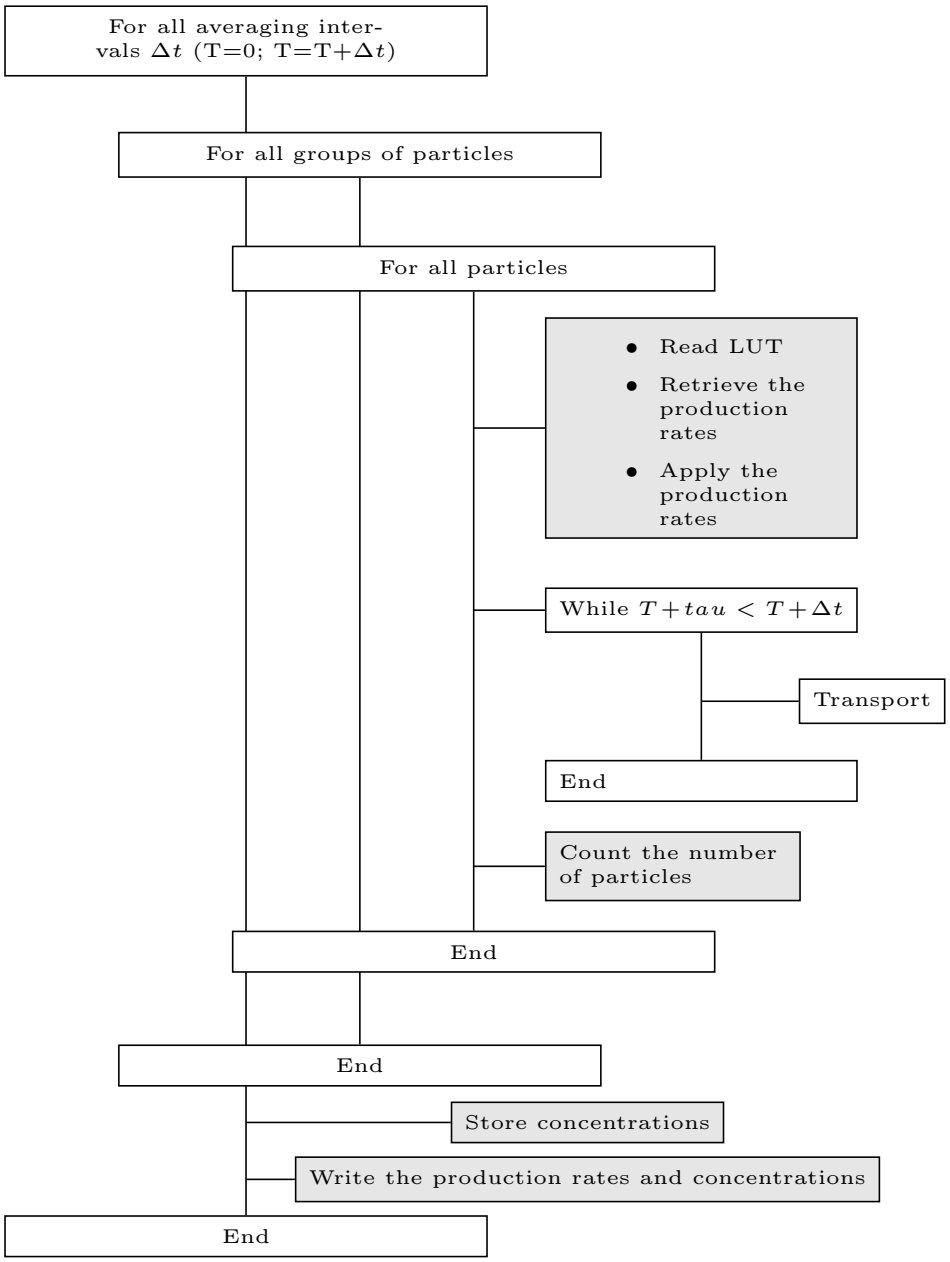

Figure E.1: Schematic representation of the code locations where the modifications have been undertaken in AUSTAL2000 model. The grey boxes represent the required changes.

Bibliography

H. Abilock, C. Bergstrom, J. Brady, A. Doernberg, A. Ek, L. Fishbone, D. Hill, M. Hirano, R. Karvanagh, S. Koyama, K. Larsson, G. Leman, M. Moy, V. Sailor, O. Sato, F. Shore, T. Sira, T. Teichman, and C.-O. Wene. Markal: A multi-period linear programming model for energy system analysis. In R. Kavanagh, editor, *Proceedings of the international conference on energy system analysis*, page 482, Dublin, Ireland, 9–11 October 1979 1980. Dordrecht: Reidel.

Plus ACCENT. Atmospheric composition change — the European Network. http://www.accent-network.org/, 2012.

Administration du Cadastre et de la Topographie du Grand-Duché de Luxembourg ACT. Le géoportail national du grand-duché de luxembourg, 2012. URL http://www.geoportail.lu/Portail/.

J. Alcamo and L. Hordijk, editors. *The RAINS model of acidification: science and strategies in Europe*. Dordrecht, The Netherlands: Kluwer Academic Publishers, 1990.

L. Aleluia Reis, D. S. Zachary, U. Leopold, and B. Peters. Selecting a fast air quality calculator for an optimization meta-model. In C. A. Brebbia and V. Popov, editors, *Air Pollution XVII*. WITPRESS Southampton, Boston, 2009.

L. Aleluia Reis, L. Drouet, U. Leopold, and D. Zachary. Luxembourg energy-air quality model. Technical report, CRTE, 2011a.

L Aleluia Reis, L. Drouet, U. Leopold, and D. Zachary. LEAQ: The luxembourg energy air quality project (2008–2012). Technical report, CRTE, CRP Henri Tudor, Esch-sur-Alzette, Luxembourg, 2011b.

L. Aleluia Reis, D. Melas, B. Peters, and D. S. Zachary. Developing a fast photochemical calculator for an integrated assessment models. In *Proceedings of the 14th International Conference os Hamonization whithin Atmospheric Dispersion Modelling for Regulatory Purposes*. HARMO14, 2012.

S. Alessandrini and E. Ferrero. A hybrid lagrangian-eulerian particle model for reacting pollutant dispersion in non-homogeneous non-isotropic turbulence. *Physica A*, 388:1375–1387, 2009.

Sofia Pinto de Almeida, Elsa Casimiro, and Jose Calheiros. Short-term association between exposure to ozone and mortality in oporto, portugal. *Environmental Research*, 111:406–410, 2011.

M. Amann, C. Heyes, M. Makowski, and W. Schöpp. An optimization model for the control of regional air quality in europe. In J.B.H.J. Linders, editor, *Modelling of Environmental Chemical Exposure and Risk*, pages 193–203. Kluwer Academic Publishers, The Netherlands, 2001.

M. Amann, I. Bertok, J. Borken-Kleefeld, J. Cofala, C. Heyes, L. Höglund-Isaksson, Z. Klimont, B. Nguyen, M. Posch, P. Rafaj, R. Sandler, W. Schöpp, F. Wagner, and W. Winiwarter. Cost-effective control of air quality and greenhouse gases in europe: Modeling and policy applications. *Environmental Modelling & Software*, 26(12):1489–1501, 2011.

H. ApSimon, R. Warren, and J. Wilson. The abatement strategies assessment model: Applications to reductions of SO_2 emissions in europe. *Atmospheric Environment*, 24(4):649–663, 1994.

S. P. Arya. *Air pollution meteorology and dispersion.* Oxford Univerity Press, 1999.

ASTA. Agrarmeteorologisches Messnetz Luxemburg, 2010. URL http://www.wetter.rlp.de/dienststellen/oppenheim/html/am/LUAM.

F. Babonneau, C. Beltran, A. Haurie, C. Tadonki, and J.-P. Vial. Proximal-accpm: a versatile oracle based optimization method. *Optimisation, Econometric and Financial Analysis*, 9:67–89, 2006.

T. Barker, A. Anger, O. Dessens, H. Pollitt, H. Rogers, S. Scrieciu, R. Jones, and J. Pyle. Integrated modelling of climate control and air pollution: Methodology and results from one-way coupling of an energy–environment–economy (e3mg) and atmospheric chemistry model (p-tomcat) in decarbonising scenarios for mexico to 2050. *Environmental Science & Policy*, 13(8):661–670, December 2010.

M. L. Bell and D. L. Davis. Reassessment of the lethal london fog of 1952: Novel indicators of acute and chronic consequences of acute exposure to air pollution. *Environmental Health Perspectives*, 3:389–394, 2001.

BMU. First general administrative regulation pertaining the federal immission control act (technical instructions on air quality control – ta luft). Technical report, Ministry for the Environment, Nature Conservation and Nuclear Safety, 2002.

R. Borge, V. Alexandrov, J. J. del Vas, J. Lumbreras, and E. Rodriguez. A comprehensive sensitivity analysis of the wrf model for air quality applications over the iberian peninsula. *Atmospheric Environment*, 42(37): 8560–5874, December 2008.

C. Borrego, A. Monteiro, J. Ferreira, M.R. Moraes, A. Carvalho, I. Ribeiro, A.I. Miranda, and D.M. Moreira. Modelling the photochemical pollution over the metropolitan area of porto alegre, brazil. *Atmospheric Environment*, 44(3):370 – 380, 2010. ISSN 1352-2310. doi: 10.1016/j.atmosenv.2009.10.027. URL http://www.sciencedirect.com/science/article/pii/S1352231009008899.

P. Capros, T. Georgakopoulos, A. Filippoupolitis, et al. The gem-e3 model: Reference manual. Technical report, National Technical University of Athens, 1997.

P. Capros, L. Mantzos, L. Vouyoukas, and D. Petrellis. European energy and co 2 emissions trends to 2020: PRIMES model v.2. *Bulletin of Science Technology Society*, 19(6):474–492, December 1999.

D. A. Carlson, A. Haurie, J. P. Vial, and D. S. Zachary. Large scale convex optimizationmethods forair quality policy assessment. *Automatica*, 40(3): 385–395, March 2004.

C. Carnevale, E. Pisoni, and M. Volta. A multi-objective nonlinear optimization approach to designing effective air quality control policies. *Automatica*, 44:1632—1641, 2008.

CEIP. Webdab search - emissions as used in emep models, 2012.

Monitoring and evaluation of the RES directives implementation in EU27 and policy recommendations for 2020, Greece, 2012. Centre for Renewable Energy Sources. URL http://www.res2020.eu.

CGIAR. Srtm digital elevation data, 2012. URL http://srtm.csi.cgiar.org/SELECTION/inputCoord.asp.

T. Y. Chang and S. J. Rudy. Ozone-precursor relationships: A modeling study of semiempirical relationships. *Environ. Sci. Technol.*, 27:2213–2219, 1993.

C. Changhong, W. Bingyan, F. Qingyan, C. Green, and D. G. Streets. Reductions in emissions of local air pollutants and co-benefits of chinese energy policy: a shanghai case study. *Energy Policy*, 34:754–762, 2006.

The EMEP Home page, 2012. CIAM, Center for Integrated Assessment Modelling. URL http://www.emep.int/.

Daniel S. Cohan, Bonyoung Koo, and Greg Yarwood. Influence of uncertain reaction rates on ozone sensitivity to emissions. *Atmospheric Environment*, 44(26):3101 – 3109, 2010. ISSN 1352-2310. doi: 10.1016/j.atmosenv.2010.05.034. URL http://www.sciencedirect.com/science/article/pii/S1352231010004176.

D. Connolly, H. Lund, B. V. Mathiesen, and M. Leahy. A review of computer tools for analysing the integration of renewable energy into various energy systems. *Applied Energy*, 87:1059–1082, 2010.

728/732 COST. *COST 728/732 - Model Inventory.* Universität Hamburg, http://www.mi.uni-hamburg.de/Summary-Tables.510.0.html, 12 March 2007.

COST728. Enhancing mesoscale meteorological modelling capabilities for air pollution and dispersion applications, 2012.

COST732. Model evaluation case studies: Approach and results, 2011.

P. Criqui, S. Mima, and L. Viguier. Marginal abatement costs of CO_2 emission reductions, geographical flexibility and concrete ceilings: an assessment using the POLES model. *Energy Policy*, 27(10):585–601, October 1999.

F. A. A. M. de Leeuw, H. J. van Rheineck Leyssius, and P. J. H. Builtjes. Calculation of long term averaged ground level ozon concentrations. *Atmospheric Environment*, 24A:185–193, 1990.

I. D'Elia, M. Bencardino, L. Ciancarella, M. Contaldi, and G. Vialetto. Technical and non-technical measures for air pollution emission reduction: The integrated assessment of the regional air quality management plans through the italian national model. *Atmospheric Environment*, 43:6182–6189, 2009.

R. Dennis. A framework for evaluating regional—scale numerical photochemical modeling systems. *Environ Fluid Mech*, 10:471—489, 2010.

Transport Department of the Environment and the Regions. Design manual for roads and bridges (dmrb). Technical report, The Stationery Office, 1999.

J. E. Diem and C. C. Andrew. Air quality, climate, and policy: A case study of ozone pollution in tucson, arizona. *Professional Geographer*, 53:469–471, 2001.

R. Djouad and B. Sportisse. Solving reduced chemical models in air pollution modelling. *Applied Numerical Mathematics*, 44:49–61, 2003.

M. C. Dodge. Chemical oxidant mechanisms for air quality modeling: critical review. *Atmospheric Environment*, 34:2103–2130, 2000.

L. Drouet. *Modélisation intégrée du changement climatique: contribuition de l'optimisation par oracle.* PhD thesis, Université de Genève, Faculté des Sciences Économiques et Sociales Section des Hautes Études Commerciales, 2006.

L. Drouet. Etem luxembourg - a reference energy scenario for luxembourg. Technical report, CRP Henri Tudor, 2011.

L. Drouet and L. Aleluia Reis. Spatial-time emission allocation module for the luxembourg energy air quality model. Technical report, CRTE, February 2012.

L. Drouet and J. Thénié. Etem - an energy/technology/environment model to assess urban sustainable development policies. reference manual—version 2.1. Technical report, Ordecsys, Place de l'Étrier 4 – Chêne-Bougeries – Suisse, November 2008.

A. J. Dyer and B. B. Hicks. Flux gradent relationships in the constant flux layer. *Quarterly Journal of the Royal Meteorological Society*, 96:715–721, 1970.

A. Ebel, R. Friedrich, and H. Rhode. *GENEMIS: Assessment, improvement, temporal and spatial disaggregation of European emission data. Tropospheric Modelling and Emission Estimation, (PART 2).* Springer, 1997, 1997.

EC4MACS. Life iii ec4macs european consortium for modelling of air pollution and climate strategies. Technical report, International Institute for and Applied Systems Analysis, June 2007.

EEA. Air pollution by ozone in europe in summer. Technical Report 1, EEA, 2006.

EEA. The european environment state and outlook 2010. Technical report, European Environment Agency, 2010a. URL http://www.eea.europa.eu/soer.

EEA. Luxembourg national emissions reported to the convention on longrange transboundary air pollution (lrtap convention) - nfr02 sector classification, July 2010b.

EEA. Luxembourg national emissions reported to the convention on long-range transboundary air pollution (LRTAP convention) - NFR02 sector classification, 06 Jul 2010c.

EEA. Air quality in Europe - 2011 report. Technical report, European Environmental Agency, Copenhagen,, 2011.

EEA. AirBase - the european air quality database, 2012a.

EEA. Air quality in europe — 2012 report. Technical report, European Environment Agency, 2012b.

European Topic Centre On Air & Climate Change EIONET. Model documentation system, 2012. URL http://pandora.meng.auth.gr/mds.

Lakes Environmental. Calpuff view, leading interface for puff dispersion. Technical report, Lakes Environmental, 2011. URL http://www.weblakes.com.

EPA. User's guide for the photochemical box model (pbm). Technical report, U. S Environmental Protection Agency, 1984.

EPA. Response to peer review comments on epa-cmb8.2 and its documentation. Technical report, U.S. Environmental Protection Agency Office of Air Quality Planning & Standards Air Quality Modeling Group, 2005.

EPA. Aerscreen user's guide. Technical report, US Environmental Protection Agency, 2011.

J.J. Erbrink and P. Bange, editors. *Modeling dispersion and NO oxidation in power plant plumes. In: Proceedings of the 19th International technical meeting of NATO-CCMS on Air Pollution Modeling and its application*, 1991. Plenum Press.

EU. Council directive 91/676/eec of 12 december 1991 concerning the protection of waters against pollution caused by nitrates from agricultural sources. Technical report, European Union, 1991.

EU. European parliament and council directive 94/63/ec of 20 december 1994 on the control of volatile organic compound (voc) emissions resulting from the storage of petrol and its distribution from terminals to service stations. Technical report, European Union, 1994.

EU. Directive 98/70/ec of the european parliament and of the council of 13 october 1998 relating to the quality of petrol and diesel fuels and amending council directive 93/12/eec. Technical report, European Union, 1998.

EU. Council directive 1999/32/ec of 26 april 1999 relating to a reduction in the sulphur content of certain liquid fuels and amending directive 93/12/eec. Technical report, European Union, 1999a.

EU. Council directive 1999/13/ec of 11 march 1999 on the limitation of emissions of volatile organic compounds due to the use of organic solvents in certain activities and installations. Technical report, European Union, 1999b.

EU. Directive 2001/81/ec of the european parliament and of the council of 23 october 2001 on national emission ceilings for certain atmospheric pollutants. Technical report, European Union, 2001.

EU. Directive 2003/17/ec of the european parliament and of the council of 3 march 2003 amending directive 98/70/ec relating to the quality of petrol and diesel fuels. Technical report, European Union, 2003.

EU. Directive 2004/107/ec of the european parliament and of the council of 15 december 2004 relating to arsenic, cadmium, mercury, nickel and polycyclic aromatic hydrocarbons in ambient air. Official Journal of the European Union, December 2004.

EU. Directive 2005/55/ec of the european parliament and of the council of 28 september 2005 on the approximation of the laws of the member states relating to the measures to be taken against the emission of gaseous and particulate pollutants from compression-ignition engines for use in vehicles, and the emission of gaseous pollutants from positive-ignition engines fuelled with natural gas or liquefied petroleum as for use in vehicles. Technical report, 2005, 2005.

EU. Commission regulation (ec) no 692/2008 of 18 july 2008 implementing and amending regulation (ec) no 715/2007 of the european parliament and of the council on typeapproval of motor vehicles with respect to emissions from light passenger and commercial vehicles (euro 5 and euro 6) and on access to vehicle repair and maintenance information. Technical report, European Union, 2008a.

EU. Directive 2008/50/ec of the european parliament and of the council of 21 may 2008 on ambient air quality and cleaner air for europe. Official Journal of the European Union, May 2008b.

EU. Regulation (ec) no 595/2009 of the european parliament and of the council of 18 june 2009 on type-approval of motor vehicles and engines with respect to emissions from heavy duty vehicles (euro vi) and on access to vehicle repair and maintenance information and amending regulation (ec) no 715/2007 and directive 2007/46/ec and repealing directives 80/1269/eec, 2005/55/ec and 2005/78/ec. Technical report, European Union, 2009a.

EU. Directive 2009/126/ec of the european parliament and of the council of 21 october 2009 on stage ii petrol vapour recovery during refuelling of motor vehicles at service stations. Technical report, European Union, 2009b.

EU. Directive 2010/75/eu of the european parliament and of the council of 24 november 2010 on industrial emissions (integrated pollution prevention and control), November 2010a.

EU. Eu energy trends to 2030 - update 2009. Technical report, European Comission, Directorate-General for energy, August 2010b.

B. A. Finlayson. *Nonlinear Analysis in Chemical Engineering.* Ravena Park Publishing, Inc, 2003.

L. G. Fishbone and H. Abilock. Markal, a linear-programming model for energy systems analysis: Technical description of the bnl version. *International Journal of Energy Research*, 5:353—-375, 1981.

R. Fourer, D. M. Gay, and B. W. Kernighan. A modeling language formulations mathematical programing. *Management Science*, 36(5):519–554, 1990.

M. W. Gery and R. R. Crouse. User's guide for executing ozipr. Technical report, U.S. Environmental Protection Agency, 1990.

M. W. Gery, J. P. Killus, and G. Z. Whitten. Development and testing of the cbm-iv for urban and regional modelling. Technical report, EPA, 1988.

M. W. Gery, G. Z. Whitten, J. P. Killus, and M. Doge. A photochemical kinetics mechanism for urban and regional scale computer modeling. *Journal of Geophysical Research*, 94:12925–12956, 1989.

J. L. Goffin and J. P. Vial. On the computation of weighted analytic centers and dual ellipsoid with the projective algorithm. *Mathematical Programming*, 60:81–92, 1993.

A. G. Grell, J. Dudhia, and D. R. Stauffer. A description of the fifth-generation penn state/ncar mesosclae model (mm5). Technical report, National Center for Atmospheric Research, 1994.

H Hass. Description of the eurad chemistry-transport-model version2 (ctm2). Technical report, Mitteilungen aus dem Institut für Geophysik und Meteorologie der Universität zu Köln, 1991.

P. J. Hurley, W. L. Physick, and A. K. Luhar. Tapm: a practical approach to prognostic meteorological and air pollution modelling. *Environmental Modelling & Software*, 20:737–752, 2005.

IMO. International convention for the prevention of pollution from ships (marpol). Technical report, International Maritime Organization, 1973.

IPCC. *Climate Change 2007, the Fourth Assessment Report.* Cambridge University Press, 2007.

D. Jacob and E. W. Gottlieb. Chemistry of a polluted cloudy boundary layer. *Journal of Geophysical*, 94:12975–13002, 1989.

M. Z. Jacobson. *Fundamental of Atmospheric Modeling.* Cambridge, 2005.

D. E. James, J. A. Chambers, J. D. Kalma, and H. A. Bridgman. Air quality prediction in urban and semi-urban regions with generalised input-output analysis: The hunter region, australia. *Urban Ecology*, 9:25–44, 1985.

Consulting Janicke. Austal2000 program documentation of version 2.4. Technical report, Janicke, Consulting, 2009.

L. Janicke. Reports on environmental physics - a random walk model for turbulent diffusion. Technical report, Ingenieurbüro Janicke, 2000.

L. Janicke. *Lagrangian dispersion modelling.* Number 235 in 235. Particulate Matter in and from Agriculture, 2002.

U. Janicke and L. Janicke. Enhancement of a diagnostic wind field model for licensing industrial facilities (TA Luft). Technical report, German Federal Environmental Agency UBA, 2004. URL http://www.austal2000.de.

L. V. Kalachev and R. J. Field. Reduction of a model describing ozone oscillations in the troposphere: Example of an algorithmic approach to model reduction in atmospheric chemistry. *Journal of Atmospheric Chemistry*, 39: 65–93, 2001.

A. Kanudia, M. Labriet, R. Loulou, K. Vaillancourt, and J. P. Waaub. The world-markal model and its application to cost-effectiveness, permit sharing, and cost-benefit analyses. In R. Loulou, J.-P. Waaub, and G. Zaccour, editors, *Energy and Environment*, pages 111–148. Springer, 2005.

K. D. Karatzas and S. Kaltsatos. Air pollution modelling with the aid of computational intelligence methods in thessaloniki, greece. *Simulation Modelling Practice and Theory*, 15:1310–1319, 2007.

G. Klaassen, M. Amann, C. Berglund, J. Cofala, L. Höglund-Isaksson, C. Heyes, R. Mechler, A. Tohka, W. Schöpp, and W. Winiwarter. The extension of the RAINS model to greenhouse gases. Technical Report IR-04-015, International Institute for Applied Systems Analysis, 2004.

J. N. Knudsen, P. A. Jensen, and K. Dam-Johansen. Transformation and release to the gas phase of cl, k, and s during combustion of annual biomass. *Energy Fuels*, 18:1385–99, 2004.

A. N. Kolmogorov. Local structure of turnulence in an incompressible fluid at very high Reynolds numbers. *Doklady Akad. Nauk.*, 30:299–303, 1941.

J. Kuenen, H. Denier van der Gon, A. Visschedijk, and H. van der Brugh. High resolution european emission inventory for the years 2003—2007. Tno report tno-060-ut-2011-00588, TNO, Utrecht, 2011. URL https://gmes-atmosphere.eu/documents/deliverables/d-emis/.

O. J. Kuik, J. F. M. Helming, C. Dorland, and F. A. Spaninks. The economic benefits to agriculture of a reduction of low-level ozone pollution in the Netherlands. *Murphy1999*, 27:75–90, 2000.

U. Kumar, A. Prakash, and V. K. Jain. A photochemical modelling approach to investigate O3 sensitivity to NOx and VOCs in the urban atmosphere of Delhi. *Aerosol and Air Quality Research*, 8(2):147–159, 2008.

Jérôme Kübler. *Integrated assessment of photochemical air pollution control strategies: method development and application to the swiss plateau.* PhD thesis, ÉCOLE POLYTECHNIQUE FÉDÉRALE DE LAUSANNE, 2001.

M. Laaidi, A. Boumendil, T. C. Tran, H. Kaba, P. Rozenberg, and P. Aegerter. Air pollution and pregnancy outcome: A review of the literature. *Environnement, Risques & Santé*, 3:287–98, 2011.

L. L. Lim, S. J. Hughesb, and Hellawell E. E. Integrated decision support system for urban air quality assessment. *Environmental Modelling & Software*, 20:947–954, 2005.

R. Loulou and M. Labriet. Etsap-tiam: the times integrated assessment model part i: Model structure. *Computational Management Science*, 5:7–40, 2008.

TA Luft. First general administrative regulation pertaining the federal immission control act (technical instructions on air quality control - ta luft). Technical report, Bundesministerium für Umwelt, Naturschutz und Reaktorsicherheit, 2002.

A. Manne. MERGE: A model for evaluating regional and global effects of GHG reduction policies. *Energy Policy*, 23(1):17–34, January 1995. ISSN 03014215.

K. Markakis, A. Poupkou, D. Melas, P. Tzoumaka, and M. Petrakakis. A computational approach based on gis technology for the development of an anthropogenic emission inventory of gaseous pollutants in Greece. *Water Air Soil Pollut*, 207:157–180, 2010.

R. Mathur, A. Hanna, Odmanm O., C. Coats, K. Alapaty, A. Trayanov, A. Xiu, C. Jang, S. Fine, D. Byun, K. Schere, R. Dennis, J. Novak, T. Pierce, J. Young, and G. Gipson. The Multiscale Air Quality Simulation Platform (MAQSIP): Model Formulation and Process Considerations. Technical report, Carolina Environmental Program, University of North Carolina at Chapel Hill, 2004.

A. Maurizi. Ozone modeling over Italy: A sensitivity analysis to precursors using bolchem air quality model. In *NATO Science for Peace and Security*

Series C: Environmental Security Air Pollution Modeling and Its Application XIX 4, 2008.

N. A. Mazzeo, L. E. Venegas, and H. Choren. Analysis of NO, NO2, O3 and NOx concentrations measured at a green area of Buenos Aires city during wintertime. *Atmospheric Environment*, 39(17):3055–3068, 2005. ISSN 1352-2310.

MDDI. Second, third, fourth and fifth national communication of Luxembourg under the united nations framework convention on climate change. Technical report, Le Gouvernement du Grand-Duché de Luxembourg Ministère du Développement durable et des infrastructures, February 2010.

MECA. Aftermarket converter technology for gasoline light-duty vehicles. Technical report, Manufacturers of Emission Controls Association, December 2009. URL http://www.meca.org.

A. Mediavilla and H. ApSimon. Urban scale assessment of options to reduce pm10 in london towards attainment of air quality objectives. *Atmospheric Environment*, 37(33):4651–4665, October 2003.

A. Milt, A. Milano, S. Garivait, and R. Kamens. Effects of 10% biofuel substitution on ground level ozone formation in Bangkok, Thailand. *Atmospheric Environment*, 43:5962–5970, 2009.

R.E. Morris, S. Lau, and G. Yarwood. Development and application of an advanced air toxics hybrid photochemical grid modeling system. *Int. J. Environment and Pollution*, 24:51–64, 2005.

N. Moussiopoulos. *MDS - Model Documentation System*, 29 August 2009. URL http://pandora.meng.auth.gr/mds.

N. Moussiopoulos, Th. Flassak, and G. Knittel. A refined diagnostic wind model. *Environmental software*, 3(2), 1988.

N. Moussiopoulos, E. Berge, T. Bøhler, F. Leeuw, K. Grønskei, S. Mylona, and M. Tombrou. Ambient air quality, pollutant dispersion and transport models. Technical report, European Topic Centre on Air Quality, 1996.

N. Z. Muller and R. Mendelsoh. The air pollution emission experiments and policy analysis model (APEEP). Technical report, Yale University, 2006.

J. J. Murphy, M. A. Delucchi, D. R. McCubbin, and H. J. Kim. The cost of crop damage caused by ozone air pollution from motor vehicles. *Journal of Environmental Management*, 55(4):273–289, 1999.

A. Mutchimwong. A methodology for the assessment of air quality in London and Bangkok. Technical report, University of Hertfordshire, 2005.

T. Nakata. Energy-economic models and the environment. *Progress in Energy and Combustion Science*, 30:417–475, 2004.

G. F. Nemet, T. Holloway, and P. Meier. Implications of incorporating air-quality co-benefits into climate change policymaking. *Environmental Research Letters*, 5(1):014007, 2010. doi: 10.1088/1748-9326/5/1/014007.

Y. Nesterov. Cutting plane algorithms from analytic centers: efficiency estimates. *Mathematical*, B(69):149–176, 1995.

D. L. Nguyen and N. Coowanitwong. Strategic environmental assessment application for sustainable transport-related air quality policies: a case study in Hanoi City, Vietnam. *Environment, Development and Sustainability*, 13 (3):565–585, 2010. doi: 10.1007/s10668-010-9277-1.

K. C. Nguyen, J. A. Noonan, and W. L. Physick. Comparison of Eulerian and Lagrangian model predictions of power station plume dispersion. *Transactions on Ecology and the Environment*, 3:1184, 1994.

W.D. Nordhaus and J. Boyer. *Warming the world: economic models of global warming*. The MIT Press, 2000.

G. Norris and R. Vedantham. EPA positive matrix factorization (pmf) 3.0 fundamentals & user guide. Technical report, EPA, 2008.

G. Norris, R. Vedantham, and R. Duvall. EPA unmix 6.0 fundamentals & user guide. Technical report, U.S. Environmental Protection Agency National Exposure Research Laboratory, 2007.

M. T. Odman, J. W. Boylan, J. G. Wilkinson, A. G. Russell, Mueller S. F., R. E. Imhoff, K. G. Doty, W. B. Norris, and R. T. McNider. SAMI air quality modeling, final report. Technical report, School of Civil and Environmental Engineering Georgia Institute of Technology, 2002.

OECD. Environmental performance reviews, Luxembourg. Technical report, Organisation for Economic Co-operation and Development, 2010.

H.R. Olesen. Datasets and protocol for model validation. *International Journal of Environment and Pollution*, 5:693–701, 1995.

J. G. J. Olivier, J. J. M. Berdowski, J. A. H. W. Peters, J. Bakker, A. J. H. Visschedijk, and J. P. J. Bloos. Applications of EDGAR. including a description of EDGAR 3.0: reference database with trend data for 1970-1995. Technical report, RIVM, 2001.

G. Omstedtt. An operational air pollution model. RMK 57, SMHI, 1988.

T. Oxley and H. M. ApSimon. Space, time and nesting integrated assessment models. *Environment Modelling & Software*, 22:1732–1749, 2007.

T. Oxley, H. ApSimon, A. Dore, M. Sutton, J. Hall, E. Heywood, T. Gonzales del Campo, and R. Warren. The UK integrated assessment model, UKIAM: A national scale approach to the analysis of strategies for abatement of atmospheric long-range transboundary air pollution. *Integrated Assessment*, 4(4):236–249, 2003.

T. Oxley, A. Valiantis, M.and Elshkaki, and H. M. ApSimon. Background, road and urban transport modelling of air quality limit values (the BRUTAL model). *Environmental Modelling & Software*, 24(9):1036–1050, September 2009.

S. Pandis and J. H. Seinfeld. Mathematical modeling of acid deposition due to radiation fog. *Journal of Geophysical Research*, 94:12911–12923, 1989.

E. A. Parson. Integrated assessment and environmental policy making: in pursuit of usefulness. *Energy Policy*, 23(4–5):463—-475, 1995.

J. K. Pearson. *Improving air quality: progress and challenges for the auto industry*. SAE-R. Society of Automotive Engineers, 2001. ISBN 9780768002362.

B. Peters and J. Smuła-Ostaszewska. Simultaneous prediction of potassium chloride and sulphur dioxide emissions during combustion of switchgrass. *Fuel*, 96:29–42, June 2012.

F. Pietrapertosa, C. Cosmi, S. Di Leo, S. Loperte, M. Macchiato, M. Salvia, and V. Cuomo. Assessment of externalities related to global and local air pollutants with the NEEDS-TIMES Italy model. *Renewable and Sustainable Energy Reviews*, 14:404–412, 2010.

A. Poupkou, T. Giannaros, K. Markakis, I. Kioutsioukis, G. Curci, D. Melas, and C. Zerefos. A model for European Biogenic Volatile Organic Compound emissions: Software development and first validation. *Environmental Modelling & Software*, 25(12):1845–1856, December 2010.

W. H. Press, S. A. Teukolsky, W. T. Vetterling, and B. P. Flannery. *Numerical Recipes*. Cambridge University Press, Cambridge, third edition, 2007. ISBN 978-0-521-88068-8. URL http://nr.com/. The art of scientific computing.

S. Rao, V. Chirkov, F. Dentener, R. Van Dingenen, S. Pachauri, Purohit. P., M. Amann, C. Heyes, P. Kinney, P. Kolp, Z. Klimont, K. Riahi, and

W. Schoepp. Environmental modeling and methods for estimation of the global health impacts of air pollution. *Environ Model Assess*, 2012. on-line.

S. Reis, S. Nitter, and R. Friedrich. Innovative approaches in integrated assessment modelling of European air pollution control strategies - implications of dealing with multi-pollutant multi-effect problems. *Environmental Modelling & Software*, 20:1524–1531, 2005.

J. Risbey, M. Kandlikar, and A. Patwardhan. Assessing integrated assessment. *Climatic Change*, 34(3–4):369–395, November 1996.

E. Romberg, R. Bösinger, A. Lohmeyer, R. Ruhnke, and E. Röth. NO-NO2-Umwandlung für die Anwendung bei Immissionsprognosen für Kfz-Abgase. *Staub-Reinhaltung der Luft*, 56(6):215–218, 1996.

R.E. Rosenthal. *GAMS: A User's Guide*. The Scientific Press, Redwood City, California, 2011.

J. Rotmans and M. B. A. Asselt. Integrated assessment: A growing child on its way to maturity. *Climate Change*, 34:327–336, 1996.

A. Russell. Regional photochemical air quality modeling:model formulations, history, and state of the science. *Annual Review of Energy and the Environment*, 22:537–588, November 1997. doi: 10.1146/annurev.energy.22.1.537.

R. Rückerl, A. Schneider, S. Breitner, J. Cyrys, and A. Peters. Health effects of particulate air pollution: A review of epidemiological evidence. *Inhalation Toxicology*, 23:555–592, September 2011. doi: 10.3109/08958378.2011.593587.

A. Sandu, J.G. Verwer, J. G. Blom, E. J. Spee, G. R. Carmichael, and F. A. Potra. Benchmarking stiff ode solvers for atmospheric chemistry problems 2. *Atmospheric Environment*, 31:3459—3472, 1997.

M. Schaap, F. Sauter, R. M. A. Timmermans, M. Roemer, G. Velders, J. Beck, and P. J. H. Builtjes. The LOTOS-EUROS model: description, validation and latest developments. *Int. J. Environment and Pollution*, 32(32): 270–290, 2005.

S.H. Schneider. Integrated assessment modeling of global climate change: Transparent rational tool for policymaking or opaque screen hiding value-laden assumptions? *Environmental Modelling and Assessment*, 2(4):229–248, 1997.

W Schoepp, M Amann, J. Cofala, C. Heyes, and Z. Klimont. Integrated assessment of european air pollution emission control strategies. *Environmental Modelling and Software*, 14(1):1–9, 1998. ISSN 13648152.

K. Segerson. Economic impacts of ozone and acid rain: Discussion. *American Journal of Agricultural Economics*, 69:970, 87.

P. Seibert and A. Frank. Source-receptor matrix calculation with a Lagrangian particle dispersion model in backward mode. *Atmospheric Chemistry and Physics*, 3:4515–1548, 2004.

J. H. Seinfeld and S. N. Pandis. *Atmospheric chemistry and physics: from air pollution to climate change*. A Wiley-Interscience publications. Wiley, 2006. ISBN 9780471720188.

Service géologique du Luxembourg SGL. Géologie du luxembourg, 2012. URL http://www.geologie.lu/.

J. Shih, A. G. Russell, and G. J. McRae. An optimization model for photochemical air pollution control. *European Journal of Operational Research*, 106:1–14, 1998.

C. Shiu, S. C. Liua, C. Chang, J. Chen, C. C.K. Chou, C. Lin, and C. Young. Photochemical production of ozone and control strategy for southern taiwan. *Atmospheric Environment*, 41:9324–9340, 2007.

S. Simões, J. Cleto, P. Fortes, J. Seixas, and H. Gjalt. Cost of energy and environmental policy in Portuguese CO2 abatement - scenario analysis to 2020. *Energy Policy*, 36:3598—-3611, 2008.

W. C. Skamarock, J. B. Klemp, J. Dudhia, D. O. Gill, D. M. Barker, W. Wang, and J. G. Powers. A description of the advanced research wrf version 2. Technical report, NCAR, 2005.

F.B. Smith. Conditioned particle motion in a homogeneous turbulent field. *Atmospheric Environment*, 2:491–496, 1968.

R. S. Sokhi, H. Mao, S. T. G. Srimath, S. Fan, N. Kitwiroon, L. Luhana, J. Kukkonen, M. Haakana, A. Karppinen, D. van den Hout, P. Boulter, I. S. McCrae, S. Larssen, K. I. Gjerstad, R. San Jose, J. Bartzis, P. Neofytou, P. van den Breemer, N. Steve, A. Kousa, B. M. Cortes, and I. Myrtveit. An integrated multi-model approach for air quality assessment: Development and evaluation of the OSCAR air quality assessment system. *Environmental Modelling & Software*, 23:268–281, 2008.

D . Solé, N. Camelo, G. F. Wandalsen, A. C. Pastorino, Jacob C. M. A., C. Gonzalez, N. F. Wandalsen, F. N. A. Rosário, G. B. Fischer, and C.K. Naspitz. Prevalence of symptoms of asthma, rhinitis, and atopic eczema in Brazilian adolescents related to exposure to gaseous air pollutants and socioeconomic status. *Jornal of Investigational Allergology and Clinical Immunology*, 17:6–13, 2007.

C. V. Souza. Emissões de compostos orgânicos voláteis de um aterro controlado e o potencial formador de ozônio. Master's thesis, Instituto de Química, Universidade do Estado do Rio de Janeiro, 2011.

B. Sportisse. A review of current issues in air pollution modeling and simulation. *Comput Geosci*, 11:159–181, 2007.

R. Srnensky. Symos'97 user guide. Technical report, Idea-Envi, 1998.

STATEC. Projections socio-économiques 2010–2060. bulletin du statec 5-10. Technical report, Institut National de la Statistique et des Études Économiques du Grand-Duché du Luxembourg, 2010a.

STATEC. Balance énergétique du Luxembourg – 2005, 2010b. Internal document.

R. Stern, P. Builtjes, M. Schaap, R. Timmermans, R. Vautard, A. Hodzic, M. Memmesheimer, H. Feldmann, E. Renner, Wolke R., and A. Kerschbaumer. A model inter-comparison study focussing on episodes with elevated PM10 concentrations. *Atmospheric Environment*, 42:4567–4588, 2008.

J. M. Stockie. The mathematics of atmospheric dispersion modeling. *Society for Industrial and Applied Mathematics*, 53(2):349—372, 2011.

J. Ström, L. Alfredsson, T. Malmfors, and O. Selroos. Health effects of particulate air pollution: A review of epidemiological evidence. *Indoor and Built Environment*, 3:58–68, 1994.

M. Tainio, J. T. Tuomisto, J. Pekkanen, N. Karvosenoja, K. Kupiainen, P. Porvari, M. Sofiev, A. Karppinen, L. Kangas, and J. Kukkonen. Uncertainty in health risks due to anthropogenic primary fine particulate matter from different source types in Finland. *Atmospheric Environment*, 44(17): 2125–2132, June 2010.

R. Thomas, J. Smith, M. Jones, J. MacKay, and J. Jarvie. Emissions modeling of specific highly reactive volatile organic compounds (HRVOC) in the houston-galveston-brazoria ozone nonattainment area. In *17th Annual International Emission Inventory Conference "Inventory Evolution - Portal to Improved Air Quality"*, Portland, Oregon, 2008. EPA.

R. M. A. Timmermans, A. J. Segers, P. J. H. Builtjes, R. Vautard, R. Siddans, H. Elbern, S. A. T. Tjemkes, and M. Schaap. The added value of a proposed satellite imager for ground level particulate matter analyses and forecasts. *IEEE JOURNAL OF SELECTED TOPICS IN APPLIED EARTH OBSERVATIONS AND REMOTE SENSING*, pages 271–283, 2010.

G. Tonnesen, J. Olaguer, Bergin M., T. Russell, A. Hanna, P. Makar, D. Derwent, and Z. Wang. Air quality models. Technical report, University of California at Riverside, 1998.

F .L. Toth and E. Hizsnyik. Integrated environmental assessment methods: evolution and applications. *Environmental Modeling and Assessment*, 3(3): 193–207, September 1998.

G. Tsilingiridis, T. Zachariadis, and Z. Samaras. Spatial and temporal characteristics of air pollutant emissions in Thessaloniki, Greece: investigation of emission abatement measures. *The Science of the Total Environment*, 1–3:99–113, 24 April 2002.

D.B Turner. *Workbook of Atmospheric Dispersion Estimates. PHS Publication.* National Air Pollution Control Administration, Cincinnati, Ohio., 1970.

L. Tzivian. Outdoor air pollution and asthma in children. *Journal of Asthma*, 48:470–481, 2011.

UNECE. Convention on long-range transboundary air pollution. Technical report, United Nations Economic Commission for Europe, 1979.

UNECE. Convention on long-range transboundary air pollution. Technical report, United Nations Economic Commission for Europe, 1999.

UNEP. Assessment of policy instruments for reducing greenhouse gas emissions from buildings. Technical report, Central European University, United Nations Environment Programme, 2007.

UNFCCC. Luxembourg — GHG inventory submission of 2010, version 1.2, 2010. URL http://unfccc.int/di/FlexibleQueries.do. http://unfccc.int/di/FlexibleQueries.do.

Alternative Models - ADAM, 2012. U.S. Environmental Protection Agency. URL http://www.epa.gov/scram001/dispersion_alt.htm.

R. Vautard, M. D. Moran, E. Solazzo, R. C. Gilliam, V. Matthias, R. Bianconi, C. Chemel, J. Ferreira, B. Geyer, A. B. Hansen, A. Jericevic, M. Prank, A. Segers, J. D. Silver, J. Werhahn, R. Wolke, S. T. Rao, and S. Galmarini. Evaluation of the meteorological forcing used for the air quality model evaluation international initiative (AQMEII) air quality simulations. *Atmospheric Environment*, 53(0):15 – 37, 2012. ISSN 1352-2310. doi: 10.1016/j.atmosenv.2011.10.065. URL http://www.sciencedirect.com/science/article/pii/S1352231011011605. <ce:title>AQMEII: An International Initiative for the Evaluation of Regional-Scale Air Quality Models - Phase 1</ce:title>.

VDI. VDI 3945 Part 3; Environmental meteorology; Atmospheric dispersion model; Particle model. Technical report, Verein Deutscher Ingenieure, September 2000.

VDI. VDI 3783 Part 8; Environmental meteorology; turbulence parameters for dispersion models supported by measurement data. Technical report, Verein Deutscher Ingenieure, September 2002.

A. Venkatram, P. Karamchandani, P. Pai, and R. Goldstein. The development and application of a simplified ozone modeling system (SOMS). *Atmospheric Environment*, 28:3665–3678, 1994.

A. Visschedijk, P. Zandveld, and H. D. van der Gon. Tno report 2007-a-r0233/b a high resolution gridded European emission database for the eu integrated project GEMS. Technical report, TNO, 2007.

J. C. Walcek and H. Yuan. Calculated influence of temperature-related factors on ozone formation rates in lower troposphere. *Journal of Applied Meteorology*, 34:1056–1069, 1994.

J. J. West, S. Szopa, and D. A. Hauglustaine. Human mortality effects of future concentrations of tropospheric ozone. *Comptes Rendus Geosciences*, 339:775–783, 2007.

J. D. Wilson and B. L. Sawford. Review of Lagrangian stochastic models for trajectories in the turbulent atmosphere. *Boundary Layer Meteorology*, 78: 191–210, 1996.

D. S. Zachary, A. Haurie, and I. Sivergina. A reduced-order photo-chemical air quality model. *Mathematical & Computer Modelling of Dynamical Systems*, 9(4):403–416, December 2003.

D. S. Zachary, U. Leopold, L. Aleluia Reis, C. Braun, G. Kneip, and O. O'Nagy. An energy and environmental meta-model for strategic sustainable planning. In *Energy and Sustainability II*, volume 121, pages 247–255. WIT Press, 2009. doi: 10.2495/ESU090221.

D. S. Zachary, L. Drouet, U. Leopold, and L. Aleluia Reis. Trade-offs between energy cost and health impact in a regional coupled energy-air quality model: the LEAQ model. *Environmental Research Letters*, 6(2):024021, 2011.

J. Zahng and Rao T. S. The role of vertical mixing in the temporal evolution of ground-level ozone concentrations. *Journal of Applied Meteorology*, 38: 1674–1691, 1999.

List of acronyms

ACCPM Analytic Centre Cutting point Method 39

ADAM Air Force Dispersion Assessment Model 31

AOT Accumulated Ozone Exposure 15

AUTH Aristotle University of Thessaloniki 12

AYLTP Asymptotic Level Transport Pollutant 10

BAT Best Available Technologies 22

CMB Chemical Mass Balance Model 30

CRTE Resource Centre for Environmental Technologies 3

CO_2 carbon dioxide 8

CO carbon monoxide 8

CPU Central Processing Unit 2

DEM Digital Elevation Model 11

EDGAR Emission Database for Global Atmospheric Research 91

EEA European Environmental Agency 7

EPA U.S. Environmental Protection Agency 90

ETEM Energy-Technology-Environment Model 3

ETSAP Energy Technology Systems Analysis Programme 20

EU European Union 1

GAINS Greenhouse Gas and Air Pollution Interactions and Synergies . . . 16

GDP Gross Domestic Product 43

GMPL GNU MathProg Language 42

IEA International Energy Agency 20

LEAQ Luxembourg Energy Air Quality 3

LRTAP Convention on Long-range Transboundary Air Pollution 15

LUT Look-up Table 6

MARKAL MARKet ALlocation 20

NO_2 nitrogen dioxide 9

NO_x nitrogen oxides 1

NO nitric oxide 9

List of Symbols

The list of symbols is given by chapter in order to ease the notation.

Chapter 2

n	number of pollutants	23
c_i	concentration of the pollutant i	23
i	pollutant species	23
t	time	23
D_i	molecular diffusivity of species i	23
$\mathbf{R_i}$	rate of change of the concentration of species i	23
T	temperature	23
S	emission rate	23
$\mathbf{x}$	position	23
$\mathbf{U}$	averaged wind velocity	24
$\mathbf{U}'$	fluctuation component of the wind velocity	24
$c_i{}'$	random component of concentration	24
$\mathbf{K}$	turbulent diffusivity tensor	24

Chapter 3

D_s	demand for sector s	43
s	commodities	43
t	time	43
f_s	social or economic factor	43
θ	elasticity	43
n_s	number of commodities	43
$\mathbf{x}$	vector of ETEM decision variables	47
$\mathbf{c}$	cost vector	47
$\mathbf{A}$	energy system	47
$\mathbf{b}$	technical coefficients of the energy system	47
$\mathbf{e}$	pollutant emissions	138
j	pollutant species	50
k	time period	50
σ	economic sector	50

$e_{j,k,\sigma}$ emissions of pollutant j, sector σ and time period k 50
$\mathbf{p}$ emission factors 47
$\bar{\mathbf{e}}$ vector of yearly maximum sectoral emissions 47
$\bar{e}_{j,k,\sigma}$ yearly maximum emissions of pollutant j, sector σ, and time period k 47
$h_\sigma(t)$ sectoral-scheduling function 49
$l_{m(t)}$ monthly load 49
$l_{d(t)}$ daily load 49
$l_{h(t)}$ hourly load 49
$n_w(t)$ number of weeks per month 49
$g_{k,\sigma}(s)$ sectoral fraction 50
$f(x)$ objective convex function 53
C convex feasible set 53
u query point 53
$h_i(x)$ form of the constraints 53
m number of constraints 53
$\mathbf{a}$ parameter of the cut 53
c parameter of the cut 53

Chapter 4

n number of pollutants 66
c_i concentration of the pollutant i 66
$\mathbf{U}$ wind velocity vector 66
t time 67
S emission rate 66
$\mathbf{K}$ turbulent diffusivity tensor 66
$\mathbf{x}$ position 66
c concentration 66
ψ probability density function 69
x' previous position 67
t' previous time 69
P probability function of a particle in $\mathbf{x}'$ at time t' to be at $\mathbf{x}$ at time t 67
n_p number of particles 67
V mean wind velocity 68
τ time step 68
Ua additional velocity 68
u' turbulent velocity 68
R_L Lagrangian autocorrelation function 68
u'' random variable 68
T_L is the Lagrangian time scale 69

Chapter 5

Chapter 7